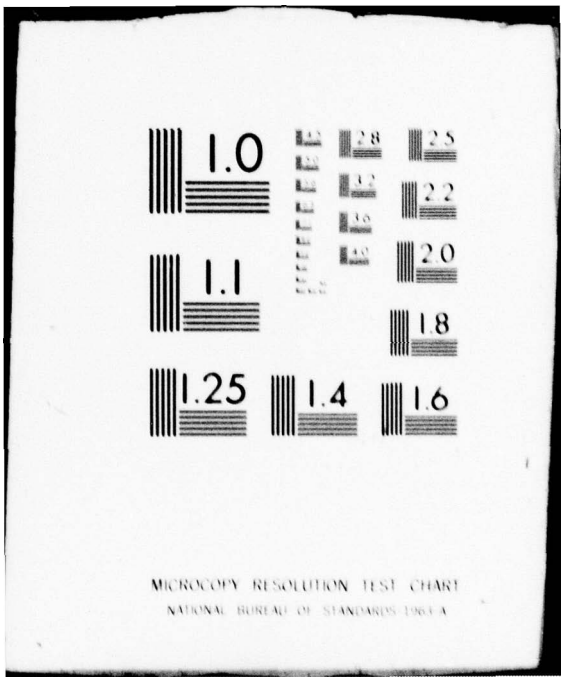
AD-A072 093 WESTINGHOUSE ELECTRIC CORP LIMA OHIO AEROSPACE ELECT--ETC F/G 10/2
PROGRAM FOR THE DEVELOPMENT OF A SUPERCONDUCTING GENERATOR.(U)
FEB 79 J L MCCABRIA F33615-71-C-1591

UNCLASSIFIED AFAPL-TR-79-2012 NL

1 OF 4
AD A072093




1.0
1.1
1.25
1.4
1.6
2.8
2.5
2.2
2.0
1.8
MICROCOPY RESOLUTION TEST CHART
NATIONAL BUREAU OF STANDARDS 1963-A

AD A072093

AFAPL-TR-79-2012

LEVEL II

A001649

PROGRAM FOR THE DEVELOPMENT OF A SUPERCONDUCTING GENERATOR

J. L. McCABRIA

Westinghouse Electric Corporation
Aerospace Electrical Division
Lima, Ohio 45802

DDC
RECEIVED
JUL 30 1979
C

DDC FILE COPY

February 1979

Technical Report AFAPL-TR-79-2012
Final Report for Period January 1974 to January 1979

Approved for public release; distribution unlimited.

AIR FORCE AERO PROPULSION LABORATORY
AIR FORCE WRIGHT AERONAUTICAL LABORATORIES
AIR FORCE SYSTEMS COMMAND
WRIGHT–PATTERSON AIR FORCE BASE, OHIO 45433

79 07 30 117

NOTICE

When Government drawings, specifications, or other data are used for any purpose other than in connection with a definitely related Government procurement operation, the United States Government thereby incurs no responsibility nor any obligation whatsoever; and the fact that the government may have formulated, furnished, or in any way supplied the said drawings, specifications, or other data, is not to be regarded by implication or otherwise as in any manner licensing the holder or any other person or corporation, or conveying any rights or permission to manufacture, use, or sell any patented invention that may in any way be related thereto.

This report has been reviewed by the Information Office (OI) and is releasable to the National Technical Information Service (NTIS). At NTIS, it will be available to the general public, including foreign nations.

This technical report has been reviewed and is approved for publication.

Hugh L. Southall

HUGH L. SOUTHALL, Capt, USAF
Project Engineer

Philip E Stover

PHILIP E. STOVER
Chief, High Power Branch
Aerospace Power Division

FOR THE COMMANDER

JAMES D. REAMS
Chief, Aerospace Power Division
AF Aero Propulsion Laboratory

"If your address has changed, if you wish to be removed from our mailing list, or if the addressee is no longer employed by your organization please notify AFAPL/POD-1, *W-PAFB, OH 45433 to help us maintain a current mailing list".*

Copies of this report should not be returned unless return is required by security considerations, contractual obligations, or notice on a specific document.

AIR FORCE/56780/18 July 1979 — 120

Unclassified

SECURITY CLASSIFICATION OF THIS PAGE (When Data Entered)

REPORT DOCUMENTATION PAGE	READ INSTRUCTIONS BEFORE COMPLETING FORM
1. REPORT NUMBER: AFAPL-TR-79-2012	2. GOVT ACCESSION NO. / 3. RECIPIENT'S CATALOG NUMBER: Rept.
4. TITLE (and Subtitle): PROGRAM FOR THE DEVELOPMENT OF A SUPERCONDUCTING GENERATOR.	5. TYPE OF REPORT & PERIOD COVERED: January 1974 - Final Report January 1979
	6. PERFORMING ORG. REPORT NUMBER: On Phases 2 and 3
7. AUTHOR(s): J. L. MC CABRIA	8. CONTRACT OR GRANT NUMBER(s): F33615-71-C-1591
9. PERFORMING ORGANIZATION NAME AND ADDRESS: WESTINGHOUSE ELECTRIC CORPORATION, AEROSPACE ELECTRICAL DIVISION, LIMA, OHIO 45802	10. PROGRAM ELEMENT, PROJECT, TASK AREA & WORK UNIT NUMBERS: 3145-32-22 / 32
11. CONTROLLING OFFICE NAME AND ADDRESS: Air Force Aero Propulsion Laboratory, AFAPL/POD-1, Wright Patterson Air Force Base, Ohio 45433	12. REPORT DATE: February 1979
	13. NUMBER OF PAGES: 316
14. MONITORING AGENCY NAME & ADDRESS (if different from Controlling Office): 331 p.	15. SECURITY CLASS. (of this report): UNCLASSIFIED
	15a. DECLASSIFICATION/DOWNGRADING SCHEDULE

16. DISTRIBUTION STATEMENT (of this Report)

Approved for public release, distribution unlimited.

17. DISTRIBUTION STATEMENT (of the abstract entered in Block 20, if different from Report)

18. SUPPLEMENTARY NOTES

The work reported here was performed in cooperation with the resources of the Westinghouse Research Laboratories, Pittsburgh, Pennsylvania, 15235 under the direction of J. H. Parker, Jr. and others.

19. KEY WORDS (Continue on reverse side if necessary and identify by block number)

superconductors, generators, cryogenics, helium, windings, light weight, high power.

20. ABSTRACT (Continue on reverse side if necessary and identify by block number)

This report summarizes work completed in Phase II and Phase III of a Program for the Development of a Superconducting Generator. A 5MW, 400 Hz, 12000 rpm generator was designed and built during Phase II. The oil cooled stator contained a 3-phase, wye connected, 5 kV, flooded winding within a laminated iron shield. The rotor contained a winding of 0.094 cm x 0.14 cm wire with 438 36 micrometers filaments of Nb-Ti superconducting alloy. A rotating dewar with a cold electro-thermal shield was used. The Phase III work consisted of a warm spin-up of the generator to design speed followed

DD FORM 1 JAN 73 1473 EDITION OF 1 NOV 65 IS OBSOLETE

Unclassified

SECURITY CLASSIFICATION OF THIS PAGE (When Data Entered)

376 170

Block 20 ABSTRACT (Continued)

by cool-downs of the rotor. A superconducting state was not obtained in a generator configuration due to high pressure in the vacuum space which resulted in excessive gas conduction into the field winding compartment. A continuous pump-down system was incorporated into the test set-up but the helium leakage rate exceeded the capability of this system. Partial disassembly of the rotor was performed to define the areas of leakage. Further disassembly and work is required to correct this problem.

FOREWORD

This final technical report covers Phases II and III development work performed under Contract F33615-71-C-1591 with the Department of the Air Force, Air Force systems command, Air Force Aero Propulsion Laboratory, Wright-Patterson Air Force Base, Ohio. The work was performed by the Aerospace Electrical Division of the Westinghouse Electric Corporation in Lima, Ohio. Work described in this report covers the period from January 1974 to November 1978. Work on this program was initiated in May 1971 under Project 3145, Task 32 and Work Unit 22. Interim Technical Report AFAPL-74-84, October 1974 covers the Phase I development.

Capt. Hugh L. Southall/AFAPL/POD-1 directed the work covered in this report. The Westinghouse Program Manager was R. H. Swanberg. Principal contributors to the research and report were:

Westinghouse
Aerospace Electrical Division
Lima, Ohio: J. L. McCabria, and A. E. King

Westinghouse
Research and Development Center
Pittsburgh, Pennsylvania:
J. H. Parker, Jr., R. D. Blaugher, A. E. Paterson, and R. E. Kolek

Accession For
NTIS GRA&I
DDC TAB
Unannounced
Justification
By
Distribution/
Availability Codes
Dist | Avail and/or special
A

TABLE OF CONTENTS

Section		Page
I	INTRODUCTION AND SUMMARY	1
II	ROTOR DESIGN IMPROVEMENTS	13
	Excessive - Cooling	13
	Current Leads	14
	Elimination of Spokes	14
	Field Winding Cooling Scheme	15
	Field Winding Insulation	17
III	DESCRIPTION OF GENERATOR	19
	Analytical Description	19
	Armature Winding	19
	Bore Seal	36
	Winding Matrix	36
	Overwrap of Armature Winding	41
	Laminated Iron Shield	41
	Aluminum Casing	45
	Stator Cooling	47
	Dielectric Capability	49
	I^2R Losses	51
	Eddy Current Losses	52
	Iron Losses	55
	Superconducting Wire	55
	Superconducting Coils	56
	Heat Exchanger	60
	Central Coil Support Structure	61
	Four Coil Assembly	61
	Containment Cylinder	65
	Anti-Drive End Shaft Assembly	65
	Drive-End Shaft	68
	Electro-Thermal Shield	69
	Outer Cylinder	75
	Helium Cooling System	75
	Cryogenic Instrumentation	77
	Bearings	79
	Dynamic Seals	79
	Bearing Brackets	79
IV	GENERATOR CAPABILITY	81
	Voltage, Power, and Field Current	81
	Static Test Results for Field Winding	85
	Stator Limitation	90
V	ROTOR TESTS	99
	Warm Spin-Up	99
	Rotor Cool-Down	102

TABLE OF CONTENTS (CONT'D)

Section		Page
VI	ROTOR REPAIRS	114
	Cold Leak at Bulkhead and Central Transfer Line	114
	Incorporation of Continuous Pumping on Vacuum Compartment	120
VII	COOL-DOWN WITH CONTINUOUS PUMPING VACUUM COMPARTMENT	123
	Rotating Cool-Down	123
	Static Cool-Down with Rotor Vertical	127
	Static Cool-Down in Liquid Helium Dewar	128
VIII	EXAMINATION OF ROTOR	123
IX	A CRITQUE OF THE GENERATOR	135
	Concluding Problem	135
	Rotor Critque	136
	Helium Leakage	136
	Field Winding	138
	Electro-Thermal Shield	141
	Stator Critque	141
	Reduction of Eddy Current Losses	141
	Armature Coils with Small Strands	142
	Magnetic Shielding	144
	Hot Spot Limitation	144
	Summary	147
Appendix		
A	BORE SEAL DEVELOPMENT FOR SUPERCONDUCTING GENERATOR	151
B	COMPOSITE COMPONENT DESIGN	169
C	INSULATING COMPONENTS FOR STATOR	192
D	EVALUATION OF ADHESIVES FOR STATOR COMPONENTS	201
E	WOUND STATOR ASSEMBLY FOR SUPERCONDUCTING GENERATOR	220
F	EDDY CURRENT LOSS FOR A RECTANGULAR CONDUCTOR	228

LIST OF APPENDIX (CONT'D)

Appendix		Page
G	HELIUM COOLING COIL FAILURES	232
H	TEST CYLINDER FOR AN OVERWRAP ON THE ELECTROTHERMAL SHIELD	235
I	OIL FLOW AND THERMAL TESTS ON ARMATURE CONDUCTORS	239
J	OIL FLOW/ELECTRIC TEST ON STATOR	260
K	TEST PROCEDURES	280
REFERENCES		315

LIST OF ILLUSTRATIONS

Figure		Page
1	Cross Section of Generator	5
2	Heat Exchanger for Isothermal Compression of Helium	16
3	Coil for Armature Winding	31
4	Armature Coil Dimensions	32
5	Armature Winding Matrix	37
6	Armature Winding with Overwrap	39
7	Coil Assembly Fixture	42
8	Fiberglass Overwrap	43
9	Completed Wound Coil Assembly	44
10	Wound Coil Assembly with Shield	46
11	Completed Stator on Test Stand	48
12	Minimum Dielectric Oil Gap in Armature	50
13	Superconducting Coil Winding Fixture	57
14	Superconducting Coil Winding Fixture	58
15	Superconducting Coil	59
16	Four Coil Assembly Before Cold Test	62
17	Cold Test of Four Coil Assembly	63
18	Four Coil Assembly After Closure Welds	64
19	Transition Pieces with Cooling Coils	67
20	Electro-Thermal Shield	72
21	Relative Temperatures of Electro-Thermal Shield and Inner Structure	74
22	Sealed Connectors and Special Tubes for Sensor Leads	78
23	Voltage Versus MVA at 12000,10000 and 8000 RPM for 228A Field Current	82

79 07 30 007

LIST OF ILLUSTRATIONS (Cont'd)

Figure		Page
24	Voltage Versus MVA at 228A, 190A and 152A Field Current at 12,000 RPM	83
25	One Pole Pitch for Generator Showing High Field Region and Field Value at OD of Winding	86
26	Superconducting Coil Load Line Comparisons	87
27	Cooling Oil Temperature Stations in Stator	91
28	Maximum Stator Hot Spot Temperature for Point Designs	94
29	Maximum Stator Hot Spot Temperature for Point Designs	95
30	Conductor Losses at Inner Radius of Armature for an Output of 5MVA with 228A Field Current	97
31	Conductor Losses at Inner Radius of Armature for an Output of 5MVA at 12,000 RPM	98
32	Test Site	103
33	Generator on Test Bed	104
34	Helium Supply System	106
35	Helium Exhaust Circuits	106
36	Compressor and Oil Removal System	108
37	Cold Box	109
38	Schematic Location of Helium Stream Thermometers	110
39	Location of Heluim Level and Pressure Indicators	110
40	Rotor Repair Drawing for Internal Transfer Line	115
41	Failure of Support Clamp for a Current Lead Conduit	118
42	New Support for Current Leads	119
43	Configuration of Continuous Pumping System	121
44	Photograph of Ferrofluidic Seal from Behind Gear Box	122

LIST OF ILLUSTRATIONS (Cont'd)

Figure		Page
45	Test Site for Cold Tests	124
46	Jacket Around Rotor for LH_2 Cooling	129
47	Cold Test with Rotor in Large Dewar	130
48	Interior of Drive-End Shaft	133
49	Specific Power of Generator Versus Field Current	140
A·1	Stator Assembly Half Section	155
A·2	Finite Element Model of Stator	158
A·3	Bore Seal Winding Mandrel	162
A·4	Sleeve Winding Mandrel	163
B·1	Finite Element Grid of Right Hand Portion of Bore Seal and Stator Stack	176
B·2	Bore Seal Axial Vs Axial Length Condition I	178
B·3	Bore Seal Hoop Stress Vs Axial Length Condition I	179
B·4	Bore Seal Axial Stress Vs Axial Length Condition II	180
B·5	Bore Seal Stress Vs Axial Length Condition II	181
B.6	Bore Seal Axial-Hoop Torsional Stress Vs. Axial Length Condition II	182
B·7	Bore Seal Tube, Winding Configuration	189
B·8	Part No. -2 and -3, Winding Configuration	190
B·9	Bore Seal Assembly	191
C.1	Conductor Channels Made from 5M54 Polyester - Glass Fabric Tape	196
C·2	Winding Tape Onto the Steel Mandrel	197
C·3	The Mandrel with Five Layers of Tape Wound on	198
C·4	Tape Wound Mandrel Sandwiched Between Flat Plates	200

LIST OF ILLUSTRATIONS (Continued)

Figure		Page
D·1	End View of Stator Section Showing Wedge Coil Channel and Bore Seal Interfaces	203
G·1	TTS - Diagrans for 304 Stainless (18-8, 18-10) Showing Sensitization Regions as a Function of Carbon Level	233
H·1	304 Stainless Steel Multifilament Yarn	236
H·2	McClean - Anderson W-1 Winding Machine and Test Cylinder	237
I.1	End View of Stator Section Showing Wedge, Coil Channel and Bore Seal Interfaces	240
I·2	Statoret for Oil Flow Test	241
I·3	Photo Micrograph of Stator Standed Conductor	243
I·4	Statoret Test Site Schematic	248
I·5	Temperature Stations for Statoret Tests	249
I·6	Stator Manifold Pressure Versus Oil Flow	255
J·1	Stator Oil Flow and Thermal Test Site	261
J·2	Schematic of Stator Cooling System	262
J·3	Location of Thermocouples in Stator	263
J·4	Installation of Thermocouple at End of Cells	264
J·5	Oil Flow Rate Through Stator	268
J·6	Pressure Drop Across Stator	269
J.7	Temperature of Knuckles Versus Loss Density	275
J·8	Temperature of Junctions Versus Loss Density	276
J.9	Temperature at End of Cells Versus Loss Density	277

LIST OF ILLUSTRATIONS (Continued)

Figure		Page
K·1	External Helium Supply System	303
K·2	Slip Ring Instrumentation System	304
K·3	Location of Rotor Thermometers	305
K·4	Open Circuit Test Instrumentation	306
K·5	Stator Cooling System	307
K·6	Thermocouple Locations in Stator	308
K·7	Short Circuit Test Instrumentation	309
K·8	Instrumentation for Sudden Application of Short Circuits	310
K·9	Unbalanced Load Test Instrumentation	311
K·10	Instrumentation for Rectified Load Test	312
K·11	Voltage Parameters for No Load Test	313
K·12	Field Current Parameters for Short Circuit Tests	314

LIST OF TABLES

Table		Page
1	Typical Leakage Currents In Phase Group	35
2	Eddy Current Losses In Conductors	54
3	Properties of 304 Stainless Steel Fiber	70
4	SS-304 Epoxy Composite Properties	71
5	Static Rotor Test	89
6	Specific Power Losses in Armature Conductor and Temperature Data	92
A·1	Stator Design and Detail Drawings	154
A·2	Resin Systems Evaluated for Using in Bore Seal	160
A·3	Physical Property Data on Candidate Material System	161

LIST OF TABLES (CONT'D)

Table		Page
B·1	Design Loads and Environmental Conditions for Stator	186
B·2	Maximum Stress and Strains During Condition I and II	187
B·3	Comparison of Maximum Stress and Strains with Allowables	188
D.1	Performance and Processing Requirements of Candidate Adhesives	205
D·2	Candidate Adhesives for Bore Seal Applications	206
D·3	Screening Tests of Candidate Adhesives; Tensile-Shear Strength on 0.063" Epoxy Fiberglass Substrates	210
D·4	Tensile Strength of Bore Seal Substrate Bonded to Coil Channel Substrate	211
D·5	Tensile-Shear Strength of Bore Seal Substrate Bonded to Coil Channel Substrate After Aging in 100°C WEMCO C Oil	211
D·6	Tensile-Shear Strength of Coil Channel Substrate Bonded to Wedge Substrate	214
D·7	Tensile-Shear Strength of Bore Seal Substrate Bonded to Wedge Substrate	214
I·1	Flow Parameters for Stator	245
I·2	Flow Calibration for Statorette #1	250
I·3	Temperature Calibration for Statorette #1	251
I·4	Summary of Losses	257
J·1	Listing of Thermocouple Reading from Charts (1) through (11)	270
J·2	Listing of Temperatures for Knuckles	271
J·3	Listing of Temperatures for Conductor/ Bus Ring Connection	272
J·4	Listing of Temperatures at Exit of Cells	273

SECTION I

INTRODUCTION and SUMMARY

Over the last decade, the development of practical high field superconductors capable of carrying large transport currents has coincided with application of these conductors to electrical rotating machines. Studies[1] have indicated in the case of ac generators that utilization of superconducting field windings gives promise of improved machine characteristics such as reduced size and weight, higher efficiency, higher output voltages and lower synchronous reactance. These potential improvements follow directly from the higher current density capability of superconductors over that of copper, the feasibility of no iron in the rotor (field) structure and the feasibility of an air gap armature winding.

Demonstrations of ac generators with superconducting field windings have ranged from the early Avco[2] and MIT[3] generators with power ratings in the kW range up to the recent 3600 rpm, two pole machines developed by Westinghouse[4,5] and MIT[6] with ratings in the MW range.

As a result of the predicted reduction in weight and volume for this new type of generator, the United States Air Force Aero Propulsion Laboratory, Wright Patterson Air Force Base initiated a technology advancement program[7] directed toward the development of a prototype ac generator with superconducting field windings. Such a generator offers outstanding features which should be of great value for an airborne application. Firstly, the rotor is small and can be directly coupled to a high speed turbine without a need for a speed changer. Secondly, it can be scaled to large ratings and, finally, it can generate a high voltage.

The program was planned as three phases, with--

Phase I

Demonstrate Feasibility of Critical Components

Phase II

Design and Construction of a Complete Generator

Phase III

Full Power Test of Generator

The first phase[8,9] of this program was successfully concluded in January 1974 with the testing of a prototype rotor. The critical components within the rotor, i.e., the dynamic cryogenic seals, power leads, and the super-conducting field winding, were experimentally evaluated concurrently with the fabrication of a rotor. This 4-pole rotor was cooled down to 4.2 K and cold tests were conducted up to the overspeed condition of 13,200 rpm. Full excitation of the field current was obtained at the operating speed of 12,000 rpm. This Phase I work is presented in Air Force Technical Report AFAPL-TR-74-84.[10]

The second phase of the program was devoted to the detail design and construction of a complete generator. The objective of the design effort was to use a rotor about the same size and configuration as the first rotor with design improvements and simplifications as warranted from the experience from the Phase I effort. Other criteria that were established at the beginning of the design phase were:

- Continuous Rating - 1.0 MW (minimum)
- Pulse Rating - 5.0 MW (minimum) for 10 seconds at a repetition rate of one 10 second pulse per minute.
- Power Factor - .95 lagging
- Phases - three phases, Y connected

- **Voltage Regulation Goal - 20% maximum**

- **Excitation Rate - rated excitation achieved in 60 seconds or less.**

- **Rotor Cool-Down Rate - cool-down from room temperature to a superconducting state in 8 hours or less.**

- **Stator Coolant - transformer oil per Federal Specification VV-I-5302, Class I.**

- **Stator Shield - silicon steel with sufficient steel to operate at no-load with full excitation.**

- **Weight Goal - 1000 pounds or less**

- **Excitation - external power supply through brushes and slip rings.**

- **Suspension - four point suspension compatible with a ground test site.**

The design effort[11,12] was completed in early 1975 and construction of the generator was started thereafter. A cross-section of the generator is presented in figure 1 (see page 5).

The stator was completed in October 1976 and static thermal and oil flow tests were performed on the stator assembly using dc power to heat the armature winding. A direct current equivalent to the phase current for a 5,000 volt, 10 MW load was applied to each phase in the winding. The results from these tests fufilled our expectation from the standpoints of oil circulation and cooling.

The projected continuous capabilities of the stator based upon the static tests results and the impact of eddy-currents are:

RPM	FIELD CURRENT AMP	VOLTAGE (L-L) VOLTS	MVA*
12,000	203	3,800	7.0
12,000	228	5,000	5.0
8,000	228	3,000	5.0

The weight of the stator is 639 pounds and with over all diameter and length of 48.26cm (19.0 inch) and 74.68cm (29.4 inch), respectively. Dielectric tests were preformed on the stator at 11 kV, or two times the design voltage plus 1 kV. However these tests represent only 57% of the continous dielectric capability of the transformer oil and solid barrier insulation system.

Certain problems arose during the fabrication of the rotor which required modifications of several components and delayed the completion of the rotor. Firstly, the bare superconducting wire was coated with enamel and an overcoat in accordance with the procedures developed during the design efforts. Post dielectric tests demonstrated the insulation was inferior to the developmental specimens. Therefore, it was necessary to strip the wire back to the original bare condition, electro-clean, and re-insulate the entire 18,000 feet of wire. Secondly, failure of the epoxy-glass pole piece occurred during the curing of the resin on the conductors in the first coil. It was necessary to modify the winding fixture, change the curing procedure, and fabricate a coil to replace the damaged coil. Thirdly, helium leak tests were made and found unsatisfactory for several of the cooling coils on the thermal transition pieces between the ambient structure and the cold structure. This situation occurred for two of the four cooling coil on the anti drive-end shaft and for all four coils on the drive-end shaft. It was necessary to eliminate the use of the defective cooling coils on the

*These capabilities are delineated in Section 4.

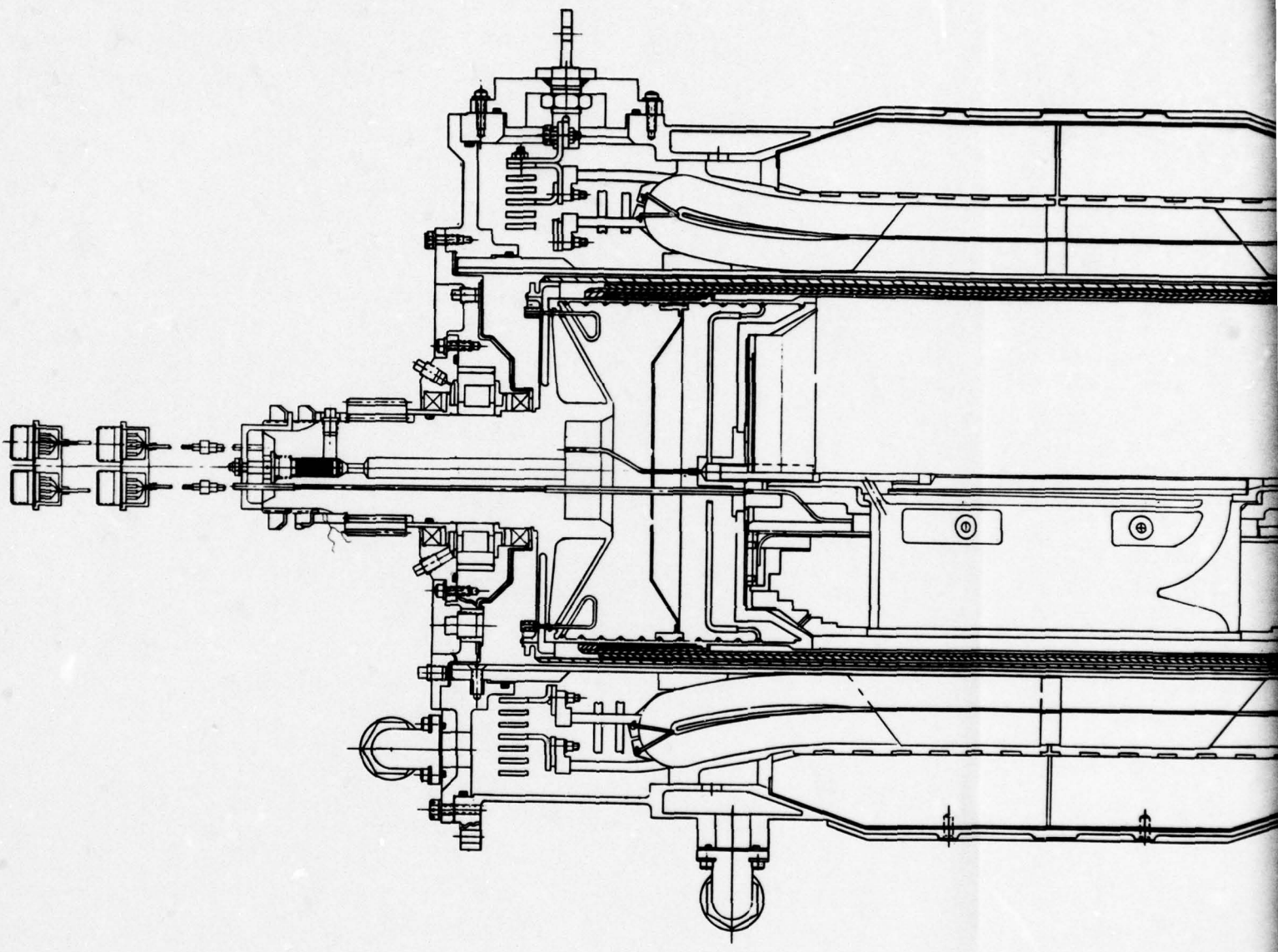
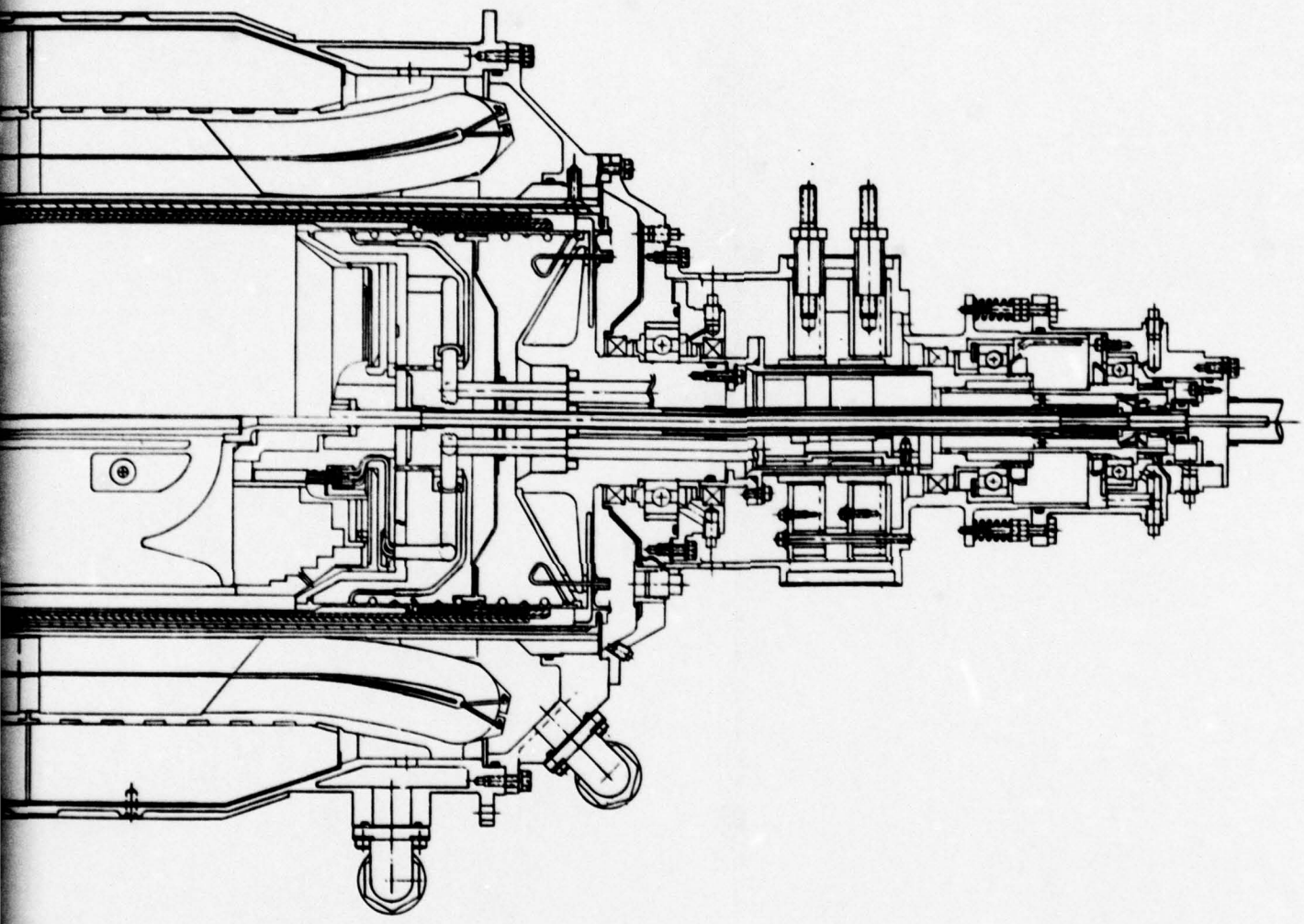


FIGURE 1. Cross Section of Gene



s Section of Generator

2

anti drive-end and to substitute new tubes which were not brazed to the transition piece. The defective cooling coils on the drive-end were removed. New coils were formed and brazed to the transition piece with a Cu-Ag brazing alloy in a vacuum furnace. Subsequently, this part was reheat treated for strength. Fourthly, attempts to fabricate an electromagnetic shield by brazement of a copper cylinder to an inner cylinder of alloy A286 were not successful. Resolution of this problem required the development of an over wrap which consisted of multifilament, stainless steel fiber and a room temperature curing epoxy resin.

Static tests of the four-coil field winding assembly were performed in a bath of liquid helium. The maximum current capability of the superconducting wire in the four-coil configuration is 440A based upon the performance of short samples of the wire. The observed current for normalization of the four coil field winding was approximately 57% (251A) of this capability. Even though the coils normalized prematurely the observed normalization was 110% of the required current (228A) for a 5,000 volt, 5MW output of the generator.

The rotor was completed in March 1977 and balanced for 12,000 rpm operation. The weight of the rotor was 340 pounds excluding the weight of the auxilary shaft for the slip rings.

During the first half of 1976 Westinghouse evaluated available facilities and equipment for full load tests on the generator. It was found that the cost to run full power tests was high, the number of available test sites are extremely limited, and the equipment required to load the generator and to control the load was a significant item. In addition, the projected schedule for the full load test was approaching the completion date of a high power test facility at the Wright Patterson Air Force Base. Therefore, the scope of the Phase III program was changed to include only no-load, steady state short circuits, sudden application of short circuits, unbalanced short circuit loads, shorted rectified output, and over speed tests.

The rotor and stator were assembled and the low power site at the Westinghouse R&D Cryogenic Laboratory was prepared for the tests. The dry weight of the generator assembly was 1021 pounds and with the stator filled with oil the weight increased to 1066 pounds. The first rotating tests consisted of a warm spin-up to 6000 rpm on 18 April 1977. A spin-up to full speed was aborted and an additional oil supply, an additional scavange port, and a new bearing was incorported at the outboard end of the slip ring shaft. The first warm spin-up to 12,000 occured on 19 April while checking vibration and general operation at intermediate speeds. At 12,000 rpm a failure of a duplex set of bearings in the high speed gear box occurred. The damage was limited to the high speed gear box and to the instrumentation leads from the slip rings. The gear box was repaired, new leads were made, and successful warm spin-ups to 12,000 rpm were performed on 13 May.

The test site was prepared for the cold tests and rotor cool-down was initiated on 6 June 1977, with liquid nitrogen. Subsequently, liquid heluim was introduced for 12 hours. During this time the temperature of the field winding did not decrease below 65 K. An investigation of the problem revealed the vacuum within the rotor had degraded which caused an excessive heat loss into the field winding compartment.

A series of leak tests were performed to establish the nature and location of the leak. It was concluded that the fault was located in or about the bulk head on the anti-drive end at a point near the penetration of the central heluim transfer tube into the low temperature structure. Also, it was established from these experiments that the fault did not leak until the bulk head was cold.

A procedure for repair of the leak was defined which limited the repair to the following tasks:

- Removal of the outer shell,
- Removal of the bearing shaft,
- Removal of the radiation disc,

- Replacement of the transfer line with an improved design,
- Replacement of the parts which were not reusable,
- Cold leak tests during the repair procedure,
- Rewelding of the rotor assembly,
- Requalification of the bearing shaft, and
- A rebalance of the rotor assembly.

The repair of the rotor was initiated 1 September 1977. This repair was completed; a satisfactory cold leak test was performed, and the rotor was balanced in January 1978. Subsequently, a cold leak test was repeated before the rotor was assembled into the stator. This test indicated a leak from the helium compartment into the vacuum space. The leak was isolated within the field winding compartment by use of a solvent which covered the fault and allowed a helium leak test above the non-filled portion. Several attempts were made to seal the fault with different resins from the helium side. Each of these attempts failed due to the fracture of the resin when the rotor was cooled to liquid nitrogen temperature. It was concluded the leak rate was low enough to permit the winding to reach a superconducting state if continuous pumping were maintained on the vacuum compartment. A continous pumping system was designed and constructed which consisted of a 3/8 inch tube conencted to the drive end of the rotor through the high speed gear box and the instrumentation slip rings that terminated in a magnetic fluid seal. This seal was designed and manufactured by the Ferrofluidics Corporation.[13]

The generator was assembled and the test site was prepared for cold test with continous evacuation of the rotor. Cool-down of the rotor was initiated on 14 August 1978 and was continued through 17 August without obtaining a superconducting state.

Failure to obtain a superconducting field winding was consistent with the steady-state temperature ($\sim$20K) observed down-stream of the field winding. An excessive heat loss into the field winding compartment was the apparent reason for this condition. However, it could not be determined during this rotating cool-down if the high heat loss was due to too high a pressure in the vacuum space or if points of contact existed between the warm structure and the cold structure.

Therefore, the rotor was removed and a calibration of the conductance of the vacuum pump-down line was made. This calibration consisted of measuring the vacuum pressure at the union for the pump-down line and the rotor versus the pressure at the vacuum pump for different helium leakage rate through the line. With this calibration and the pressures observed at the vacuum pump during the cool-down, it was established that pressures between 10^{-3} and 10^{-2} mmHg existed in the vacuum compartment of the rotor during the previous cool-down cycle. These pressures were approximately 10 times greater than the allowable vacuum pressure for acceptable gas conduction losses.

A static cool-down of the rotor was then performed with the rotor in a vertical position and with continuous pumping through a high conductance vacuum line. A jacket was placed around the outer shell of the rotor and filled with liquid nitrogen. The helium temperatures observed within the field winding compartment were consistant with a superconducting state for the coils. However, the winding did not go superconducting. This fact gave rise to new questions such as:

- possible high resistive interconnection(s) or lead connection(s) which prevented the winding from going superconducting, and
- possible blockage of coolant passages by the sealant resin which caused a non uniform cooling of the coils.

To answer these questions the resin was dissolved and flushed from the helium compartment. Subsequently, the rotor was suspended within a large stationary dewar. Helium was supplied from the Westinghouse liquefaction unit and was circulated through the rotor in a closed cycle with the vacuum compartment vented into the dewar. After ∿50 hours the sensor within the rotor indicated 7K and the field winding became superconducting. Subsequently, the dewar was filled with liquid helium until the rotor was submerged. The field winding was excited until it normalized at 236A with a helium inlet temperature of 4.3K.

This test demonstrated that the winding and internal coil connections are electrically sound and that previous inabilities to obtain a superconducting state were due to inadequate and nonuniform cooling of the winding. The resolution of this problem requires elimination of the leakage of helium so adequate insulation of the winding compartment can be provided and maintained.

USAF approval was obtained on 11/29/78 to remove the outer shell and electrothermal shield and to perform leak tests to define the area(s) of leakage. The internal region of the drive-end shaft showed a significant leakage into the field winding compartment when helium gas was introduced from the outside. The location of this leak was isolated from other areas by partially filling the hollow shaft with liquid (alcohol) and checking with helium gas above the liquid. This leak is located at the level of the central bulkhead. Two possible areas exits for the leak . They are: (1) the braze joint(s) between the radial conduits and the cooling coils on the thermal transition tube, and (2) at or near the bulkhead penetration of a lead conduit for resistance thermometers. A second leak was found inboard of a terminal brazement for a helium conduit and the anti drive-end shaft. Extensive disassembly of the rotor is required to repair these faults.

SECTION II

ROTOR DESIGN IMPROVEMENTS

The Phase I rotor development was reviewed and those areas which warranted improvement were defined. A review of areas which were given special consideration are discussed here.

Excessive-Cooling

It was observed during the cool down cycle and during the cold running tests of the Phase I rotor that excessive cooling occurred in the power leads, slip rings, guide bearing and transfer seals. In fact electric heaters were used to maintain the operating temperatures of these components at an acceptable level. The basic problem is that 250 to 300A power leads require ∿1/10 the cooling flow rate as the field windings under cold running conditions. Even less coolant is required for the cool down cycle. Thus, when all of the helium from the field winding was expelled through the power leads, excessive cooling of these parts occurred. The resolution of this problem for the Phase II rotor was to contrive the exhaust system so the helium expelled from the field winding was divided. A small portion of the flow was used to cool the power leads and the remainder was diverted outward to cool shields and to intercept the heat influx from the ambient structures. These parallel exhaust circuits were arranged so the coolant flow rate through the power leads is self regulative or can be regulated externally. The other flow circuit was designed so that a high flow rate of cold helium vapor will not cause a problem. Accordingly, these exit ports were located so excessive cooling of oil lubricated parts will not occur and ice formation will not cause a problem.

PRECEDING PAGE BLANK

Current Leads

A pair of concentric leads with respect to the axis of rotating was used to supply current to the field winding in the Phase I rotor. The reasons for this selection were (1) the flow distribution would probably be superior to that obtainable with off axis leads; (2) the center of the rotor core could be used to produce long conduction stabilized leads, and (3) experience with other types of leads was minimal. Unfortunately, the installation of these concentric leads in the Phase I rotor required a complex arrangement of tubular parts and many critical weldments. Provision for accommodation of thermal contraction of the inner structure relative to the ambient shell was marginal. From the standpoint of mechanical reliability the concentric power lead configuration was not satisfactory and design improvements were warranted for the Phase II rotor. The resolution of this problem was to use simple off-axis leads in separate conduits. The number of critical welds in this arrangement was reduced to six. Provisions for accommodating the thermal displacement was made by forming non-straight (curved) conduits.

Elimination of Spokes

A system of radial spokes was used to connect the cold inner structure to the ambient shell on the anti torque-end of the Phase I rotor. These spokes accommodated thermal displacement. However, they had to support the most massive part of the rotor. The heat leak into the cold structure from the spokes was large and an extra heat load was imposed upon the electro-thermal shield via the spokes. In addition the stress in the spokes was the highest stress intensity in the rotor. The particular problem associated with the high loads on the spoke system was that these loads were transferred to the other structures through mechanical joints (screw threads). Since these loads varied with the dynamic state and thermal state of the rotor the mechanical joints were subjected to cyclic loading. With this arrangement the alignment of the inner structure relative to the rotor bearing can change due to the fact that the applied pre-load on the joints can not begin to approach the cyclic loading that occurs during cool down, start-up, shut-down, and warm-up.

The resolution of the spoke problem was to eliminate them entirely and make the inner structure the primary shaft for the rotor. This was accomplished by making the outer shell accommodate thermal displacement by virtue of flexible end members and by a thin wall, vapor cooled, tubular section on each end of the cold inner structure. The stress intensity in the flexible end of the outer shell is $\sim$1/2 the stress intensity in a spoke system. The extra tubular thermal transition section provided a second cooling station for the electro-thermal shield and a portion of the helium flow from the field winding was used cool this structure. An additional advantage of making the inner structure the primary shaft of the rotor was that it simplified the fabrication of the rotor since it was not necessary to transfer the axis of the massive inner structure to the bearing axis.

Field Winding Cooling Scheme

The helium flow channels in the SC coils for the Phase I field winding caused the helium to flow outward on one end of the coils and inward on the opposite end. Along the straight length of the coils the flow was parallel to the axis of rotation. The rationale for selection of this scheme was that forced convection cooling through the SC winding is required for this application. It was observed from the cold running tests the temperature gradient parrallel to the axis of rotation was weak at the outer raduis of the winding. For the most part the removal of heat at the outer radius depended upon radial conduction within the copper separators. Under these conditions, it was difficult to maintain a low temperature through out the winding during field excitation.

In view of the experience from the Phase I program a new cooling scheme was used for the Phase II rotor. The new scheme contained the following features:

1. A heat exchanger, shown in Figure 2, which is removed from the SC winding and produces an isothermal flow of helium as it flows radially outward to the maximum radius of the field;

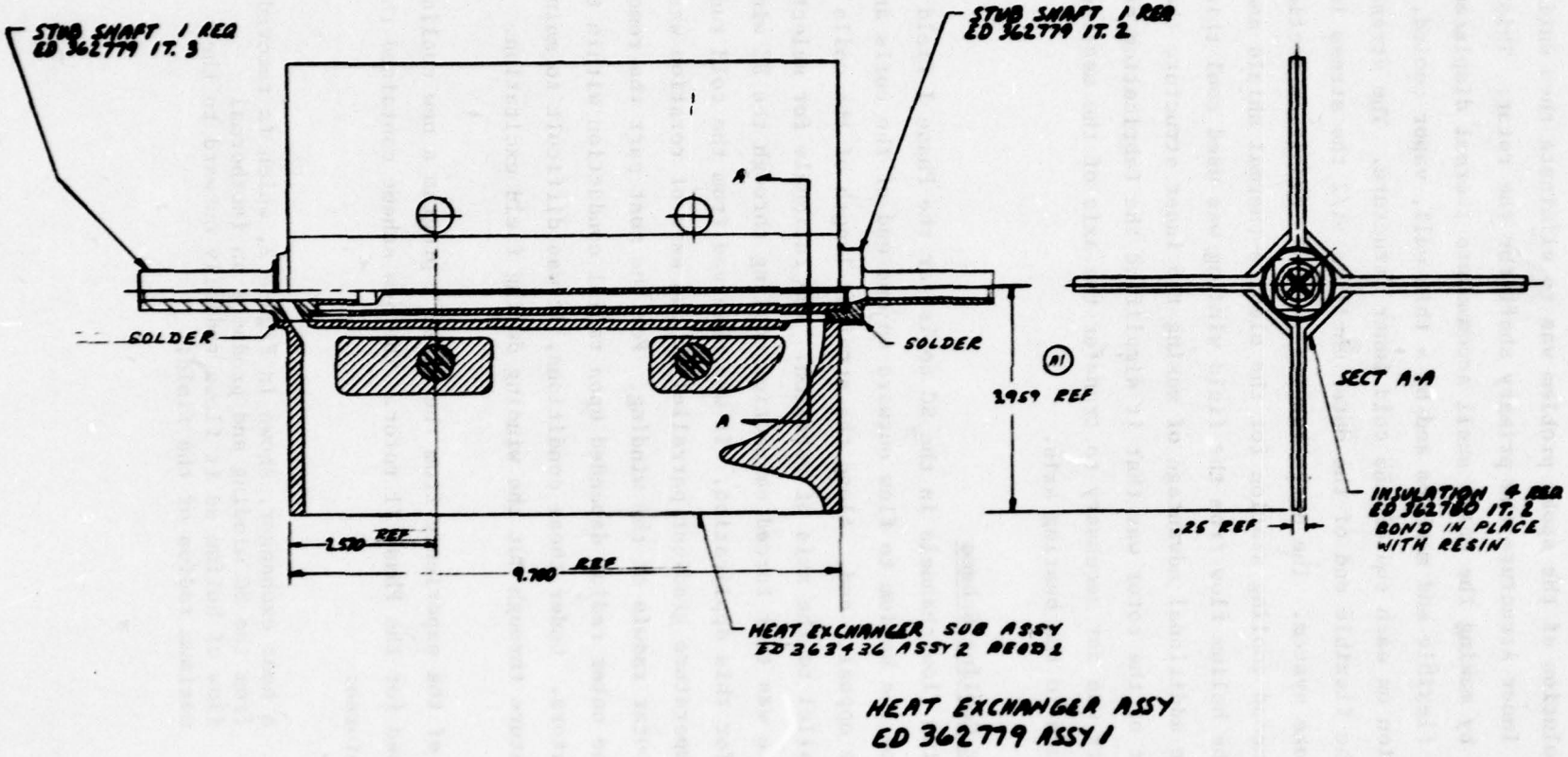


FIGURE 2. Heat Exchanger for Isothermal Compression of Helium

2. Radial flow passages in the SC coils which cause the helium to flow inward as it absorbes heat; and

3. Cooling of the heat exchanger in the center of the rotor with the helium that flows into the cooling coils on the torque tube.

The advantages this scheme offers are:

- the temperature rise due to off-axis compression of the helium is eliminated,
- heat is absorbed in the field winding during decompression of the helium as it flows inward without undergoing a temperature rise - the reverse of isothermal off-axis compression,
- the radial passages in the winding produce a negative feedback upon the flow distribution - a high heat influx in a particular passage causes the flow rate in this passage to be a maximum; and
- positive circulation of helium through-out the field winding is produced by expelling the helium after it has passed through the coils at a radius less than the inner radius of the winding.

Field Winding Insulation

A severe shorting problem in the field was experienced through out the fabrication and testing of the superconducting winding in the Phase I rotor. These shorts limited the rate the coils could be charged due to the I^2R heating by virtue of the L di/dt voltage across the shorts.

The resolution of the shorting problem required improvement of the insulation on the SC wire and improvement of insulation between the winding and ground. A series of experiments were performed on several candidates for the wire insulation. Polyimide ML enamel was selected for the undercoat and Polysulfone enamel was selected for the over-coating.

Cleaning of the bare wire consisted of electro-etching the metal by applying a low voltage high current across a section of the wire while it was immersed in a cleaning solution of sodium carbonate and trisoduim phosphate. Following this operation, the wire was rinsed in an ultrasonic cleaning bath containing water only. The wire was then coated in the enameling tower with 6 passes of Polyimide ML at 25 fpm followed by 2 passes of polysulfone at 25 fpm. The temperature of the tower at the top and bottom was respectively 410° and 300° C for both enameling processes.

The polysulfone over coat is a thermo-plastic enamel that flows at 225°C and was used to provide a bond between adjacent wires after the coil was wound.

SECTION III

DESCRIPTION of GENERATOR

Analytical Description

One part of the design process for the generator was to determine a set of basic dimensions for the electrical conductors and the magnetic shield. A Westinghouse Computer Program was used to synthesize these dimensions and other parameters of interest as presented on pages 20 through 29 . Basic dimensions, inductances, reactances, and winding parameters are given on pages 20 and 21. The magnetic field distribution is based upon a two-dimensional solution. However, empirical factors were applied to the actual length to represent the effective lengths. The magnetic field distribution within the generator is presented on pages 22, 23, 25 and 26. Similarly, the forces acting upon the armature and field conductor are given on page 24.

Armature Winding

The armature winding is composed of twelve identical coils. Each coil contains twenty-four, series connected turns which form a phase group for one pole. The total winding has two parrallel circuits; thus, each conductor carries one-half of the phase current and each phase group per pole generates one-half of the phase voltage. A conductor consists of a 3x6 array of rectangular strands. These strands were formed from 16 gauge round wire and were insulated with polyimide ML enamel with a polysulfone overcoating.

The coils were designed specifically so they could be manufactured by methods and resources common to windings for airborne alternators. All of the conductors in one phase group were wound in straight lengths and around pins that were held apart at a distance equal to the true length of each conductor and strand in their final shape.

DESIGN DATA FOR 5.015 MVA 1200C.0 RPM 4. POLE MACHINE
AT 0.950 POWER FACTOR 400.0 CYCLES
-- IRON STATOR SHIELD --

DIMENSIONS

DIAMETERS

ROTOR
ID 3.880 INCHES OD 9.00C INCHES
DAMPER SHIELD
ID 9.000 INCHES OD 9.20C INCHES
ARMATURE
ID 10.320 INCHES OD 13.884 INCHES
STATOR SHIELD
ID 14.418 INCHES OD 17.985 INCHES

LENGTHS

ACTIVE LENGTH = 9.700 INCHES
END TURNS - ACTUAL AT EACH END
FIELD 1.485 INCHES
ARMATURE 4.920 INCHES
END TURNS - EFFECTIVE TOTAL
FIELD 1.980 INCHES
ARMATURE 4.920 INCHES
MUTUAL 2.441 INCHES

INDUCTANCES

FIELD SELF INDUCTANCE - LF	0.1221E 01 HENRIES
ARMATURE PHASE INDUCTANCE - LA	0.3385E-03 HENRIES
PHASE - PHASE INDUCTANCE - LAB	-.1692E-03 HENRIES
FIELD - ARMATURE MUTUAL - M	0.7907E-02 HENRIES
DAMPER SHIELD INDUCTANCE - LD	0.9172E-07 HENRIES
FIELD - SHIELD MUTUAL - LFD	0.1936E-03 HENRIES
ARMATURE - SHIELD MUTUAL - LAD	0.4198E-05 HENRIES

REACTANCES

SYNCHRONOUS OPEN CIRCUIT - XA	0.2296 PER UNIT
SYNCHRONOUS FULL LOAD - XS	0.2539 PER UNIT
TRANSIENT	0.2155 PER UNIT
SUBTRANSIENT	0.0922 PER UNIT

FIELD WINDING

OVERALL CURRENT DENSITY	116.57 MEGAMPS/SQ.METER
CONDUCTOR CURRENT DENSITY	124307.8 AMPS/SQ. IN.
POLE FACE ANGLE	38.00 ELEC. DEGREES
NUMBER OF TURNS	5000.
SPACE FACTOR	0.605
CONDUCTOR CROSS SECTION	0.193E-02 SQUARE INCHES
TOTAL CONDUCTOR LENGTH	1191.2 FEET
RATED FIELD CURRENT	228.07 AMPERES

ARMATURE WINDING

OVERALL CURRENT DENSITY	3.80 MEGAMPS/SQ.METER
CURRENT DENSITY IN COPPER	8094.22 AMPS/SQ. IN.
PHASE BELT ANGLE	60.00 ELEC. DEGREES
NUMBER OF TURNS	48.
WINDING PITCH	0.708
SPACE FACTOR - WINDING	0.725
- CONDUCTOR	0.418
- OVERALL	0.303
CONDUCTOR CROSS SECTION	0.171E 00 SQUARE INCHES
TOTAL CONDUCTOR LENGTH	593.5 FEET
STRAND DIAMETER	50.20 MILS
NUMBER STRANDS/CONDUCTOR	36.
VOLTS PER TURN	60.38 VOLTS
LINE-NEUTRAL VOLTAGE	2898.4 VOLTS
LINE-LINE VOLTAGE	5020.2 VOLTS
RATED CURRENT	576.7 AMPERES
WINDING CONDUCTIVITY	0.778 RELATIVE TO COPPER

STATOR SHIELD

FRACTION OF END TURNS COVERED	0.100
SATURATION FLUX DENSITY	13.25 KILOGAUSS

MISCELLANEOUS DATA

LOAD ANGLE =	12.559 DEGREES
MACHINE TORQUE =	0.339E 05 IN-LB
REC. TO REC. LENGTH =	37.11 INCHES
FRAME THICKNESS =	0.100 INCHES
HEADING WIDTH =	7.02 INCHES

FIELDS AND FORCES

TOTAL RADIAL FIELD

ANGLE - DEGREES

RADIUS - INCHES	0.0	15.0	30.0	45.0	60.0	75.0	90.0	105.0	120.0	135.0	150.0	165.0	180.0
0.194	0.05	0.88	1.65	2.31	2.81	3.11	3.21	3.09	2.75	2.23	1.56	0.78	-0.05
0.970	0.27	4.37	8.20	11.49	14.03	15.61	16.11	15.47	13.76	11.11	7.72	3.85	-0.27
1.940 - RFI	0.55	7.53	14.53	21.40	28.31	33.00	33.09	32.72	27.77	20.62	13.59	6.47	-0.55
2.352	0.66	7.82	15.26	22.92	31.85	38.08	37.00	37.74	31.19	21.98	14.12	6.54	-0.66
2.764	0.78	7.96	14.73	22.33	31.74	38.34	36.78	37.93	30.96	21.23	13.39	6.05	-0.78
3.176	0.89	6.96	13.43	20.35	29.46	35.91	33.77	35.44	28.57	19.09	11.89	5.23	-0.89
3.588	1.01	6.23	11.78	17.59	25.60	31.35	28.80	30.83	24.59	16.17	10.04	4.28	-1.01
4.000 - RFO	1.13	5.53	10.08	14.72	20.39	24.32	23.09	23.73	19.26	13.14	8.14	3.36	-1.13
4.387	1.25	4.97	8.66	12.34	15.91	18.16	18.32	17.50	14.66	10.61	6.55	2.58	-1.25
4.773	1.35	4.50	7.52	10.40	12.88	14.39	14.61	13.67	11.49	8.52	5.27	1.90	-1.39
5.160 - RAI	1.56	4.14	6.62	8.93	10.77	11.84	11.97	11.06	9.21	6.91	4.27	1.34	-1.56
5.516	1.68	3.87	5.97	7.91	9.36	10.17	10.23	9.34	7.68	5.80	3.56	0.93	-1.68
5.873	1.73	3.63	5.45	7.12	8.32	8.95	8.96	8.11	6.59	4.98	3.04	0.65	-1.73
6.229	1.72	3.41	5.03	6.51	7.53	8.05	8.02	7.21	5.82	4.39	2.65	0.46	-1.72
6.586	1.66	3.22	4.69	6.03	6.94	7.38	7.33	6.57	5.28	3.98	2.38	0.36	-1.66
6.942 - RAO	1.56	3.04	4.42	5.65	6.50	6.90	6.83	6.12	4.94	3.70	2.19	0.31	-1.56
7.075	1.51	2.96	4.33	5.54	6.36	6.76	6.68	5.99	4.85	3.62	2.14	0.31	-1.51
7.209 - RSI	1.48	2.93	4.25	5.43	6.24	6.63	6.55	5.88	4.76	3.55	2.09	0.30	-1.48

-- KILOGAUSS --

TOTAL TANGENTIAL FIELD

RADIUS - INCHES	ANGLE - DEGREES 0.0	15.0	30.0	45.0	60.0	75.0	90.0	105.0	120.0	135.0	150.0	165.0	180.0
0.194	-3.21	-3.09	-2.75	-2.23	-1.56	-0.78	0.05	0.88	1.65	2.31	2.81	3.11	3.21
0.970	-15.98	-15.38	-13.76	-11.20	-7.85	-3.93	0.27	4.46	8.32	11.58	14.03	15.52	15.98
1.940 - RFI	-30.26	-29.38	-27.44	-23.68	-18.08	-8.44	0.55	9.50	19.03	24.45	27.98	29.67	30.26
2.352	-20.49	-19.88	-18.41	-15.77	-11.64	-5.61	0.66	6.89	12.79	16.71	19.07	20.22	20.49
2.764	-11.23	-10.81	-10.04	-8.65	-6.42	-2.77	0.78	4.27	7.76	9.75	10.82	11.22	11.23
3.176	-1.82	-1.56	-1.39	-1.17	-0.85	0.25	0.89	1.48	2.39	2.43	2.28	2.03	1.82
3.588	7.88	8.07	7.80	7.12	5.62	3.54	1.01	-1.58	-3.88	-5.69	-6.79	-7.50	-7.88
4.000 - RFO	17.91	17.81	17.62	16.24	13.92	6.59	1.13	-4.41	-11.98	-14.66	-16.49	-17.21	-17.91
4.387	13.50	13.60	13.20	12.01	9.63	5.49	1.24	-3.10	-7.50	-10.29	-11.96	-12.93	-13.50
4.773	10.24	10.42	10.07	9.08	7.23	4.46	1.36	-1.84	-4.93	-7.24	-8.71	-9.65	-10.24
5.160 - RAI	7.78	8.06	7.77	7.02	5.66	3.71	1.46	-0.84	-3.19	-5.09	-6.31	-7.12	-7.78
5.516	5.74	5.94	5.73	5.15	4.15	2.75	1.13	-0.56	-2.25	-3.65	-4.60	-5.26	-5.74
5.873	4.08	4.21	4.06	3.63	2.92	1.95	0.81	-0.38	-1.56	-2.55	-3.25	-3.74	-4.08
6.229	2.65	2.76	2.65	2.36	1.89	1.25	0.50	-0.29	-1.04	-1.68	-2.15	-2.48	-2.69
6.586	1.51	1.51	1.44	1.27	0.99	0.62	0.19	-0.26	-0.65	-0.98	-1.25	-1.44	-1.51
6.942 - RAO	0.48	0.40	0.39	0.30	0.18	0.05	-0.10	-0.30	-0.35	-0.38	-0.49	-0.56	-0.48
7.075	0.24	0.16	0.19	0.15	0.09	0.02	-0.05	-0.14	-0.17	-0.19	-0.24	-0.27	-0.24
7.209 - RSI	0.0	0.0	0.0	0.0	0.0	0.0	0.0	0.0	0.0	0.0	0.0	0.0	0.0

-- KILOGALSS --

FORCES DUE TO FIELD WINDING ALONE

RADIAL FORCE ON THE FIELD WINDING CONDUCTORS
(POUNDS/INCH)

RADIUS - INCHES	ANGLE - DEGREES 0.0	15.0	30.0	45.0	60.0	75.0	90.0
1.940	3.98	3.85	3.65	3.16	2.44	0.0	0.0
2.352	2.77	2.64	2.49	2.15	1.62	0.0	0.0
2.764	1.53	1.45	1.41	1.24	0.93	0.0	0.0
3.176	-0.31	-0.30	-0.30	-0.28	-0.23	0.0	0.0
3.588	-1.45	-1.34	-1.28	-1.12	-0.88	0.0	0.0
4.000	-2.25	-2.20	-2.15	-1.95	-1.64	0.0	0.0

TANGENTIAL FORCE ON THE FIELD WINDING CONDUCTORS
(POUNDS/INCH)

RADIUS - INCHES	ANGLE - DEGREES 0.0	15.0	30.0	45.0	60.0	75.0	90.0
1.940	0.0	-0.92	-1.85	-2.77	-3.49	0.0	0.0
2.352	0.0	-0.93	-1.94	-2.96	-4.15	0.0	0.0
2.764	0.0	-0.90	-1.86	-2.88	-4.14	0.0	0.0
3.176	0.0	-0.81	-1.68	-2.62	-3.84	0.0	0.0
3.588	0.0	-0.71	-1.44	-2.25	-3.32	0.0	0.0
4.000	0.0	-0.60	-1.23	-1.88	-2.66	0.0	0.0

MAXIMUM FORCES ON THE ARMATURE CONDUCTORS
(POUNDS/INCH)

HARMONIC	RADIUS 5.160	5.516	5.873	6.229	6.586	6.942
1	3.98	3.40	2.97	2.65	2.41	2.25
3	0.12	0.08	0.05	0.04	0.03	0.02
5	0.02	0.03	0.03	0.04	0.03	0.03
7	0.02	0.02	0.03	0.03	0.03	0.02
9	0.00	0.00	0.00	0.00	0.00	0.00
11	0.00	0.00	0.00	0.00	0.00	0.00

HARMONIC FIELD COMPONENTS
<KILOGAUSS

HARMONIC	RADIUS = 1.94 INCHES FIELD RAD.	FIELD TAN.	ARMATURE RAD.	ARMATURE TAN.	RADIUS = 4.00 INCHES FIELD RAD.	FIELD TAN.	ARMATURE RAD.	ARMATURE TAN.
1	32.412	-32.413	0.635	0.635	23.163	19.152	1.310	1.310
3	-1.976	1.970	0.0	0.0	-2.142	-2.142	0.0	0.0
5	-0.100	0.101	-0.000	-0.000	-0.138	-0.138	-0.007	-0.007
7	0.372	-0.373	0.000	0.000	0.577	0.577	0.002	0.002
9	-0.315	0.315	0.0	0.0	-0.520	-0.520	0.0	0.0
11	0.183	-0.183	-0.000	-0.000	0.314	0.314	-0.000	-0.000

HARMONIC	RADIUS = 5.16 INCHES FIELD RAD.	FIELD TAN.	ARMATURE RAD.	ARMATURE TAN.	RADIUS = 5.52 INCHES FIELD RAD.	FIELD TAN.	ARMATURE RAD.	ARMATURE TAN.
1	12.443	7.245	1.690	1.690	10.832	5.301	1.774	1.299
3	-0.367	-0.354	0.0	0.0	-0.235	-0.211	0.0	0.0
5	-0.008	-0.008	-0.065	-0.065	-0.004	-0.004	-0.094	-0.039
7	0.013	0.013	0.049	0.049	0.005	0.005	0.078	0.025
9	-0.004	-0.004	0.0	0.0	-0.001	-0.001	0.0	0.0
11	0.001	0.001	-0.006	-0.006	0.000	0.000	-0.011	-0.002

HARMONIC	RADIUS = 5.87 INCHES FIELD RAD.	FIELD TAN.	ARMATURE RAD.	ARMATURE TAN.	RADIUS = 6.23 INCHES FIELD RAD.	FIELD TAN.	ARMATURE RAD.	ARMATURE TAN.
1	9.625	3.741	1.801	0.930	8.725	2.479	1.784	0.574
3	-0.155	-0.133	0.0	0.0	-0.113	-0.080	0.0	0.0
5	-0.002	-0.002	-0.106	-0.023	-0.001	-0.001	-0.110	-0.009
7	0.002	0.002	0.089	0.014	0.001	0.001	0.092	0.005
9	-0.000	-0.000	0.0	0.0	-0.000	-0.000	0.0	0.0
11	0.000	0.000	-0.012	-0.001	0.000	0.000	-0.013	-0.001

HARMONIC	RADIUS = 6.59 INCHES FIELD RAD.	FIELD TAN.	ARMATURE RAD.	ARMATURE TAN.	RADIUS = 6.94 INCHES FIELD RAD.	FIELD TAN.	ARMATURE RAD.	ARMATURE TAN.
1	8.042	1.435	1.731	0.224	7.528	0.567	1.647	-0.124
3	-0.087	-0.045	0.0	0.0	-0.074	-0.016	0.0	0.0
5	-0.001	-0.001	-0.104	0.008	-0.000	-0.000	-0.089	0.032
7	0.000	0.000	0.086	-0.008	0.000	0.000	0.068	-0.033
9	-0.000	-0.000	0.0	0.0	-0.000	-0.000	0.0	0.0
11	0.000	0.000	-0.012	0.001	0.000	0.000	-0.008	0.006

IMPORTANT FLUX DENSITIES

TYPE	LOCATION	SOURCE	MAGNITUDE	RADIUS	ANGLE
MAXIMUM	FIELD WINDING	FIELD WINDING	38.814 KILOGAUSS	2.352	75.0
MAXIMUM	FIELD WINDING	BOTH WINDINGS	38.492 KILOGAUSS	2.352	75.0
MAXIMUM	ARMATURE WINDING	BOTH WINDINGS	12.410 KILOGAUSS	5.160	75.0
1 - HARMONIC					
LIN. AVERAGE	ARMATURE WINDING	FIELD WINDING	9.443 KILOGAUSS		
RMS AVERAGE	ARMATURE WINDING	BOTH WINDINGS	8.966 KILOGAUSS		
3 - HARMONIC					
LIN. AVERAGE	ARMATURE WINDING	FIELD WINDING	-0.163 KILOGAUSS		
RMS AVERAGE	ARMATURE WINDING	BOTH WINDINGS	0.185 KILOGAUSS		
5 - HARMONIC					
LIN. AVERAGE	ARMATURE WINDING	FIELD WINDING	-0.002 KILOGAUSS		
RMS AVERAGE	ARMATURE WINDING	BOTH WINDINGS	0.099 KILOGAUSS		
7 - HARMONIC					
LIN. AVERAGE	ARMATURE WINDING	FIELD WINDING	0.003 KILOGAUSS		
RMS AVERAGE	ARMATURE WINDING	BOTH WINDINGS	0.081 KILOGAUSS		
9 - HARMONIC					
LIN. AVERAGE	ARMATURE WINDING	FIELD WINDING	-0.001 KILOGAUSS		
RMS AVERAGE	ARMATURE WINDING	BOTH WINDINGS	0.001 KILOGAUSS		
11 - HARMONIC					
LIN. AVERAGE	ARMATURE WINDING	FIELD WINDING	0.000 KILOGAUSS		
RMS AVERAGE	ARMATURE WINDING	BOTH WINDINGS	0.011 KILOGAUSS		

VOLTAGE REGULATION - PERCENT #1C.6

CURRENT AMPERES	VOLTAGE VOLTS L-L	POWER MVA
0.0	5551.9	0.C
115.3	5467.1	1.1
230.7	5371.6	2.1
346.0	5264.4	3.2
461.4	5148.3	4.1
576.7	5022.2	5.C

LOSSES

ARMATURE WINDING I2R - 28.497 KILOWATTS
OR
125.6786 WATTS/POUND
OR
0.0057 PER UNIT

EDDY CURRENT LOSSES - RADIUS W/CUBIC-CM

RADIUS	W/CUBIC-CM
5.166	38.514
5.518	26.801
5.873	19.521
6.225	15.029
6.584	12.206
6.642	10.602
TOTAL	196.672 KILOWATTS

OR
1.7942 WATTS/POUND
OR
0.0092 PER UNIT

STATOR SHIELD LOSS - 6.466 KILOWATTS
OR
25.6399 WATTS/POUND
OR
0.0013 PER UNIT

WINDAGE LOSSES - 1.451 KILOWATTS
OR
0.0003 PER UNIT

TOTAL LOSS = 233.087 KILOWATTS
= 0.0465 PER UNIT

WEIGHTS

BORE SEAL	19.5 POUNDS	
STATOR END PLATES	2.8 POUNDS	
STATOR OUTER FRAME	59.7 POUNDS	
IRON SHIELD	252.2 POUNDS	
OUTER WRAPPING ON WINDING	15.8 POUNDS	
COPPER IN ARMATURE WINDING	162.9 POUNDS	
COPPER IN PHASE CONNECTIONS	9.3 POUNDS	
INSULATIONS IN STRAIGHT LENGTH	20.0 POUNDS	
INSULATIONS IN CROSS-OVERS	15.4 POUNDS	
INSULATIONS IN HAIR-PIN TURNS	6.5 POUNDS	
TOTAL STATOR WEIGHT		549.7 POUNDS
SUPERCONDUCTOR	75.2 POUNDS	
FIELD WINDING SUPPORT	83.2 POUNDS	
ROTOR CONTAINMENT	29.2 POUNDS	
DAMPER SHIELD	13.0 POUNDS	
TORQUE TUBE	4.8 POUNDS	
SHAFTS	30.5 POUNDS	
TOTAL ROTOR WEIGHT	235.9 POUNDS	
TOTAL MACHINE WEIGHT	809. POUNDS	

MECHANICAL PROPERTIES

DESIGN STRESS	100000. P.S.I.
ROTOR CENTRIFUGAL PRESSURE	5130.8 P.S.I.
ROTOR MAGNETIC PRESSURE	130.1 P.S.I.
ROTOR INTERNAL PRESSURE	5260.9 P.S.I.
ROTOR CONTAINMENT THICKNESS	0.2104 INCHES
TORQUE ON FIELD WINDING	0.356E C5 IN-LB
AVERAGE TORQUE PER INCH, FIELD	-0.305E C4 IN-LB/IN
HORIZONTAL FORCE, LEFT	-3584.4 LB/IN
HORIZONTAL FORCE, RIGHT	3210.0 LB/IN
VERTICAL FORCE PER POLE	1316.4 LB/IN
REACTION FORCE	3262.3 LB/IN
CONTAINMENT THICKNESS BASED ON REACTION AND CENTRIFUGAL FORCES	0.2988 INCHES

Z1	Z2	Z3	Z4	Z5	Z6	Z7	Z8	Z9	ES	
7.751	0.500	0.400	4.000	0.094	0.010	3.750	5.849	0.988	4.920	
Z10	Z11	Z12	Z13	Z14	Z15	Z16	Z17	Z18	Z19	ACL
8.251	7.250	10.684	29.167	9.043	9.143	8.251	8.651	0.048	0.007	9.700
Z20	Z21	Z22	Z23	Z24	Z25	Z26	Z27	Z28	AWLEY	
0.150	3.761	29.355	6.051	5.150	5.338	5.744	5.000	6.860	21.323	

TORQUE TUPE AND SHAFT DATA -

MAXIMUM TRANSIENT TORQUE, IN-LB	YIELD POINT PSI	HOT TEMP. DEGREES K.	COLD TEMP. DEGREES K.
0.134E 06	100000.	300.0	4.2

THERMAL DISTANCE LENGTH= 12.000 INCHES TYPE 347 SS

SOLID SHAFT-R= 1.28 IN. SS= 41038. PSI RS= 336. PSI Q= 32.72 WATTS

R,IN	H,IN	SS,PSI	SR,PSI	Q,WATTS	TCR,IN-LB	TCL,IN-LB
2.000	0.107	49945.	4695.	2.52	0.723E 06	0.252E 06
2.255	0.084	49911.	4571.	2.23	0.488E 06	0.147E 06
2.511	0.068	49963.	7399.	2.01	0.344E 06	0.908E 05
2.766	0.056	49798.	8981.	1.82	0.251E 06	0.589E 05
3.022	0.047	49712.	10717.	1.67	0.189E 06	0.398E 05
3.277	0.040	49601.	12605.	1.55	0.145E 06	0.278E 05
3.533	0.041	42217.	14646.	1.69	0.134E 06	0.134E 06
3.788	0.044	33747.	16841.	1.97	0.134E 06	0.134E 06
4.043	0.048	27413.	19189.	2.27	0.134E 06	0.134E 06
4.299	0.051	22589.	21689.	2.59	0.134E 06	0.134E 06

Spreading of the upper conductors relative to the lower conductors to form the coil pitch occurred without relative movement between strands. All bending in the conductors occurred at four bend lines - the portion of the conductors between bend lines remained straight. Figure 3 shows a coil before it was assembled into the armature winding and Figure 4 shows the manufacture drawings for the coil. The procedures for manufacture of the coils were as follows:

- Three strands were wound simultaneously in a fixture that contained eight slots for the upper side of the coil, eight slots for the lower side, and pins to form the hair pin turns.
- This step (above) was repeated until eighteen layers (three conductors) were placed in the slots.
- A .25x4.5 mm ribbon of insulation was placed between the 6th and 7th layers and between the 12th and 13th layers of strands to separate adjacent conductor.
- After the strands were clamped in the winding fixture the coil was spread to a 17/24 coil pitch.
- Subsequently, the fixture and coil were placed in an oven and heated to a sufficient temperature to melt the polysulfone overcoating on the strands and the ribbon separators.
- After the assembly was cooled to room temperature, the coil was removed from the fixture. The conductors in the coil were in a rigid, bonded state as shown in Figure (3) and could be handled easily as a unit.
- A 2000 volt conductor-to-conductor dielectric test was performed with the coil submerged in Stoddard Solvent before the 3 groups of 16 conductor were connected in series. Typical leakage currents versus voltage potential are given in Table 1.
- After the dielectric test was performed the conductors were connected in series and terminal connectors were installed.

A total of twenty coils were wound by the National Electric Coil Co. with delivery of the first coil in February, 1976 and the last coil in June, 1976. One coil failed on dielectirc test. Each coil was checked for dimensional accuracy and one coil was rejected for excessive dimensional variations beyond the point of correction. Terminal and lead connections were completed on fourteen of eighteen acceptable coils.

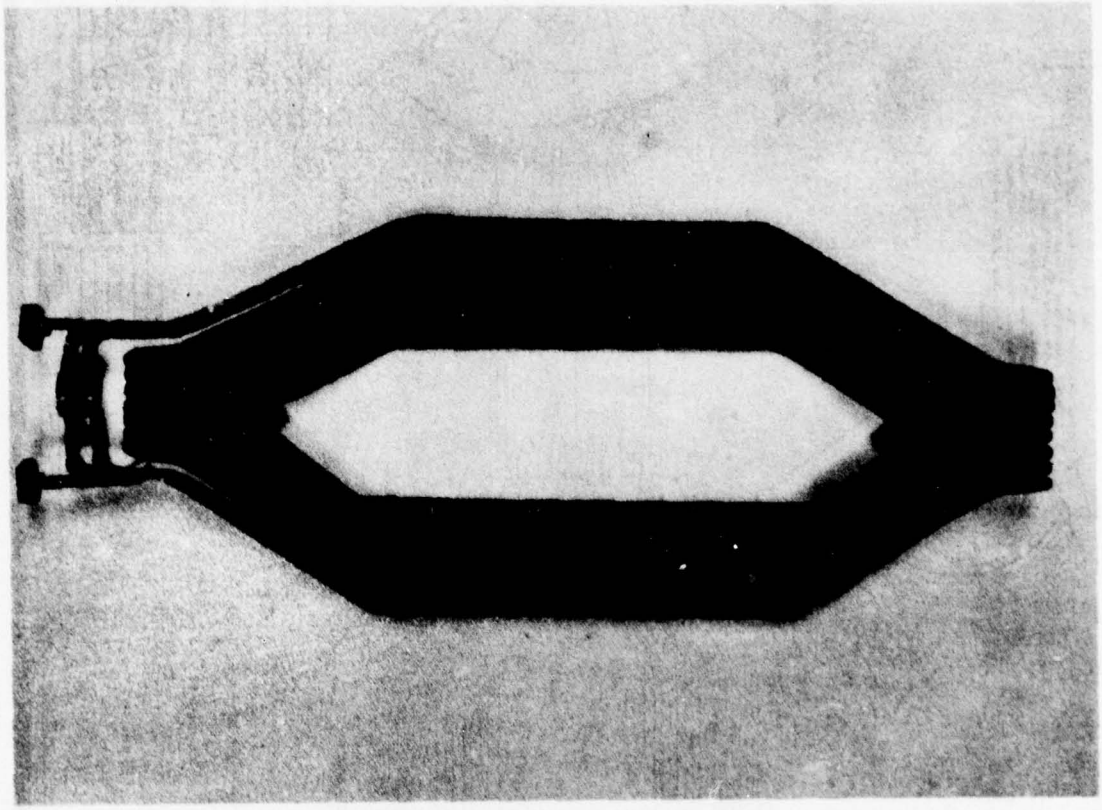


FIGURE 3. Coil for Armature Winding

THIS PAGE IS BEST QUALITY PRACTICABLE
FROM COPY FURNISHED TO DDC

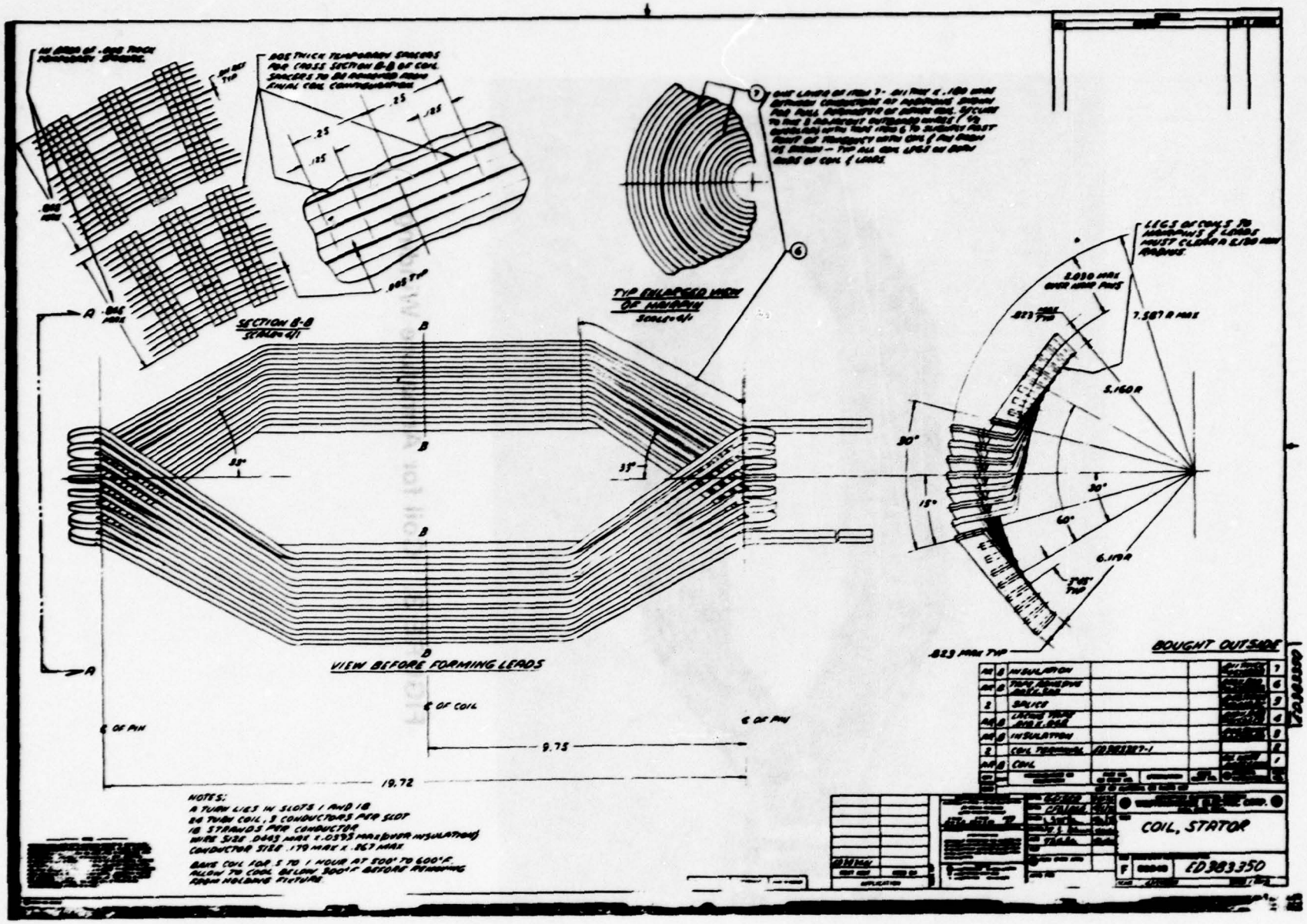


FIGURE 4a. Armature Coil Dimensions

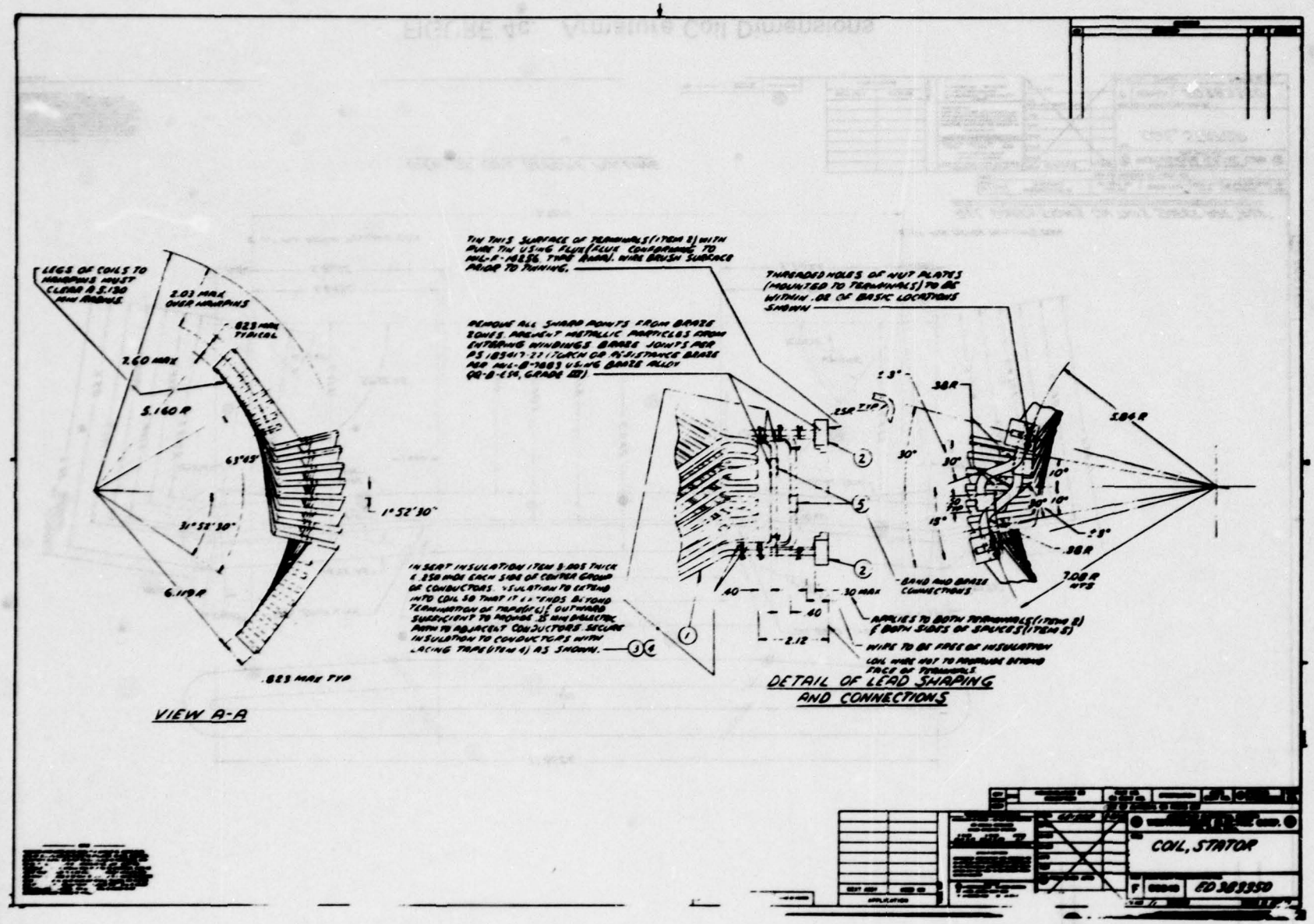
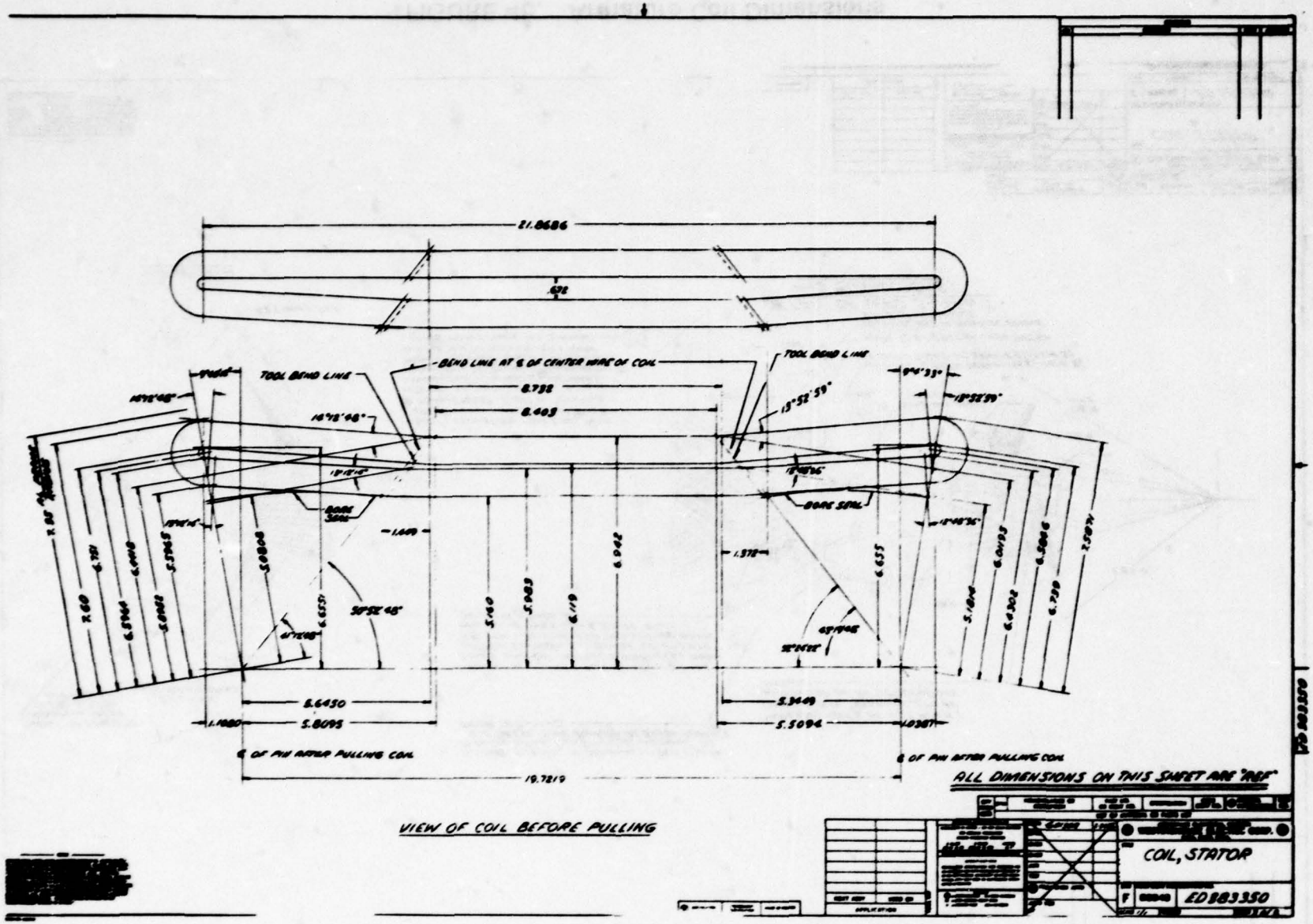


FIGURE 4b. Armature Coil Dimensions

THIS PAGE IS BEST QUALITY PRACTICABLE
FROM COPY FURNISHED TO DDC

THIS PAGE IS BEST QUALITY PRACTICABLE
FROM COPY FURNISHED TO DDC



VIEW OF COIL BEFORE PULLING

FIGURE 4c. Armature Coil Dimensions

TABLE 1

TYPICAL LEAKAGE CURRENTS

IN

PHASE GROUP

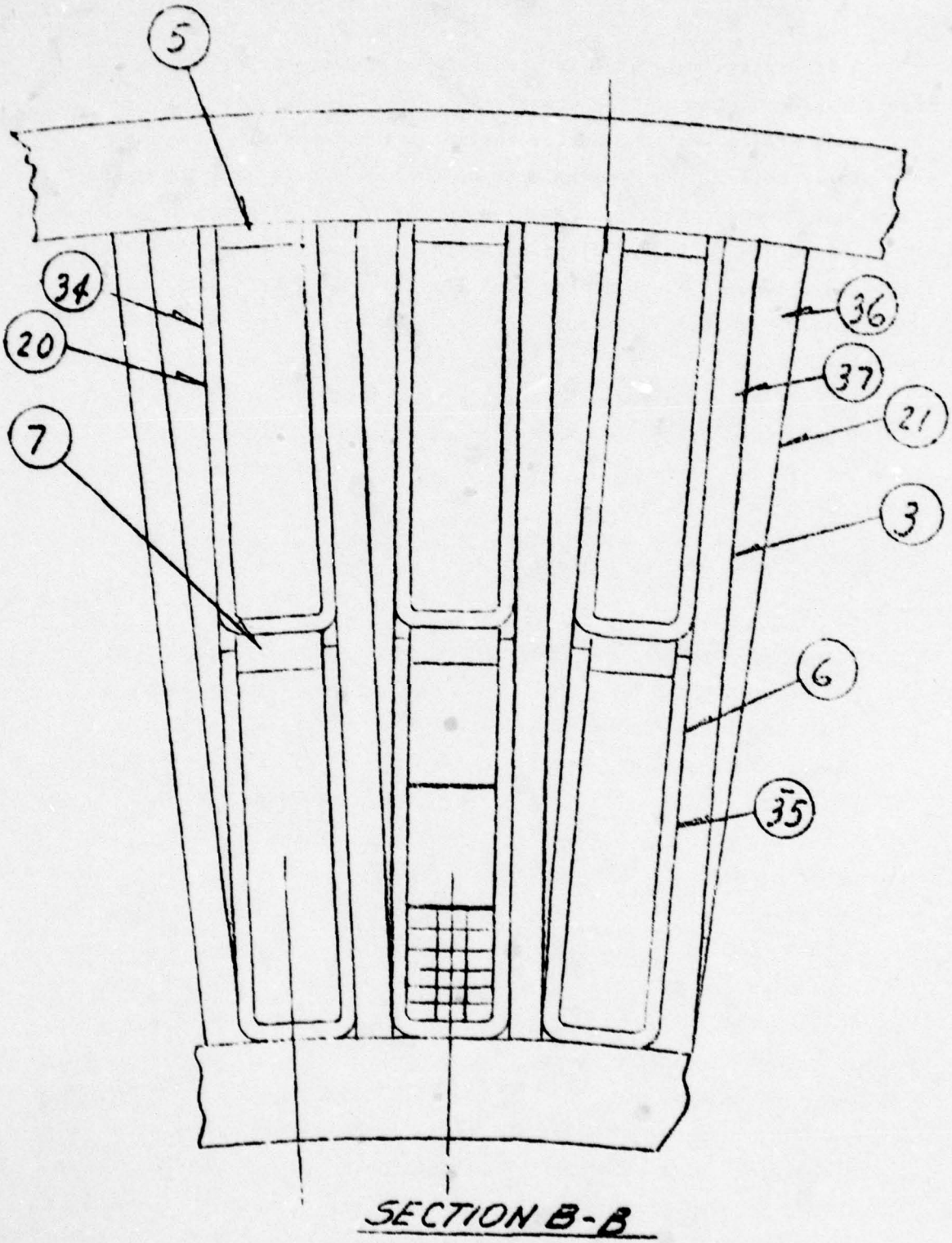
VOLTAGE	LEAKAGE CURRENT (μA)	
(Volts)	Conductor #1 to #2	Conductor # 2 to #3
250	50	80
500	75	170
750	170	260
1000	230	340
1250	290	430
1500	350	500
1740	400	570
2000	450	660

Bore Seal

A fiberglass bore seal is used between the stator compartment and the rotor compartment. The primary functions of this cylindrical structure are to seal the stator cooling oil and to supply support for the stator coils. A moment balance on the conductors as a monolithlic structure showed that 54% of machine torque is distributed to the bore of the winding and 46% is distributed to outer surface. The bore seal tube has a bore of 9.920 inches with a minimum wall thickness of .172 inches and is 28.880 inch long. At the tube ends, thick walled composite sleeves are provided to engage the end brackets. A stress analysis and strength analysis for the bore seal was performed using a finite element model of the bore seal and the other structure associated with the stator. A description of the winding configuration, material and tools used to manufacture the bore seal is given in Appendix A and the stress analysis of the bore seal in given in Appendix B.

Winding Matrix

The winding matrix was assembled on the outside surface of the bore seal and secured by an adhesive bond. The matrix includes the copper conductors and filler material arranged in close packed and bonded channels for the conductors as shown in Figure 5. The fabrication of the insulating components in the matrix is descirbed in Appendix C. This matrix extends over the active straight length of the conductors excluding a 0.5 inch gap at the mid point of the coils as shown in Figure 6. The purpose of this gap is to provide a manifold for the cooling oil which enters and passes through the interstices with in the conductors and between the walls of the channels and the conductors. The purpose of the "U" channels in addition to providing dielectric space was to keep the epoxy paste away from the conductors to insure oil flow through the channels. For this reason the "U" channels and spacers were located and bonded on the conductors before the coils were mounted on the bore seal. After the coils and sleeves were mounted on the bore seal, a thin coating of adhesive was applied to the exterior surfaces of the U-channels and the two fiberglass wedges.



(Reference Fig. 6)

Fig. 5 Armature Winding Matrix

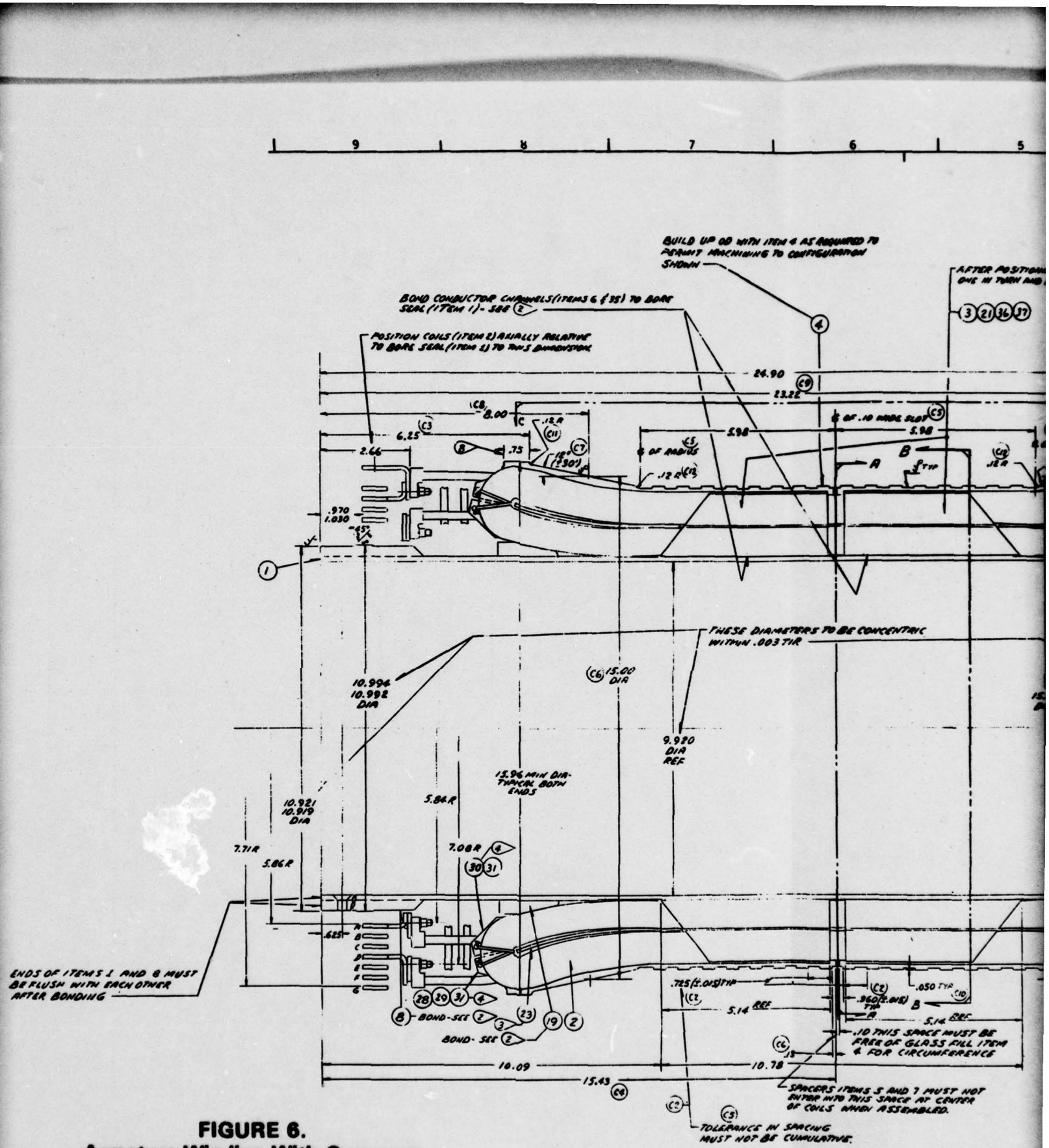
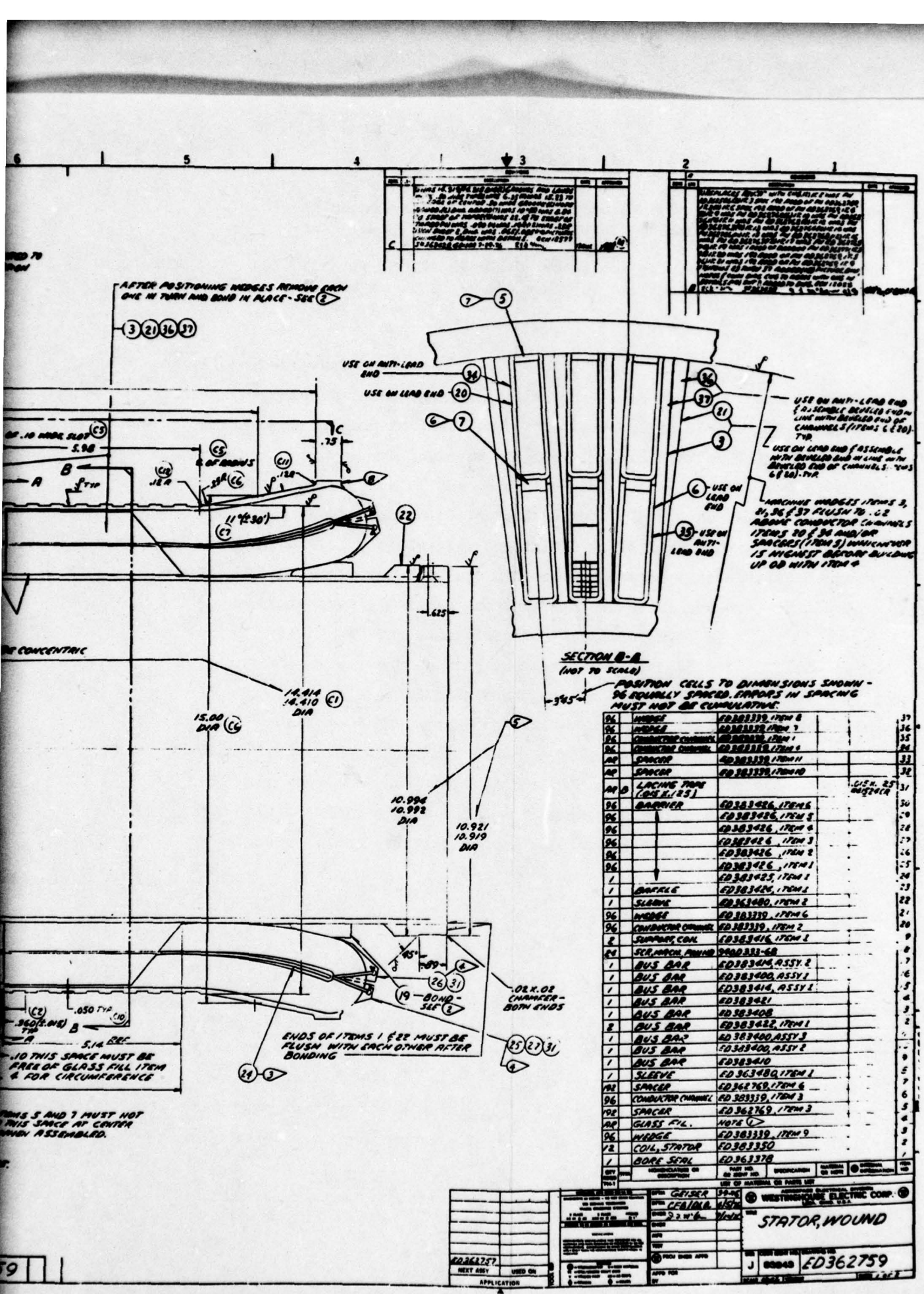


FIGURE 6.
Armature Winding With Overwrap



2

THIS PAGE IS BEST QUALITY PRACTICABLE
FROM COPY FURNISHED TO DDC

Subsequently, the entire assembly was cured in a wall-in oven. The all-composite nature of stator components necessitates heavy reliance on adhesives to provide a monolithic structure. An investigation was made to select the best adhesive candidate for each application and to provide related performance data. This evaluation is presented in Appendix D. The entire building procedure for the wound armature assembly (362759), Figure 6, required thirty-eight assembly operation which are outlined in detail in appendix E. Figure 7 through 8 are photographs of part of the assembly operations.

Overwrap of Armature Winding

The exterior portion of the coil and wedges was wound with fiberglass/epoxy overwrap to form a dielectric space and a rigid structure which was machined to mate with the iron shield. Figure 8 shows the overwrap applied to one-half of the winding and Figure 9 shows the overwrap after it was machined to mate with the iron shield. Phase-to-Phase dielectric tests were performed at 11 kV (60 Hz) for 30 seconds with the armature submerged in transformer oil.

Laminated Iron Shield

The ends of the coils, which produce the cross-overs to adjacent poles, were formed without curvature between bend lines. Therefore, the knuckles at the ends of the conductors have a much greater envelope (39.6cm diameter) than the straight portion (35.9 cm diameter). With this situation is not possible to use a one-piece punching to construct the laminated iron shield unless the shield has a bore diameter greater than the diameter of the knuckles. The original armature coil design called for sufficient curvature in the cross-overs so as to make the diameter of the knuckle envelope slightly greater than the envelope of the straight length. However, the dimensional accuracy of coils made with curvature in the cross-over was not acceptable due to the spreading of the stranded conductors. This dilemma was resolved by elimination of the curvature in the cross-overs and by accommodation of a greater envelope diameter (39.6cm) for the knuckles. In order to maintain

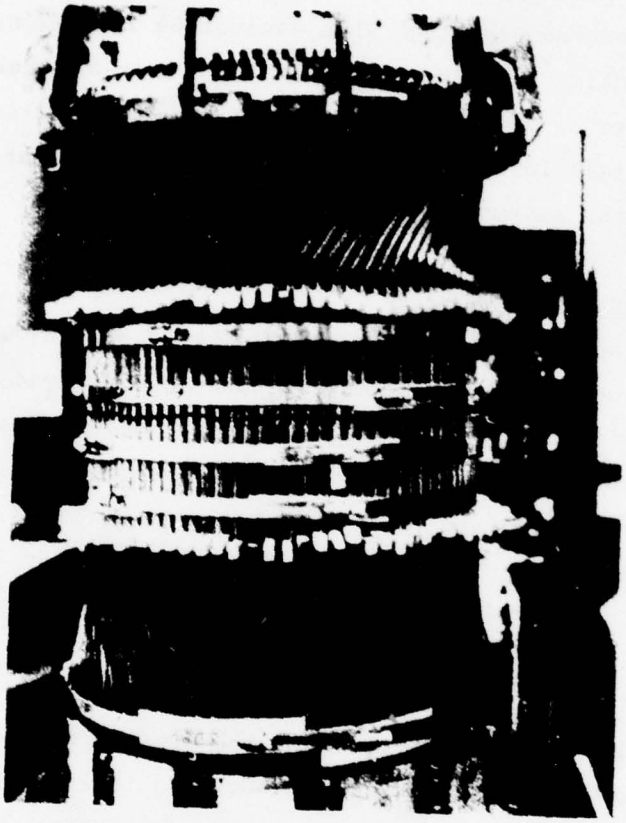


FIG. 7 Coil Assembly Fixture

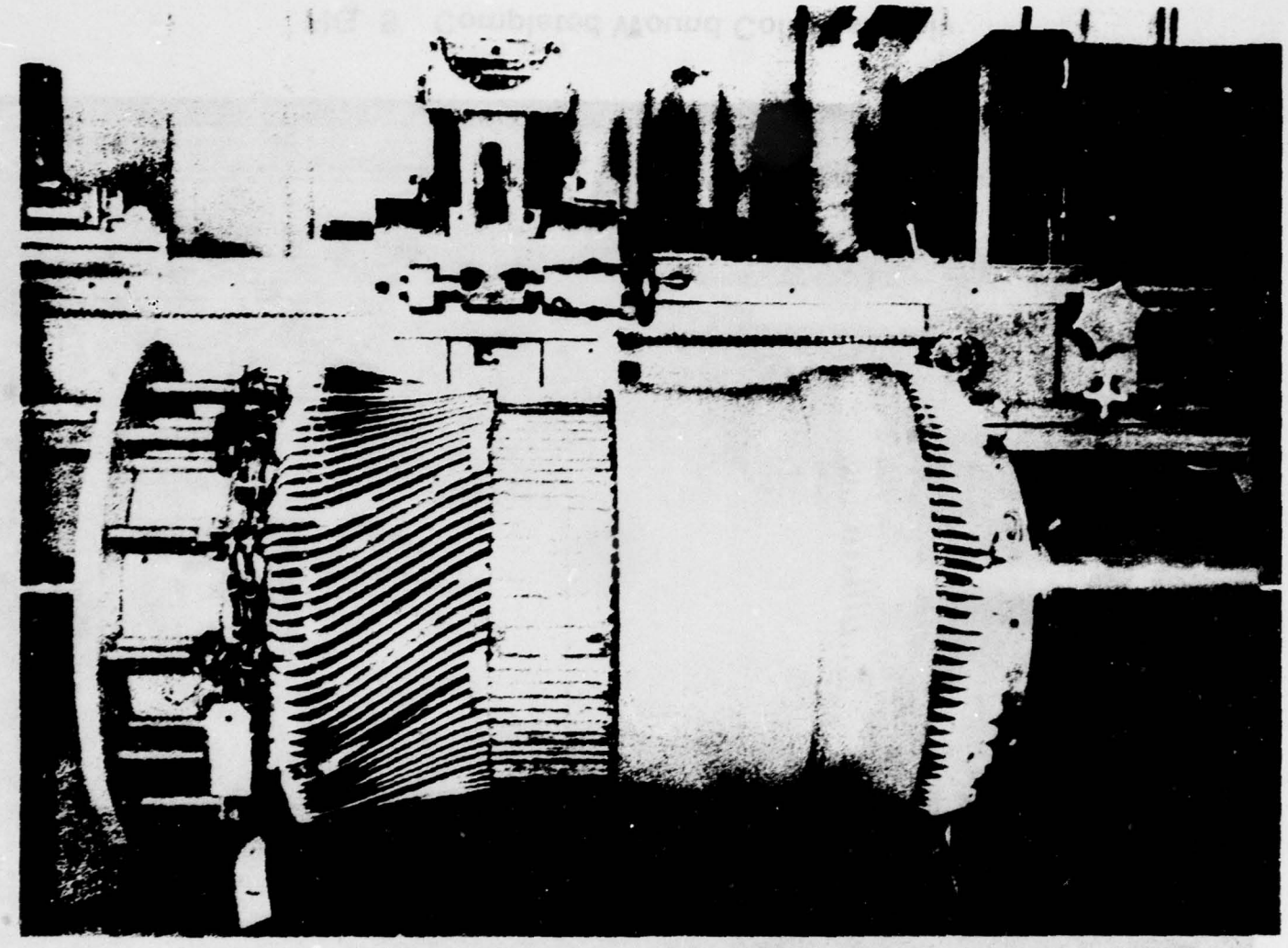


FIG. 8 Fiberglass Overwrap

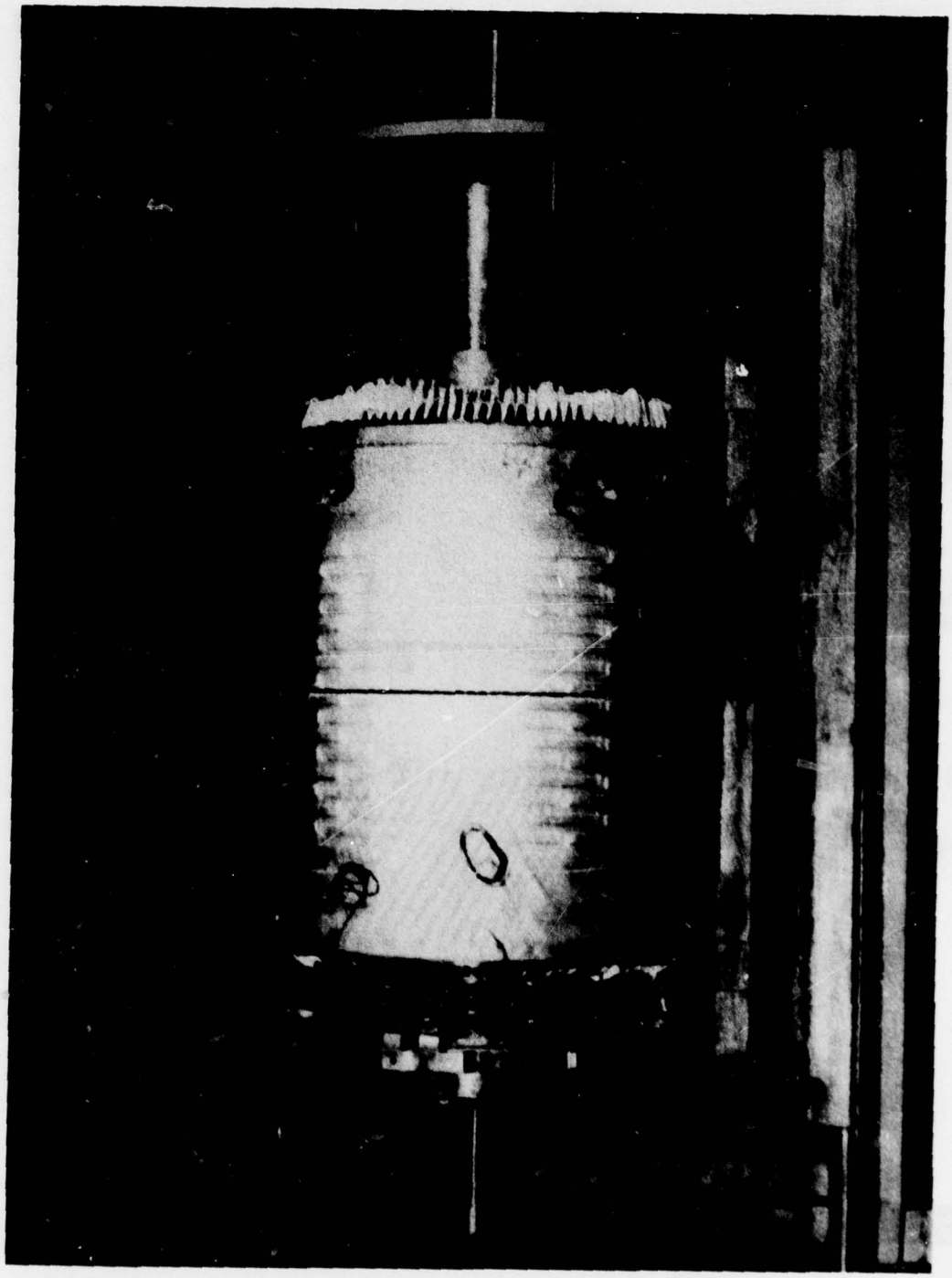


FIG. 9 Completed Wound Coil Assembly

a minimum bore (36.62cm) for the shield, it was constructed from fifteen laminated rings with separate halves. These rings were bonded to the winding assembly and were welded together on their outer surface to form a unibody sturcture as show in Figure 10. Subsequently, the shield was machined to mate with the aluminum casing.

Aluminum Casing

The casing consisted of two cylindrical frames and two end brackets. The cylindrical frames were heated to 500°F and shrunk onto the iron shield and the glass-epoxy overwrap around the end turns of the winding. Installation of the frames occurred without problems. However, upon cool-down a crack developed in one of the frames. The stress intensity caused by the interference at the point where the crack started was 23,200 psi. This frame was machined from a casting (21"ODx15"IDx17½") of alloy 350.T6. Certification of the material demonstrated a yield strength of 30,000 psi and a tensile strength of 36,600 psi with an elongation of 3.0%. One would not have expected this material to fracture under the skrink stress unless a flaw or series of flaws were present. Fracture toughness data (K_{1c}) was not specified as a condition for purchase or acceptance of the material. However, typical values for this alloy range between 15 and 25 ksi$\sqrt{in}$ and the critical crack size for these values of K_{1c} in the region of concern is between 0.1 and 0.3 inches. Post inspection of the frame around the region of fracture revealed porosity over an area of approximately 7 inches by 5 inches. In this region the oil in pores caused discoloration of the aluminum frame by virtue of the 500°F preheat for the shrink fit. The size of the flaws on the surface indicates that a flaw of the critical size was present. Thus, failure occurred during cool-down of the assembly. Repair of the frame by welding in a new section and remachining the part was considered impractical in light of other options. These options included the fabrication of a frame from a new casting or over-wrapping the stator assembly with a glass/epoxy composite to form a sound and non permeable structure. The latter option was chosen since it had less impact upon cost and schedule.

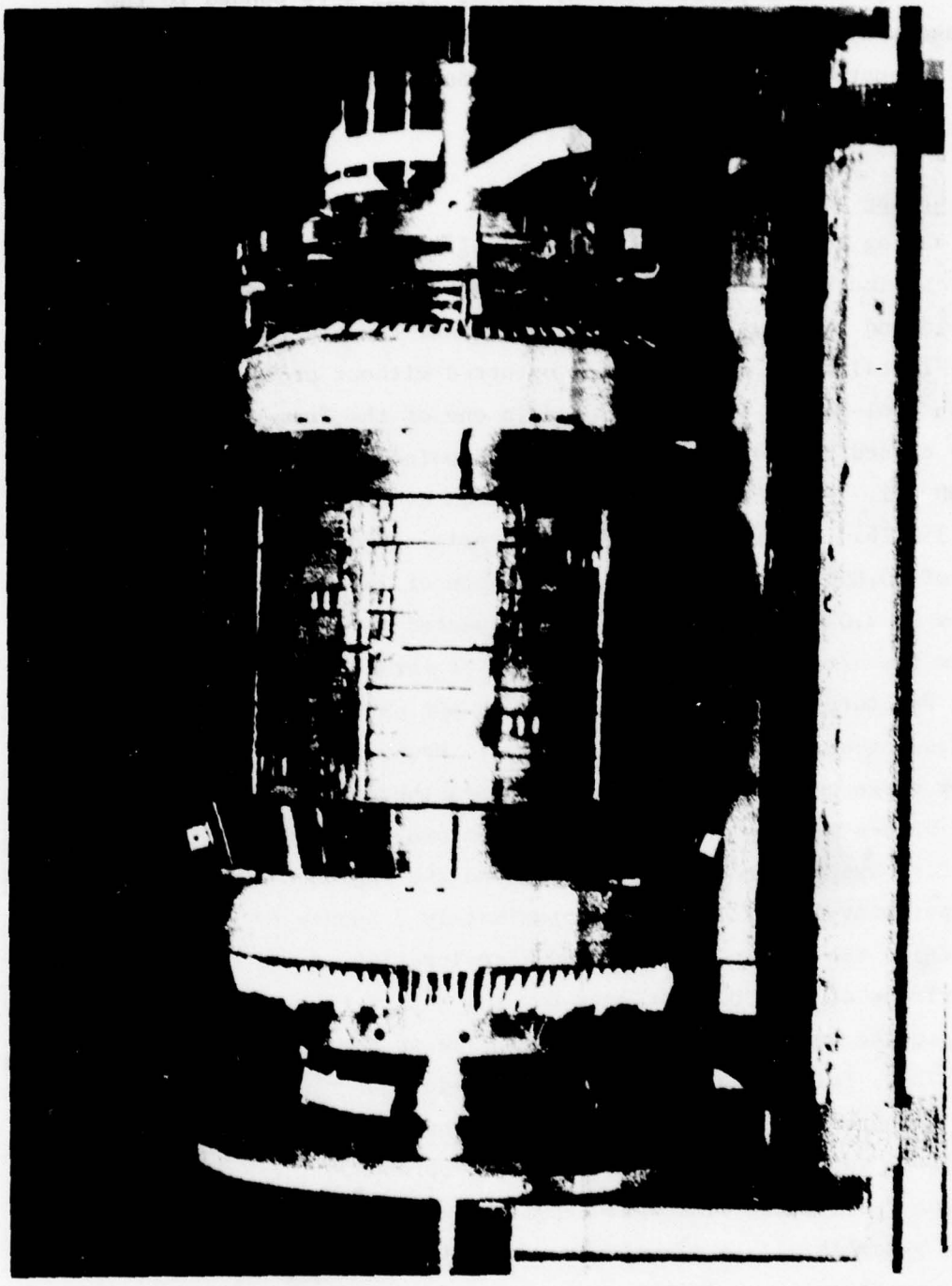


FIG. 10 Wound Coil Assembly With Shield

The torque imposed upon the bore seal is transferred to the outer frame by way of the stator end brackets. To accomplish this the end brackets were mounted on the outer frame and the brackets and the bore seal were line-drilled for attachment. As previously noted the iron shield was bonded to the outer wraping on the winding. Transfer of torque imposed upon the shield is transferred to the outer frame through twenty-four 1/4 inch roll-pins. The completed stator assembly is shown in Figure 11.

Stator Cooling

Cooling oil enters the stator from four ports which are located 180° apart on each end of the outer casing illustrated in Figure 11. Manifolds within the casing cause the oil to be distributed around the iron shield. Oil flows axially between sheild and the casing and between shield and the outer wraping on the winding. The oil flow passage in the overwrap are shown in Figure 9. At the center of the shield the oil enters a Manifold and is diverted into the winding. At this point it passes through the interstices within the conductors and between the conductors and the walls of the channels. The heat transfer mechanism from the shield and conductors is purely laminar conduction with a uniform heat flux along the flow path. For this situation Nusselt Number (hl/k) approaches a value of 4.36 by theory[14]. Thus, the heat transfer coefficient between the conductors and the oil is a strong function of the width of the oil path. For this reason baffles, shown in Figure 8, were placed within the array of conductors at the ends of the coils to decrease the width of the oil gap and increase the heat transfer coefficients. Also, solid insulation was placed between the upper layer and the inner layer of conductors to cause the cooling oil to flow between the conductors and baffles. The material for these solid barriers was polytetrafluorethylene (PTFE Teflon). The primary function of the overwrap on the ends of the coil is to support the conductors. In addition the overwrap confines the oil flow path to the space between the baffles and conductors. A short tapered cylindrical coil support between the bore seal and the ends of the coils also caused

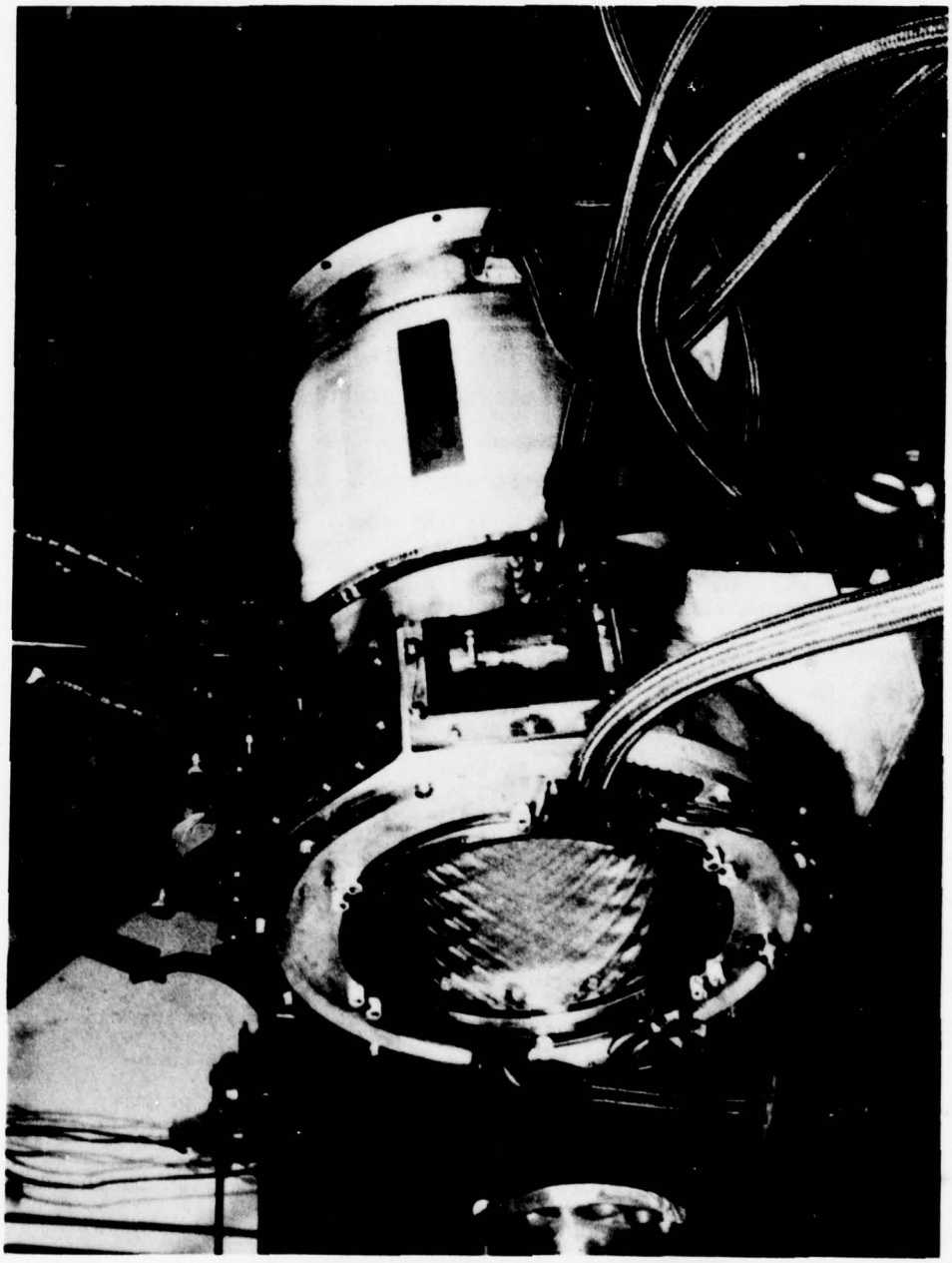


FIG. 11 Completed Stator On Test Stand

the oil to flow between the baffles and the conductors. They were bonded to the bore seal with Scotchweld 2214 NMF adhesive. After the cooling oil passes through the ends of the coils, it leaves the stator assembly through two ports on each of the end brackets.

The oil in the stator serves three functions. Firstly, circulation of the oil removes the heat generated in the stator as previously discussed. Secondly, it serves as a dielectric barrier between adjacent conductors and ground. Thirdly, it provides viscous damping for the conductors and related components.

Dielectric Capability

Solid dielectric barriers were used at several locations within the winding. The primary functions of the solid barriers were to provide support and to maintain adequate space between the conductors and between the conductors and the ground plane. These barriers do not provide adequate electrical insulation of the conductor until gaps in the barriers are filled with the insulating oil.

The results of several years study of the dielectric breakdown in transformer oil with uniform field and non uniform field situations were used to determine the voltage for the on-set of breakdown (corona).

The phase-to-phase separation for inner conductors in the ends of the coils presents the maximum voltage stress in the winding. A minimum gap of 2.13mm (.084 inches) occurres where the crossovers are tangent to the bore seal as demonstrated in Figure 12. If the field were uniform across this gap the breakdown voltage would be 24.5 kilovolts. However, the corners of the conductor cause a concentration of the field which reduces the breakdown voltage at the rounded edge to 19.3 kilovolts. A 11.0 kilovolt dielectric test was performed on the winding assembly with the neutral connections isolated. This test represented only 57% of the dielectric capability of the armature.

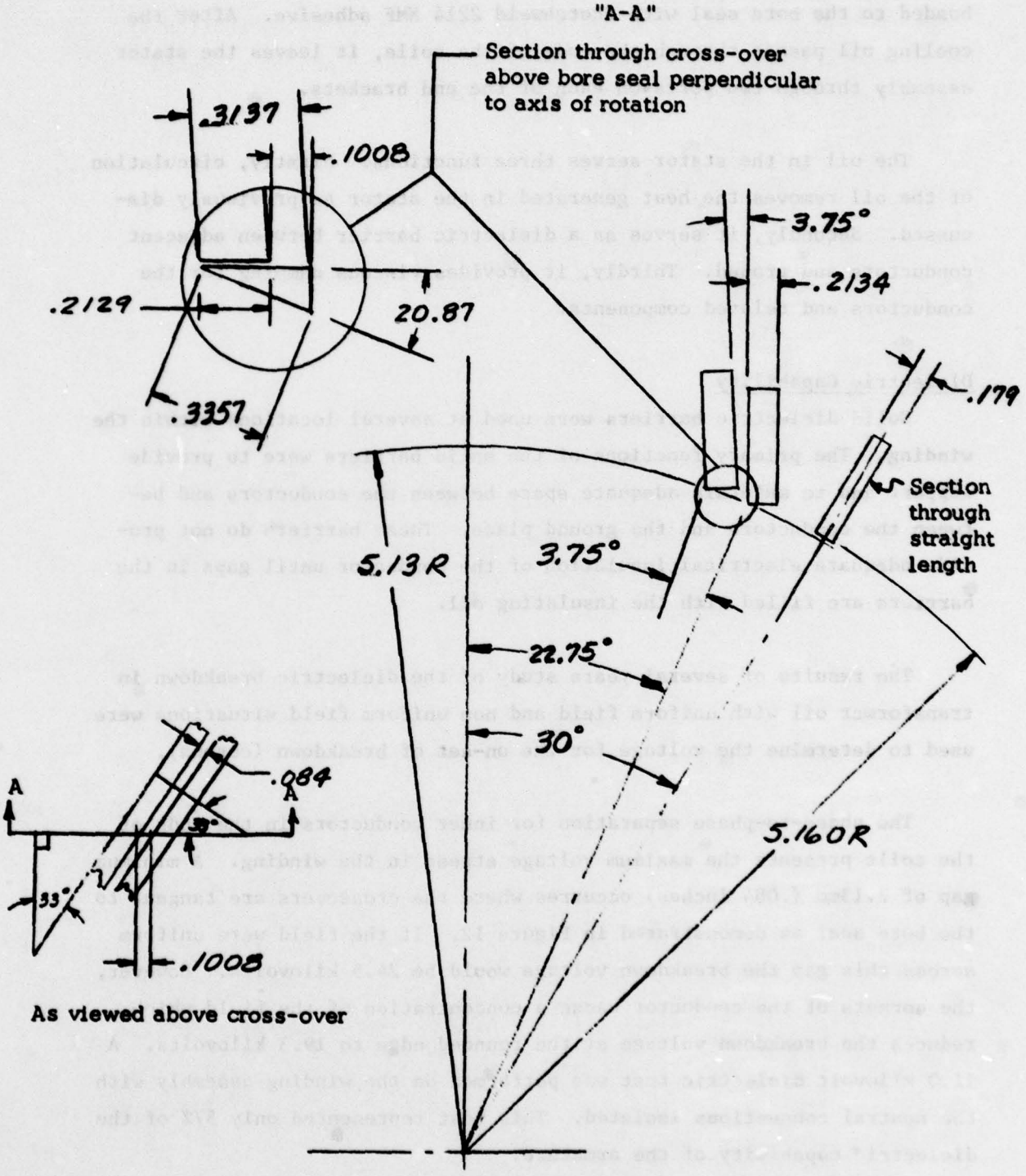


FIGURE 12. Minimum Dielectric Oil Gap in Armature

I^2R Losses

There are 34647cm (1137ft) of conductors in the winding. The winding contains two parallel circuits so each conductor carries one-half of the phase current. The conductor has a copper cross section of .230cm^2 and each 4.35 cm of length contains one cubic and of conductor. The specific power loss due to the phase currents is given by

$$\frac{P}{V} = \rho \frac{\ell}{A} \frac{I^2}{4} \qquad \text{(III-1)}$$

where

$\frac{P}{V}$ = watts per cubic cm

I = Phase current (rms) in amp

A = .230 cm^2

ℓ = 4.35 cm

$\rho = 1.72 \times 10^{-6} (390.1 + t)/467.1$ ohm - cm

t = Temperature of conductor in degrees F

P = (P/V) X 7965 cm^3, watts

For a 300°F conductor the specific power loss for several phase currents are shown below:

Stator OutPut	Voltage L-L	I_p	$\frac{P}{V}$	I^2R
10. MVA	5000 volts	1154.7 A	10.02w/cm^3	127.6 KW
7.7	3800	1170	10.29	131.0
5.0	5000	577.4	4.01	31.9
5.0	3000	962.2	11.12	88.6

Eddy Current Losses

During the design phase of this generator eddy current heating was based upon methods previously used by others for the design of 60Hz machines with an air gap winding. The equation used was:

$$\frac{P}{V} = \frac{\pi^2}{8} \frac{f^2}{\rho} D^2 B^2 \qquad \text{III-2}$$

where B was the maximum vector sum with respect to time of the two component field. An examination of this equation showed that it is only valid for a field which pulsates sinusoidally with respect to time in one direction - the field can not rotate about the conductor. This is not the real situation for the armature conductors in an air gap winding. Near the iron shield the magnetic field approaches a pulsating, one directional field. However, at the inner radius of the winding the field has a strong tangenial component which leads to a field that rotates around the conductors. This situation produces twice the loss in a cylindrical conductor as a one directional, pulsating field of the same amplitude[15].

The field which penetrates the strands in the armature conductors is defined on page 22 and 23. This field is represented by

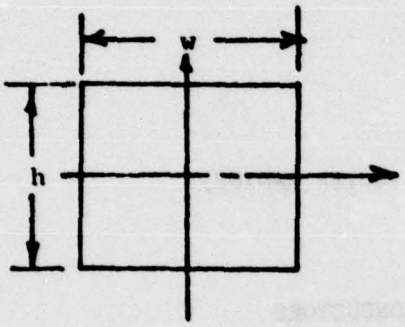
$$B_\Theta = \hat{B}_\Theta \text{ Cos } \omega t \qquad \text{III-3}$$

$$B_R = \hat{B}_R \sin (\omega t + \alpha) \qquad \text{III-4}$$

where $\hat{B}_\Theta$ and $\hat{B}_R$ are the amplitude of the tangential and radial component, respectively, at each radius and α is the phase angle between these time varying components.

The eddy current loss per unit volume of conductor is formulated in Appendix (F) using a rectangular model for the strands and the magnetic field as described above. The results of this formulation are given here.

$$B_R = \hat{B}_R \sin(\omega t + \phi)$$



$$B_\theta = \hat{B}_\theta \cos \omega t$$

$$\frac{P}{V} = \frac{1}{6} \frac{\pi^2 f^2}{\rho} (h^2 \hat{B}_\theta + w^2 \hat{B}_R) \times 10^{-7} \quad (\text{watts/cm}^3) \qquad \text{III-5}$$

f - Hz

ρ - abohm - cm (1 abohm-cm = 10^9 ohm - cm)

h - cm

w - cm

$\hat{B}_\theta$ - gausses

$\hat{B}_R$ - gausses

The eddy current loss distribution in the winding for the 12,000 rpm, 5,000 V, 5 MVA design point is presented in Table 2.

Temperature of conductor = 300°F
f = 400 Hz
h = .0947 cm
w = .1346 cm
ρ = 2541 abohm-cm

Armature radius (inches)	$\hat{B}_\theta$	$\hat{B}_R$	P/V	
5.160	8040	12000	33.03	(INNER RADIUS)
5.516	5920	10260	23.01	
5.873	4200	8900	16.40	
6.229	2750	8080	12.95	
6.586	1510	7410	10.52	
6.942	490	6930	9.03	(OUTER RADIUS)
		Average	17.51	

TABLE 2 EDDY CURRENT LOSSES IN CONDUCTORS

The eddy current loss has a maximum value of 33.03 watts/cm^3 at the inner radius since the field attenuates through the winding.

If the eddy current loss is calculated as a non rotating, pulsating field on an equivalent round wire, the maximun eddy current power density is 19.54 watts/cm^3. Similarly, the average eddy current power density throughout the winding becomes 12.86 watts/cm^3. Thus, the ratio of the losses based upon the new and the original method of calculation for the 5.0 MVA, 5,000 V and 12,000 rpm design point are

$$\frac{33.03}{19.54} = 1.69$$

At the inner conductor and

$$\frac{17.86}{12.86} = 1.39$$

for the overall heating of all of the conductors.

As noted above the eddy current heating at the inner radius of the winding is 69% higher than originally anticipated. Unfortunately it was not possible to correct this discrepancy when it was discovered without refabrication of the armature coils. Reduction of the eddy current heating could have been accomplished by decreasing the size of the strands in the conductors. With the present size strands these losses have a dominant impact upon the capability of the stator. This impact is discussed in Section IV.

Iron Losses

The losses in the laminated shield (.015 inches) silicon steel were based upon the specific loss (15.45 watts/pound) observed for this steel at a frequency of 400 Hz under a magnetic induction (B) of 10 kilogausses. The losses for other frequencies and inductions were calculated as:

$$\text{watts/Lb} = 15.45\ (\text{freq}/400)^{1.6}\ \ (B/10)^{1.8} \qquad \text{III-6}$$

The weight of the shield is 248 pounds and iron losses for three operating conditions are given below:

RPM	MVA	VOLTAGE	B KILOGAUSSES	IRON LOSS KILOWATTS
12,000	5.0	5,000	13.25	6.36
8,000	5.0	3,000	13.25	3.32

Superconducting Wire

A rectangular superconducting wire (.094cmX.140cm) with rounded corners (radii ∿ .025cm) of Nb-Ti alloy, 2/1 - cu/sc ratio, 438 filaments, ∿ 36/μm filament diameter was used for the windings.

The short sample test results for this conductor demonstrated 830A at 4 Tesla at 4.2K. A comparisons of short sample results and the field winding load line is given in Section IV, Figure 26.

The insulation on the wire is comprised of an undercoating of Polyimide ML enamel with an overcoating of a polysulfone thermosetting resin. The procedure for application of this insulation system was developed during the design phase of the program as discussed in Section II, Page 17 . The first application of these enamels was unstatisfactory due to an insufficient build-up of insulation on the wire. Dielectric tests showed the insulation was inferior to previous samples. Thus, it was necessary to strip back to a bare condition and re-insulate to produce an adequate build-up and acceptable dielectric properties.

Superconducting Coils

The coils were wound in the fixture, shown in Figures 13 and 14, which controlled their physical dimensions. The number of turns in the layers was varied to obtain the step arrangement indicated in Figure 15. However, the coils for the north and south poles had different dimensions (shape) along their union line. The shape of the union line was selected to produce the maximum number of conductors within the field winding boundaries with approximately the same number of turns in each coil. The north pole coils have 1229 turns and the south pole coils have 1239 turns (or vice versa).

Spacers (.76mm X .19mm) were inserted between adjacent layers in each step to provide a (.76mm X 6mm) radial passage for helium as shown in Figure 15. Also, spacers were inserted in the end region between each layer of wire. These spacer provide access for longitudinal flow of helium through interstices that were created by the turn-to-turn position of the wire.

After completion of the winding operation, the coil and fixture were placed in an oven to obtain turn-to-turn bonding of the resin system. Failure of the pole piece and spacers occurred during the bonding reaction for the first coil. Later investigations showed the oven was at a higher temperature then desired (270°C instead of 225°C).

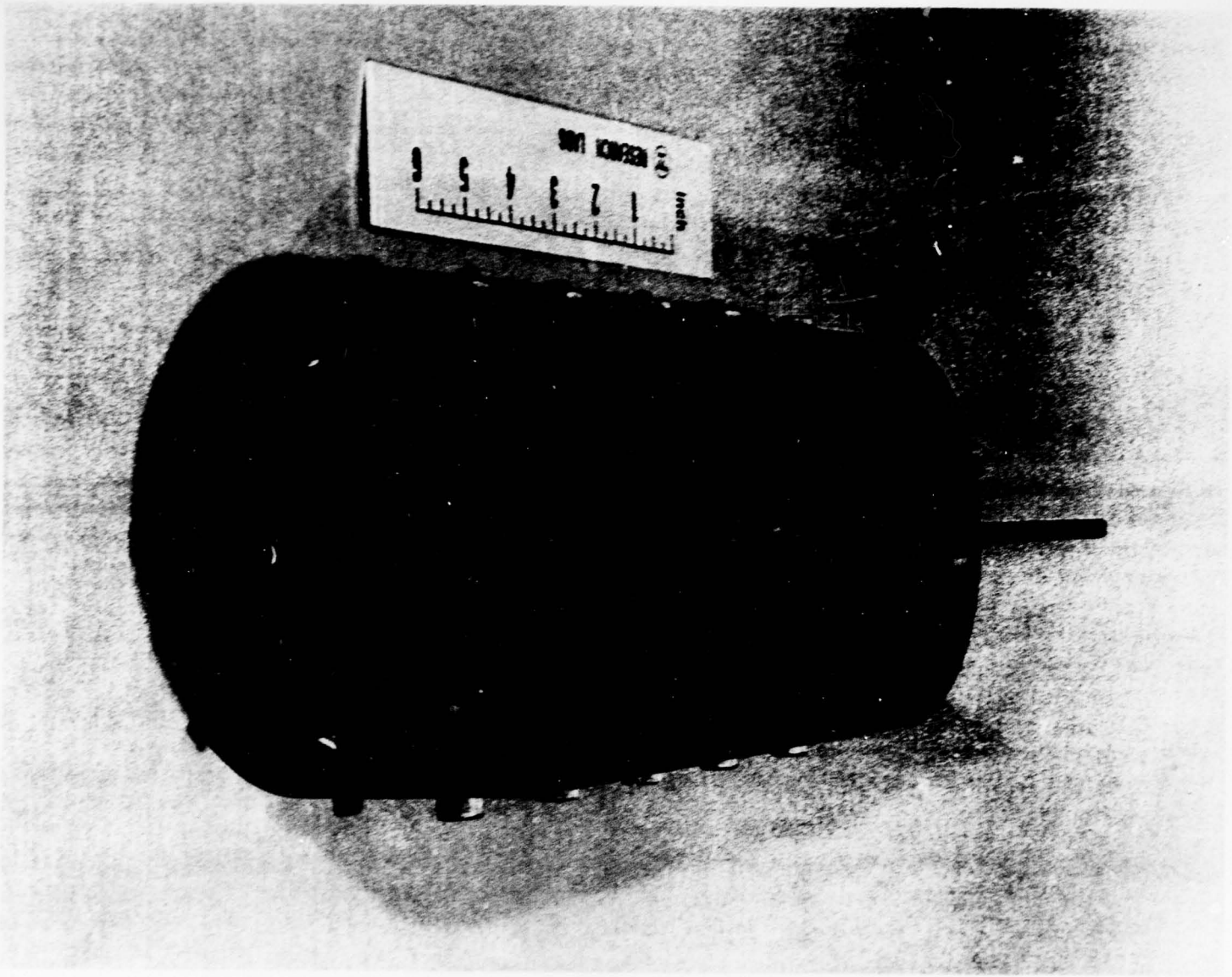


FIG. 13 Superconducting Coil Winding Fixture

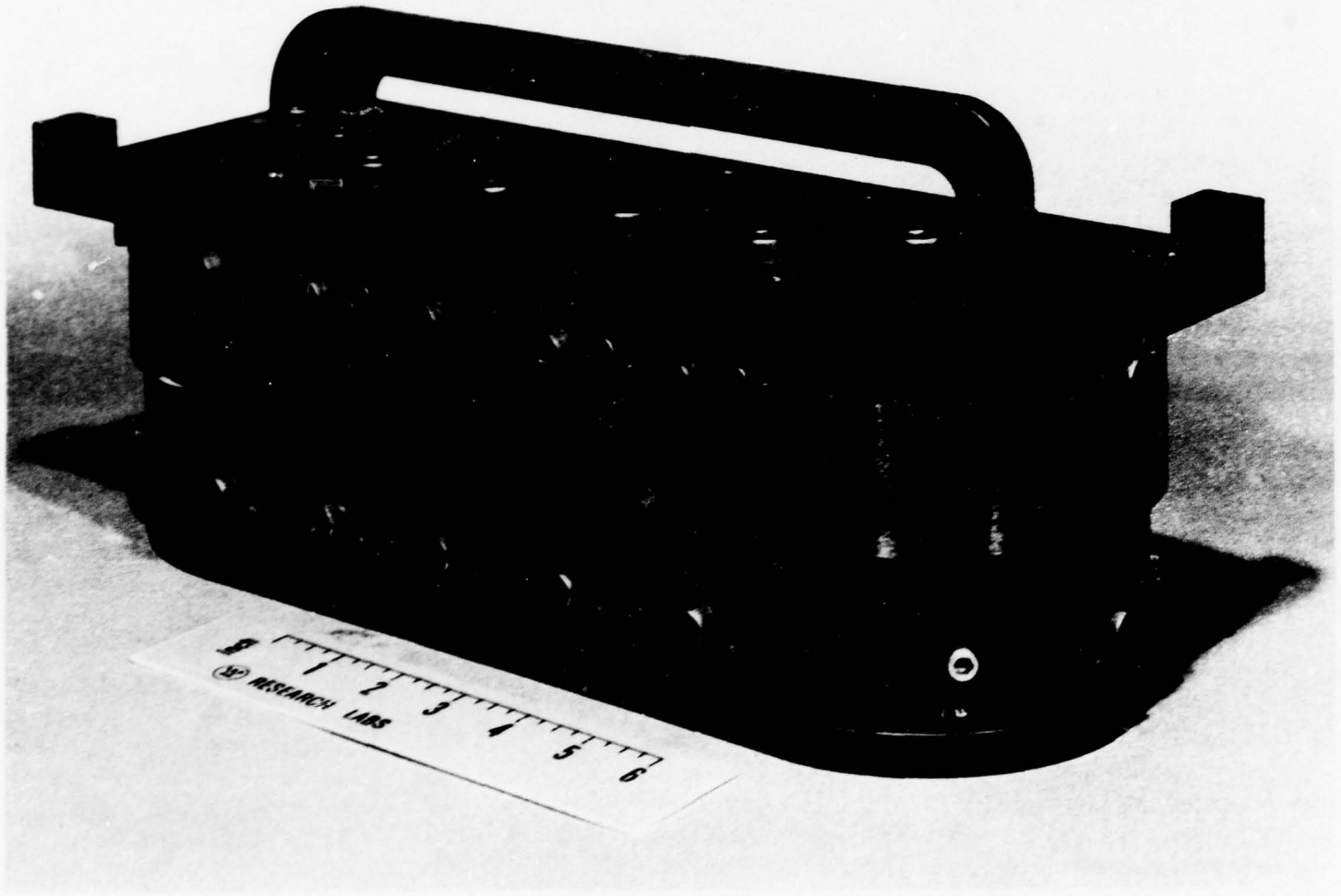


FIG. 14 Superconducting Coil Winding Fixture

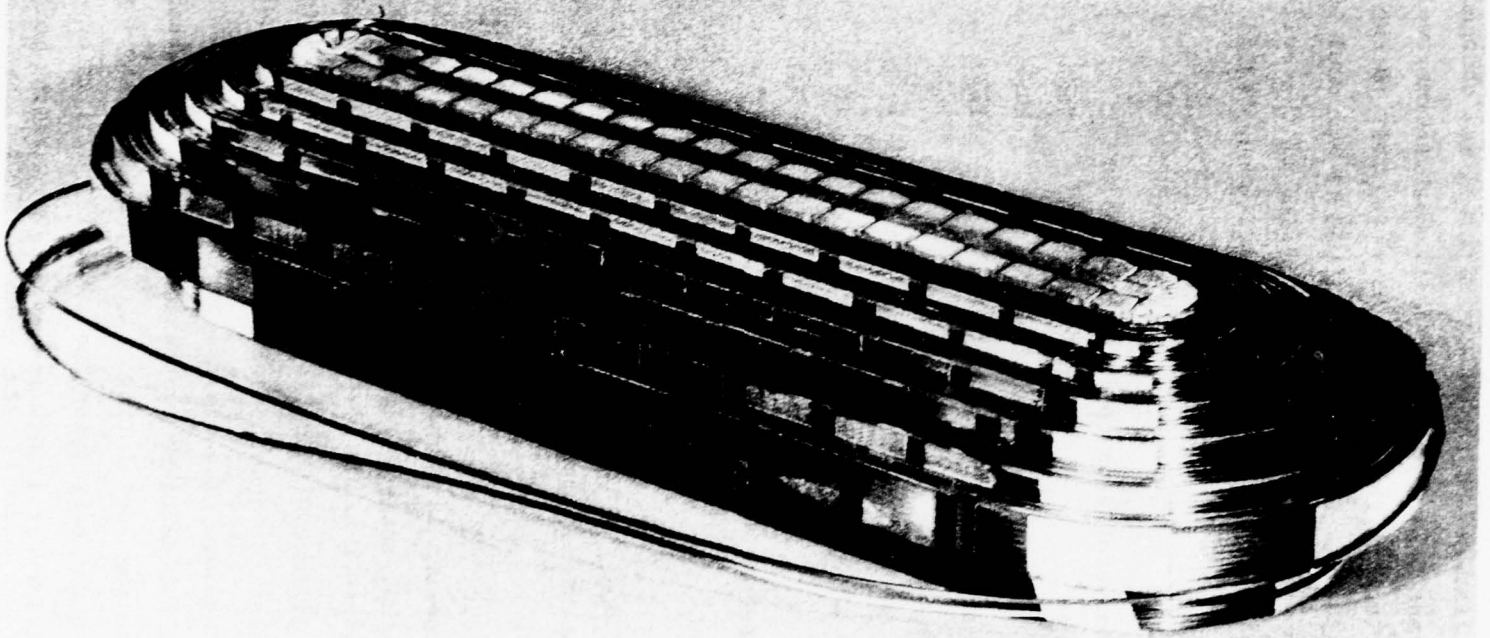


FIG. 15 Superconducting Coil

Subsequently, the winding fixture was modified by insulation of the insulating pole piece from the steel winding fixture. Thermocouples were installed within the fixture and the spacer material was changed from Nema Grade G-10 to Grade G-11. After the inner most thermocouple temperature reached 220°C, the fixture and coil were (1) left in the oven for 15 minutes, (2) then removed, and (3) allowed to air cool to room temperature. The end result was successful bonding of the coils. They were easily removed from the fixture and mounted in the field winding support structure.

The weight and resistance of each coil is given below:

	TOTAL WEIGHT*	COIL RESISTANCE	TURN
Coil 1	23 Lbs.	16.3 Ohms	1239
Coil 2	23 Lbs - 2 oz	16.2 Ohms	1239
Coil 3	22 Lbs - 15 oz	16.0 Ohms	1229
Coil 4	23 Lbs	16.1 Ohms	1229

*Pole piece weighs 1 Lb - 2 oz
Dead turns weigh 6 oz
Spacers weigh 1 Lb - 6 oz

Heat Exchanger

A heat exchanger is used in the central region of the winding compartment to produce isothermal compression of the helium as it moves off-axis along the axis of the pole. An impeller was incorporated on the central axis of the exchanger to separate the two-phase mixture from the inlet stream. This impeller is required since the flow velocity of the inlet stream is such that the holding time for the dense helium in the central inlet tube is short compared to the time needed to accelerate and separate a two-phase mixture without an impeller. Also, this impeller provides additional surfaces for absorbing the heat produced by isothermal compression of the dense helium. The central portion of the exchanger is contrived so the dense helium makes two passes through the exchanger before it is diverted into the radial fins. The off-axis movement of liquid in the fins under goes compression due to centrifugal effects which for adiabatic conditions at 12,000 rpm would increase the helium

Pressure to ∿ 12 atm with a temperature rise of ∿1K. For an isothermal compression the heat released by the dense helium is ∿2J/g at 12,000 rpm. The cross sectional area (51 cm^2) of copper in the fins is adequate to conduct 2W of heat back to the central exchanger with a temperature rise of ∿.1K. Hence, near isothermal compression is produced in the fins for up to 30 Liter/hour with only a .1K temperature rise. Boil-off in the central exchanger and vapor from the inlet stream is diverted out to cooling coils on the torque tube. In order to maintain isothermal conditions, the heat exchanger is isolated from the superconducting field winding by thermal insulation consisting of a G-11 composite spacer. A view of the heat exchanger system is shown in Figure 2.

Central Coil Support Structure

The inner coil support consists of a square frame (7.584cm X 7.584cm) of alloy 600 (AMS5665) with a bore diameter of 6.30 cm. The frame was fabricated in halves and subsequently welded together with the central heat exchanger in the bore. Nema Grade G-11 insulating parts were added to isolate the heat exchanger fins and coils from the frame. The final dimensions of the square frame, including the thickness of the insulation, was 8.219cm X 8.219cm.

Four Coil Assembly

All four coils were mounted on the central support and encased in structures that contained the counter form of the coils. This encasement structure was bolted together to accommodate a static cold test before the final closure welds were made. The assembly shown in Figure 16 and 17 was precooled with liquid N_2 followed by liquid helium cooling to 4.2K. Liquid level monitors were positioned at the top of the assembly to insure liquid coverage during the course of the test. Carbon thermometers mounted within the heat exchanger were checked during this static test to verify their low-temperature performance against their initial calibration. The four coil assembly was excited at various sweep rates until normalization occurred. The observed static test results are discussed in Section IV.

Following the cold test, closure welds were made on the casing as shown in Figure 18. Subsequently, the exterior surface was machined for a .508mm (.020 inch) shrink fit with the containment cylinder.

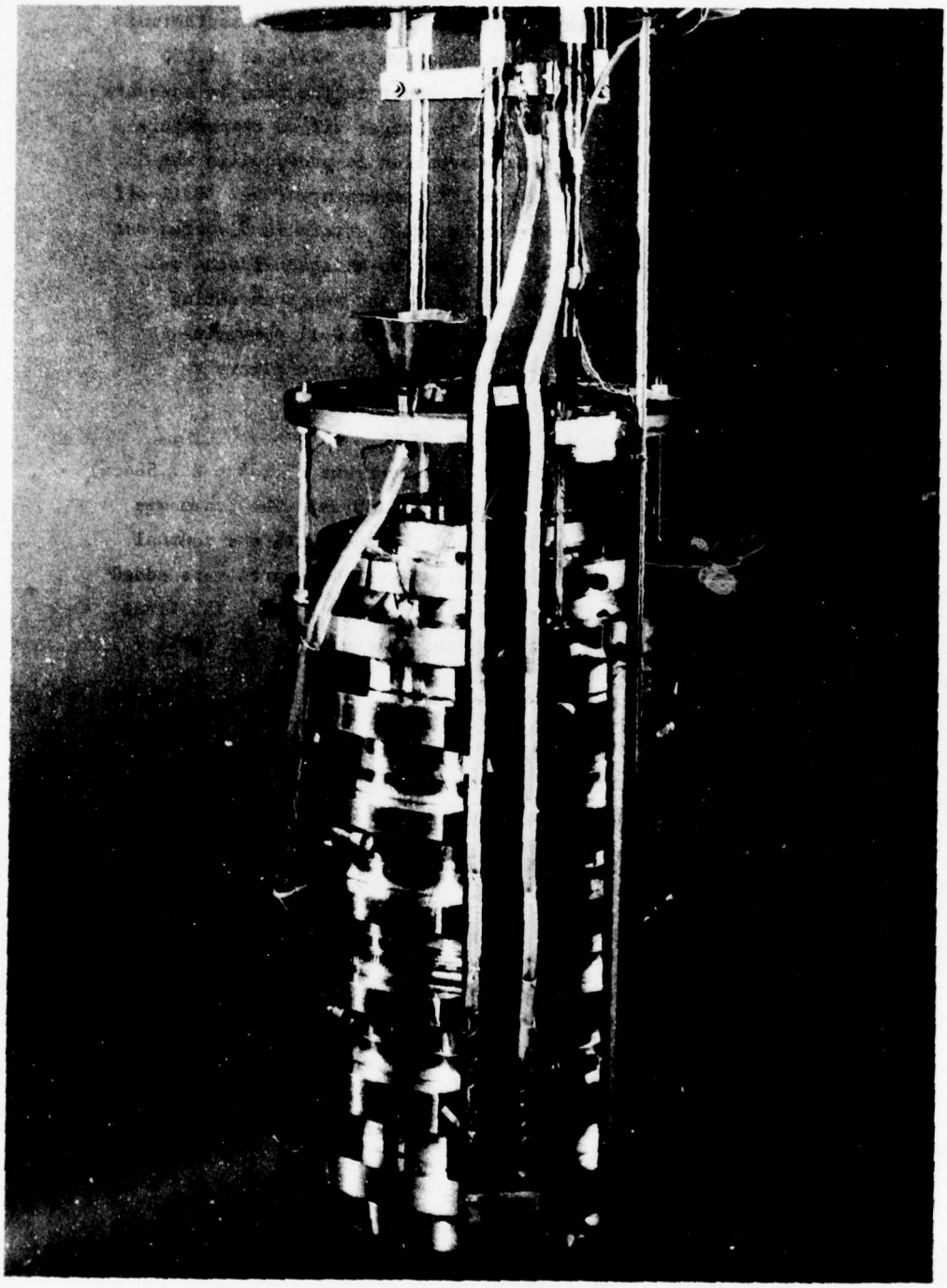


FIG. 16 Four Coil Assembly Before Cold Test

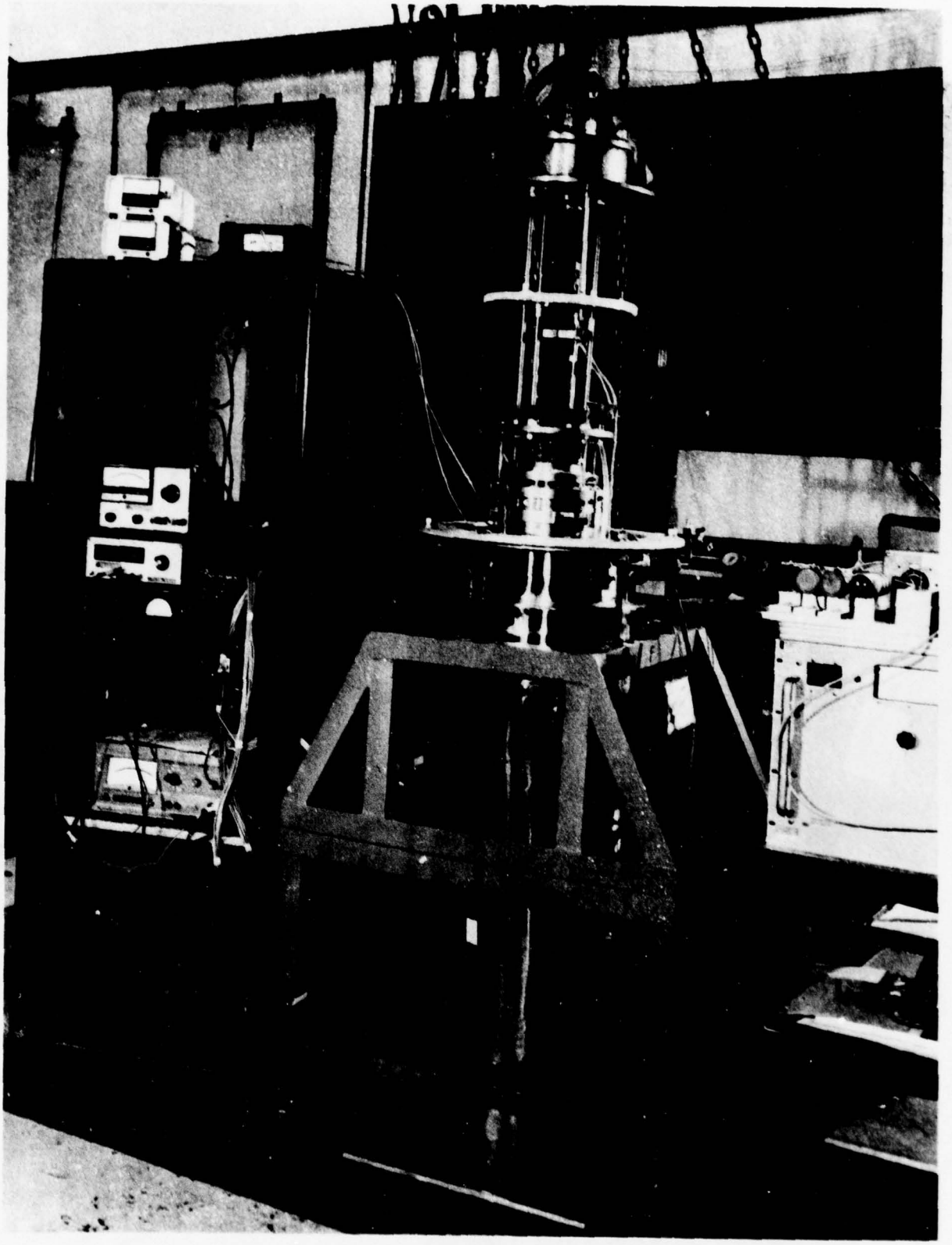


FIG. 17 Cold Test of Four Coil Assembly

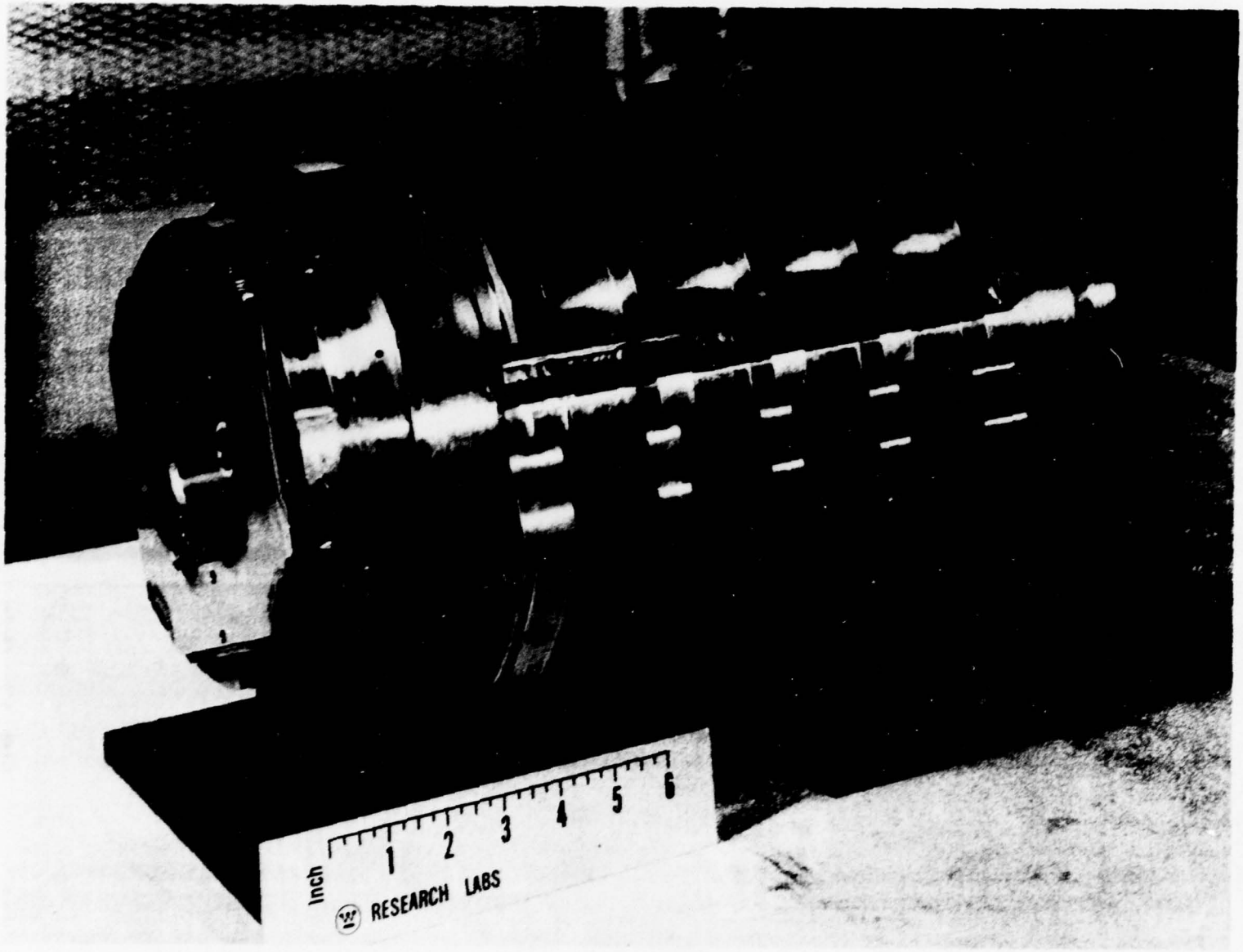


FIG.18 Four Coil Assembly After Closure Welds

Containment Cylinder

The containment cylinder had a length of 31.938cm (12.574 inches) and a bore of 21.112 (8.321 inches). The shrink fit caused the diameter of the winding assembly to decrease .406mm (.016 inches) and the outside diameter of the cylinder to increase .101mm (.004 inches). Subsequently, the outer diameter was finished to a 22.860cm (9.000 inches) diameter. Alloy 718 was used for this part and was given a solution treatment plus a double aging, precipitation hardening treatment.

The centrifugal hoop stress in the cylinder for a plane strain situation (a long cylinder) is 23,982 psi at 12,000 rpm. A centrifugal pressure of 5131 psi and a magnetic pressure of 82 psi is applied on the bore of the cylinder by the field winding. These loads plus the centrifugal stress in the cylinder generate a total hoop stress of 76,500 psi at 12,000 rpm at the bore which results in an elastic growth of .533mm (.021 inches). A net growth of .017 inches is produced by rotation and the magnetic forces or .021 inches minus the expansion (.004 inches) produced by the shrink fit. The philosophy associated with the design of the containment cylinder was that the elastic growth under rotation (.017 inches) would be approximately equal to the reduction of the field winding diameter (.016 inches) due to the shrink fit. With this situation the compression of the field winding under rotation will be approximately equal to the compression during the static test on winding.

The field winding assembly with the containment cylinder was balanced by making a correction of 5.16 oz-inches at the anti drive-end and a correction of 1.462 oz-inches at the drive-end. Subsequently, the anti drive-end stub shaft assembly was welded to this assembly.

Anti Drive-End Shaft Assembly

The anti drive-end shaft assembly contained the following sub assemblies:

(1) A vapor cooled thermal transition tube between the warm end and the cold end,

(2) shaft journals for the anti drive-end bearing system with a flexible end-member (disc) that accommodates axial contraction of the cold structures,

(3) a support station for the field winding electro-thermal shield,

(4) a radiation shield (disc) between the warm end and the cold end,

(5) conduits and current leads for the field winding,

(6) the central helium supply line, and

(7) the bulk-head between the helium compartment and the vacuum compartment.

The thermal transition tube is 15.75cm (6.20 inches) long and has a diameter of 22.3cm (8.775 inches) with a minimum wall thickness of 1.4mm (.055 inches). Spiral grooves were provided for two coils of .083 inch diameter X .010 wall tubing and two coils of .188 inch diameter X .030 wall tubing. These coils were furnace brazed to the transition piece as shown in Figure 19(a). Orignally , the scheme used all of the coils to cool the transition piece. However, helium leak tests before the bulk-head was welded to the assembly showed the large cooling coils were not usable. The cooling scheme for the transition piece was reviewed in light of the facts that (1) the large tubes would have to be replaced if the original scheme was used, or (2) if these tube were not use, adequate coolant flow would have to be provided by the remaining coils. It was concluded that adequate cooling would be provided by the remaining (equally spaced) coils if they were connected to the dense helium ports in the bulk-head. However, the defective coils would have to be replaced with tubing that would provide adequate venting of the field winding compartment for cool-down and during normalization of the field winding.

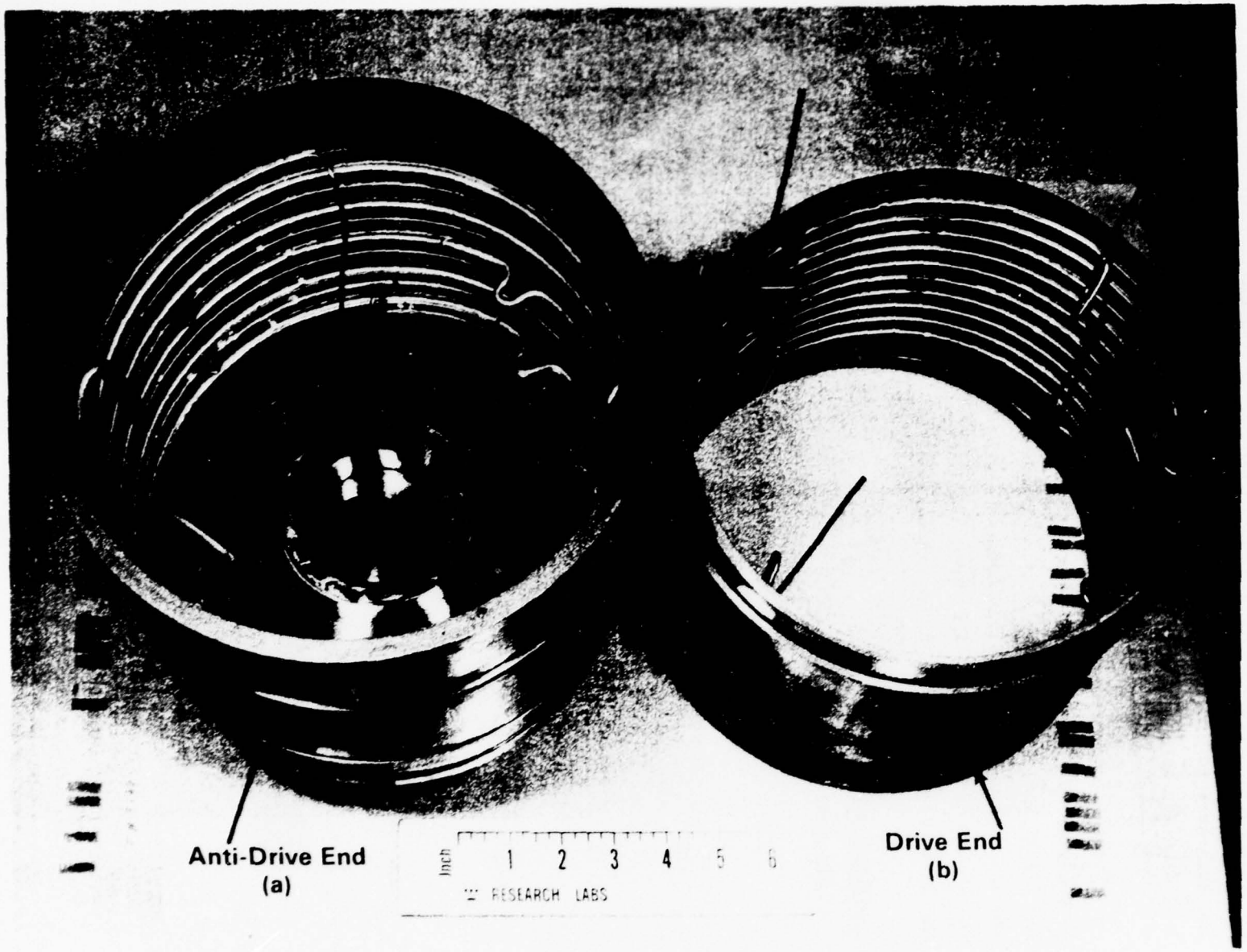


FIG. 19 Transition Pieces With Cooling Coils

New tubes were substituted for defective coils which were not brazed to the transition piece. They were connected to vapor ports in the bulk-head to provide adequate ventilation of helium vapor during cool-down and normalization of the field winding.

The anti-drive end shaft assembly was welded to the field winding assembly by multiple passes using gas tungsten arc welding with Inconel 718 filler rod. The welding schedule around the joint was varied to produce minimum run-out of the bearing journal. Critical dimensions on the shaft were qualified after the welding operation was completed using the outer diameter of the field winding assembly as a datum surface.

Drive-End Shaft

The drive-end shaft assembly contained the following sub-assemblies:

(1) A vapor cooled thermal transition tube between the warm end and the cold end,

(2) shaft journals for the bearing with a flexible end-member that accommodates axial contraction of the cold structures,

(3) a support station for the electro-thermal shield,

(4) a radiation shield (disc),

(5) conduits for sensor leads from the field winding compartment,

(6) the bulk-head between the helium compartment and the vacuum compartment, and

(7) a vacuum pump-down valve and a spline for torque transmission.

The thermal transition tube is identical to the tube on the anti drive-end except all four cooling coils were made from .083 inch diameter X .010 inch wall tubing (See Figure 19). Leak tests of these tubes after the first brazement of the tubes and further processing of the transition piece showed failure of the coils. The defective coils were replaced with new tubes. A failure analysis of cooling coils is presented in Appendix G.

The drive-end shaft was welded to the field winding assembly using the procedures as employed for the anti drive-end.

Electro-Thermal Shield

The electro-thermal shield consisted of a copper shield supported on an inner cylinder of alloy A286. The dimensions of the inner cylinder are 9.260 inches O.D X .087 inches wall thickness X 24.16 inches long. Originally, the thickness of the copper was 0.105 inches. The approach used to join the two parts was based on a diffusion technique. This technique was as follows:

- A thin layer of Ag (.001 inch) was plated onto the Copper and the A286 was flash coated with Ni.
- The two parts were then clamped and furnace treated at a temperature in excess of 1475°F to form the copper-silver eutectic.
- This alloy wets the two surfaces and affects a braze joint.

This procedure was followed with very poor results. Later discussion with Wallcolmony, who performed the vacuum heat-treatment, indicated that the results could have been improved if Cu had been flashed over the nickel on the A286. The silver would then have been sandwiched between Cu, reducing the diffusion distance and accelerating the eutectic reaction.

To improve the bond the assembly was reclamped and reheat-treated at a higher temperature (1865°F) for one hour followed by a fast cool. Subsequently Bag-8 powder was added to the ends and seams and through holes drilled in the Copper. The assembly was heat to 1500°F for 15 minutes and cooled. This treatment was followed by a reaging heat treatment to restore the high strength properties of the A286 alloy by heating the assembly to 1325°F for 16 hours.

An ultrasonic inspection of the part showed a poor bond. Thus, it was decided to hand torch the part using a lower melting (1435°) braze alloy commonly called BT compound and Easy-Flo flux with a melting point of 1160°F. The flux was introduced through 1/4 inch holes in the copper shell using hydraulic pressure. The part was heated on both sides using two torches and then braze rod was fed into the holes.

A final ultrasonic inspection of the braze joint for the copper to A286 support tube was made. This inspection showed the bond was unsatisfactory. Further attempts to improve the braze joint were considered impractical and it was decided to over wrap the copper shield with Brunsmet metal fibers to provide the necessary structural support under rotation.

A 304 stainless steel, multifilament fiber was selected for this application. The filament diameter was 8 microns and the yarn consisted of 1159 filaments and exhibited the same desirable fabrication characterictics as multifilament glass fibers. The properties of the fibers are listed in Table 3.

TABLE 3

PROPERTIES OF 304 STAINLESS STEEL FIBER

Property	Value
Ultimate Tensile Strength	300,000 psi (typical)
	230,000 psi (minimum)
Modulus of Elasticity	27×10^{6} psi
Elongation	1.2 to 1.5%
Specific Gravity	7.9 gm/cc
Coefficient of Thermal Expansion	17×10^{-6} m/m °K
Electrical Resistivity	72×10^{-6} ohm-cm

*Brunswick Corporation, Technical Products Division, Brunsmet Metal Fibers

After consideration of the structual requirements under rotation, it was decided to provide this protection by a .040 inch overwrap of the copper by reduction of the thickness of the copper shield from .100 to .060 inches. Mechanical test specimens were prepared and tested as described in Appendix H. From these tests the properties of the composite used to make the overwrap were evaluated and are shown in Table 4.

TABLE 4

SS-304 EPOXY COMPOSITE PROPERTIES

Composite	Constituents	vf	Long. Tensile KSI	Long Tensile Mod. psi	Shear KSI	Long Exp. m/m/°K x 10^{-6}	Trans. Exp. m/m/°K x 10^{-6}
SS-304/Ep.	*Brunsmet/DER330 8/1159/PT	0.63	130	14 x 10^{6}	15	15.2	16.5

*Trademark of Brunswick Corp., Technetics Division.

If the bond between the 0.060 copper tube and A286 support tube is neglected, the centrifugal pressure of the copper on the overwrap is 366 psi at 12,000 rpm which produces a hoop stress of 43,200 psi in the 0.040 inch overwrap. The hoop stress in the overwrap itself due the 12,000 rpm rotation is 21,700 psi. Hence, the combined hoop stress in the overwrap is 64,900 psi at design speed and 78,500 at the overspeed (13,200 rpm) condition. The observed tensile strength in the hoop direction for the composite at 77°oK is $\sim$ 130,000 psi. Hence sufficient structural protection under rotation was provided by the overwrap. Figure 20 is a photograph of the overwrapped electrothermal shield before it was assembled on the rotor.

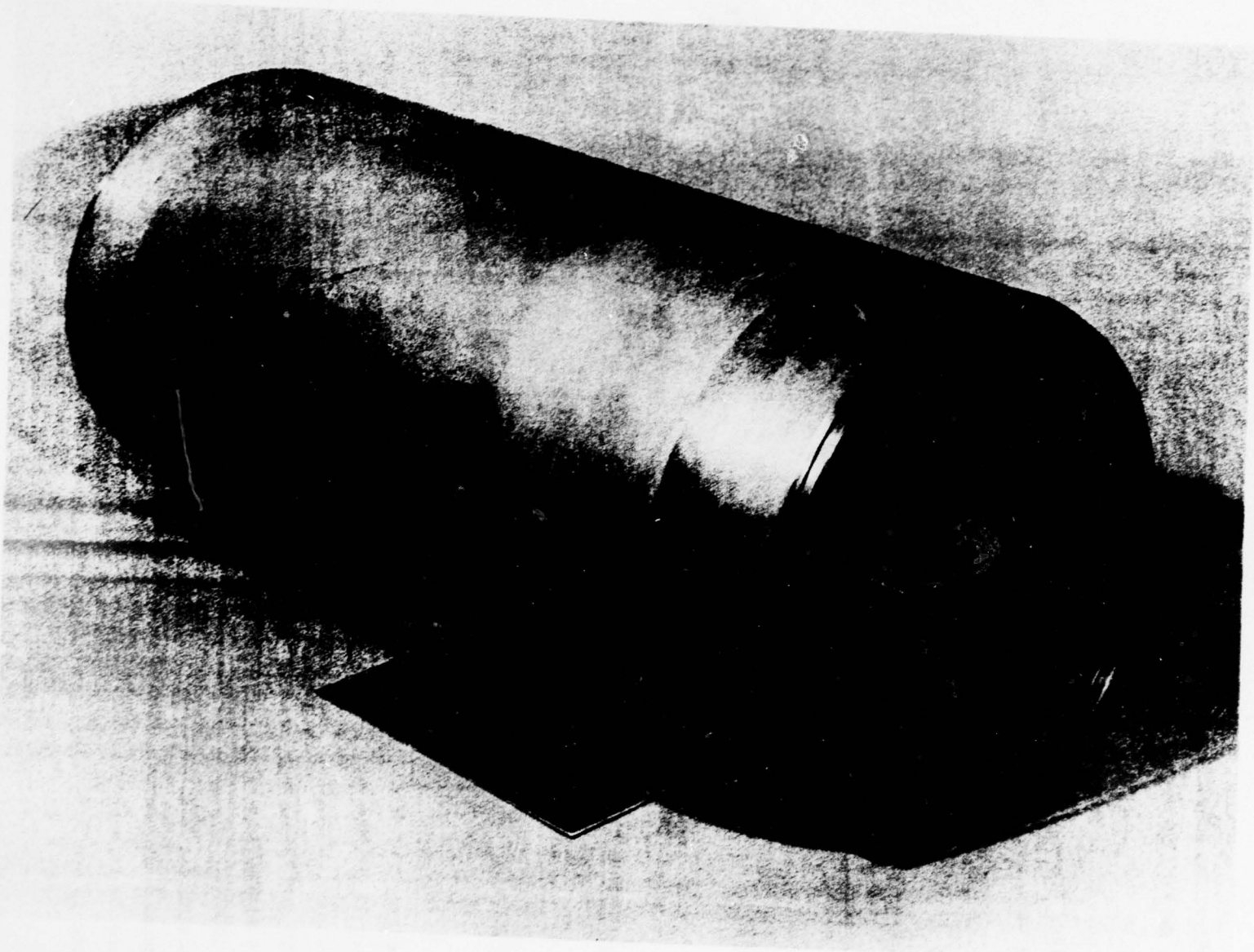


FIG. 20 Electro-Thermal Shield

The electro-thermal shield is supported at each end by a flange on the thermal transition tubes. A shrink fit was employed on one end with 360° weldment of the joint. A slight press fit was employed for the opposite end. The weldment for this joint was contrived so that axial movement between the flange and the inner cylinder of the shield can occur without restraint from the welds. The philosophy for the design of the support system for the shield was that accommodation for relative axial contraction of the shield and the inner structure is not essential.

The contraction for the shield (Alloy A286) is greater than the contraction of the inner structure (Alloy 718) at the same subambient temperature. However, the shield operates at a higher temperature than the inner structure which off-sets this situation. Figure 21 shows the relative temperatures for each component that produces equal contraction. Also, the stress intensity (axial) introduced by both components operating at the same temperature is indicated.

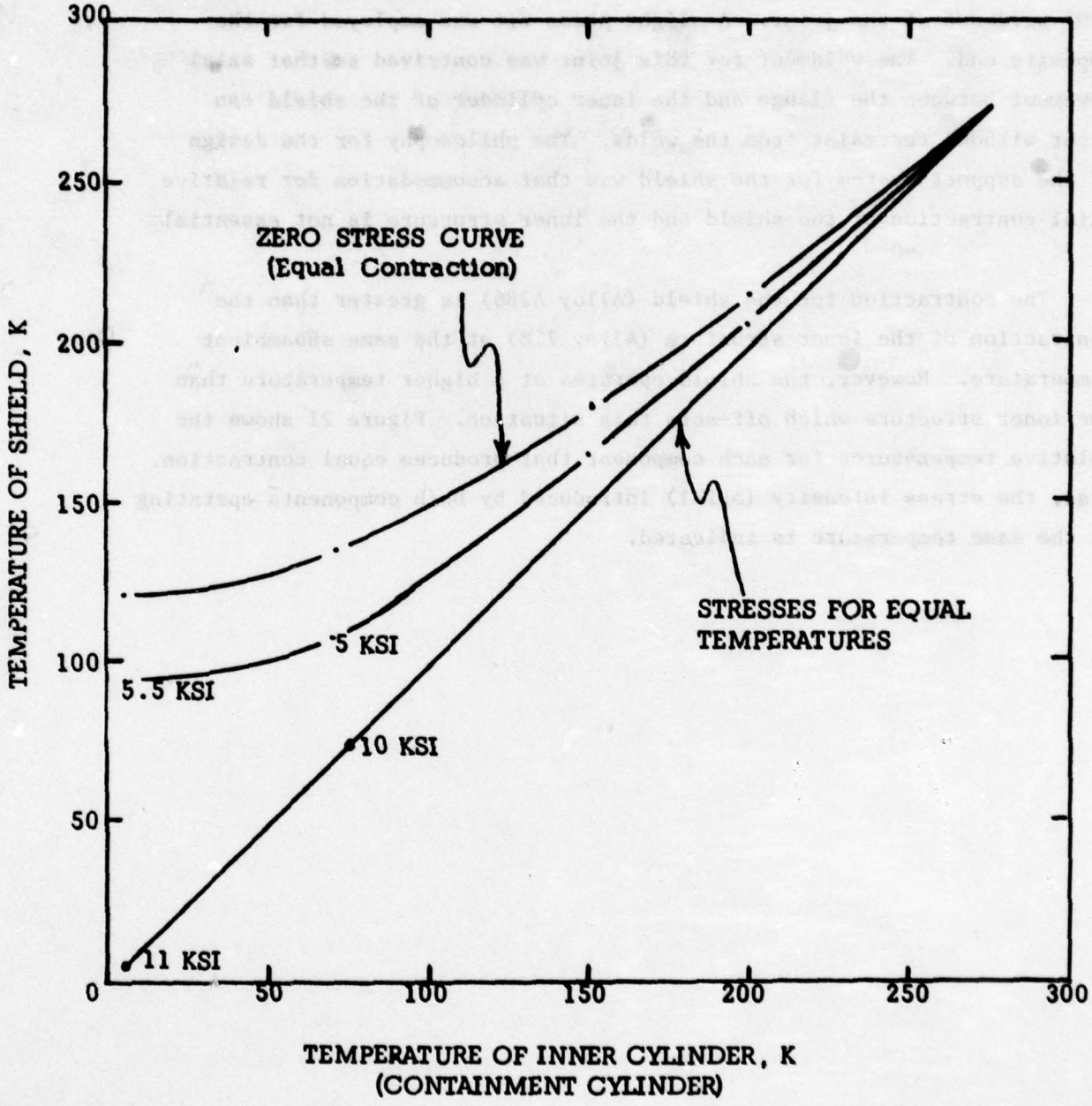


FIGURE 21 AXIAL STRESS INTENSITY CURVES

Outer Cylinder

The outer cylinder has a diameter of 24.79 cm (9.760 inches) with a wall thickness of 2.35 mm (.093 inches) and is 66.83 (26.31 inches) long. This cylinder forms a vacuum jacket around the cold inner structures. It was welded to flexible members which accommodate the contraction of the inner cold structures. The radial clearance (single air gap) between the rotor and stator is 2.03 mm (.080 inch). Alloy 600 (AMS 5662) was used for this cylinder. It was gold plated on the vacuum side to minimize radiant heating of the cold structures.

Helium Cooling System

Helium is introduced by means of a stationary bayonet within a rotating tube at the center of the rotor as shown in Figure 1. The cold-to-warm helium in the annular clearance between the bayonet and the rotating tube is isolated from the warm, exhaust helium from the current leads by a carbon face seal. Bayonet and seal concentricity relative to the rotating tubes is maintained by a ball bearing which has the inner race mounted on the rotating tubes with the bayonet/seal housing mounted on the outer race. This housing is independently mounted with respect to the main stator through a system of pins and springs which impose an axial force ($\sim$ 200 lb) on the auxiliary housing and bearing.

Transfer losses were measured for the bayonet, seal, and an external transfer line by using a double transfer system[16] through a hollow rotating shaft. The external transfer lines contained a union which made them dismountable and separate components. The losses in the system were 6 watts at 12,000 rpm with a transfer rate of 30 liters per hour in the transfer system. However, this boil-off does not constitute a waste since this vapor is used later to cool the electro-thermal shield and the thermal transition tube at the drive-end of the rotor.

An impeller and heat exchanger shown in Figure 2, along the axis of the rotor produces phase separation. The dense helium is diverted outward through copper fins in the center of the poles. These fins are thermally connected to the exchanger on the axis of the rotor and

are thermally isolated from the helium in the field winding. As the helium moves off-axis in the fins, it undergoes compression by virtue of the rotational forces. At 12,000 rpm, the pressure at the outer diameter of the rotor is ∿ 11 atmospheres. This compression process is isothermal because the heat of compression, thermodynamically represented as (temperature x change of entropy), is conducted back to the central exchanger. At this point, it is released by evaporation in the exchanger. The boil-off which occurs in the transfer system and within the central exchanger is expelled on the axis of the drive-end through radial tubes which are connected to the cooling coils on the thermal transition tube.

Decompression of the helium occurs as it moves toward the axis of rotation within and around the field coils. During this decompression a heat influx of ∿ 2 J/gram may occur at 12,000 rpm without a temperature rise of the helium. The mass flow rate through the winding at design speed is ∿ .56 grams per second. Hence, a heat influx of 1.1 watts may be accommodated before the temperature at the exit rises above that at the entrance. A distinguishing feature of the cooling scheme is that a high influx of heat in a particular region causes a negative feedback upon the flow distribution. A higher influx causes a greater change of density relative to the other regions, thus rotational forces cause the flow rate in this region to increase. Circulation of the dense helium through the field winding is produced by expelling it at a radius of 3.0 cm. Phase separation occurs at a radius less than 3.0 cm. The liquid-vapor interface in the separator adjusts as required to displace dense helium in the field winding compartment. All of the helium in the field winding compartment flows inwardly from the outer radius of the winding to the central, off-axis location before it leaves the field winding compartment. After the helium leaves the winding compartment, the dense helium flows outward to a radius of 4.5 cm through a two-phase region. At this radius it enters a pool of dense helium. The helium for the current leads continues to flow outward to a radius of 7.5 cm where it enters the conduits. A self regulated flow rate through the leads is produced by the path of the conduits. The conduits cause the helium to move inward to a radius of 2.4 cm before the temperature of the exhaust helium changes significantly.

The pool of helium at the entrance cannot support dense helium when it completely fills the conduits. Thus, a liquid-vapor interface occurs in the conduits at a radius which produces equilibrium of the rotational forces. The boil-off (.08 g/sec.) at the liquid-vapor interface flows toward the warm ends and intercepts the heat conducted and generated within the leads.

The dense helium (.487 g/sec.) which is not expelled through the current leads is expelled at a radius of 4.5 cm. This off-axis position sets the location of the pool previously discussed. The overflow is expelled through tubes which are connected to the cooling coils on the thermal transition tube. These tubes contain a vapor trap which isolates the warm vapor in the cooling coils from the cold vapor within the two-phase compartment. Vapor within the two-phase compartment is expelled through ports near the axis of rotation. Compression of this vapor up to ambient pressure is produced by the centrifugal force as it flows outward to a radius of 9.7 cm.

Cryogenic Instrumentation

Internal thermometers were incorporated into the rotor during its assembly. These thermometers are ordinary 1/10W Allen-Bradly carbon resistors which were calibrated between 3 - 100°K using a calibrated Ge thermometer. Each thermometer was housed in a Cu support sleeve and was designed to fit within a 0.125 diameter hole. The Teflon insulated voltage and current leads were sufficiently long to reach outside the rotor. The leads were fed through special tubes, shown in Figure 22, to hermetically sealed connectors located in the drive coupling. These leads were passed through a bored hole in the gear box drive shaft to high speed instrumentation slip rings. Internal thermometer leads penetrated both the vacuum and He space through conduits to ascertain the temperature of the centerline inlet helium, the helium into the copper fins, the helium out of the fins, the helium out of the coils, and the electro-thermal shield.

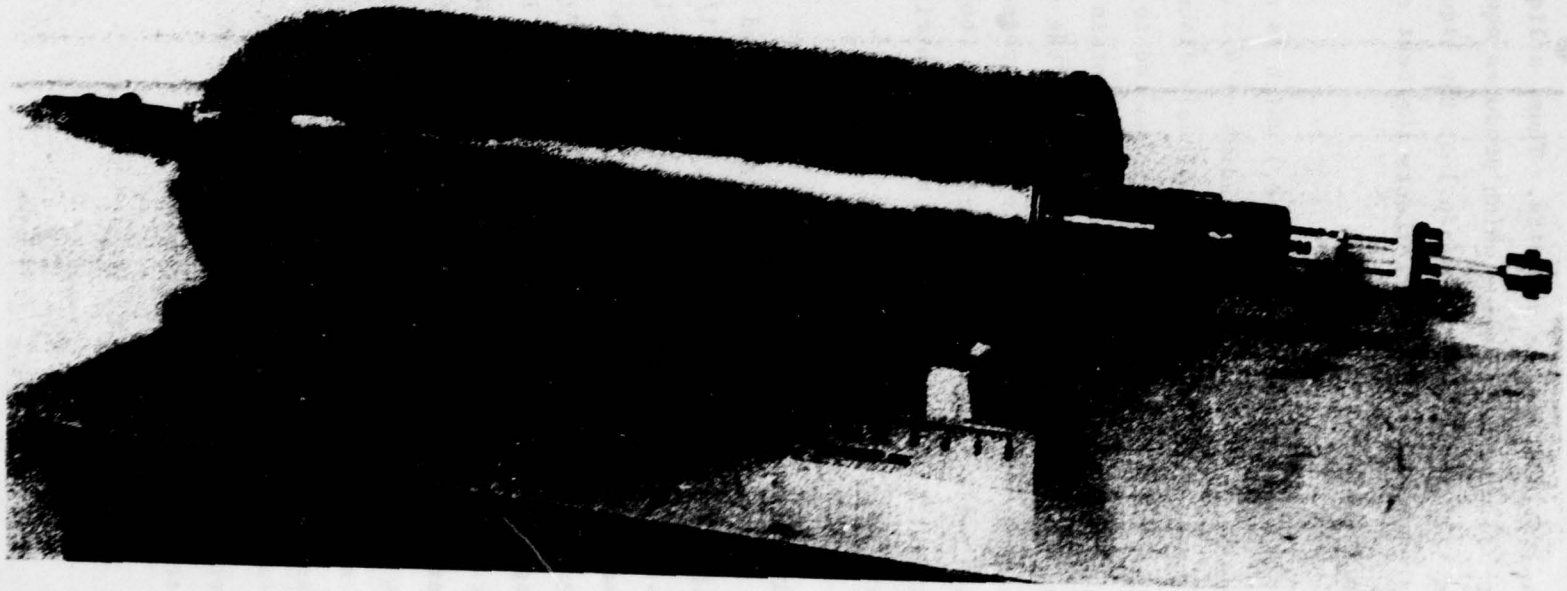


FIG. 22 Sealed Connectors and Special Tubes for Sensor Leads

Bearings

The drive-end is supported on a 70mm x 125 mm roller bearing and the anti drive-end is supported on a 70 mm x 110 mm angular contact ball bearing. A second angular contact ball bearing (55 mm x 90 mm) was used at the end of the auxiliary shaft for the slip rings. This bearing is pre-loaded with springs to provide thrust on this ball bearing and the main ball bearing. A third angular contact bearing (45 mm x 75 mm) is used for alignment of the helium transfer seals and for alignment of a stationary helium transfer bayonet within the central, rotating tube. The pre-load on this bearing is maintained by coil springs which act upon the seal and bearing housing. This pre-load is opposed by a tensile load on the tube which forms a vacuum space around the central, rotating helium transfer tube. The tensile load on this tube is opposed by a thrust load on the 70 mm x 110 mm angular contact ball bearing.

Dynamic Seals

The bearing oil is confined by floating, circumferential, carbon ring seals. The carbon rings are split and were designed to make contact with the shaft at installation. A garter spring caused the ring to close after a wear-in period. The helium transfer seals were face seals which consisted of a magnetized ring pushed into the housing and a carbon-faced steel ring on the shaft. Magnetic force held the seal surface in contact and "O" rings in both the shaft and magnet elements prevented leakage around this seal. The inner seal confines the supply helium and is contrived so it operates in a dry helium environment at temperatures near ambient temperature. The outer seal confines the helium from the current leads and is contrived so it operates at a temperature near ambient temperature with oil lubrication from the bearing side of the seal.

Bearing Brackets

The brackets for mounting the rotor bearings were made of aluminum. Each bracket contained a steel insert to mate with outer race of the bearing. An infringing flux from the rotating field encroachs upon

these stations in the generator. Hence, the aluminum brackets were contrived with a cooling jacket so eddy-current heating could be removed by circulation of oil or water. The thickness of the aluminum around the bearing was selected to prevent penetration of a high frequency fields into the steel bearing structures since these fields would produce heating in these critical components.

SECTION IV
GENERATOR CAPABILITY

Voltage, Power, and Field Current

Line-to-line voltage for a 3-phase, wye connected generator are shown in Figures 23 and 24 for constant value (broken lines) of phase current. These parameters are not unique for this particular generator since they only graphically represent the equations below:

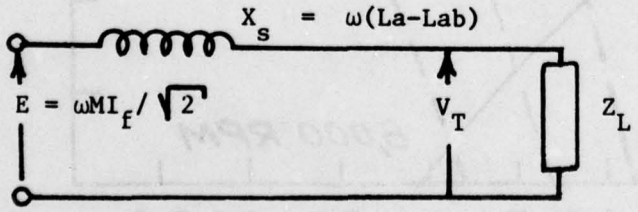
$$V_{T(L-L)} = \sqrt{3}\, V_{T(L-N)} \qquad (1)$$

$$MVA = 3\, V_{T(L-N)}\, I_p \times 10^{-6} \qquad (2)$$

$$V_{T(L-L)} = \frac{MVA \times 10^6}{\sqrt{3}\, I_p} \qquad (3)$$

However, the parameters shown in Figures 23 and 24 become unique once field currents are superimposed for a given power factor and operating speed.

A synchronous reactance model for the generator was used to establish voltage versus load for constant values of field current. An electrical circuit representing each phase for such a model is shown below.



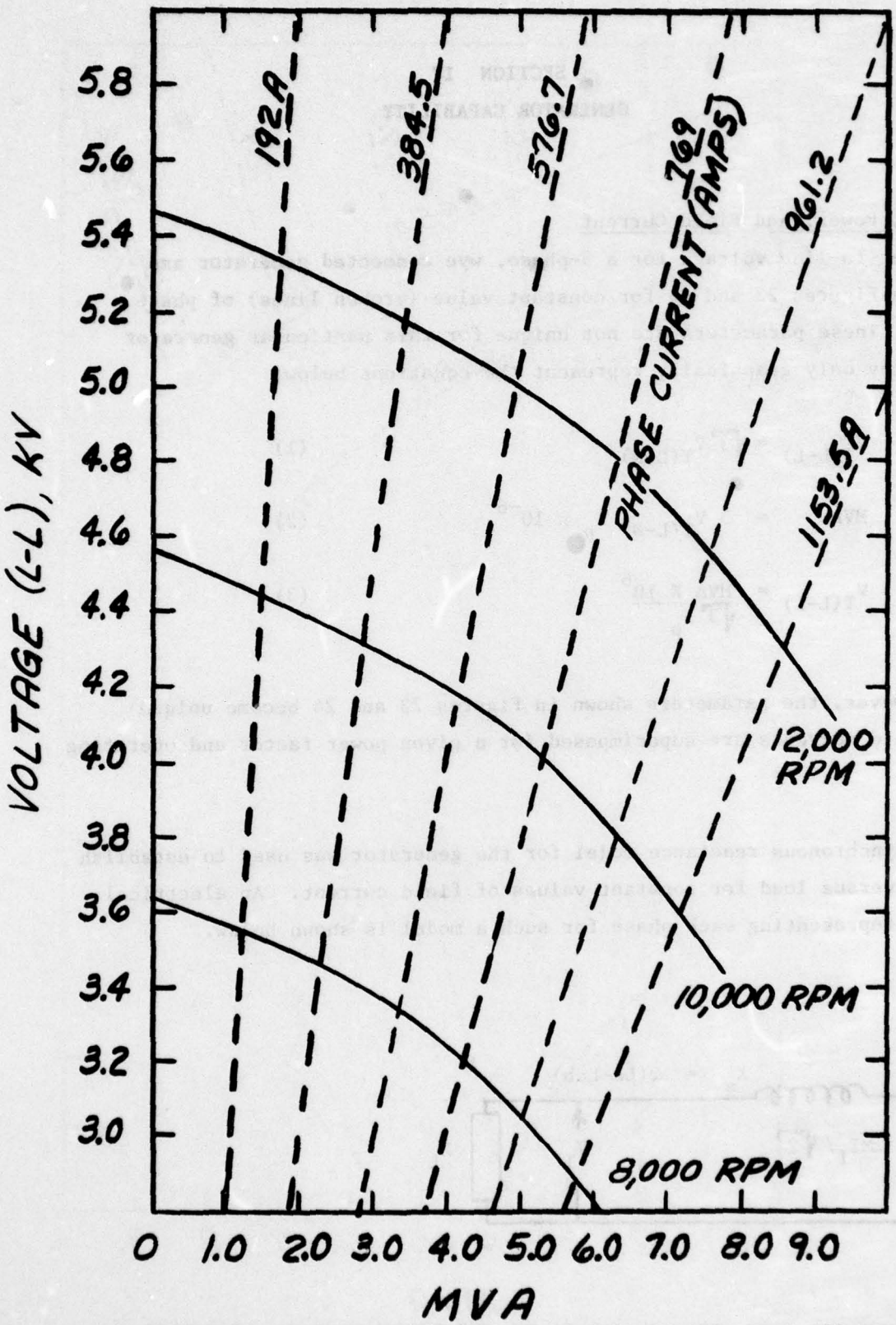


FIGURE 23 VOLTAGE VERSUS MVA AT 12,000, 10,000 AND 8,000 RPM FOR 228A FIELD CURRENT

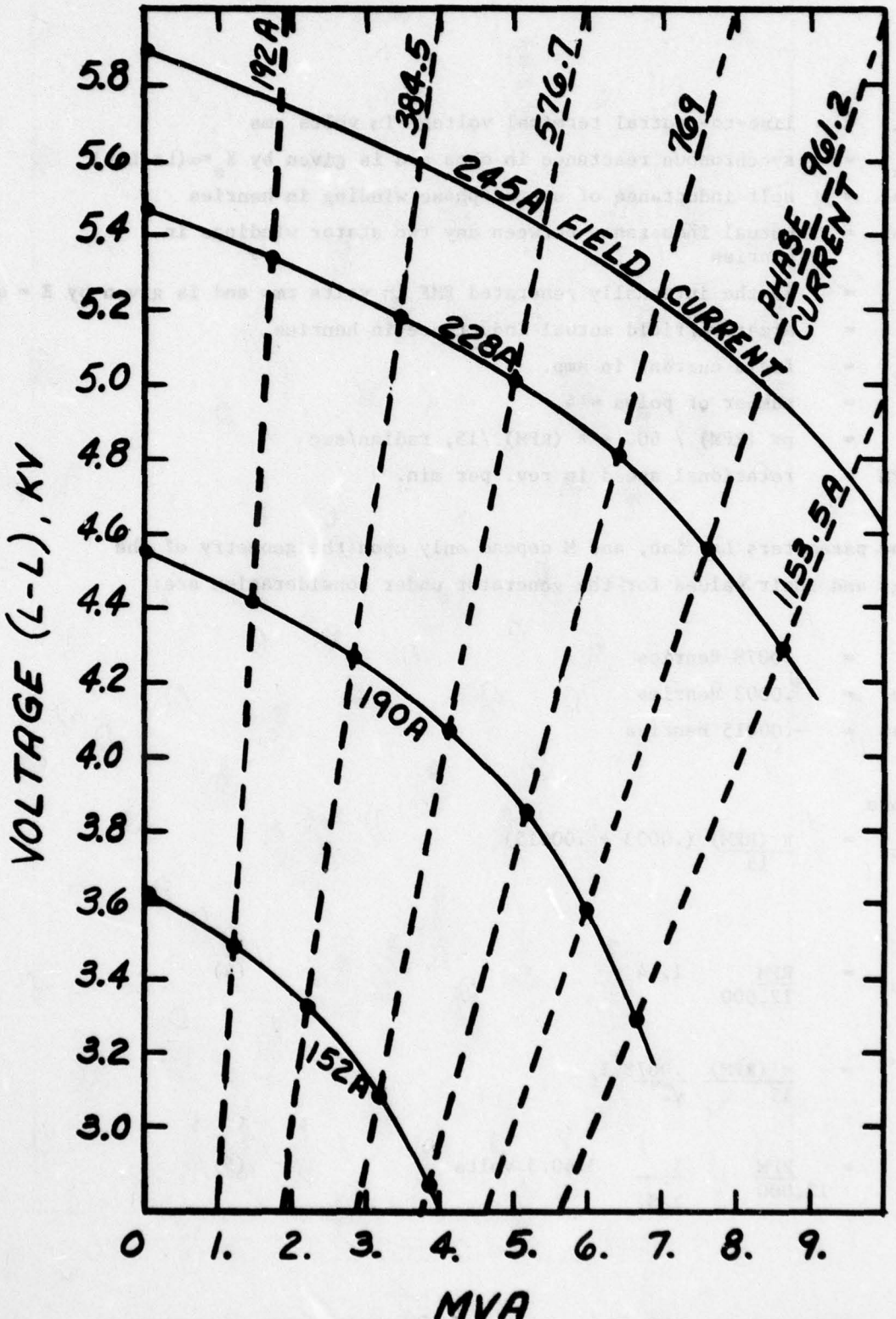


FIGURE 24 VOLTAGE VERUS MVA AT 245, 228, 190 AND 152A FIELD CURRENT AT 12,000 RPM

Where

V_T = line-to-neutral terminal voltage in volts rms

X_s = synchronous reactance in ohms and is given by $X_s = \omega(La - Lab)$

La = self inductance of stator phase winding in henries

Lab = mutual inductance between any two stator windings in henries

E = is the internally generated EMF in volts rms and is given by $E = \omega M I_f / \sqrt{2}$

M = Armature/field mutual inductance in henries

I_f = field current in amp.

p = number of poles = 4

ω = $p\pi$ (RPM) / 60. = π (RPM) /15, radian/sec

RPM = rotational speed in rev. per min.

The parameters La, Lab, and M depend only upon the geometry of the windings and their values for the generator under consideration are:

M = .0078 Henries

La = .0003 Henries

Lab = -.00015 Henries

Therefore

$$X_s = \frac{\pi\ (RPM)}{15}\ (.0003 + .00015)$$

$$X_s = \frac{RPM}{12{,}000}\ 1.14 \qquad (4)$$

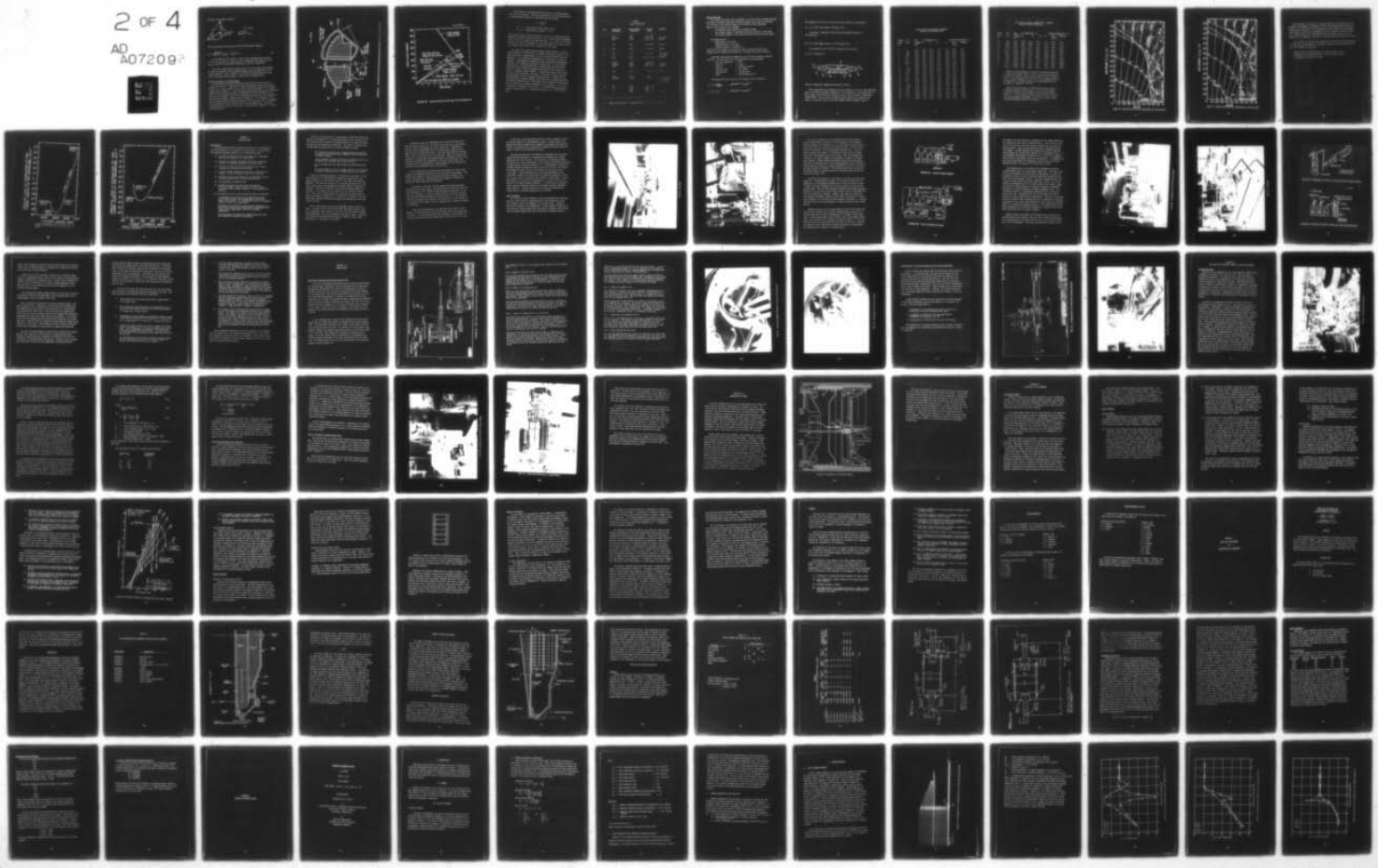
$$E = \frac{\pi\ (RPM)}{15}\ \frac{.0078}{\sqrt{2}}\ I_f$$

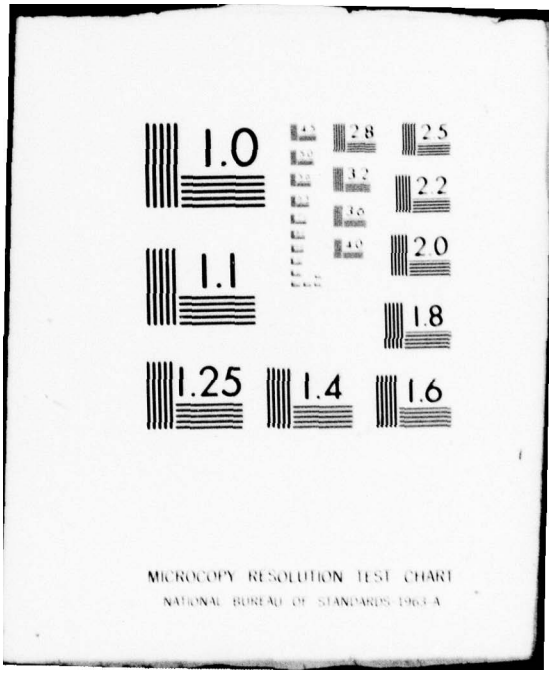
$$E = \frac{RPM}{12{,}000}\ \frac{I_f}{228}\ 3160.5 \text{ volts} \qquad (5)$$

AD-A072 093 WESTINGHOUSE ELECTRIC CORP LIMA OHIO AEROSPACE ELECT--ETC F/G 10/2
PROGRAM FOR THE DEVELOPMENT OF A SUPERCONDUCTING GENERATOR.(U)
FEB 79 J L MCCABRIA F33615-71-C-1591

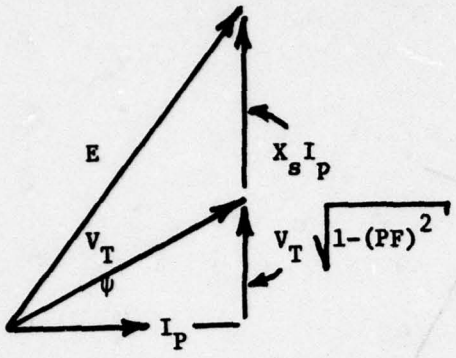
UNCLASSIFIED AFAPL-TR-79-2012 NL

2 OF 4
AD A072093




1.0
1.1
1.25
1.4
1.6
2.8
3.2
3.6
4.0
2.5
2.2
2.0
1.8
MICROCOPY RESOLUTION TEST CHART
NATIONAL BUREAU OF STANDARDS 1963-A

The steady state phasor diagram is



$$PF = \cos \psi$$

$$\sqrt{1-(PF)^2} = \sin \psi$$

and the following relation can be derived from the phasor diagram:

$$V_T^2 + (2\sqrt{1-(PF)^2}\, X_s I_p) V_T + X_s^2 I_p^2 - E^2 = 0 \qquad (6)$$

If I_f, RPM, and PF are given, X_s and E can be determined from equations (4) and (5), respectively. Hence, V_T can be determined from Equation (6) and $V_{T(L-L)}$ and MVA are determined by Equations (1) and (2), respectively.

The field currents shown on Figures 23 and 24 by the solid lines indicate the impact of observed field winding performance upon the capabilities of the overall generator. Field currents up to 251A were observed during the static test on the field winding assembly. These test are discussed below.

Static Test Results for Field Winding

The generator can produce 5.0 MVA when the field coils are excited to a current level of 228 A. This current level should produce a high field point of 38.8 KG at a 2.352 in. radius (5.97 cm) with an electrical angle of 75° as shown schematically in Figure 25. This field value is determined from the two-dimensional computer field plot which includes an approximate 10% field enhancemant due to the iron stator shield. The four-coil superconducting load line can be generated from these field-current values as shown in Figure 26. It is important to note that the maximum current that can be achieved in the four-coil rotor is determined by the intersection of the load line with the short sample limit. The current carrying limit for the four coils is thus $\sim$ 410 A which will generate $\sim$ 7.1 tesla at the field point.

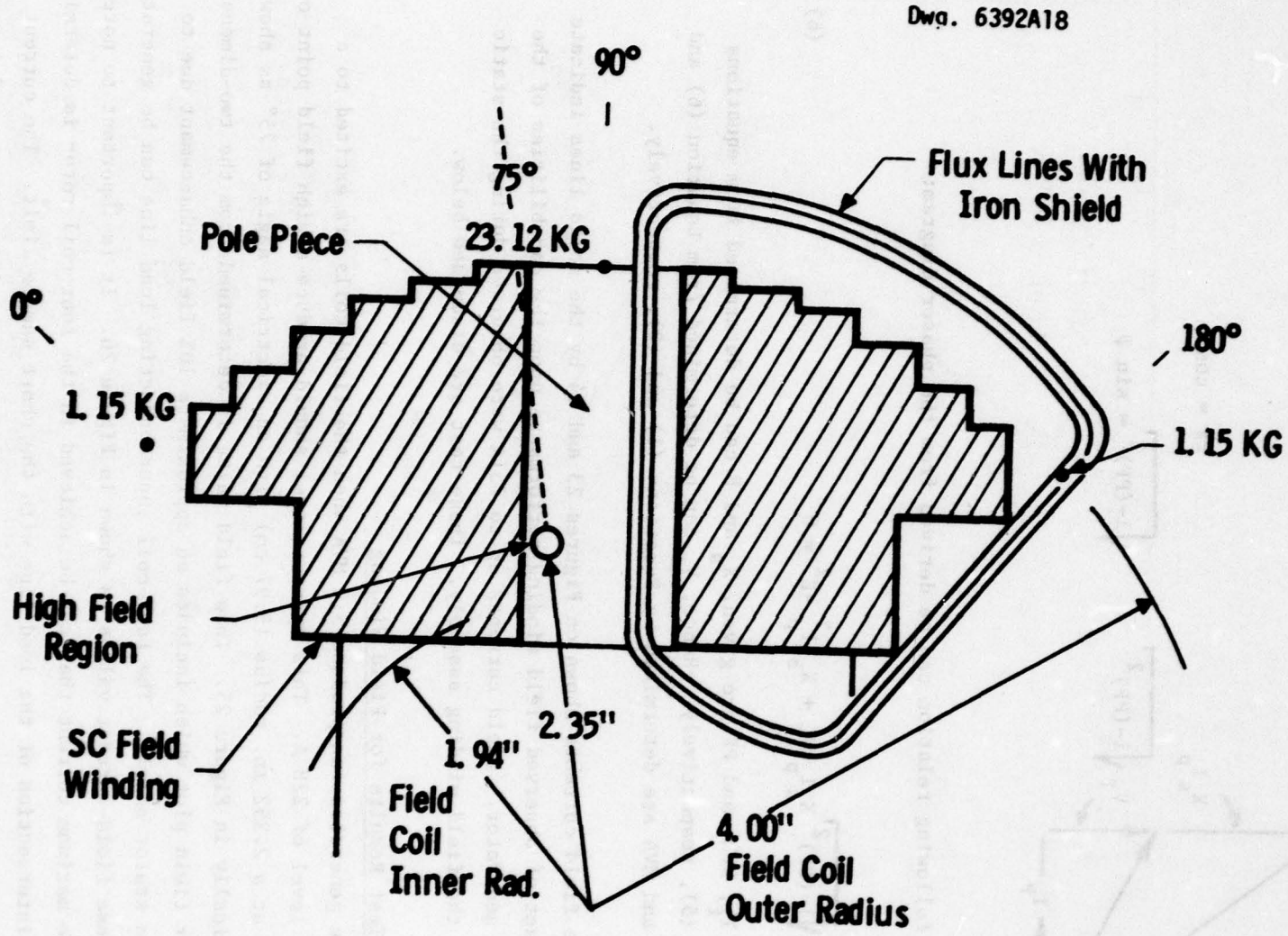


FIGURE 25. One Pole Pitch for Generator Showing High Field Current at 12000 RPM

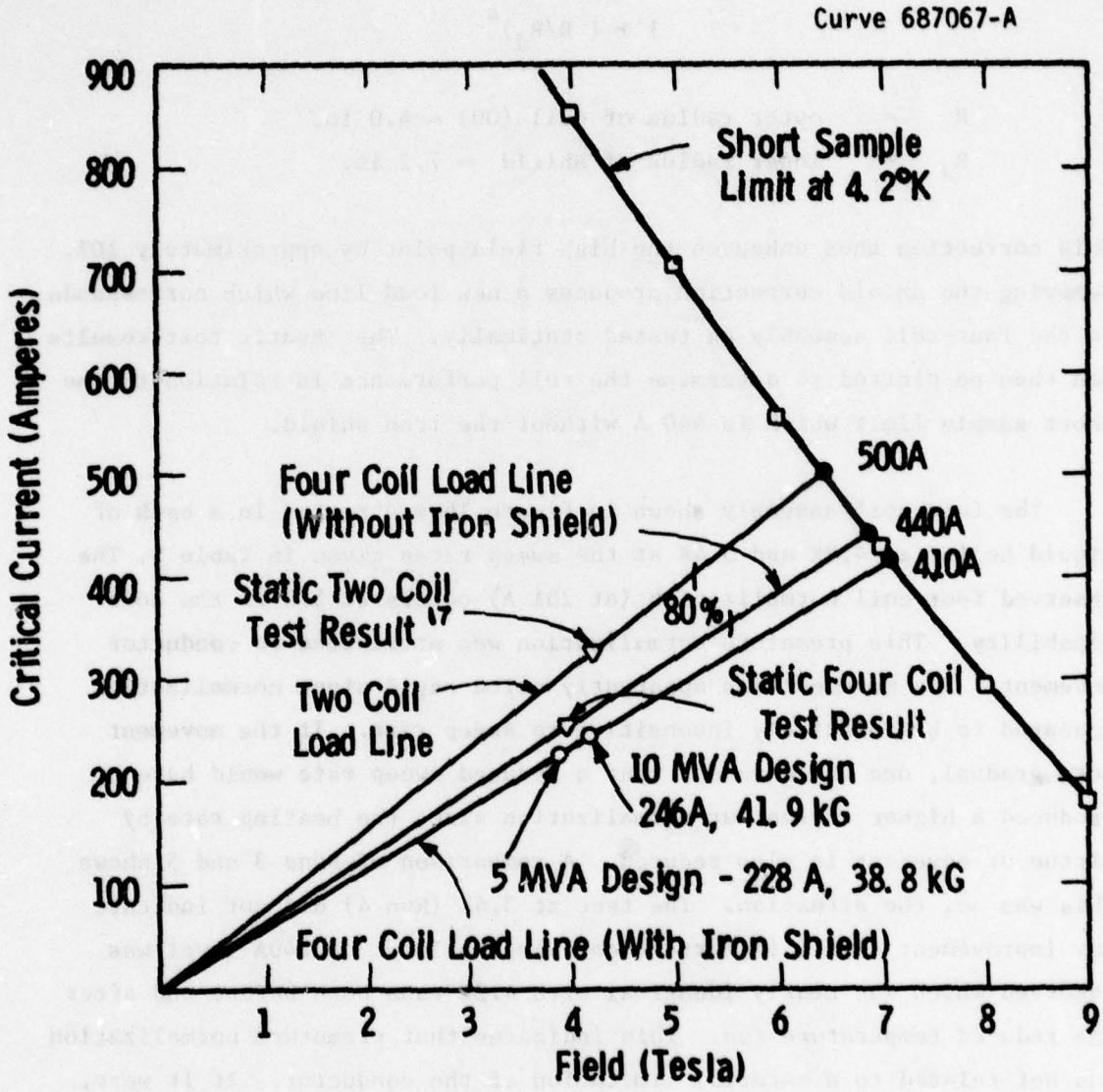


FIGURE 26. Superconducting Coil Load Line Comparisons

The field plot as mentioned earlier includes a field enhancement due to the iron shield. The field correction due to the iron shield for a two-dimensional machine is calculated from the relation

$$1 + (R/R_J)^4$$

R = outer radius of coil (OD) $\approx$ 4.0 in.
R_J = inner radius of shield $\approx$ 7.2 in.

This correction thus enhances the high field point by approximately 10%. Removing the shield correction produces a new load line which corresponds to the four-coil assembly as tested statically. The static test results can then be plotted to determine the coil performance in relation to the short sample limit which is 440 A without the iron shield.

The four coil assembly shown in Figure 16 was tested in a bath of liquid helium at 4.2K and 3.4K at the sweep rates given in Table 5. The observed four-coil normalization (at 251 A) occurs at 57% of the coil capability. This premature normalization was attributed to conductor movement. The movement was apparently quite rapid since normalization appeared to be relatively insensitive to sweep rate. If the movement were gradual, one would expect that a reduced sweep rate would have produced a higher current at normalization since the heating rate by virtue of movement is also reduced. A comparison of Runs 3 and 5 shows this was not the situation. The test at 3.4K (Run 4) did not indicate any improvement at all in current carrying ability. A 240A level was observed which was nearly identical with 4.2K runs both before and after the reduced temperature run. This indicates that premature normalization was not related to a material limitation of the conductor. If it were, a reduction in temperature from 4.2K to $\sim$ 3.5K should have increased the current carrying ability by a significant amount, i.e., $\sim$ 20% for this test.

TABLE 5

STATIC ROTOR TEST

Run	Sweep Rate (Amp/Min.)	Time Interval (Minutes)	Current (Amps)	Comments
1	112	1.80	0 to 200	
	Holding	3.56	200 to 213	Drifting
	45.5	0.31	213 to 227	Quench
2	140	1.66	0 to 232	Quench
3	369	0.66	0 to 243	Quench
4	23.4	1.13	0 to 30	Subcooled to 3.3°K*
	56.1	3.56	40.2 to 240	Quench
5	57.83	3.72	0 to 215	
	Holding	0.71	215 to 221	Drifting
	6.09	3.62	221 to 243	Quench
6	144	1.7	0 to 241	Quench
7	144	1.5	206	
	Holding	Drift	248	Quench (drifted for 25 sec. up to 248A)
8	58	3.25	0 to 190	
	10	2.9	190 to 225	
	5	2.8	225 to 240	
	3	3.8	240 to 254	Quench

* Temperature was stable to within 0.1°K over a six minute interval.

Stator Limitation

The results from static tests of Appendix I and J were used to define algorithm which give the maximum temperature difference between the oil and the conductors as a function of the specific losses in the conductor. These algorithms apply at three location in the winding;

- the knuckles (often referred to as hairpin turns),
- the straight lengths of conductors where they connect to a bus rings,
- the straight lengths of the conductors where they exist from the matrix.

The algorithms are

$\Delta T(\text{Knuckles}) = 8.67\ (P/V)$

$\Delta T(\text{Connections}) = 7.248\ (P/V)$

$\Delta T(\text{End of matrix}) = 4.418(P/V) + 5$

where P/V is the losses in watts per cubic cm of conductor and ΔT is the maximum observed temperature difference in °F between the oil and conductor.

Algorithms which give the temperature of oil at these stations, reference Figure 27, are presented here for the following oil flow conditions:

Oil inlet temperature	=	100°F
flow rate	=	64 gpm
density	=	.884 g/cm at 100°F
mass flow rate	=	72.2 Lb/min
specific heat	=	.469 BTU /Lb°F
$\dot{\Delta H}/\Delta T$	=	3.89 Kilowatts per °F

The temperature rise of the oil for cooling of the iron shield is

$$T_1 - T_o = \frac{8.07\text{kw}}{3.89\text{kw°F}^{-1}} \times (\text{RPM}/12000)^{1.6}(I_f/228)^{1.8}$$

$$T_1 - T_o = 2.07 \times (\text{RPM}/12000)^{1.6}(I_f/228)^{1.8}$$

The temperature rise of the oil along the inner radius of the winding is

$$T_2 - T_1 = ((P/V) \text{ eddy current} + (P/V)_I{}^2{}_R) \ .839.$$

The average temperature rise of the oil through the matrix of the winding is:

$$\bar{T}_2 - T_1 = ((P/V) \text{ eddy current} \times .53 + (P/V)_I{}^2{}_R) \ .839$$

The temperature rise of the oil through the end turns is:

$$T_3 - \bar{T}_2 = (P/V)_I{}^2{}_R \ 1.21$$

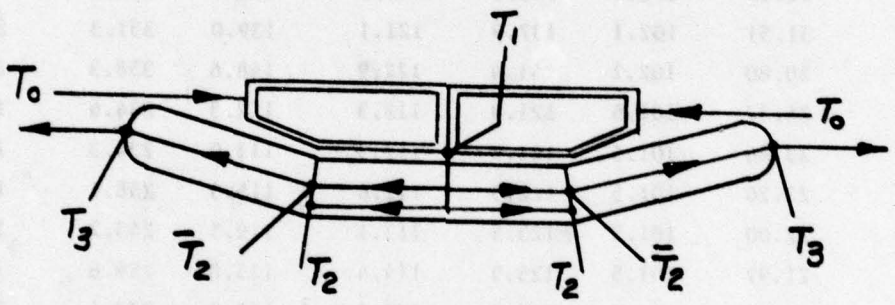


Figure 27 Cooling Oil Temperature Stations In Stator

These alogrithms were combined with the alogrithms for the oil film temperature drop to establish the maximum temperature of the conductors. The shaded area on these figures shows where over heating of stator occurs -conductor temperature exceeds 300°F. Table 6 gives the specific power losses in the conductor and temperature data for each of the point designs noted on Figures 28 and 29.

TABLE 6 SPECIFIC POWER LOSSES in ARMATURE CONDUCTORS AND TEMPERATURE DATA

DESIGN POINT NO.	I^2R Wcm^{-3}	EDDY CURRENTS Wcm^{-3}	OIL TEMPERATURES (°F) T_1	T_2	$\bar{T}_2$	T_3	CONDUCTOR TEMPERATURES (°F) END OF MATRIX	KNUCKLES
0	0	35.10	102.1	131.5.	117.7	117.7	291.5	117.7
1	.445	34.12	102.1	131.3	117.6	118.3	290.3	122.2
2	1.782	33.79	102.1	131.9	117.9	120.8	294.0	136.2
3	4.01	33.03	102.1	135.2	118.6	125.0	301.8	159.8
4	7.13	32.10	102.1	135.0	119.5	130.9	313.3	192.7
5	11.14	31.51	102.1	137.9	121.1	139.0	331.3	235.6
6	16.04	30.80	102.1	141.4	122.9	148.6	358.3	290.8
7	0	24.37	101.5	121.9	112.3	112.3	234.6	112.3
8	.445	23.86	101.5	121.9	112.3	113.0	234.3	116.9
9	1.782	23.26	101.5	122.5	112.6	115.5	238.1	130.9
10	4.01	22.00	101.5	123.3	113.1	119.5	243.2	154.3
11	7.13	21.97	101.5	125.9	114.4	125.8	259.6	187.6
12	11.14	21.41	101.5	128.8	115.5	133.9	277.6	230.5
13	16.04	20.70	101.5	132.3	117.8	143.5	299.6	287.0
14	0	15.60	101.0	114.1	107.9	107.9	188.0	107.9
15	.445	15.19	101.0	114.1	107.9	108.6	188.2	112.5
16	1.782	14.68	101.0	114.8	108.3	111.2	192.5	126.6
17	4.01	14.14	101.0	116.2	109.1	115.5	201.4	150.3
18	7.13	13.70	101.0	118.5	110.3	121.7	215.5	226.3
19	11.14	14.05	101.1	126.3	114.5	140.2	264.2	282.4
20	7.13	20.89	101.4	124.9	113.9	125.3	253.9	187.0
21	0	40.53	102.4	136.4	121.0	121.0	315.5	121.0

TABLE 6 (cont'd) SPECIFIC POWER LOSSES in ARMATURE CONDUCTORS AND TEMPERATURE DATA

DESIGN POINT NO.	I^2R Wcm^{-3}	EDDY CURRENTS Wcm^{-3}	OIL TEMPERATURES (°F) T_1	T_2	$\bar{T}_2$	T_3	CONDUCTOR TEMPERATURES (°F) END OF MATRIX	KNUCKLES
22	.445	23.91	101.6	122.0	112.6	113.1	234.6	117.0
23	1.782	23.67	101.6	122.8	113.6	115.7	239.4	131.1
24	4.01	21.93	101.6	123.4	114.6	119.6	243.0	154.4
25	7.13	22.47	101.6	126.4	120.6	129.2	262.3	191.0
26	11.14	21.88	101.6	129.3	124.3	137.8	280.2	234.5
27	16.04	21.39	101.6	133.0	129.0	148.4	303.4	287.5
28	.445	15.31	101.1	114.3	108.3	108.8	188.9	112.7
29	1.782	15.02	101.1	115.2	109.3	111.4	194.4	126.8
30	4.01	14.68	101.1	116.8	111.0	115.7	204.4	150.5
31	7.13	14.27	101.1	119.1	113.4	122.0	218.6	183.8
32	11.14	14.00	101.1	122.2	116.7	130.2	283.3	226.8
33	16.04	13.69	101.1	126.0	120.6	140.0	262.3	279.1

Figure 23 shows the influence of speed upon the machine rating with a constant field current. From this data a plot of the loss density in the conductor versus rotor speed is given in Figure 30 for an output of 5 MVA. It can be noted from this plot that at a rotor speed of $\sim$ 8400 the loss density is a minimum. However, the output voltage decreases from 5000V to $\sim$ 3000V for a 5 MVA load.

Figure 24 shows the influence of field current upon the machine rating with a constant rotational speed. A plot of the loss density versus field current is given in Figure 31 for an output of 5 MVA at 12,000 rpm. It can be noted from this plot that at a field current of 175A, the loss density is a minimum. In this case the output voltage decreases from 5000V to 3300V for a 5 MVA load.

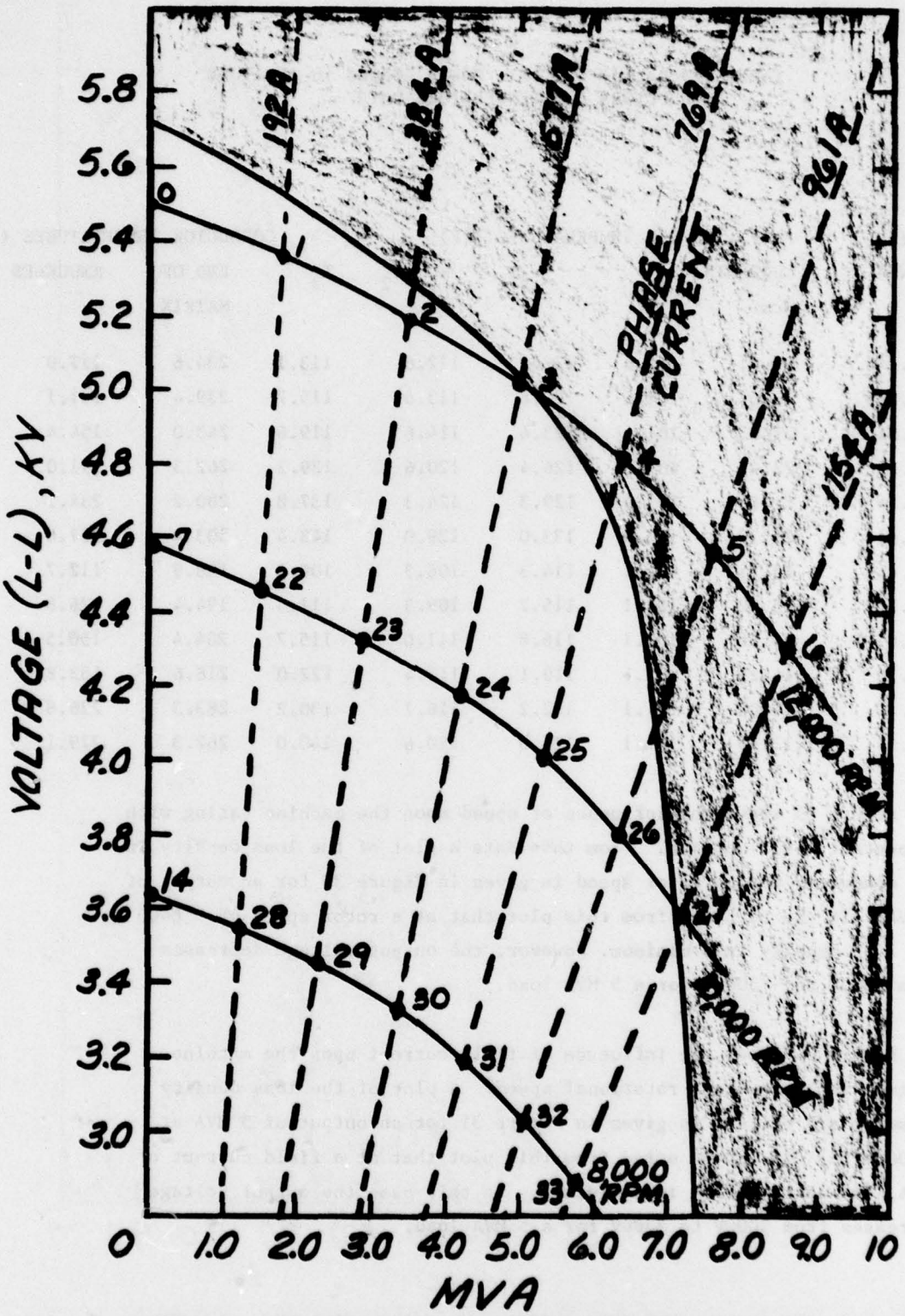


FIGURE 28 MAXIMUM STATOR HOT SPOT TEMPERATURE FOR POINT DESIGNS

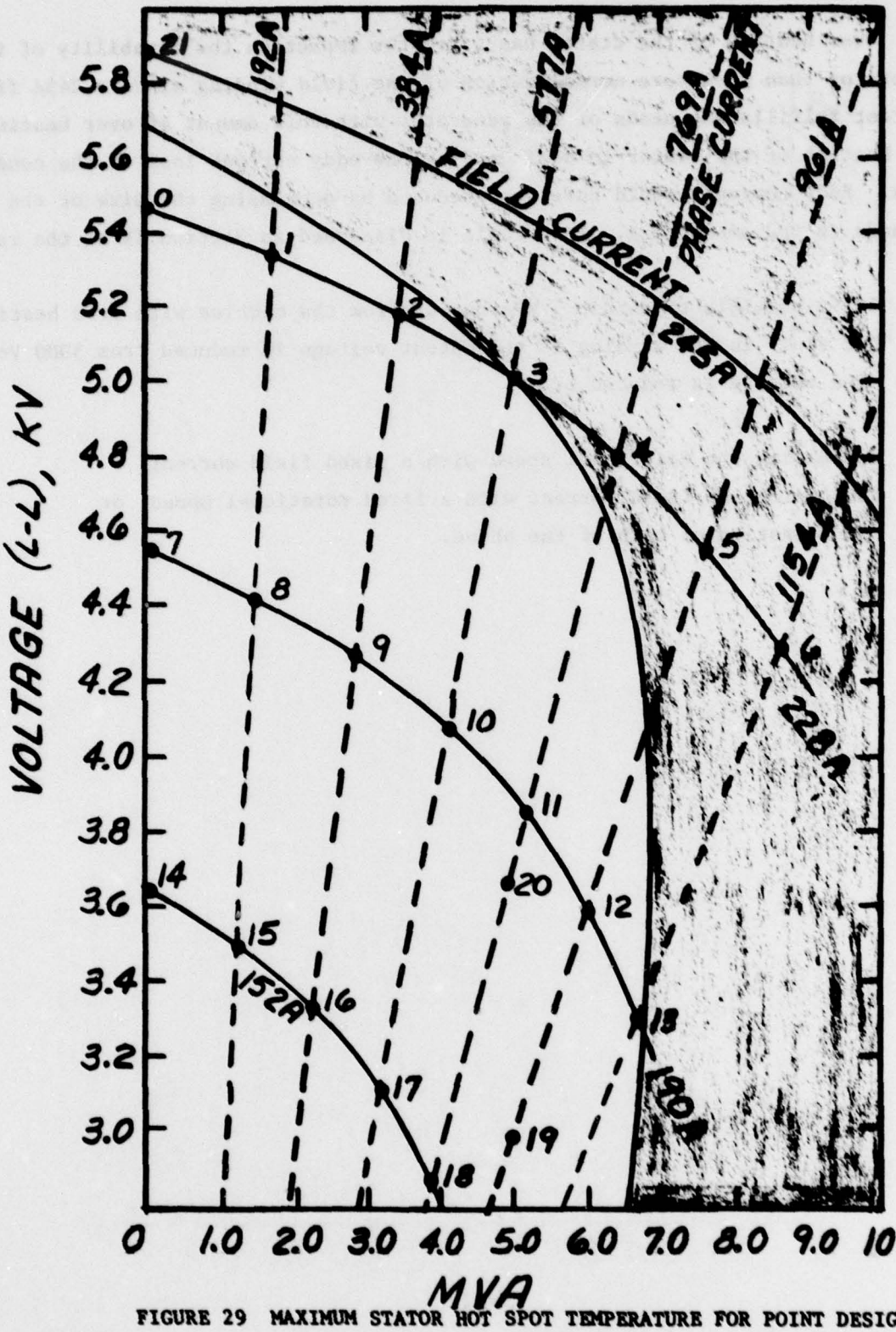


FIGURE 29 MAXIMUM STATOR HOT SPOT TEMPERATURE FOR POINT DESIGNS

Over heating of the stator has a greater impact on the capability of the generator than premature normalization of the field winding since a 245A field current fulfills the needs of the generator with this amount of over heating. The heating of the stator is dominated by the eddy current loss in the conductors. Eddy currents could have been reduced by decreasing the size of the strands in the conductors. This topic is discussed in Section IX of the report.

It is possible to obtain 5 MVA output from the machine with less heating at the "hot spot" in the winding if the output voltage is reduced from 5000 Volts L-L. The voltage is reduced by

- decreasing the rotational speed with a fixed field current,
- decreasing the field current with a fixed rotational speed, or
- a combination of both of the above.

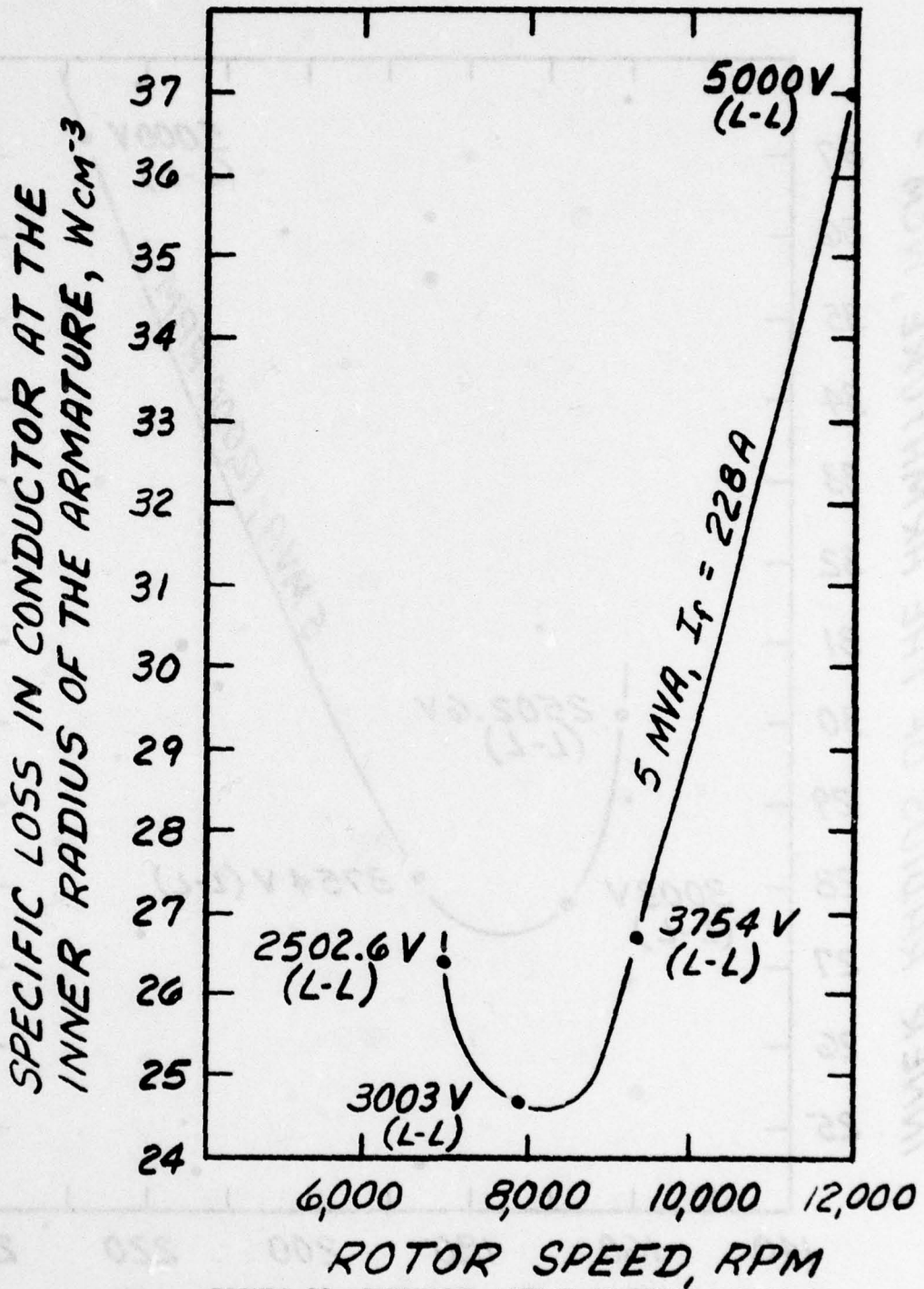


FIGURE 30 CONDUCTOR LOSSES AT INNER RADIUS OF ARMATURE FOR AN OUTPUT OF 5 MVA WITH 228A FIELD CURRENT

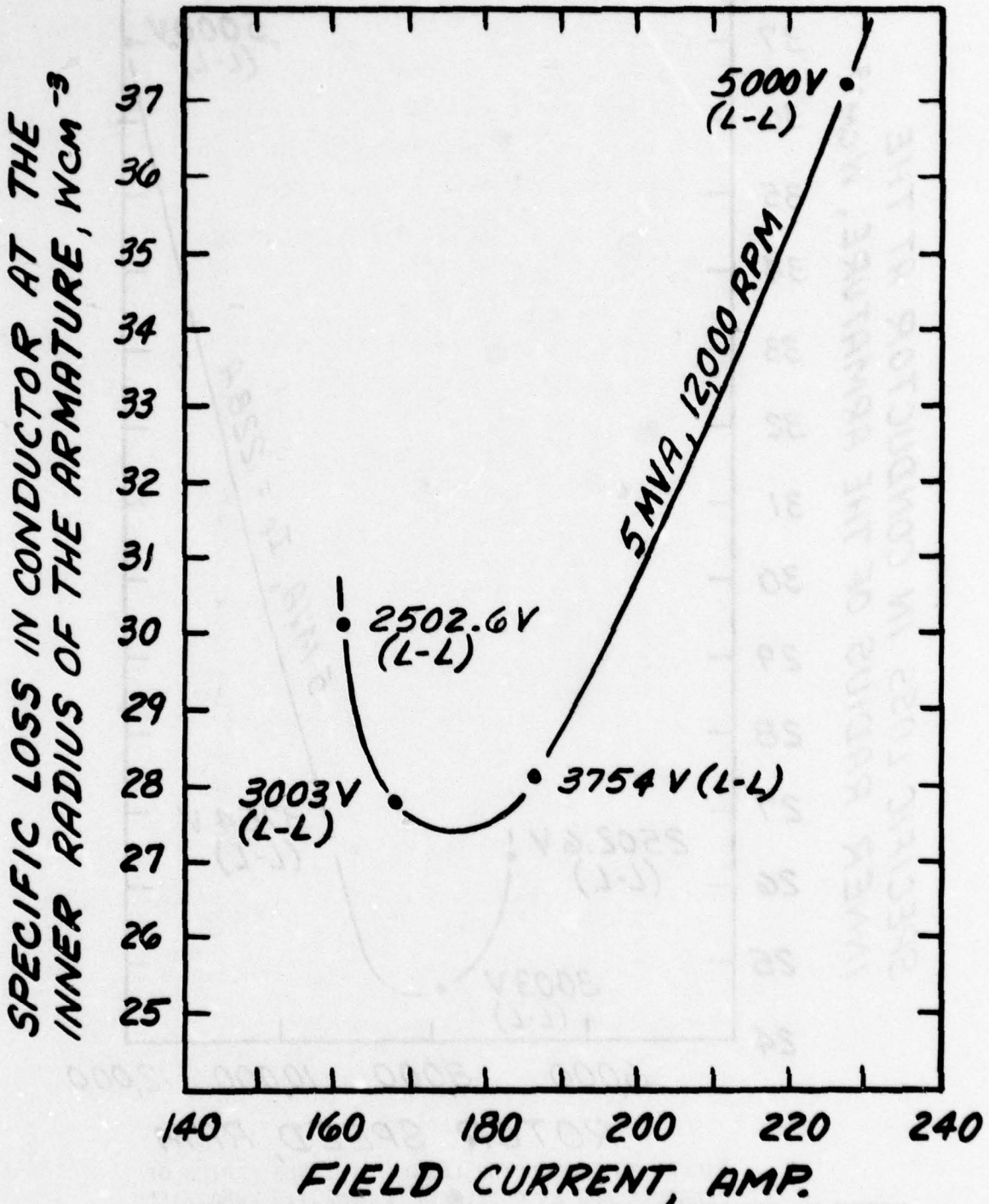


FIGURE 31 CONDUCTOR LOSSES AT INNER RADIUS FOR AN OUTPUT OF 5 MVA AT 12,000 RPM

SECTION V

ROTATING TESTS

Warm Spin-Up

The Westinghouse Research Laboratories facility for testing superconducting generators was prepared for a warm spin-up of the generator. The permanent equipment employed for this warm spin-up were:

(1) A 300 hp dc drive motor with a low-speed and a high-speed gear box that provide a 19:1 drive ratio;

(2) A panel in an adjacent instrument and control room which controls all permanent equipment on the test stand;

(3) Two ac-dc, 150 hp, 250 vdc motor generator sets located elsewhere but controlled from the panel;

(4) A stator cooling system with a 125kw oil to water heat exchanger, a 7½ hp, 3450 RPM oil pump, and oil filters;

(5) Lubrication and cooling systems for the bearings in the experimental generator and the high speed gear box;

(6) Two independent tachometers; and

(7) Automatic protection by drive motor line breakers for an over speed, a loss of stator oil flow, a loss of lubrication flow, excessive vibration, or an excessive temperature.

The instrumentation for the warm spin-up included the following:

- Accelerometers were mounted on the high speed gear box, front bearing bracket, rear bearing braket, and helium transfer seal housing. An accelerometer output was displayed either on a meter or a strip chart.

- Thermometry was provided for monitoring and displaying on a cyclic chart recorder the bearing and seal temperatures, oil inlet and exit temperatures, and stator conductor temperatures.

- Slip ring inputs and outputs for sensors within the rotor were checked for continuity and operation.

The first test consisted of a warm spin-up to 6000 RPM. During this spin-up the temperature of the bearing and seal on the out-board end of the excitation slip ring shaft increased rapidly as the speed increased and did not reach equilibrum at 6000 RPM. The spin-up to design speed (12,000 RPM) was aborted and the following changes were made:

- The deep-groove bearing with a stamped ball-piloted retainer was replaced with high precision angular-contact bearing with a phenolic retainer;
- A jet was added to supply oil between the in-board side of the bearing and the out-board side of the oil seal;
- An oil scavange port was added between the bearing and seal; and
- The outer diameter of the oil flinger adjacent to the seal was decreased to allow more oil to splash onto the seal surface.

During the second warm spin-up. The speed was increased up to the operating speed of 12,000 RPM while checking the vibration and the general operation at intermediate speeds of 150, 2000, 4000, 6000 and 8000 RPM. The vibrations observed on the bearing housings were acceptable, 4 mils peak to peak maximum with maximum vibration occurring at 9400 RPM. The level of vibration on the helium transfer bayonet was excessive. This bayonet was not connected to the external transfer line. Thus, the 2.5 pound bayonet over hung the seal housing by 11.2 inches and imposed a moment of 8.5 in-lbs upon the housing. This over hang caused excessive vibration as observed by placement of one's hand around the union.

After a short period of time at 12,000 RPM an unusual noise was heard. The power relay to the dc motor was opened and the motor, gear box, and generator were allowed to coast for 35 seconds down to approximately 6400 RPM. The noise continued during this run down. Therefore, the voltage was decreased and the relay was closed to cause a rapid deceleration of the machine (12 seconds).

Inspection of the site immediately after shut down revealed the high speed gear box was hot. Oil vapor and an the odor of over heated phenolic material was present at the oil drain line. Subsequently, the gear box was disassembled and it was found that a duplex set of angular-contact bearings had failed. These bearings supported the high speed shaft on the motor side of the gear box. Repair of the gear box consisted of requalifying the bearing journal, replacement of all of the bearings in the gear box, replacement of the slip ring coupler, and replacement of the instrumentation leads between the slip ring and the connectors on the generator side of the gear box.

It was concluded the bearing failure was caused by a thrust load produced by restrained axial motion in the splines on the spindle. The splines were lapped to remove the high points and the edges on the teeth. Provisions were incorporated on the spindle for injection of grease into the splines teeth periodically.

A leak check on the rotor and the bayonet device was performed during gear box repair period. The bayonet device failed this test and was disassembled. The internal helium passage was replaced with new tubes and brazements. Failure of these parts was caused by the excessive vibration observed during the previous spin-up. It was concluded from this experience that failure of this bayonet will occur unless it is connected to the transfer line and supported from a pedestal designed for this duty.

A leak test was performed on the pump-down valve before it was opened. A leak was found in the bellow and the valve was removed from the rotor. The bellow connections were resoldered. Subsequently, the valve operated satisfactorily during several leak checks on the rotor.

A leak test on the vacuum space within the rotor revealed a leak in an external conduit for instrumentation leads. An epoxy sealant was applied and then the conduits were wrapped with graphite fiber material. Finally, the entire array of conduits was wrapped with glass fibers and epoxy to provide a self supported structure.

The next warm spin-up to 12,000 RPM was performed with the helium transfer system connected to the generator and supported in a manner appropriate for the cold test. The vibration at the bearing housings (measured as G's) was approximately 4 times higher than observed (measured in displacement) during the previous run. An investigation revealed the alignment between the generator and the gear box was off by .030 inches. The alignment of gear box was corrected and the rotor was run up to 12,000 again. This decreased the "g" level by approximately 25% at 12,000 RPM. However, the output from the transducers measured in "g's" did not agree with the vibration when measured in dispalcement. Filters were added to the vibration instrumentation to filter out the low frequency and the high frequency components. It was found the the high "g" output from the transducers was due to very high frequency components (above 1000 Hz). With the filters the "g" levels of vibration were satisfactory for continous operation at 12, 000 RPM.

Rotor Cool-Down

The test site shown in Figure 32 and 33 was prepared for cool-down and the no load tests by incorporating the helium management system. This cryogenic system was composed of three sub-systems: logistics, helium flow circuitry, and liquefaction. Helium logistics consisted of four 500-liter shuttle dewars which were used to transport liquid helium from an external supplier and from the internal liquefaction system.



FIG. 32 Test Site

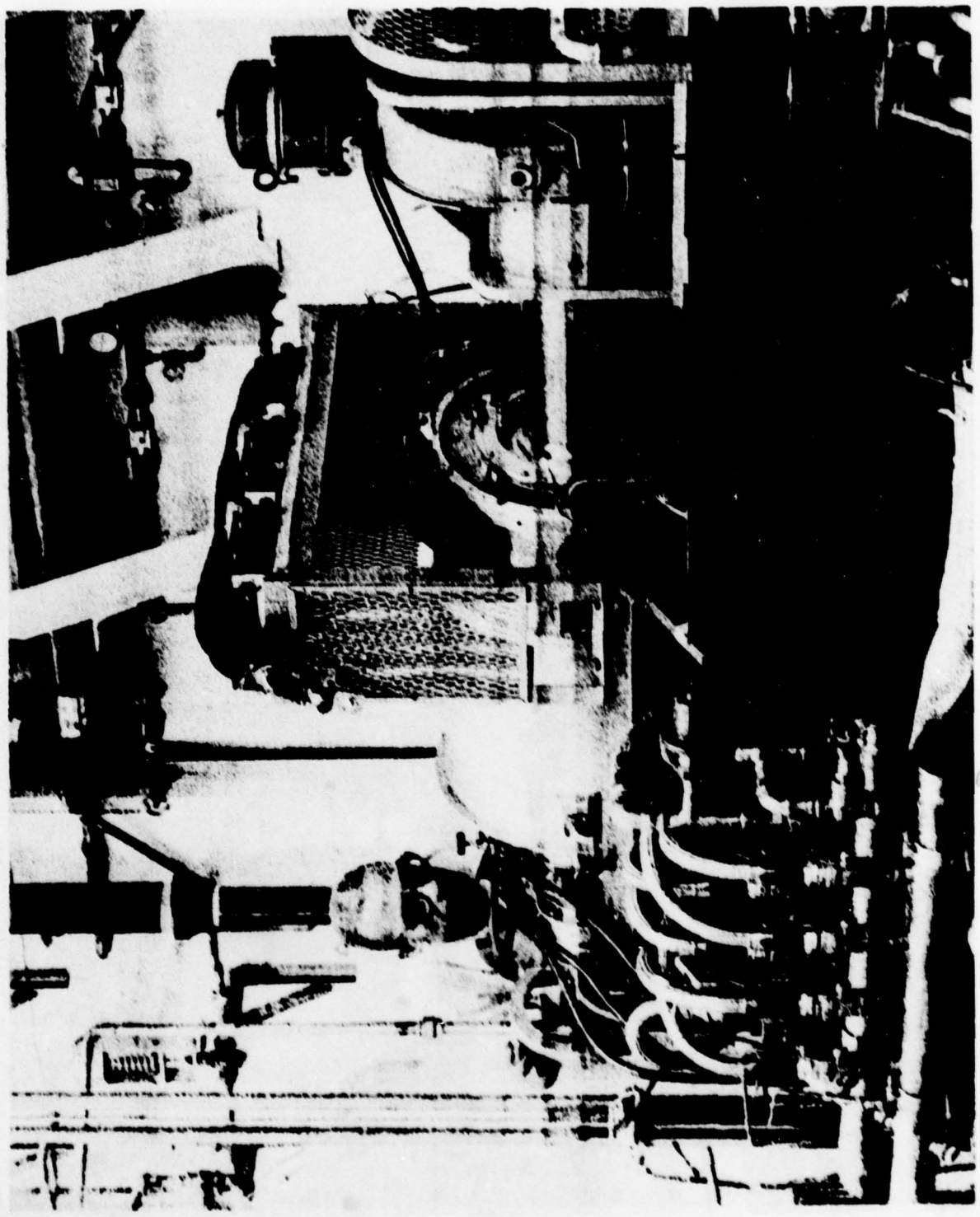


FIG. 33 Generator on Test Bed

The circuit started with two independently controlled 250-liter helium storage dewars connected to a heat exchanger (cryo-exchanger). These two dewars, once connected to the cryo-exchanger remained connected and were refilled in place from a 500-liter dewar. All other bayonets once connected to the cryo-exchanger remained intact. This procedure minimized the danger of collecting ice particles in the input valves and Joule-Thompson valves of the unit. The cryo-exchanger was connected to the input bayonet of the generator through its rotating seal assembly. Figure 1 shows the transfer line and the seal system. There was an additional inlet to the cryo-exchanger to which a 100-liter helium dewar was connected to supply supplemental helium for the bath of the main stream heat exchanger. This feature negates main stream flow fluctuations when the system operates in a subcooled mode and when the flow rate is high or low.

The helium flow sequence of the supply circuit was as follows (see Figure 34). Pressurization of either of the 250-liter dewars and the opening of its corresponding manifold valve allowed the helium to enter a counter flow heat exchanger unit which was cooled by the gas vented from the bath. Next the stream passed through the main stream exchanger located at the very bottom of the inner volume of the cryo-exchanger and into the rotating seal assembly. However, just before it enters the exit bayonet's housing, a portion of the stream, was diverted if necessary, through a J-T valve into the bath volume to replenish it. Filling the bath this way was an alternative to using the 100-liter dewar supply system.

Exhausts from the rotor occurred within the bore of the stator and from the seal housing with the latter representing the flow from the current leads and the former representing the remainder of the helium flow. An additional exhaust from the bath in the cro-exchanger existed, also. The circuits for the exhausts are shown in Figure 35. The flow from the bore of the stator bore and flow from the leads were collected in separate circuits and diverted through flow meters. Subsequently, all exhausts were collected in a common circuit.

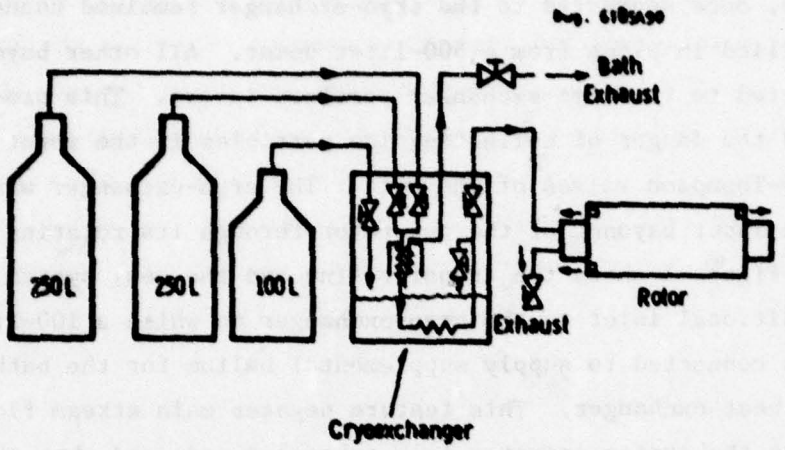


FIGURE 34. Helium Supply System

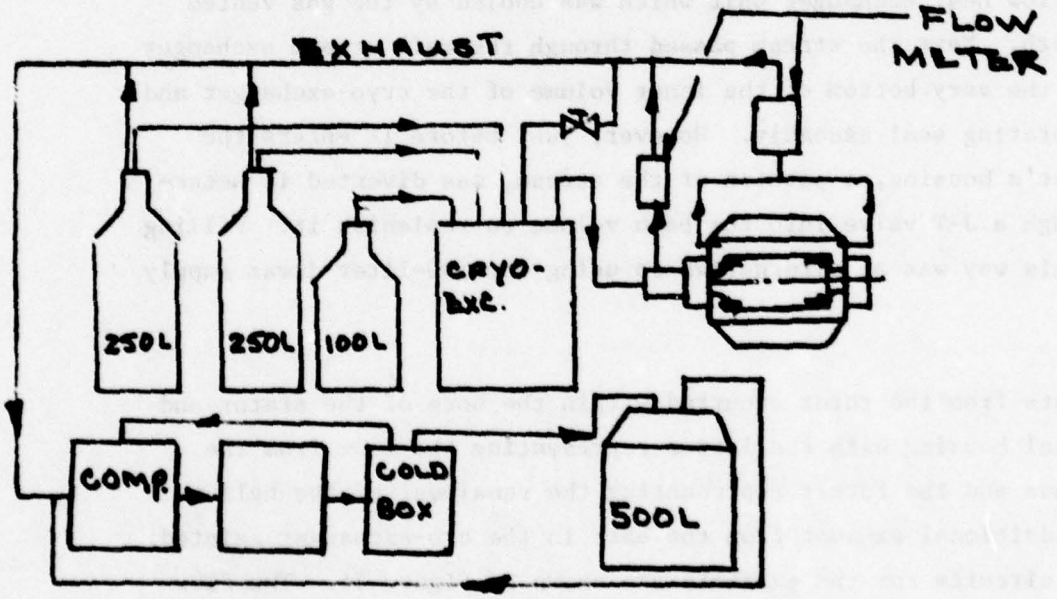


FIGURE 35. Helium Exhaust Circuits

The exhaust flow then entered the compressor and oil removal system for the liquefaction unit shown in Figure 36 and 37. This unit has a capacity of 30 liters per hour and the liquid produced was collected in a 500-liter dewar. This recycled helium was used to replenish the 250-liter dewars. In many instances the combined flow rates through the cryo-exchanger did not match the capacity of the liquefaction unit. In this situation warm helium was vented into the room by way of pressure relief valves in the exhaust lines from the generator. In addition, the gas storage tank between the compressor system and the cold box was maintained below a set pressure by venting into the room.

Instrumentation for the external helium management system was concerned mainly with the cryo-exchanger (Figure 38). There were eight resistance thermometers and eight gas bulb thermometers. A gas bulb thermometer was used to monitor nitrogen temperatures during the cool-down of the cryo-exchanger cryostat. The other thermometers were used to monitor various points along the helium flow circuit. All of the resistance thermometers were of the four-terminal type and were either one-tenth watt carbon resistors or commercial germanium thermometers. They were all calibrated against a standard thermometer which has a certified calibration. At operating temperatures their accuracy is better than 0.1°K. Thermometers in the cryo-exchanger were used to monitor its inlet, outlet and bath temperatures. The units in the inlet and outlet transfer lines indicated the rise in temperature of the main stream helium, due to heat leaks through the lines, joints and rotating seals as it transversed through the circuit. The voltage across any of these thermometers was cabled and connected to a rotary selector switch whose output was read on a digital voltmeter.

Figure 39 shows the location of the three types of helium level indicators which were utilized. One type senses change in capacitance due to helium density, and was located in each of the 250-liter dewars and in the cryo-exchanger. This type was calibrated to perform in two

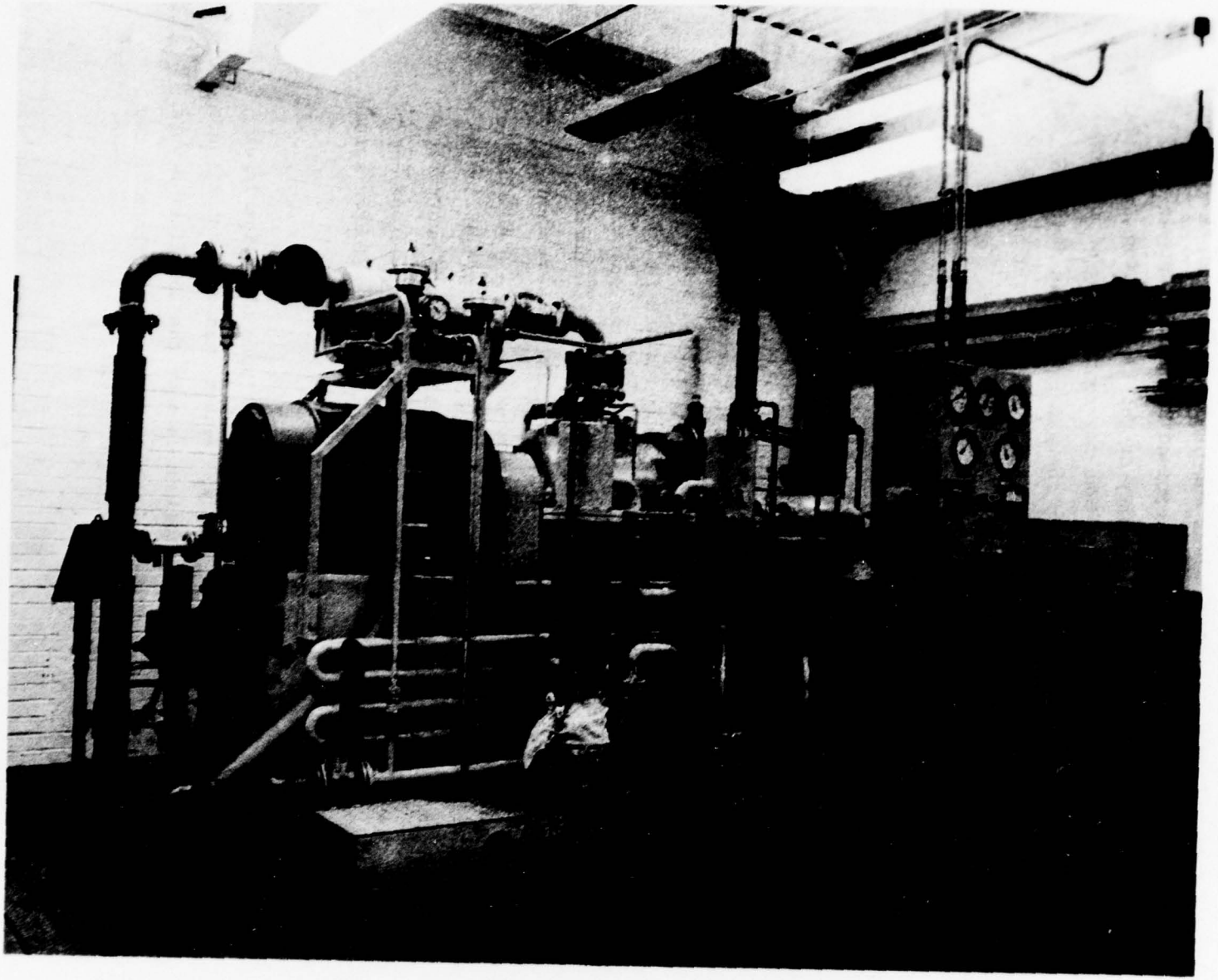


FIG. 36 Compressor and Oil Removal System

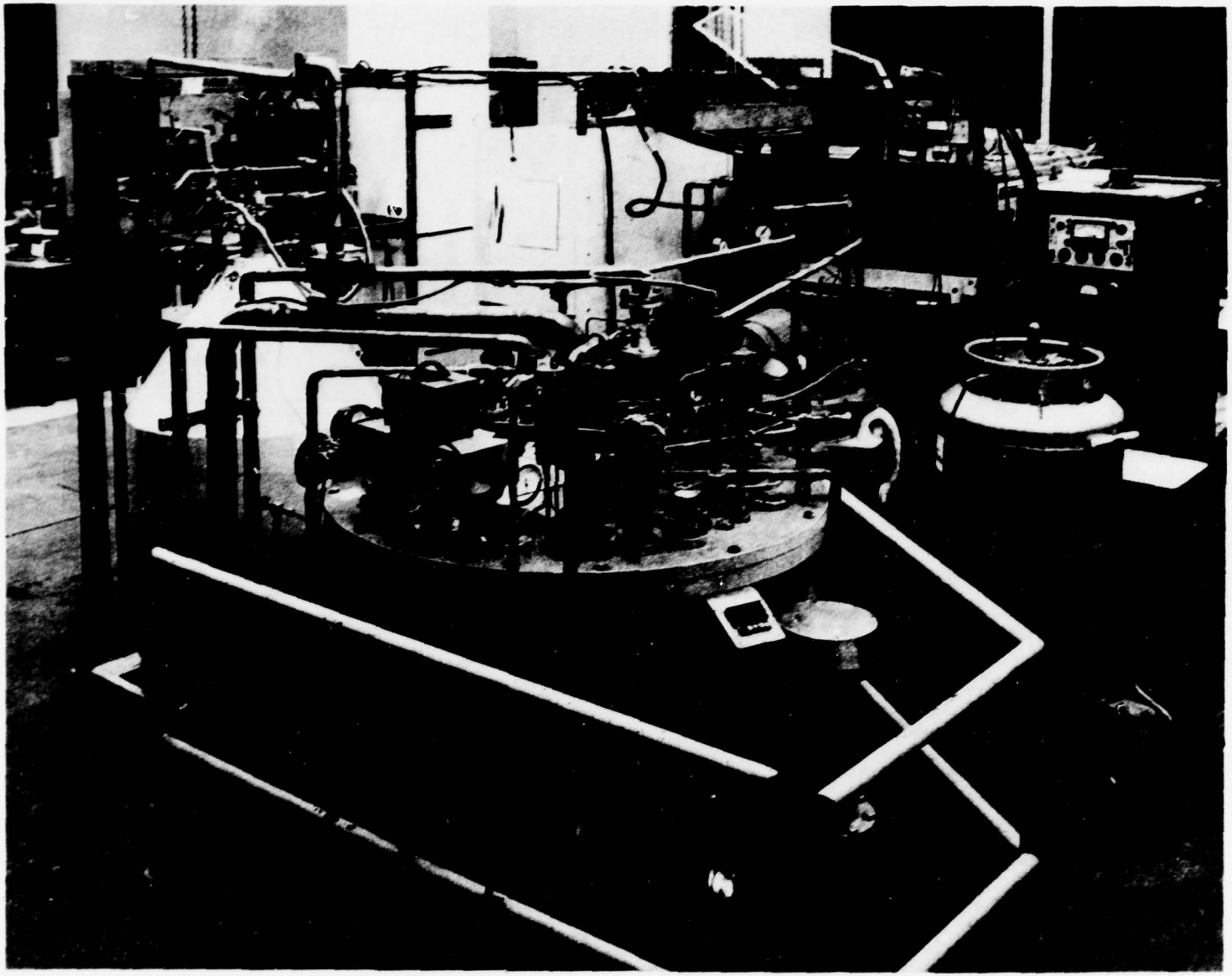


FIG. 37 Cold Box

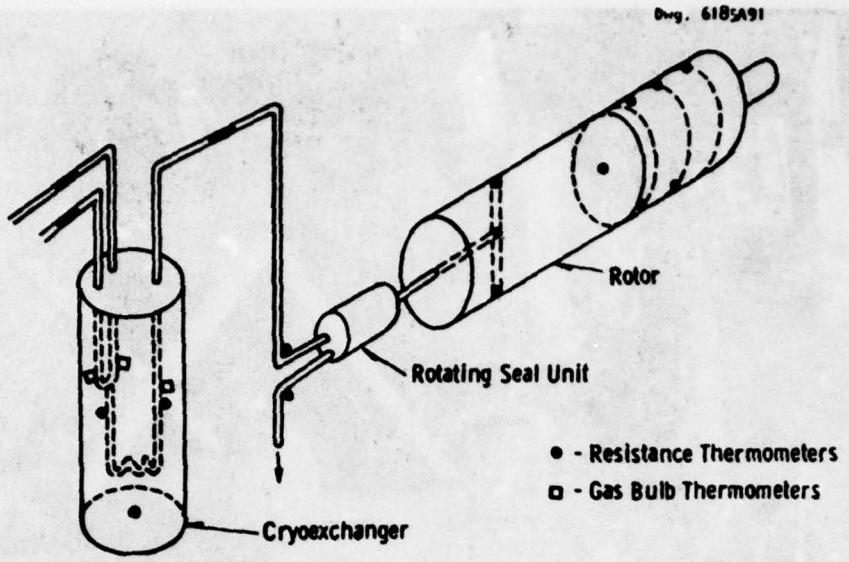


FIGURE 38 SCHEMATIC LOCATION OF HELIUM STREAM THERMOMETERS

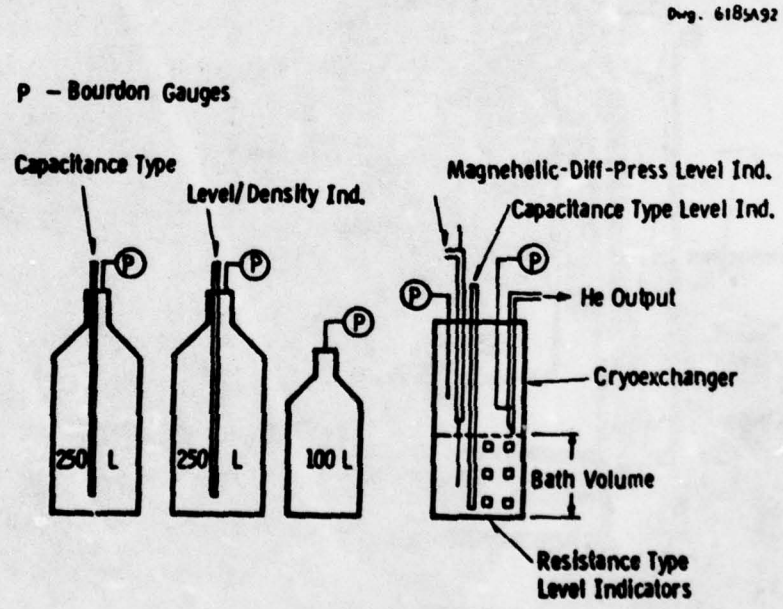


FIGURE 39 LOCATION OF HELIUM LEVEL AND PRESSURE INDICATORS

modes. When operating in subcritical helium where there was no distinct liquid level or phase interface, it measured the average helium density as an indication of helium quantity.

Another type of level indicator consisted of a calibrated length (50 cm) of superconducting wire whose ratio of normal to superconducting lengths is displayed by a pointer scale to indicate level calibrated to read the level at 4.2°K and 3.5°K through a bridge measuring circuit. The third type of level indicating device was the Magnahelic or differential pressure gauge.

Five Bourdon-type pressure gauges (Figure 39) were used to indicate the pressures within the storage dewars, over the helium bath in the cryo-exchanger, and at the inlet of the rotor.

Rotor cool-down was initiated with liquid nitrogen through a temporary transfer line. Subsequently, liquid helium was introduced and the temperatures of the rotor and the resistance of the field winding were monitored for twelve hours. During this time the temperatures within the rotor did not decrease below 65K and reached this equilibrum approximately 8 hours after liquid helium was introduced. The rotation of the rotor was stopped and the vacuum pump was connected to the pump-down valve. When the valve was opened the vacuum pump was deluged by gas flowing out of the rotor. This demonstrated that a leak had developed in the rotor and allowed the vacuum space to become filled with gas.

The loss of vacuum produced an excessive heat influx which explains why the rotor could not be cooled down to a superconducting state. Transfer of liquid helium was terminated and warm-up of the rotor was accelerated by introducing warm nitrogen gas. During the warm-up period the vacuum space in the rotor was pumped-down and back-filled with

nitrogen several times to remove the helium gas from the vacuum space and increase the sensitivity of the helium leak detector. Four hours after warm-up was initiated helium gas was introduced in the transfer line. At this time the leak detector indicated a leak from the helium compartment into the vacuum space. This leak test was repeated nine hours after warm-up was initiated. By this time the vacuum pump had reduced the pressure in the rotor to 1×10^{-5} mm Hg or less and the leak detector did not indicate a helium leak when helium gas was introduced into the rotor.

A series of leak tests were performed after the rotor was removed from the stator to establish the nature and location of the leak. From these experiments the following facts were established.

1. With a warm rotor, the vacuum space could be pumped down to 10^{-5} mm Hg or less.

2. With a warm rotor and with closure of the pump down valve on the rotor, the pressure within the rotor did not rise above 10^{-5} mm Hg over a 12 hour period.

3. Introduction of cold nitrogen gas through the central transfer tube caused the pressure in the vacuum space to increase from 10^{-5} to approximately 10^{-3} mm Hg over a 4 minute time period.

4. Cooling the central transfer line with a stopper (a moveable plug) at the inboard end of the central transfer tube caused a leak. In this experiment the pressure in the vacuum space increased as noted for the previous case. The central tube was cooled with cold nitrogen gas from a small tube inside the central tube.

5. The leak detector did not indicate a helium leak when helium gas was introduced up stream of the plug even though the pressure rise indicated the fault was leaking.

6. The leak detector indicated a leak when helium gas was introduced downstream of the plug and the central transfer line was cold. Experiments 6. and 7. demonstrated the fault is not in the wall of the transfer line but at some point outside of the tube.

7. The cooling time required for the fault to leak was a minimum (approximately 2 minutes) when the plug was located at or beyond the point where the tube passes through the bulk head for the the winding compartment.

8. When the plug was moved forward of the bulkhead by approximately one inch, cooling times of 6 minutes did not cause the fault to leak. Experiments 7. and 8. demonstrated that the leakage through the fault is strongly influenced by the radial contraction of the tube and the bulkhead since axial contraction of the long tube did not cause the fault to open when the plug was upstream from the bulkhead.

9. The time required for the fault to open was low (2 to 3 minutes) when the cooling was concentrated at the point where the tube passed through the bulkhead. This data and experiment 6. indicated that the fault is in the bulkhead and probably close to the central tube. If the fault were not located in the bulkhead a longer and greater degree of cooling would be required to cause the fault to respond to temperature.

10. The response time of the helium leak detector did not change when the helium gas was introduced by different but identical routes. For example, the response time was the same for both current lead conduits, the same for both the small cooling coils on the thermal transition tube, and the same for both of the large coils. These experiments show the fault was not located in these tubes or close to points where they penetrate the bulkhead. If it were at one of these locations the response time of the helium leak detector would have been lower when that particular passage was used for introducing the helium gas.

These experiments indicated the fault was located in the bulkhead near the penetration of the central helium transfer tube. Two joints were employed to attach the tube to the bulkhead. Both of these joints were primary candidates for the leak and a procedure for repair of this kind of internal leak was defined.

SECTION VI
ROTOR REPAIRS

Cold Leak at Bulkhead and Central Transfer Line

A review of the design considerations for the central helium transfer tube was made. Originally, Invar was selected for this tube since the thermal contraction of this alloy on cool-down did not cause an excessive axial stress in the tube even though the outer tube remained at room temperature. This option was selected over stainless steel for both tubes and incorporation of a bellows to accommodate the thermal contraction of the inner tube during cold-down. Based upon our experience with the first cool-down it appeared that joining the Invar tube to the bulkhead through a weldment of a stainless steel sleeve and a brazement of the sleeve to the Invar tube was a problem. This problem is intensified by the rotating stress in the bulkhead and any axial stress in the tube.

It was concluded that a repair of the internal leak could be performed and at the same time improve the design of the central transfer line. The improvement consisted of an Inconel tube for both the transfer tube and the warm outer tube. The inboard end of the transfer tube would be welded to an Inconel flange which would in turn would be welded to the bulk head. This flange would surround the previous faulty joint. An Inconel bellows would be incorporated to accommodate the relative thermal contraction of the warm structure and the cold inner tube. The modification of the rotor for incorporation of the improved design is shown in Figure 40.

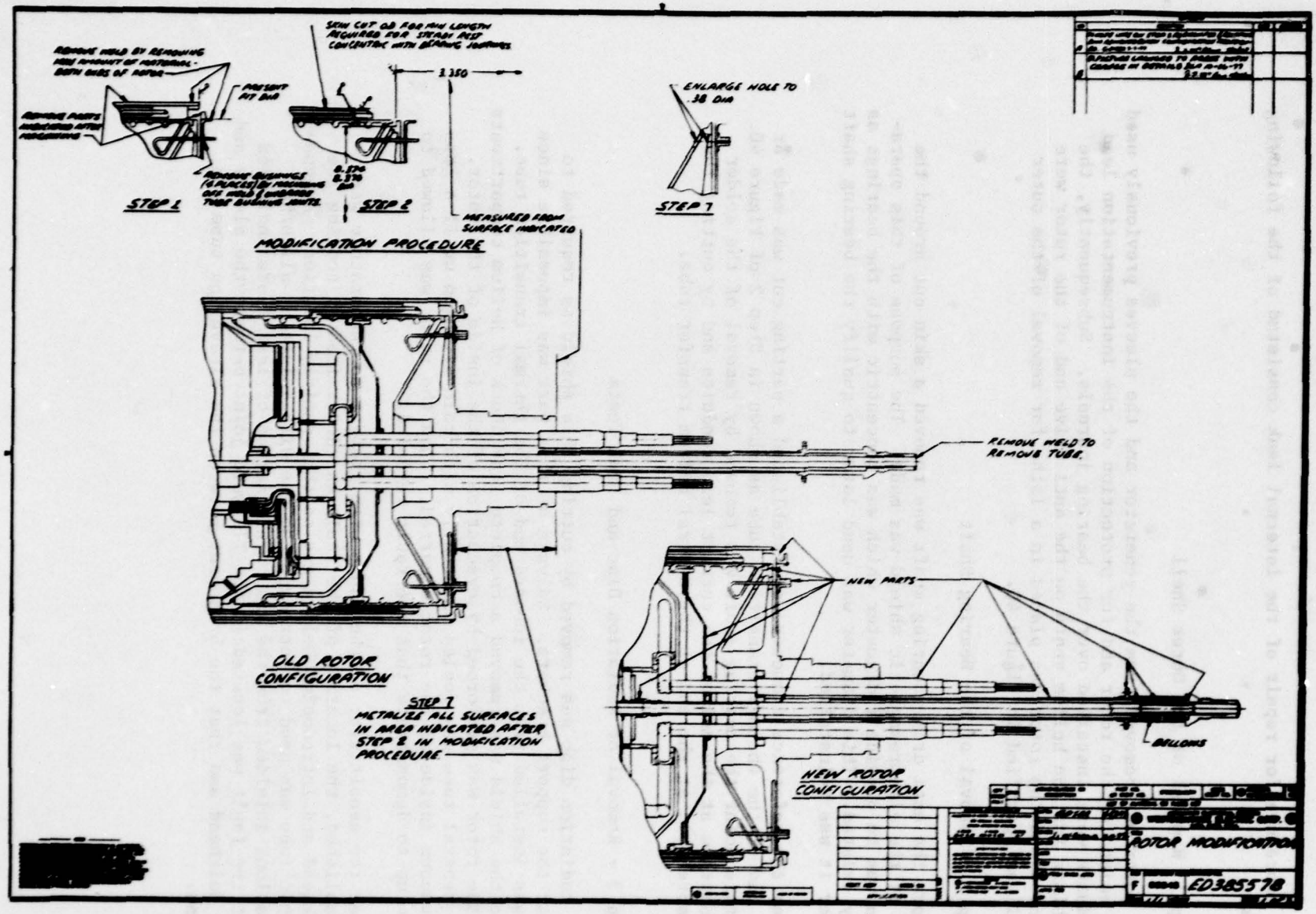


FIGURE 40. Rotor Repair Drawing for Internal Transfer Line

The procedure for repair of the internal leak consisted of the following task:

Step 1 Removal of the Outer Shell

The rotor was removed from the generator and the sleeves previously used for balancing the rotor and for protection of the instrumentation lead conduits were installed over the bearing journals. Subsequently, the bushings for the helium vents on the anti drive end of the rotor were removed and the rotor was placed in a lathe for removal of the outer shell as specified in Figure 40.

Step 2 - Removal of the Bearing Shaft

Before the anti drive bearing shaft was removed a skin cut around the end of the electromagnetic shield was made. The purpose of this operation was to provide a diameter which was concentric with the bearings as they existed. This diameter was used later to qualify the bearing shaft after it was reinstalled.

After the reference diameter was established a parting cut was made at the end of the thermal transition tube as shown in Step 2 of Figure 40. At this point the bearing shaft was removed by removal of the solder connection at the end of the current lead conduits and by cutting the closure weld at the end of the central helium transfer tube.

Step 3 - Removal of Radiation Disc and Leak Tests

The radiation disc was removed by cutting this shield as required to clear the support brackets. Salvage of this part was impossible since it was installed from the inboard end of the thermal transition tube. Once the shield was removed a complete leak check of helium compartments in the rotor was performed by evacuation of the inside of the rotor. The central tube was cooled externally with cold nitrogen until a loss of vacuum inside of the rotor occurred. Then the rotor was allowed to warm up to demonstrate that the fault resealed.

After the sensitivity of the fault with respect to temperature was established, the location of the fault was determined by cooling the bulkhead and introducing helium gas at the specific location. A hypodermic tube was used to introduce the gas with joints at all other locations shielded from the gas. This series of leak tests indicated that the fault was located in the TIG weld joint between the sleeve and the bulkhead and that the brazement between the sleeve and tube was sound.

Inspection of the bulkhead indicated why this joint failed. It can be noted in a photograph, Figure 41, of the bulkhead with the radiation shield removed that failure of a support clamp for one of current lead conduits occurred under rotation (12,6000 RPM max.)

Failure of this clamp caused the support system to move off-axis and bend (deform) the central helium supply tube. Subsequently, the central tube held the other conduit and prevented further off-axis movement of this conduit. Hence, failure of the joint between sleeve on the tube and bulkhead was probably caused by the failure of the clamp.

Step 4 - Repair of Transfer Line

The repair of the transfer line was accomplished by replacement of the Invar, 3/8"OD x .010" wall tube with a 3/8" OD x .030" wall Inconel tube. The inboard end of the tube was welded to a flange which in turn was welded to the bulk head. This new flange surrounded the existing sleeve on the original Invar tube.

Thermal contraction of the central tube relative to the warm structure was accommodated by concentric, telescopical tubes on the outboard end of the 3/8" OD tube as shown in Figure 40. Sealing of this union was provided by a bellows. The bellow material was Inconel with an OD and ID of 0.535 and 0.376 inches, respectively. The inside tube was Inconel with an OD of 0.312 inches and a 0.010 wall. A new spool, similar to the old spool, was made of Inconel to accommodate this union.

Step 5 - Replacement and Rework of Parts

Parts, such as the radiation disc, were made to replace the parts which were not reusable. This rework included installation of a new support for the current leads as shown in Figure 42. The other new parts incorporated into the final condiguration are shown in Figure 40. All new tubes, welds, and solder joints were cold leak tested in an organized sequence to insure that all parts and joints were sound.

Step 6 - Rotor Balance and Leak Check

The rotor was balanced after the repair was completed and a final leak test was performed before assemblage of the rotor into the stator. This test indicated a leak from the helium compartment into the vacuum space. This leak was isolated to be within the field winding compartment.

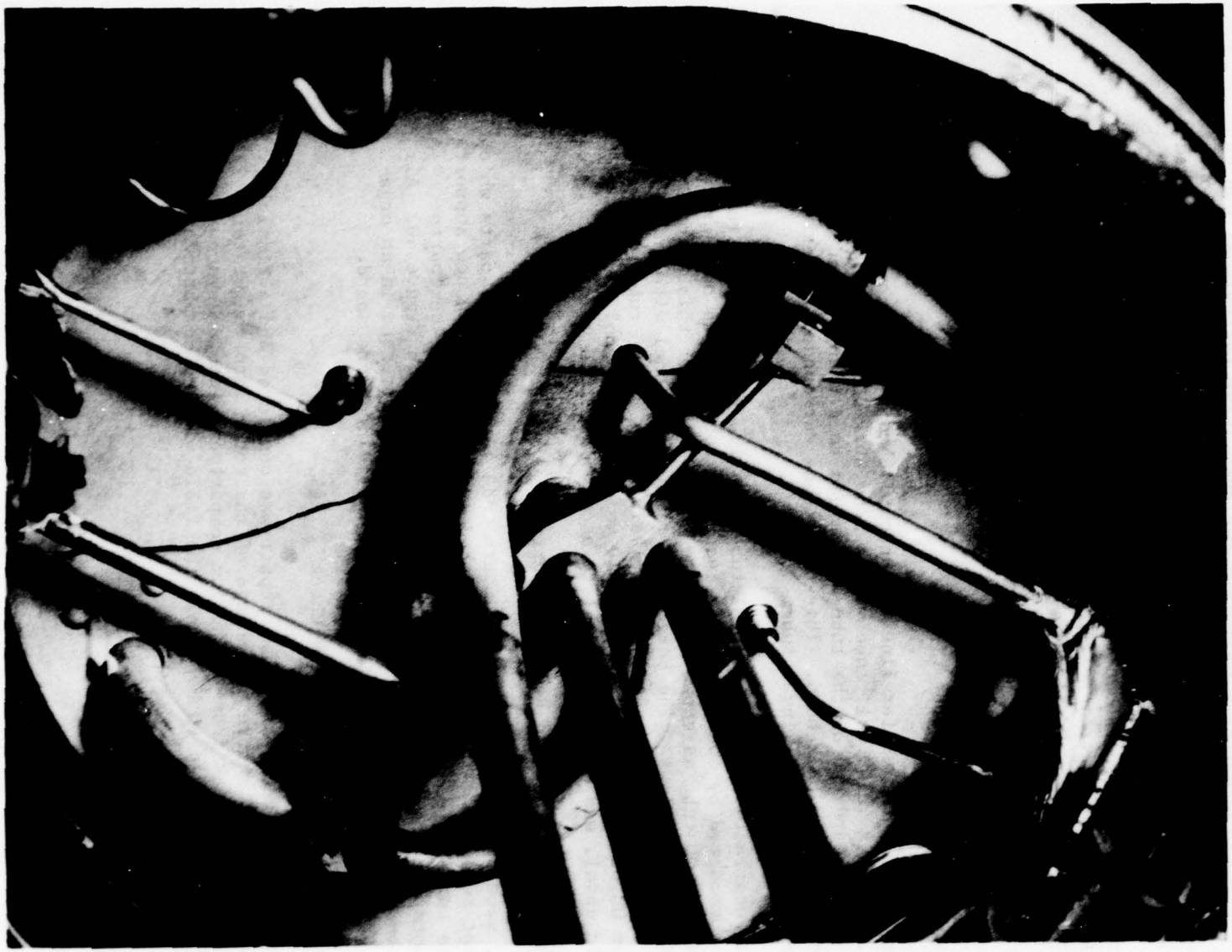


FIG. 41 Failure of Support Clamp for a Current Lead Conduit

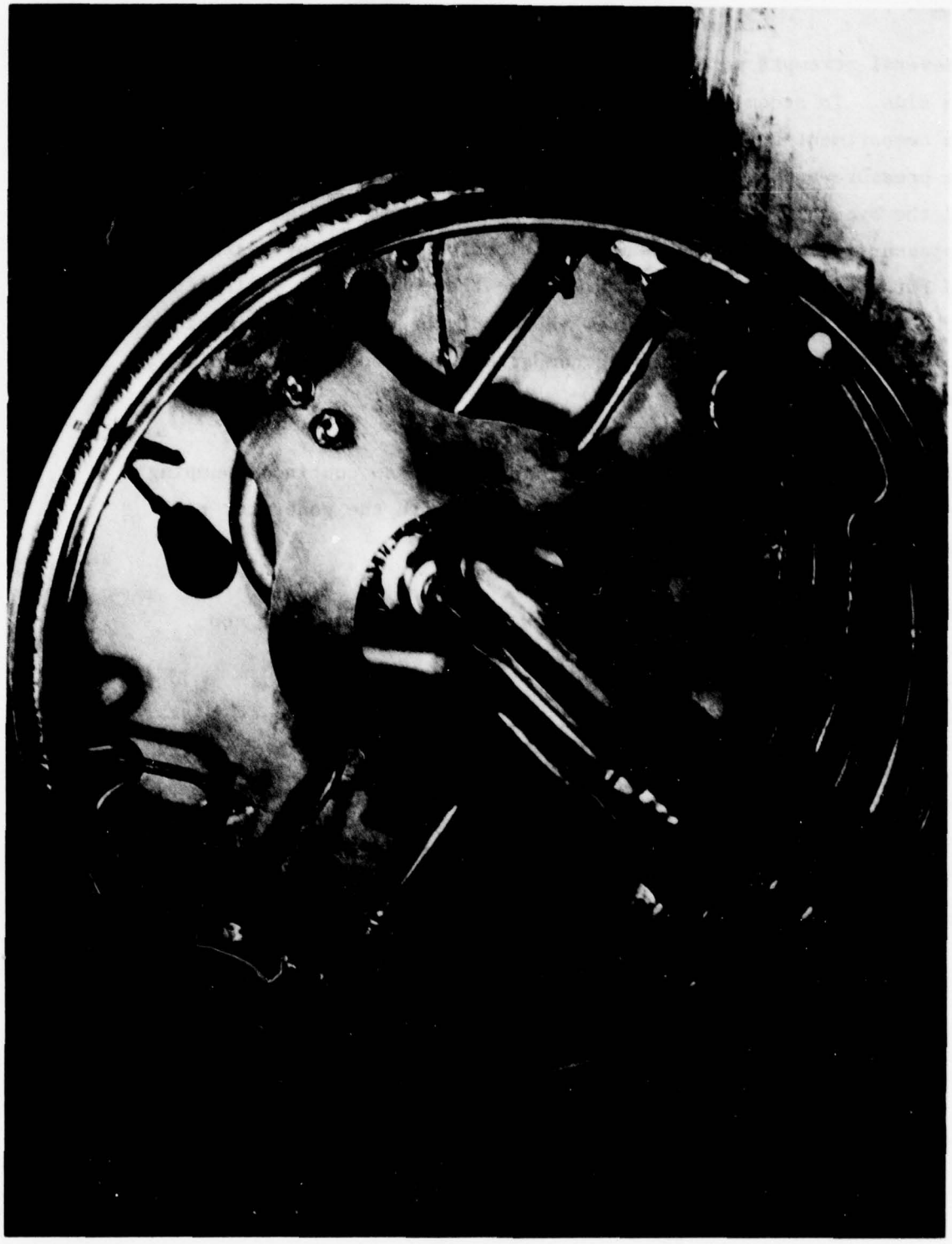


FIG. 42 New Support for Current Leads

Incorporation of Continous Pumping on the Vacuum Compartment

Several attempts were made to seal the leak with a resin from the helium side. To accomplish this, the resin was introduced into the helium compartment until the fault(s) was sealed as observed by the vacuum pressure and by a helium leak detector. Once the fault was sealed the excess resin was drained and flushed from the compartment with pressurized gas. Subsequently, the resin was cured by heating the entire rotor to 200°F for 24 hours. These treatments were satisfactory with the rotor at room temperature. However, the resin did maintain a seal of the fault when the winding compartment was cooled to liquid N_2 temperature.

It was decided to modify the test insulation so continous pumping on the vacuum compartment could be maintained with the generator rotating. This was accomplished by:

- replacement of the pump-down value with a union for connection of a 3/8 inch, stainless steel tube;
- enlargement of the bore in the high speed shaft to accommodate the pump-down line; and
- installation of a Ferrofluidic seal and a vacuum pump.

The configuration of continous pumping system is shown in Figure 43 and a photograph of the installation from behind the gear box is shown in Figure 44.

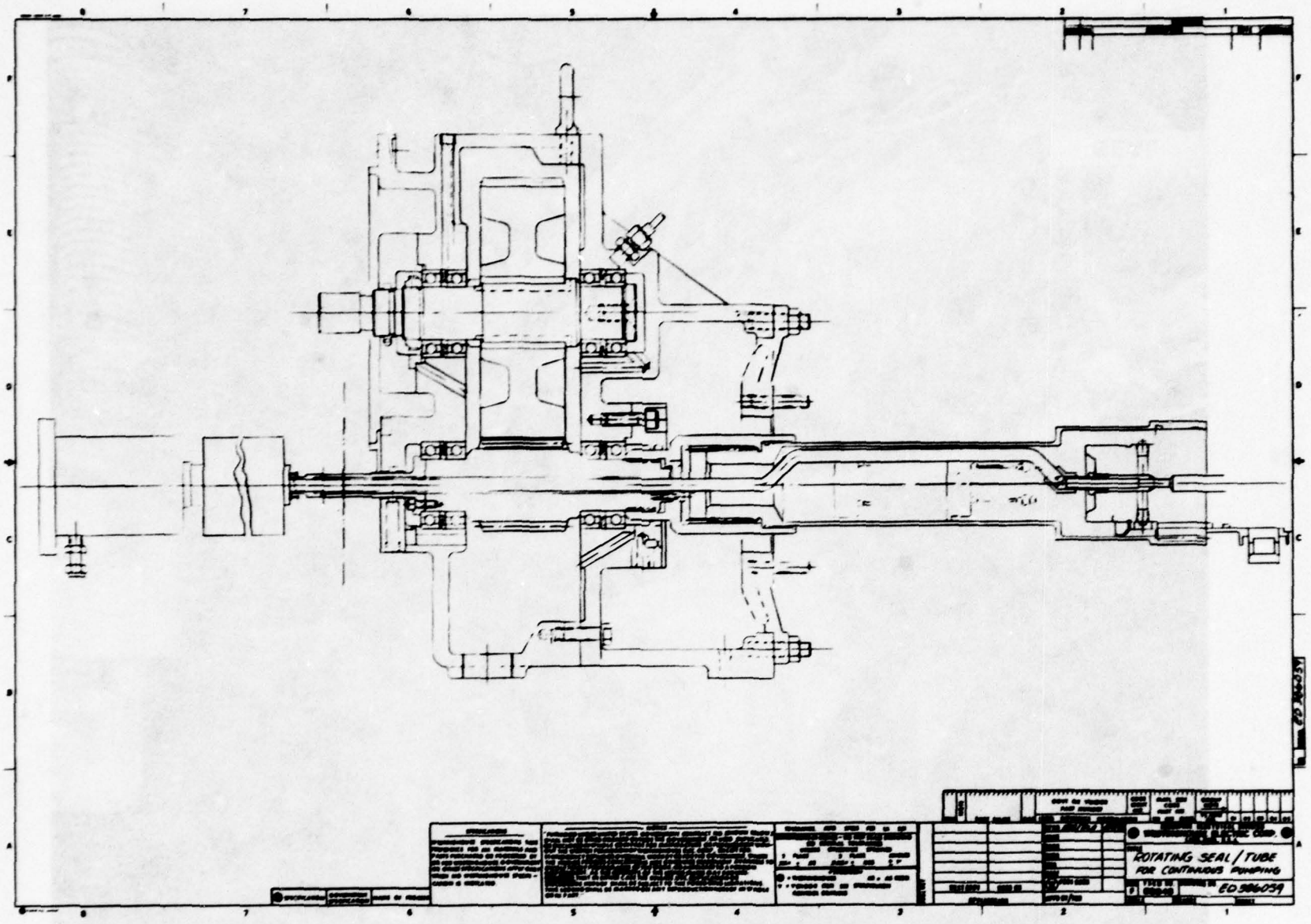


FIG. 43 Configuration of Continuous Pumping System

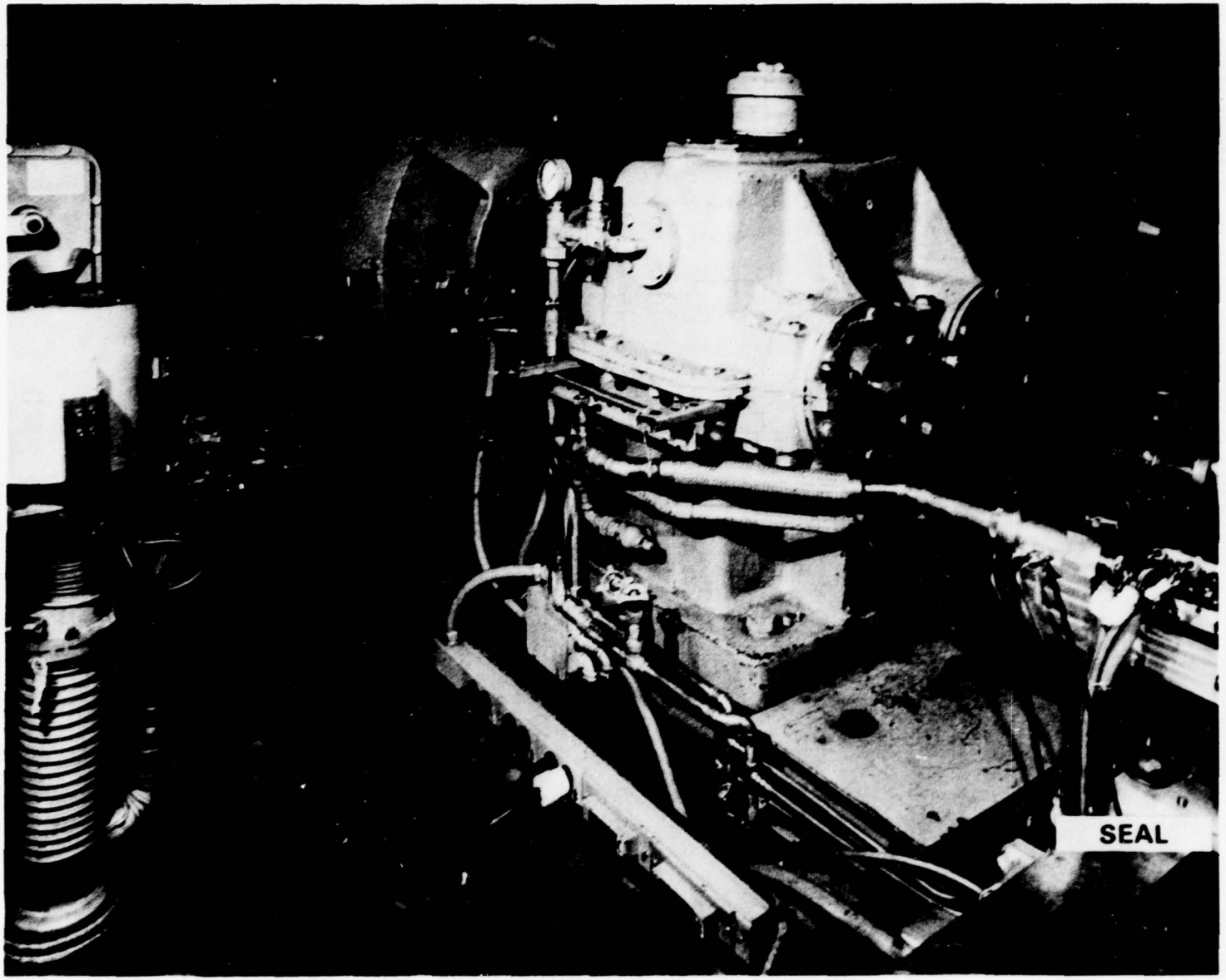


FIG. 44 Photographs of Ferrofluidic Seal from Behind Gear Box

SECTION VII

COOL-DOWN WITH CONTINUOUS PUMPING ON VACUUM COMPARTMENT

Rotating Cool-Down

The test site was prepared for cold tests as shown in Figure 45 in accordance with Revision "D" of the test plan. This test plan is presented in Appendix K. The revised test plan call for a "proof-of-integrity" test which would demonstrate that a superconducting state could be maintained at speeds up to 4000 RPM. This test would be followed by a series of calibrations at speeds up to 4000 RPM at conditions well away from a possible quench of the field winding. The objectives of these initial low risk tests were to obtain critical data for characterization of the generator. Subsequently, the plan called for tests at 8000 RPM and at conditions which would quench the superconducting field winding.

Cool-down of the generator was started on Monday, 8/14/78, by circulating helium gas through the rotor. This gas was pre-cooled in a LN_2 exchanger. Subsequently, it was cycled through a refrigerator and liquified. This procedure was continued until the field winding approached LN_2 temperature, whereupon liquid helium was introduced by way of the CTI and dual 250 liter storage dewar management system. Both the exhaust from the CTI and the rotor were cycled through the W liquefier. The 250 liter storage dewars were refilled from a 500 liter shuttle dewar. This helium was obtained from an outside supplier and from the in-house liquefier. Cool-down was continued until 1600 hours, Tuesday 8/15. Attempts to cause the field winding to go superconducting were made by increasing the flow rate and flow division within the rotor at speeds up to 4000 rpm. Voltage measurement versus field current indicated the field winding did not reach a superconducting state. However, this observation was not conclusive since ice and moisture had accumulated on the slip rings for the current leads. Thus, excessive voltage drop may have occurred between the brushes and the slip rings. Also, an ice point formed at the union in the external transfer line. This ice demonstrated that the bayonet portion of the union was in contact with the outer wall which caused an extra heat loss in the external transfer system.

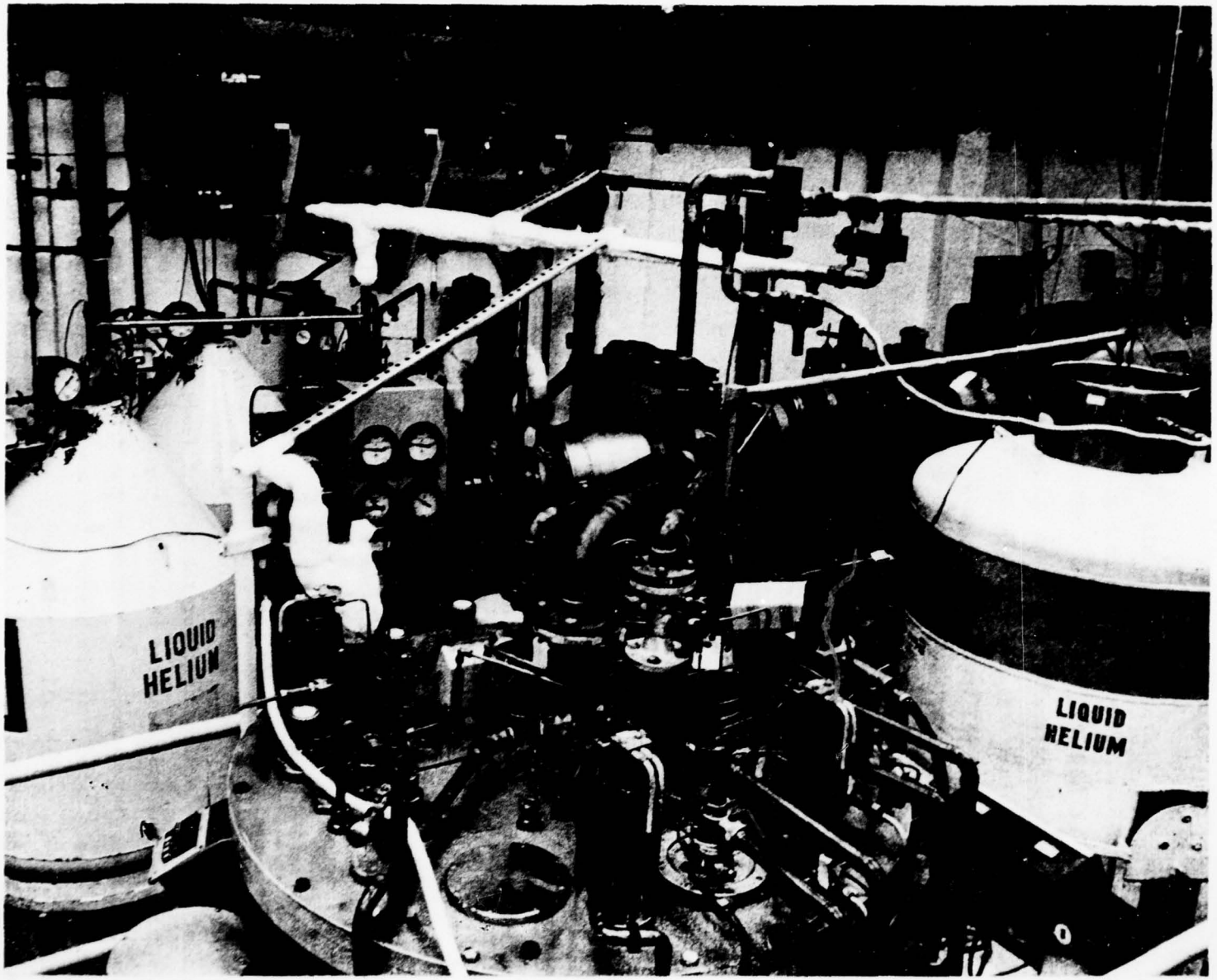


FIG. 45 Test Site for Cold Tests

The cooling system was placed on stand-by operation by using helium gas from a LN_2 exchanger and the transfer line from the CTI to the rotating seal was removed to clear the contact point. During this period the brushes were inspected; the brush to slip ring resistance was measured; and a pre-heated gas supply was connected to the cooling air manifold for the brushes and slip rings.

Cool-down was started again at approximately 1200 hours on 8/16 and was continued until 1800 hours, 8/17. The temperatures within the rotor and the flow rate through the current leads, and the total flow rate were obtained from 200 to 8000 rpm. A superconducting state was not achieved. Voltage versus field current showed a normal resistance for the field winding.

Failure to obtain a superconducting state was consistent with the temperatures observed for helium up stream ($\sim$ 12 K) and down stream ($\sim$ 20 K) of the field winding. Flow rates up to 80 liter per hour of dense helium were introduced into the rotor. The exit temperature of the helium from the winding compartment did not go below 20 K. This observation indicated the heat removal rate was approximately $\sim$ 300 watts. Thus, excessive heat loss into the field winding was the apparent reason for not obtaining a superconducting state. It was concluded the high heat loss into the cold structure was due to the high pressure in the vacuum space or contact between the warm structure and the cold structure. Further attempts to cool the rotor in the generator would not provide any more facts relative to the cause of the excessive heat loss into the winding compartment. Therefore, the cool-down was terminated and the rotor was removed from the generator for remote investigations.

A calibration for the conductance of the pump-down system was made. This was accomplished by measuring the pressure at the union of the line and rotor versus the pressure at the vacuum pump for different helium leakage rates through the line. With this calibration data the pressure observed at the vacuum pump during the previous cool-down was used to establish the pressure at the union. A pressure between 10^{-3} and 10^{-2} mm Hg probably existed in the vacuum compartment during the cool-down.

The residual gases (helium for the most part) in the vacuum space between the electro-thermal shield and the field winding compartment probably gave rise to the excessive heat load. This heat load by molecular conduction can be calculated from Knudsen equation

$$\frac{Q}{A} = \Psi P (T_2 - T_1) \qquad \text{VII-1}$$

Where

$$\Psi = \frac{\sigma+1}{\sigma-1} (R/8\pi MT_g)^{\frac{1}{2}} F_\alpha \qquad \text{VII-2}$$

and

$$F_\alpha = \left[\frac{1}{\alpha_1} + \frac{A_1}{A_2}\left[\frac{1}{\alpha_2} - 1\right]\right]^{-1} \qquad \text{VII-3}$$

α = the accommodation coefficient α_1, α_2

A = cross sectional area to heat flow, $A_1 = A_2$

σ = ratio of specific heats, cp/cv = 1.667

R = universal gas constant

P = the absolute pressure of the gas

T_g = gauge temperature at which P is measured = 540°R

M = molecular weight of gas = 4.003

and the subscripts 1 and 2 refer to the cold surface and hot surface respectively.

The values given by Scott [18] for helium are shown below

Temperature °K	Temperature °R	Accommodation Coefficient
4.2	7.6	1.0
20	36	0.6
78	140	0.4
300	540	0.3

For gas conduction from the electro-thermal shield $A_1 \approx A_2$ and T_2 (shield temperature) was approximately 150 K (270 R) during the final stage of the cool-down. Assuming T_1 (winding compartment temperature) of 20 K (36R), the accommodation coefficient become $\alpha_1 = .37$ and $\alpha_2 = .6$ Hence, $F_\alpha = .297$ and $\Psi = 1.144$ Ft $sec^{-1}{}^\circ R^{-1}$. Assuming a pressure of 10^{-2} mm Hg (2.79×10^{-2} Lb/Ft^2) the heat flux becomes

$$\frac{Q}{A} = 1.144 \frac{FT}{sec^\circ R} 2.79 \times 10^{-2} \frac{Lb}{Ft^2} (270 - 36)^\circ R$$

$$= 7.47 \frac{Lb\text{-}Ft}{sec\ Ft^2}$$

$$= 10 \text{ watts/Ft}^2$$

The area for conduction is about 3 FT^2. Therefore, the heat input by molecular conduction at 10^{-2} mm Hg could be about 30 watts or $\sim$ 1/10 of the heat removal rate based upon the total enthalpy rise of the helium. This fact suggested the pressure within the helium compartment was higher than 10^{-2} mm Hg during the previous attempted cool-down or that a direct contact(s) between the warm structure and the cold inner structure was present. Further investigations were performed to determine if direct contacts were present.

Static Cool-Down With Rotor Vertical

A static cool-down was attempted with the rotor in a vertical position. A high conductance line was connected to the rotor and vacuum pump. Liquid helium was introduced from a 250 liter dewar from the upper end of the rotor. The temperatures observed for the helium stream through the winding were consistent with a superconducting state. However, a superconducting state was not obtained. The pumping on the vacuum compartment did not prevent frost from forming on the outer cylinder. However, the frost pattern did not indicate contact between the shell and the inner structure.

A casing was placed around the outer cylinder and liquid N_2 was employed to cool the outer structure as shown in Figure 46. With this arrangement the pressure at the union of the rotor and the pump-down line was about 5×10^{-3} mm Hg and the electro-thermal temperature decreased to $\sim$ 40 K. The heat input to the field winding compartment by molecular conduction for these conditions was probably reduced by a factor of 4. Temperatures observed for the helium up-stream and down-stream of the winding were 4.2 K and approximately 4.6K, respectively. Based upon the total entholpy rise of the helium, the heat removal rate was between 35 and 70 watts. A superconducting state was not obtained. The observed resistance of the winding appeared to be less than expected for a normal state but higher than anticipated for a complete super-conducting winding.

Further investigations were performed to determine if the winding failed to go superconducting because of (1) a high resistance connection within the winding or (2) partial blockage of the cooling channels by the sealing resin.

Static Cool-Down in Liquid Helium Dewar

The sealing resin was dissolved and flushed from the helium compartment. This was done by filling the compartment with solvent and allowing it to dissolve the resin for 24 hours. Then it was flushed and replaced with new solvent. This treatment was repeated for a period of one week. Subsequently, the rotor was suspended within a large stationary dewar as shown in Figure 47.

Helium from the liquefaction unit was circulated through the rotor and out into the dewar in a closed cycle. Also, the vacuum compartment of the rotor vented into the dewar.

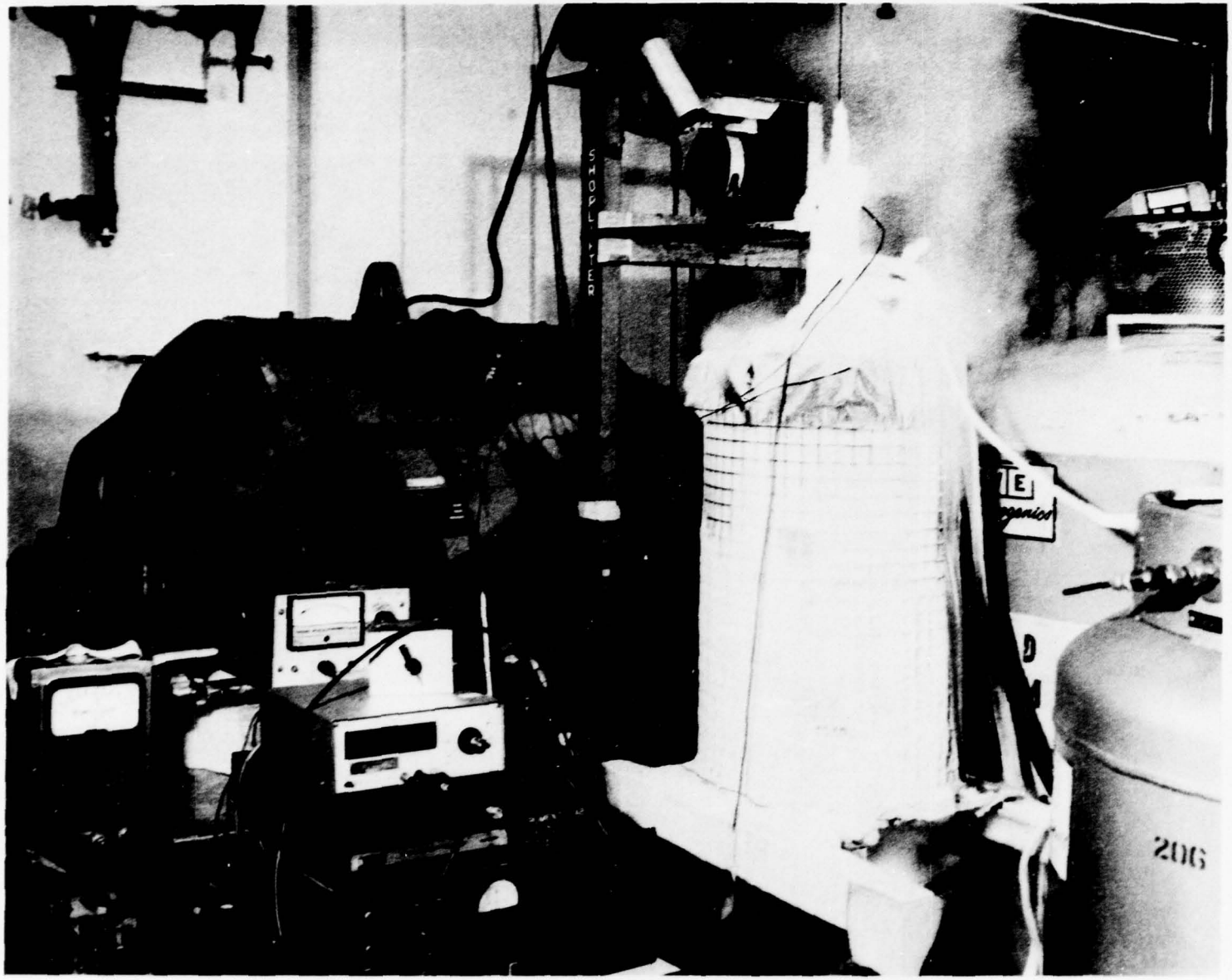


FIG. 46 Jacket around Rotor for LN_2 Cooling

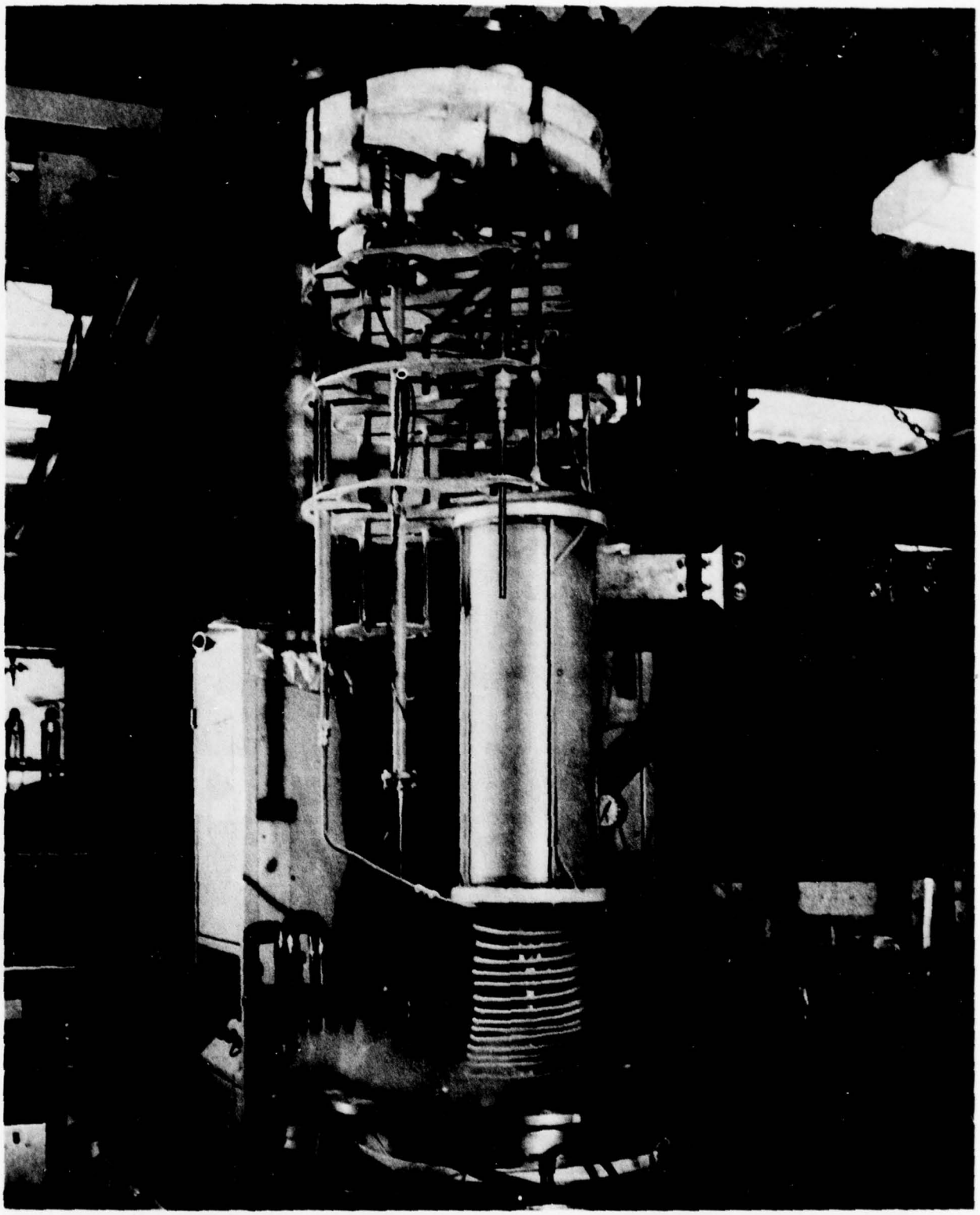


FIG. 47 Cold Test with Rotor in Large Dewar

This process was continued until the sensor within the rotor indicated 7K, $\sim$ 3°K below the critical temperature of the conductors. At this time a current of 10A was introduced in the current leads and the field winding demonstrated a superconducting state. Subsequently, the dewar was filled with liquid helium from an external source until the rotor was submerged.

All sensors in the rotor indicated a temperature below 5K and the inlet temperature was 4.6 to 4.8K. The field current was increased until normalization occurred. The first normalization occurred at 201A. The sensors showed an increase in temperature to about 15K. After 10 min. of continuous cooling the sensors indicated temperatures below 5K The flow rate through the winding was decreased which reduced the inlet pressure. This caused the inlet temperature to decrease to 4.3K. Two normalizations were produced with this inlet conditions at a field current of 236A. These normalizations demonstrated that the field winding, the lead connections, and coil connections are sound.

The critical problem of the rotor is the leak from the helium compartment into the vacuum space. The leakage rate is excessive and sufficient vacuum can not be maintained even with continous pumping. The rotor was examined internally to determine the area of leak. This investigation is discussed in Section VIII.

SECTION VIII

EXAMINATION OF ROTOR

The outer cylinder and the electro-thermal shield were removed and three areas of the helium compartment were examined for leaks. The first area was the structural welds which join the winding containment cylinder to the anti drive-end shaft and to the drive-end shaft. These welds were checked by exposure from the outside with helium gas with a vacuum in the winding compartment. They were found to vacuum tight. Secondly, helium gas was introduced into the interior region of the anti drive-end shaft. This test indicated a slight leak near the terminal brazement for one of the small tubes and the flexible end of the shaft. Fortunately, this fault was outside of the interior region so it was possible to seal it and continue to test the interior of the shaft.

Further checks proved the bulkhead, helium supply line, cooling coils and current lead conduits were vacuum tight. Thirdly, helium gas was introduced into the interior region of the drive-end shaft. This region showed a significant leak of helium into the field winding compartment. The exact location of the leak(s) could not be defined since the helium gas was exposed simutaneously to several critical areas. The areas of particular concern are noted in Figure 48. They included (1) the weld around the bulkhead and the thermal transition piece, (2) the cooling coils on the transition piece, (3) the joints between the cooling coils and radial conduits, (4) the conduits for the sensor leads, and (5) the brazements for the tube terminals at the center of the bulkhead. In order to individually investigate the integrity of one of these areas it is necessary to disassemble other areas of concern. Therefore another option was selected to further isolate the fault(s).

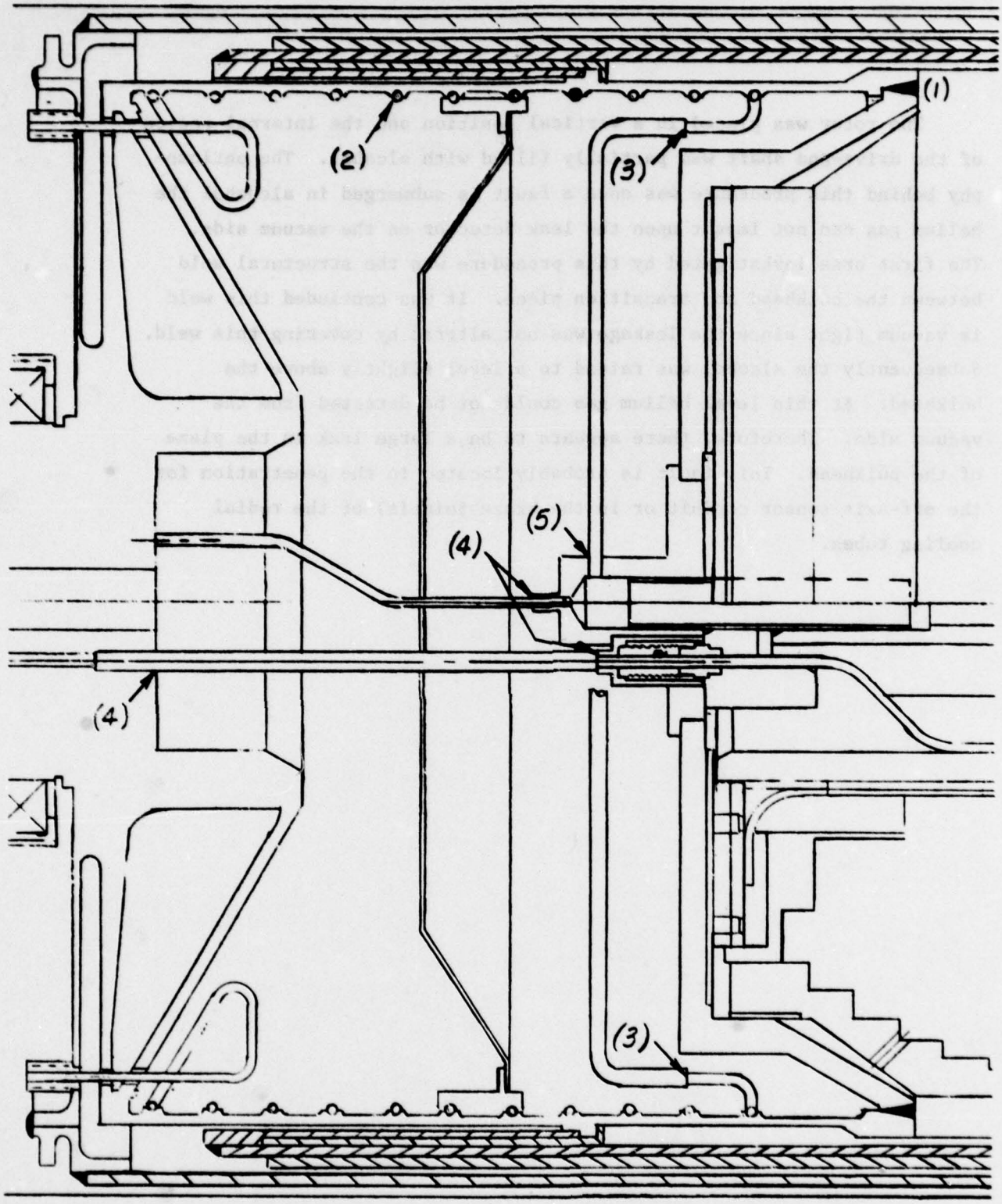


FIGURE 48 INTERIOR OF DRIVE-END SHAFT

The rotor was placed in a vertical position and the internal region of the drive-end shaft was partially filled with alcohol. The philosophy behind this procedure was once a fault is submerged in alchohol the helium gas can not impact upon the leak detector on the vacuum side. The first area investigated by this procedure was the structural weld between the bulkhead and transition piece. It was concluded this weld is vacuum tight since the leakage was not altered by covering this weld. Subsequently the alcohol was raised to a level slightly above the bulkhead. At this level helium gas could not be detected from the vacuum side. Therefore, there appears to be a large leak in the plane of the bulkhead. This fault is probably located in the penetration for the off-axis sensor conduit or in the braze joint(s) of the radial cooling tubes.

SECTION IX

A CRITIQUE OF THE GENERATOR

Concluding Problem

Leakage of helium into the vacuum compartment was the concluding problem. Even with continuous pumping through a dynamic, rotating seal, the pressure in the vacuum space apparently reached ∿0.1 mmHg. Consequently, the heat conduction into the winding was too high to obtain a superconducting state in the rotor winding.

The vacuum pressure within the rotor was limited by the conductance of the gas flow path within the vacuum compartment and by the conductance of the 3/8 inch pump-down line. Unfortunately, continuous evacuation of the rotor was not considered during the design phase of the program and high conductance to an external pump was not considered to be essential. Consequently, the restrictions within the rotor and the maximum size for a pump-down line were set by other design considerations. The leakage rate was thus too high to be accommodated by the restrictive flow paths.

Leaks were found at two locations. One leak is located in the wall of a small tube that terminates in the flexible end of the anti drive-end shaft. This fault appears to be a small pin hole just inboard of the terminal brazement. The leak at this location is the result of several factors. First, time was involved in the failure process since this tube was leak checked several times during the construction and repair of the rotor. Second, the sensitization of the 304 stainless steel tube during the brazement of this tube to the transition piece (as explained in Appendix G) increased the susceptibility of this tube to corrosive attack. Third, on several occasions moisture from ambient air condensed and froze at the termination of this helium conduit. This moisture, during warm-up and shut-down, probably entered the tube and created a condition for corrosive pitting of the 0.010 inch wall tubing.

The second leak is located inside of the drive-end shaft. This leak could be caused by (1) a faulty brazement between a cooling coil and its radial conduit or (2) a fracture (crack) in the manifold for the four radial conduits. This manifold was altered to accommodate the installation of a bellows union between the bulkhead and a conduit for sensor leads which produced a thin wall adjacent to the bellows housing as shown in Figure 48 in Section VIII.

Rotor Critique

Helium Leakage -

Helium leakage within the rotor was a continous problem throughout the construction and testing of the generator, although the vacuum performance of the Phase I rotor was excellent. Features of these rotors and critieria for adequate vacuum containment are discussed below.

(1) The Phase I rotor employed one warm vacuum conduit and one helium conduit for sensor leads. Two helium conduits and two vacuum conduits were used in the present rotor for sensor leads. Incorporation of these additional conduits created a higher probability for leakage and may have created the situation which produced the terminal leakage problem. Conduits for sensor leads must be kept to a minimum and it is prudent to arrange the thermometers within the helium compartment so the leads can be accommodated through one conduit. Also, sensor leads within the vacuum compartment should be passed through a single conduit. The only complication this procedure may create is that the lead wires may require internal joints in order to assemble the components of the rotor.

(2) The cooling coils for the Phase I rotor had a wall thickness of 0.03 inches. Whereas, the wall thickness for the coils in the present rotor is 0.01 inches. Premature failure may have been prevented if heavy wall (0.03 inches) tubing had been used. Also, braze mock-ups should have been made and tested for susceptibility to corrosion and for the impact of the thermal treatments (time at temperature) upon the materials. In addition, future cooling coils should be made of Inconel tubing if they are to be brazed to an Inconel thermal transition piece. Subsequent heat treatment of the thermal transition piece will have less impact upon the Inconel tubing than upon stainless steel tubing.

(3) A helium leak test at room temperature was not conclusive relative to the soundness of a structure at cold temperatures. In some instances thermal cycling to liquid nitrogen temperature exposed a faulty joint. However, this kind of leak test does not prove the structure will remain sound after it is cold. Warm leak tests of the Phase II rotor showed the rotor did not leak when it was warm. However, a leak developed when the inner structure was cooled to near liquid nitrogen temperature which resealed upon warm-up of the rotor as described in Section V. Cold leaks are produced by strain due to contraction of the material(s). However, cold leaks in the Phase II rotor were not observed until the rotor had undergone warm spin-ups to design speed (12,000 RPM). Thus, the fault(s) may have been created by the rotational stress rather than by a thermal stress. Thereafter thermal stress was enough to cause the fault to leak.

Leak tests of structures before they are assembled into the rotor are essential. Most defects can be detected at room temperature and thereby eliminated before the part is assembled into the rotor. Thermal cycling may expose other faults which otherwise would not have been detected.

In some instances cold leak tests can be performed as demonstrated by the tests discussed in Section V. Final proof requires a leak test at conditions that simulate the conditions which the part will experience in service. However, simulation of both thermal strain and rotational strain in a sub-component during a leak test is a formidable task and other options must be considered. These options include:

(1) redundant sealing of joints,
(2) providing easy access to the internal structure of the rotor so repair of leaks can be accomplished without major destructive disassembly of the rotor, and
(3) redundancy of the vacuum system by providing a back-up dynamic system.

Field Winding -

Premature normalization of the field winding occurred based upon the results observed from a short sample of the wire. The maximum normalization current observed with the rotor removed from the stator was 251A or ∿57% of the limit established from the short sample test results as discussed in Section V. Degradation of the current carrying ability is most likely related to mechanical movement of the conductors. Coils[17] made with the same materials, procedures, tools and cross-sectional dimensions have been examined. Conductors around the pole piece were loose and other were not bonded sufficiently. The combination of resetting and rebonding these experimental coils increased the normalization current from 270A to 353A.

In principle the current carrying capability of the winding for the rotor can be improved to 80% (353A) of short sample performance by improvement of the bonding and compression operations. To accomplish these improvements the following procedures and features should be applied to the coil winding process.

(1) Winding of the coil should be performed on rigid (unyielding) steel pole pieces. These pole pieces should be designed so they can be mechanically expanded before the coil is bonded and so they can be removed from the coil after it is bonded.

(2) An appropriate nonconducting pole piece should be inserted into the coil after the winding pole pieces are removed.

(3) The winding fixture, reference Figures 13 and 14 in Section III, should be designed so the top and bottom sections can be mechanically manipulated to provide compression of the coil during the bonding operation.

The impact of increasing the current carrying capability upon the specific power of the generator is illustrated in Figure 49. Presently, the specific power at the 5.0 kV, 5 MVA design point is 4.46 Kw/Lb (0.224 Lb/Kw) at .95 power factor. Increasing the current carrying capability to 80% (353A) of short sample performance would increase the potential specific power of the generator by a factor of three or more.

The experiences with the present rotor coils have shown that a coil design should not be committed for assembly into the rotor until the design and manufacturing procedures have undergone evaluation and improvements. The following steps must be performed to achieve a high (80% of short sample performance) and reproducible level of performance.

(1) Sufficient wire should be procured so both experimental coils and the coils for the rotor can be made from the same parcel of wire.

(2) Insulations should be applied on the entire parcel by continuous processes so the dimensions over the insulation are identical throughout the entire parcel of wire.

(3) The first coil should be wound, compressed, and bonded in the winding fixture followed by sectioning the coil to determine the uniformity of compaction and bonding of the turns.

(4) If necessary, the dimensions of the winding fixture must be altered to produce uniformity throughout the coil.

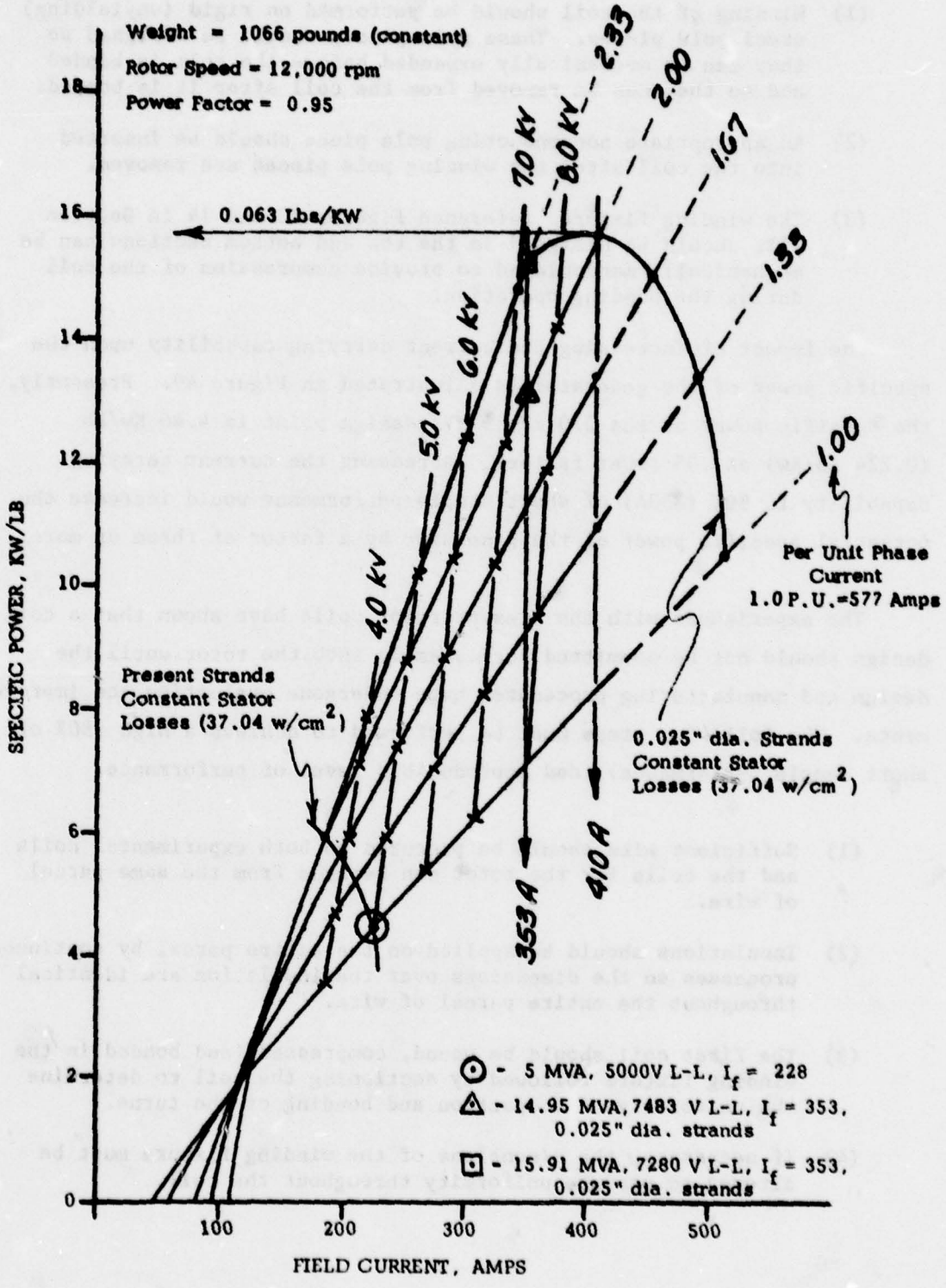


FIGURE 49 SPECIFIC POWER OF GENERATOR VERSUS FIELD CURRENT

(5) If necessary, a second coil should be wound and examined for uniformity throughout the array of conductors.

(6) Finally, coils should be wound for cold tests. Extra coils should be wound so the superior coils can be selected for the rotor assembly.

Electro-Thermal Shield -

Problems arose with the fabrication of an electro-thermal shield with copper around an inner support cylinder. Bonding of the copper to the cylinder was not achieved, as explained in Section III. Placement of the copper inside of the conductive support cylinder would have increased the losses in the shield by 20%. Thus, the demands upon the cryogenic cooling system for the shield would have increased by ∿20%. Therefore, an overwrap of a stainless steel fiber was developed which has a resistance 170 times greater than an equivalent 304 stainless steel cylinder of the same dimensions (see Appendix H). With this resistance, the overwrap only increased the losses in the shield by ∿0.16%. The only problem defined for the overwrap approach was that the work hardened 304 stainless steel fiber was magnetic and saturated at 12.5 kilogausses at 4.2°K. Other high strength metal fibers, such as Inconel, should be investigated for this application since low level of magnetic saturation is desired. The inner support cylinder can be eliminated if the overwrap approach is used.

Stator Critique

Reduction of Eddy Current Losses -

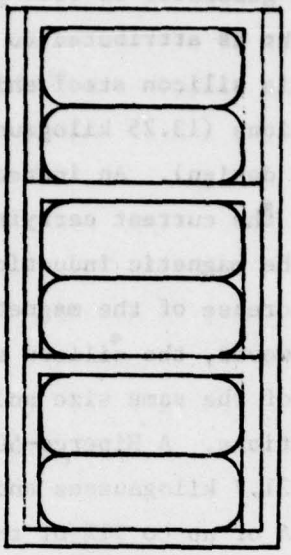
Heating of the armature conductors is dominated by eddy current losses produced by the rotating field. Even with normalization at 57% (251 amps) of the maximum capability of the field winding, this excitation produces excessive heating of the armature conductors at 12,000 RPM under no-load as is illustrated in Figure 29 in Section IV. Reduction of the eddy current losses is required. If these losses are not reduced, improvement of the field winding current carrying capability can not be utilized by this generator.

Eddy Current losses can be reduced by decreasing the size of the strands in the stator conductors. Strands for the present conductor were formed from 16 gauge (0.051 inches diameter) round wire. In the event the current carrying capability of the field winding is increased from 57% to 80% of the limit, the strand size must be reduced to about 0.025 inches. The impact of using round strands of 0.025 inches diameter in place of the present strands (0.037 inches by 0.053 inches) is illustrated in Figure 49. This strand size produces the same maximum specific power loss (37.04 watts/cm^3) at 2 per unit armature current and 410 amps field current as presently exists for the 5 MVA point design (one per unit armature current and 228 amps field current). The 0.025 inch round strand would allow the field winding to operate up to 100% of its capacity.

Armature Coils with Small Strands -

Winding armature coils with wire that has a strand size of $\sim$0.025 inches is practical if a cable configuration is used. Firstly, a rectangular braid with a small strand size would be made. The cross section of this braid would be a fractional part of the total cross section of a complete conductor for a phase group.

Secondly, "U" channels would be fabricated with internal dimensions equivalent to a complete conductor. Thirdly, "U" channels would be fabricated with internal dimensions equivalent to the overall envelope of a conductor/channel array on one side of the coils as shown below.



Winding of a phase group could be accomplished by using the procedures developed for the present coils with some modifications. The "U" channels would be placed in the fixture during the winding operation and bonding of the coil would consist of curing a resin between the sides of the channels.

Presently, the armature winding has two parallel circuits. Thus, each conductor is one-half the size of the conductor required for a single three-phase circuit. This option was selected because it was easier to wind and form forty-eight conductor bars with a 3X6 array of strands than twenty-four conductor bar with a 6X6 array of strands. If the conductor bar is formed from a braid of small round strands it will become easier to wind and spread twenty-four conductors. Thus, a single three-phase circuit could be used for the armature winding which would decrease the number of insulation pieces and allow more space for the conductors.

Magnetic Shielding -

The wet weight of the generator is 1066 pounds. A large portion (248 pounds) of this weight is attributed to the iron stator shield. It should be noted that this silicon steel shield was designed to operate at low magnetic inductions (13.25 kilogausses for the 5 MVA, 5000 V, 228 A field current, point design). An increase of the excitation current to 293 A (71.5% of the current carrying limit of the field winding) would increase the magnetic induction in this shield to ∿17.0 kilogausses. A further increase of the magnetic induction would be too high for silicon steel; however, the silicon steel shield can be replaced with Hiperco-50 shield of the same size and weight which would carry the flux for higher excitations. A Hiperco-50 shield can be operated at magnetic inductions up to 21.7 kilogausses and would carry the flux for field currents up to 373 A or up to 91% of the current carrying limit of the field winding. Static tests of complete coils made from the superconducting wire have only demonstrated 80% of the current carrying limit. Thus, a Hiperco-50 shield of the same size and weight as the present shield represents a conservative design.

Hot Spot Limitation -

The temperature of the hot spot in the armature is limited to 300°F by the thermal stability of the transformer oil. This mineral oil is a mixture of molecules of different sizes and changes occur with high temperature aging even in the absence of oxygen. Lower molecular weight fractions may be volatilized and higher molecular weight fractions may be deposited upon the heated surface of the conductors forming a resinous layer. Any cracking of the molecular chains results in formation of some highly volatile compounds and a larger proportion of gums and resinous materials.

In principle the thermal stability of transformer oil can be increased by "super-refining" - a term given to a process in which conventional oils are dewaxed and otherwise treated to produce a higher allowable temperature. The maximum temperature of mineral oil can be increased by ∿100°F. However, it is much more expensive than conventionally refined oil and no large market has developed for it. Accordingly it can not be readily procured.

The silicone oils that are used for the dielectric fluid for high voltage transformers for air borne applications could be used for the cooling and insulating oil for the stator. These oils offer thermal stability in a non-oxidizing environment up to 200°C and their viscosity does not experience a large variation with temperature. Furthermore, the level of viscosity of a particular grade of silicone oil can be controlled by the degree of polymerization of the basic constituents. An oil with a viscosity between 4 and 8.6 centipoises can be produced and would be satisfactory for the stator coolant. Such a coolant would allow the maximum temperature of the armature conductors to reach 390°F. Thus, a higher current density could be sustained which would increase the power density of the generator. An increase of the hot spot temperature from 300 to 390°F would result in a power density increase of 20%.

The conductor channels were wound from Class F B-staged polyesterglass tape as described in Appendix C. Prolonged operation above 140°C (302°F) would degrade these composite structures. A combination of materials which would increase the service temperature of this component consists of multiple layers of 0.003 inch polyimide film bonded into a dense laminated form conforming to the channel dimensions using B-staged amide-imide resin, PD George 981. Information concerning the electrical properties of this material (Kapton film) is given in reference 19. In addition to an increase in thermal stability, this material offers superior dielectric strength and a lower dielectric dissipation factor than the polyesterglass tape composite. Also, the dielectric constant closely matches the dielectric constant of the insulating oils. Thus, a more favorable electrical stress distribution can be provided between

the oil and the solid insulation. The wedges for the armature assembly were machined from G-11 epoxy laminate. A laminate made from polyimide film and amide-imide resin could be used to increase the service temperature and dielectric strength of these components, also.

The coil supports, the sleeves for the bore seal, and the overwrap for the winding were wound from Fiberglass grade S-901 and a resin system composed of XB2793 epoxy and Methylene Dianiline. All of these parts can be hoop wound. Thus, the new F502 Resin - S glass fabric tape which is available from U.S. Ploymeric can be used to make these composite parts. Test results with this tape for banding rings for containment of rotor windings for spray oil cooled generators have demonstrated that this composite can operate at 200°C for a prolonged period in a synthetic oil environment. This composite will increase the allowable service temperature of the coil supports, the sleeves, and the overwrap for the armature winding to 200°C. The bore seal (see Appendix A and B) requires both helically wound layers and hoop wound layers of glass filaments for strength and thermal expansion considerations. A resin system composed of XB2793 epoxy and Methylene Dianiline was used for this structure. Data is required to characterize the performance of the Fiberglass grade S-901 and this resin system up to 350°F in order to determine the allowable stresses within this structure for high temperature service.

SUMMARY

The heat loss (∿ 300 watts) into the field winding compartment was too high to cool the winding to a superconducting state. The excessive heat loss was caused by gas conduction due to leakage of helium into the vacuum compartment. Two leaks were found. Major destructive disassembly of the rotor and replacement of several components are required to repair the leaks.

Static cold tests showed premature normalization of ∿ 51% of the field winding capability based upon test results from short samples of the wire. Examination of coils like the ones used in the field winding showed that the premature normalization is probably due to inadequate bonding and compression of the conductors.

The capability of the stator is limited by high eddy current losses in the armature conductors, by a low (300°F) allowable hot spot temperature, and by the low allowable magnetic induction (17 kilogausses) for the silicon steel shield.

The generator in the absence of the helium leakage problem is capable of producing 5 MVA at 5kV (L-L) at a specific power of 4.45 kW/Lb. Technical aspects of the problems were considered with recommendations for overcoming the difficulties with the vacuum containment and for improvement of the capability of the generator. They include:

(1) elimination of unnecessary helium conduits for sensor leads;

(2) use of heavy wall, Inconel tubing for the cooling coils and other conduits;

(3) redundant sealing of joints;

(4) providing access to the internal structure so repair of potential leaks can be accomplished without major destructive disassembly of the rotor;

(5) providing redundancy of the vacuum system by providing a back-up dynamic system;

(6) cold leak testing of a structure, if possible, before this structure is assembled into the rotor;

(7) development of manufacturing procedures and experimental evaluation of the coils for the field winding before the coils are committed for assembly into the rotor;

(8) reduction of eddy current losses in armature conductors by using small strands (.025 inch diameter)

(9) use of Hiperco-50 shield in place of a silicon steel shield;

(10) use of silicon oil for the stator coolant in place of mineral oil so the allowable hot spot temperature can be increased to 390°F;

(11) use of multiple layers of polyimide film bonded into dense laminated form conforming to channel dimensions in place of polyester glass tape;

(12) use of a laminate made from polyimide film and amide-imide resin for the wedges in place of G-11 epoxy laminate;

(13) use of a composite composed of F502 Resin - S glass fabric tape, available from U. S. Polymeric for armature coil supports, the sleeves for the bore seal, and the overwrap for armature winding;

(14) use of a single three-phase circuit in place of two parallel circuits for the armature winding.

With these improvements incorporated in a generator of the same size and weight as the present generator, the capability would be increased from 5 MVA, 5kV to 15.91 MVA, 7.28kV with a specific power of 14.93 kw/Lb (.067 lbs/Kw). The hot spot temperature for the armature winding for this design would be the same as the present 5 MVA design (300°F).

ACKNOWLEDGEMENTS

I would like to acknowledge the following major contributors to the Phase II and Phase III programs. These programs were a joint effort between the Research Laboratories and the Aerospace Electrical Division.

Aerospace Electrical Division	Research Labs
A. E. King	J. H. Parker, Jr.
R. H. Swanberg	R. D. Blaugher
H. O. Oglesbee	A. E. Patterson
	A. S. Venturino
	R. L. Kolek

I would also like to acknowledge the following people who made substantial contributions to the programs.

Aerospace Electrical Division	Research Labs.
C. C. Kouba	W. R. Kuba
L. Cardone	Z. N. Sanjana
D. L. Arnett	E. M. Petrie
G. J. Geiser	T. J. Fagan
D. R. Heintz	J. G. Bich
F. D. Kahle	H. E. Ricks
	H. E. Haller III

I would like to especially thank those who devoted their efforts to the construction and testing of the generator.

Aerospace Electrical Division
C. H. Parker
R. L. Swanberg
J. A. Smith

Research Labs.
A. E. Patterson
J. Buttyan
P. J. Steve
M. A. Janocko
P. D. Vecchio
J. H. Upholl
H. C. Pohl
R. D. Blaugher
E. J. Backa
A. B. Cohen
D. S. Pysh
R. L. Shelby

The support and generous encouragement given by Hugh L. Southall, Capt. USAF, Project Manager, is gratefully acknowledged. Finally, the typing of many progress reports by Pam Warwick and the typing of the final report by Maxine Harris are greatly appreciated.

APPENDIX A

BORE SEAL DEVELOPMENT

FOR

SUPERCONDUCTING GENERATOR

BORE SEAL DEVELOPMENT FOR SUPERCONDUCTING GENERATOR RESEARCH REPORT 75-8B7-BORSE-R1

Robert L. Kolek
Polymers & Plastics

September 3, 1975
Revised November 4, 1978

ABSTRACT

Three fiberglass structural components were designed and fabricated for use in the stator assembly. These consisted of a bore seal, two sleeves and two coil supports. Their primary functions are to supply support for the stator coils and to seal in the stator cooling oil. Materials for these components were selected based on screening tests and available data. They were successfully produced per specifications.

INTRODUCTION

The stator design called for the following structural insulation components with which this report deals:

1. One bore Seal
2. Two Sleeves
3. Two Coil Support Rings

The bore seal is a fiberglass-epoxy cylinder which supports the stator coils and seals the stator cooling oil. The sleeves are fiberglass-epoxy flanges which fit on the ends of the bore seal and serve as connectors to the stator end brackets. The coil supports are tapered fiberglass-epoxy rings which slide under the ends of the stator coils for support and divert oil into the conductors. This report describes the design and fabrication of these components.

DESCRIPTION

The relation of the superconducting generator structural insulation components to the stator assembly are documented in the Detail Drawings presented in Table A·1. These drawings and their revisions were used for developing tooling dimensions to produce the composite structures and to arrive at finished dimensions for the fabricated items. Owing to the designed lines of symmetry, a half-section of the stator is adequate for the purposes of description. A simplified half-section of the stator assembly is shown in Figure A·1. The bore seal tube is a fiberglass-epoxy composite tube. The nominal overall dimensions are 9.92" I. D. x 28.8" long x 0.195" wall thickness. At the tube ends, thick walled composite sleeves are provided to engage the end brackets. The winding matrix is assembled on the outside diameter of the bore seal and secured by adhesive bonding. The winding matrix includes the electrical copper conductors and filler material arranged in a close packed and bonded matrix. The copper conductors extend axially from the winding matrix. In this arrangement, the copper conductors exterior to the winding matrix are supported only by the winding matrix and not the bore seal. The banding consists of fiberglass-epoxy wound around the winding matrix and copper conductors. After being banded, the exterior surface is machined to close tolerances in preparation for the steel laminate. The fitting procedure consists of applying adhesive to the steel laminate prior to clamping the steel laminate around the banding. Fiberglass-epoxy barrier rings are part of the banding and form a seal between

TABLE A·1

AED SUPERCONDUCTING GENERATOR DESIGN AND DETAIL DRAWINGS

AED Drawing	Description
ED-363378	Bore Seal Tube
ED-362773	End Bell
ED-362774	End Bell, Stator
ED-363378	Bore Seal Tube, L. H. & R. H. End Views
ED-363480	Sleeve
ED-362769	Stator Details
ED-362775	Stator Assembly
ED-362759	Wound Stator
ED-362757	Stator Stack, Wound Assembly
ED-362776	Stator Assembly

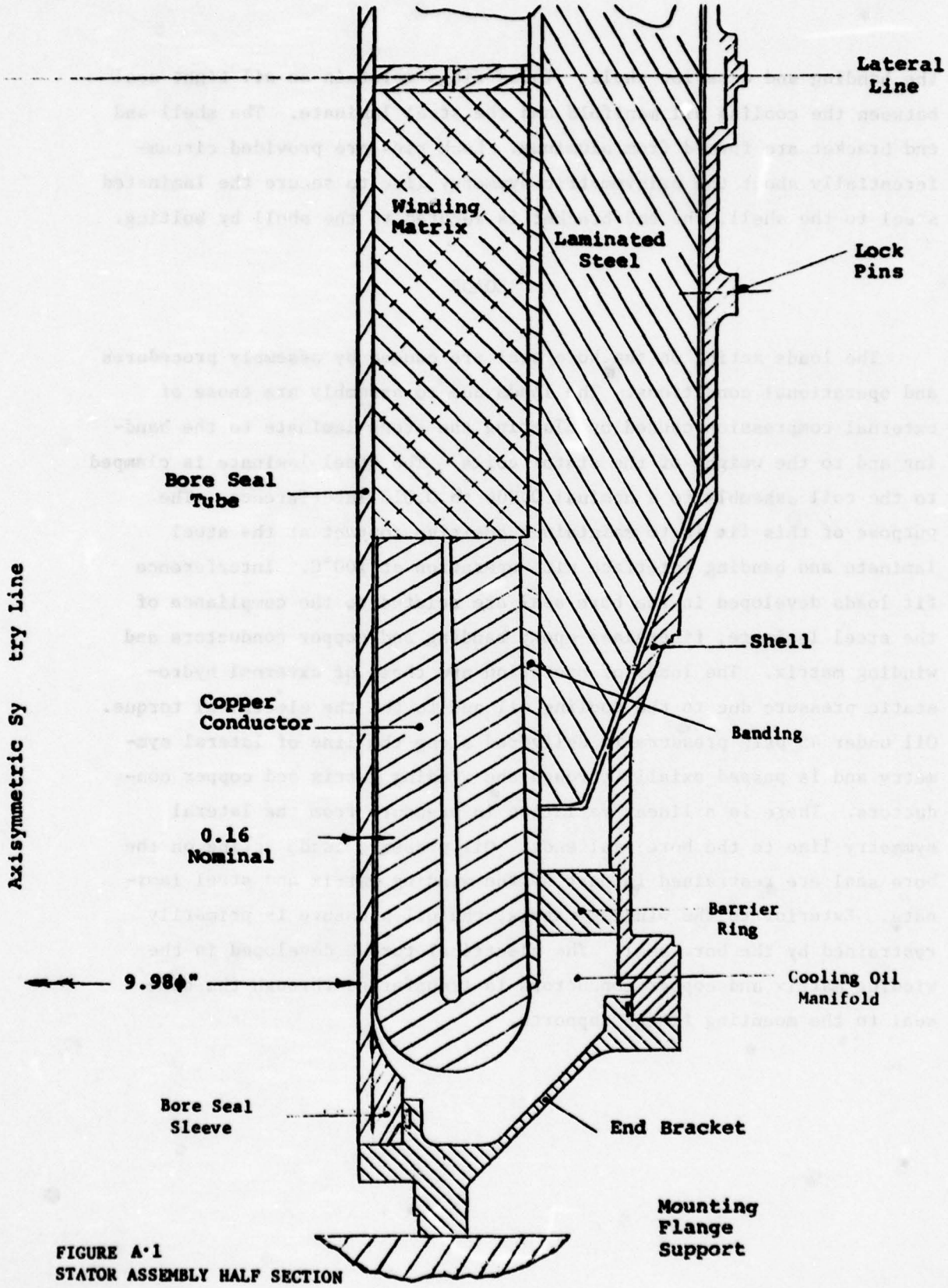


FIGURE A·1
STATOR ASSEMBLY HALF SECTION

the banding and exterior shell. These rings maintain an oil tight seal between the cooling oil manifold and the steel laminate. The shell and end bracket are formed from aluminum. Lock pins are provided circumferentially about the axisymmetric symmetry line to secure the laminated steel to the shell. The end bracket is secured to the shell by bolting.

LOADS

The loads acting on the bore seal are caused by assembly procedures and operational conditions. The loads due to assembly are those of external compression caused by clamping the steel laminate to the banding and to the weight of the stator coils. The steel laminate is clamped to the coil assembly to a nominal 0.006 to 0.010 interference. The purpose of this fit is to maintain a positive contact at the steel laminate and banding interface with operation at 100°C. Interference fit loads developed in the bore seal are related to the compliance of the steel laminate, fiberglass-epoxy banding and copper conductors and winding matrix. The loads of operation are those of external hydrostatic pressure due to the cooling oil and to the the electrical torque. Oil under 45 psig pressure is delivered along the line of lateral symmetry and is passed axially through the winding matrix and copper conductors. There is a linear variation in pressure from the lateral symmetry line to the bore seal ends. Oil pressure loads acting on the bore seal are restrained in part by the winding matrix and steel laminate. Exterior to the winding matrix, the oil pressure is primarily restrained by the bore seal. The electrical torque developed in the winding matrix and copper conductors is transferred through the bore seal to the mounting flange supports.

STRESS ANALYSIS AND DESIGN

The method of analysis used for the bore seal utilizes an axisymmetric finite element model to determine the stress states in the composite components. The features of the model are shown in Figure A-2. A comparison of the model with the stator assembly shown in Figure 1 shows that simplifications have been made in the model without sacrifice in accuracy of the bore seal stress solutions. The macromechanic approach utilized experimentally determined elastic constants and stress-strain responses of individual lamina. These data were subsequently used in the computer model together with the assumptions of thin plate or shell theory to determine the stress-strain response of any laminate composed of any orientation of the characterized lamina. The stress analysis was conducted by Hercules, Inc. under Purchase Order 34-RP-15366A. The design aspects were handled jointly by Lima, AED, Hercules, Inc. and Westinghouse Research. A final report on all three study areas was submitted by Hercules, Inc. and appears in Appendix B. Their report concludes that the bore seal can be manufactured to function satisfactorily under the predicted loads and environmental conditions. The report details the fiber orientation and stacking sequence required in the bore seal and sleeves as well as a redesigned method of attaching the bore seal ends to the end brackets.

MATERIALS EVALUATION

Several material systems were considered for use in the bore seal and sleeve components. The torsional shear and external pressure requirements called for a fiber with high interlaminar shear strength and high modulus. A high reliability fiber was also felt necessary because of the critical nature of the application. A failure of the bore seal to support the stator coils would result in a failed generator. On balance, Owens Corning Fiberglass precision grade S-901 20 end roving was selected for testing as the best reinforcement for the bore seal. Five resin systems

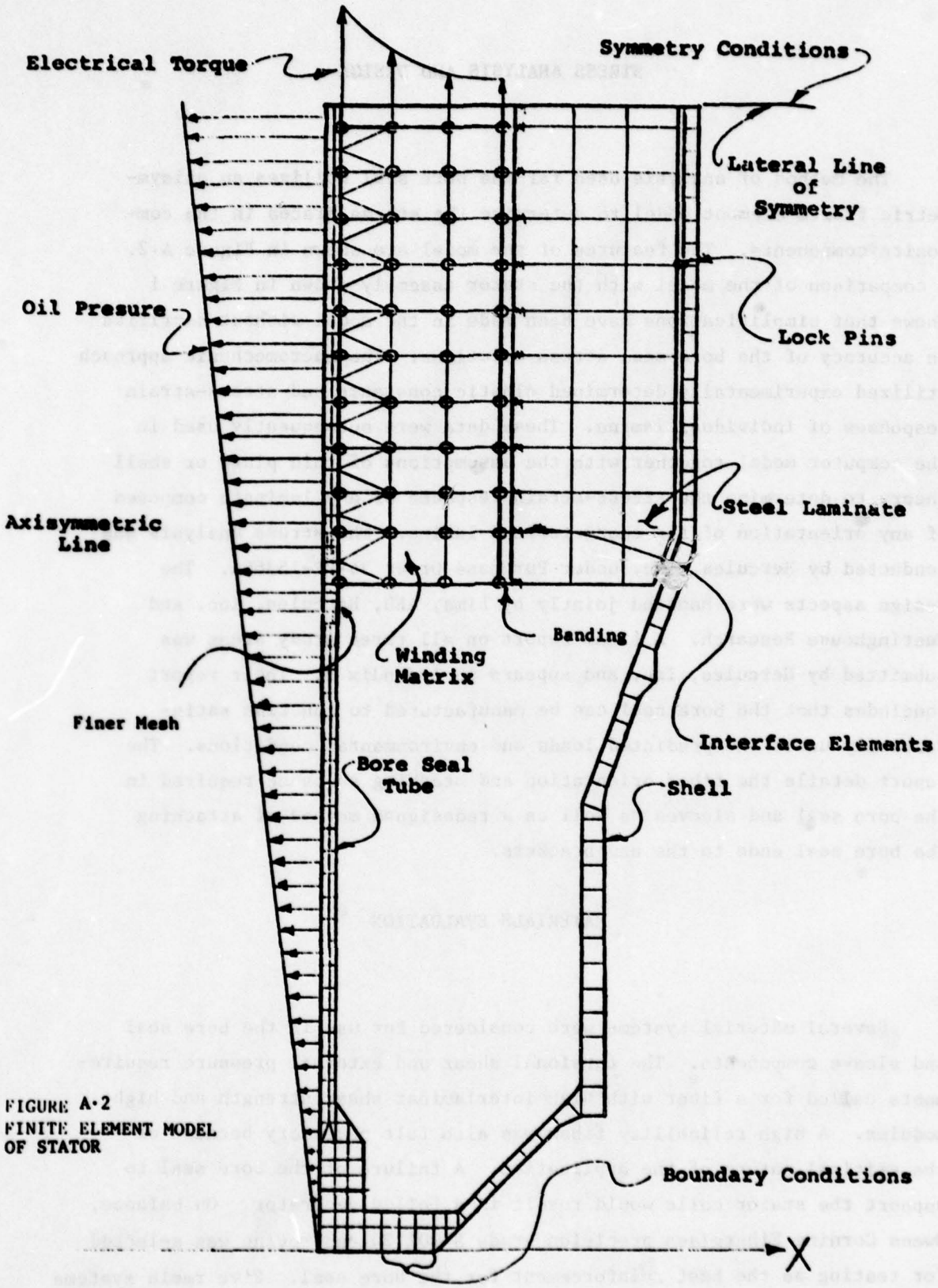


FIGURE A·2
FINITE ELEMENT MODEL OF STATOR

were evaluated for use with this fiber. The formulations are shown in Table A·2. The materials were selected based on in-house fracture toughness and composite material property data as well as suppliers' thermal testing data. Physical properties were measured on both resin castings and S-901 composite test specimens cut from filament wound cylinders. Where possible, data was collected at both room temperature and at 100°C. The data is shown in Table A·3. Limited data after aging for 30 days at 100°C in Wemco C oil is included for the two candidate materials thought to be best for the application. All data collected at room temperature could not be collected at 100°C because of temperature effect on the strain gauges used and because of limited time. Resin system five was chosen as the best resin system for use with S-901 fiberglass in the fabrication of the bore seal sleeves and coil supports.

BORE SEAL AND SLEEVE FABRICATION

Mandrels

Winding mandrels were fabricated by Tooling Specialists, Inc., Latrobe, PA, from seamless, cold drawn steel tubing. The mandrel drawings are shown in Figures A·3 and A·4. The finished bore seal mandrel had an O.D. of 9.924". However, because of tool bit chatter marks in the center, it was ground to a final O.D. of 9.919" in order to achieve the desired surface finish. This mandrel was intended for future use as a building tool for construction of the stator assembly. For this reason the stub shafts are attached with eight equally spaced, ½", thirteen hex head bolts on 3½" bolt hole centers. These bolts permit removal of the stub shafts for replacement

TABLE A·2

RESIN SYSTEMS EVALUATED FOR USE IN BORE SEAL

Material	Resin Systems				
	1	2	3	4	5
Dow XD-7818	70			100	
CIBA XB-2793		70			100
DEN-431			100		
DGENPG*	30	30			
Methylene Dianiline	34	34		34	34
Nadic Methyl Anhydride			100		
BDMA**			1		

*Diglycidylether of Neopentyl Glycol.

**Benzyl Dimethyl Amine.

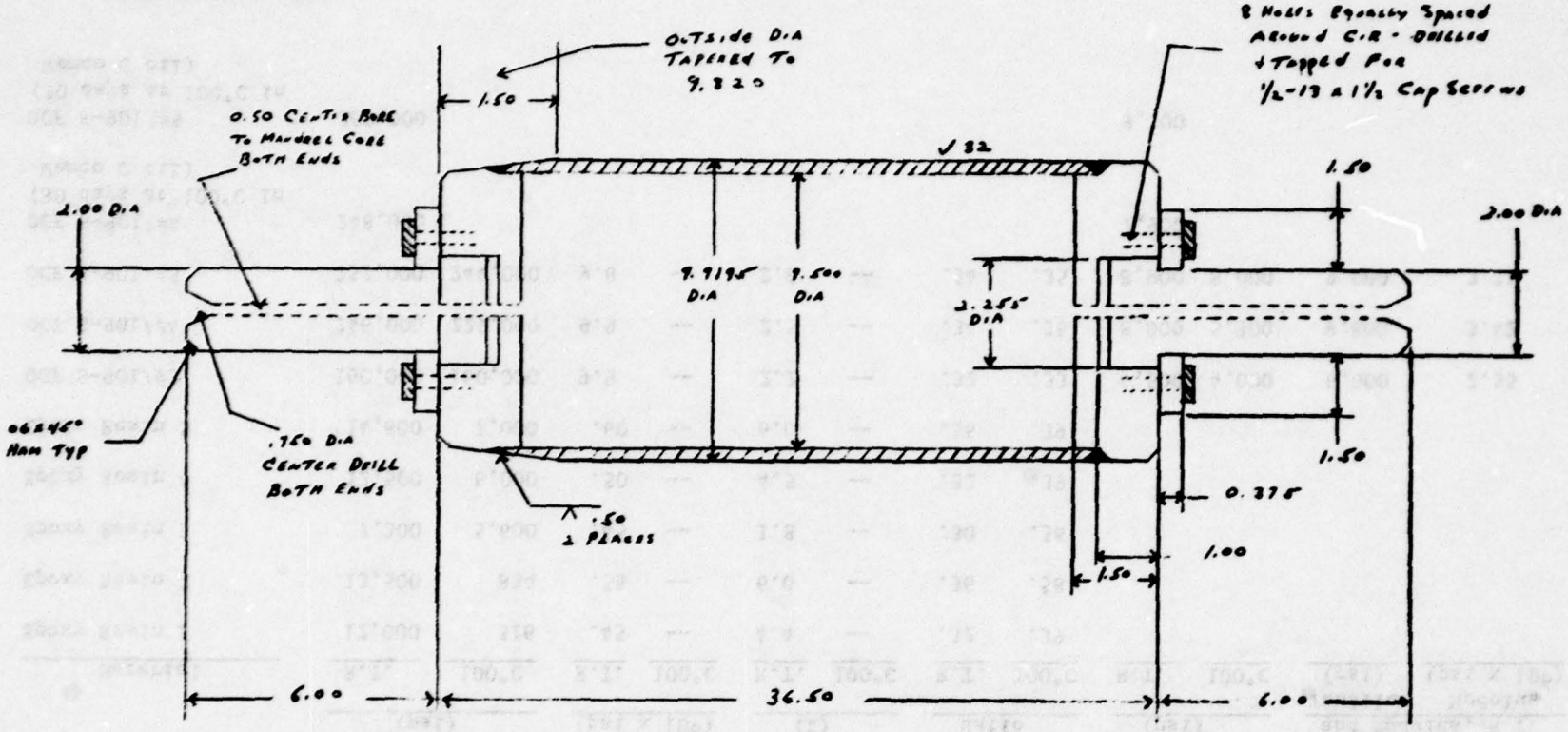
Cure Conditions: 2 hours at 100°C
16 hours at 160°C

TABLE A·3

PHYSICAL PROPERTY DATA ON CANDIDATE MATERIAL SYSTEMS

Material	Tensile Strength (psi)		Modulus (psi x 10^6)		Elongation (%)		Poisson's Ratio		Shear Str. (psi)		Transverse Tensile and Modulus, R.T.	
	R.T.	100°C	R.T.	100°C	R.T.	100°C	R.T.	100°C	R.T.	100°C	Tensile (psi)	Modulus (psi x 10^6)
Epoxy Resin 1	12,000	516	.45	--	4.4	--	.32	.39				
Epoxy Resin 2	13,500	834	.55	--	6.0	--	.36	.58				
Epoxy Resin 3	7,300	5,600	.45	--	1.8	--	.30	.36				
Epoxy Resin 4	12,500	6,000	.50	--	4.5	--	.32	.39				
Epoxy Resin 5	14,600	7,000	.60	--	6.0	--	.36	.39				
OCF S-901/#3	160,000	160,000	9.9	--	2.2	--	.32	.33	4,500	4,000	6,000	2.55
OCF S-901/#4	246,000	224,000	9.9	--	2.5	--	.34	.36	8,000	5,300	8,800	3.42
OCF S-901/#5	252,000	244,000	9.8	--	2.6	--	.34	.35	8,900	8,000	9,000	3.71
OCF S-901/#4 (30 days at 100°C in Wemco C oil)	248,000								7,900			
OCF S-901/#5 (30 days at 100°C in Wemco C oil)	260,000								9,300			

FIGURE A-3
BORE SEAL WINDING MANDREL

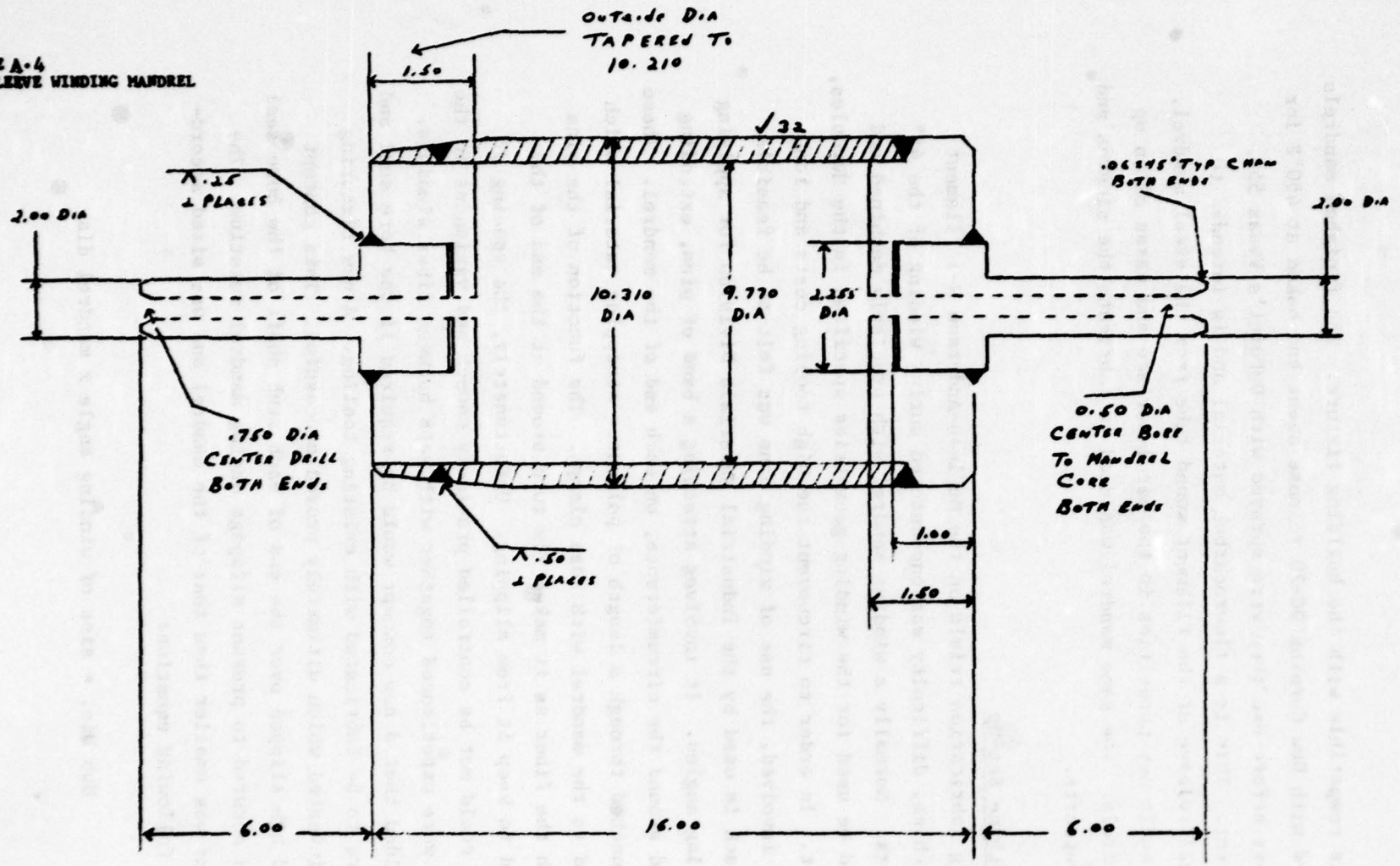


MTLS. PLATE = H.R. STL
Tubing = Seamless Cold Drawn STL
Rod = C.D. STL.

Westing House Winding Mandrel
For Superconducting Generator
Stator Bore Seal

R. L. Kolek
4/14/75

FIGURE A-4
SCG SLEEVE WINDING MANDREL



MTLs: Plate = H.R STL
Tubing = Seamless Cold Drawn STL
Rod = C.D. STL

R.E. Nolen
4/24/80

WESTINGHOUSE WINDING MANDREL
FOR SUPERCONDUCTING GENERATOR STATOR SLEEVES
AND COIL SUPPORTS

with shafts compatible with the building fixture. The finished mandrels were coated with Dow Corning DC-20 release agent and baked at 450°F for 24 hrs. Just before use they were sprayed with DuPoint's Vydax 550 release agent. This is a fluorocarbon material and is intended to insure final release of the filament wound tube from the steel mandrel. The DC-20 seals any porosities in the metal surface and eases clean up of the mandrels. The same mandrel was used to fabricate the sleeves and the coil supports.

Winding Machine Set-Up

During fabrication trials on the McClean-Anderson W-1 filament winding machine, difficulty was encountered during winding of the 45° fiber layers. Normally a winding mandrel with precisely machined end domes would be used for the winding geometries specified in the Hercules, Inc. report. In order to circumvent the high tooling costs and long lead times involved, the use of winding pins was felt to be feasible. This approach is used by the Industrial Materials Division for applying steep winding angles. It involves attaching a band of pins, extending outward and around the circumference, on each end of the mandrel. These pins are punched through a length of polyester strapping material which is attached to the mandrel with hose clamps. The function of the pins is to catch the fiber as it makes its turn around at the end of the mandrel and to keep it from slipping. Unfortunately, the spacing of these pins could not be controlled precisely enough and variances in the wind angle were experienced together with gaps between fiber windings. It was decided that a new concept would be required if the bore seal and sleeves were to be fabricated with existing tooling. A new fixturing setup was invented which ultimately proved successful. This concept used a wood hub slipped over the end of each stub shaft of the bore seal mandrel and secured to prevent slippage during mandrel rotation. The hub diameter was smaller than that of the mandrel and was sized according to the following equation:

Hub Dia. = sine of winding angle x mandrel dia.

The fiber band during fabrication would be permitted to traverse over the end of the mandrel onto the hub. As the fiber band made its turn around on the hub, it would bear against the end of the mandrel which would prevent fiber slippage. The hub diameter is critical in order to maintain the proper turn around dwell for maintenance of the desired wind angle. Winding trials showed that a hub length of 4" was necessary to accommodate the buildup of fiber winding. The winding machine setup calculations to implement this concept had never been used before at the Research Labs. They were obtained from the McClean-Anderson Co. of Milwaukee, WI. During the calculations, a major problem developed with the sleeve winding mandrel. The machine setup required a precise and fixed ratio between the number of teeth in the traverse sprocket gears (Sa) and the number of pins in the traverse drive chain (N). The ratio automatically fixes a minimum required winding length (L). Changes in the N/Sa ratio can increase L but never reduce it beyond the fixed minimum. Unfortunately, the sleeve winding mandrel was 7" shorter than the as calculated L. The problem was solved by welding 4" extensions to the existing stub shafts. Wood discs 3½" in length, having the same diameter as the mandrel were slipped over the end of each stub shaft and covered with Teflon tape. The mandrel extensions permitted the sleeve to be fabricated in the same manner as the bore seal. In both cases, however, a problem existed since the steel mandrel is now sealed inside a cylindrical overwrap by end dome windings. The following technique was used to remove the mandrel. Three layers of ½" wide by 5 mil thick Teflon tape were wound concentrically on each of the mandrels flush with both ends. After cure, a carbide hack saw blade was used to make a circumferential cut throuth the fiberglass into this tape. A hose clamp was used as a saw guide. After cut through, the fiberglass end windings together with the wood hubs and discs could be slipped off. The mandrel was then pushed out of the fiberglass cylinder by means of a hydraulic jack and a stripping rack.

Fiber Tensioning

Tensioning of the fiberglass roving during winding was achieved by means of a Type 800C012 constant tension device from Compensating Tension Controls, Inc., Orange, NJ. The applied tension was eight pounds per roving end. Fabric tensioning and pay off was achieved with a special constant tension unwind stand fitted with a Mount Hope roll. Applied tension was two pounds. The Mount Hope roll prevented fabric wrinkling to achieve a tight winding.

Roving and Fabric

Four roving packages of OCF, HTS-901 roving were consumed during winding trials and fabrication. These are identified as follows:

Package No.	Code No.	Operators Clock No.	Shift	Doff No.
75220	71C50144	609	C-3	019
75170	"	609	C-3	002
96993	"	609	B-1	049
96967	"	840	C-2	040

The fabric used in the sleeve winding was obtained from Burlington Glass Fabrics Co. and is identified as Style I9132. It was supplied in a slit width of 22" and consists of a 31 x 24 construction using G75 1/2 fiberglass yarn having an epoxy resin compatible size. This fabric deviates from the S-glass fabric called for in the Hercules, Inc. report in that it uses E-glass yarn. The S-34-901 glass cloth specified by Hercules was no longer available from Owens Corning Fiberglass and no suitable equivalents were commercially available. Subsequent discussions with Mr. Joseph Burch and Dr. Ernest Jones of Hercules prompted additional design work which indicated that an E-glass fabric would be suitable if it had the same tensile strength in the fill direction as the S-34-901 cloth. The fill direction would correspond to the axial direction in the wound sleeve. Tensile modulus was not of prime importance for this component of the sleeve. S-glass had been specified only because the required roving was S-glass.

Fabrication Lay Up Sequence

The bore seal was fabricated using a lay up sequence consisting of:

+45°
-45°
90°
90°

Seven of these sequence units were required for a total of twenty-eight layers of fiber. The final O.D. of the wound bore seal was 10.3540". The thickness per layer was 0.0078". The I.D. of the bore seal after mandrel removal was checked at 9.922 - 9.923"

The sleeve cylinder was fabricated using a lay up sequence of:

90°
+45°
-45°
Cloth
Cloth

Nine of these sequence units are required for a total of forty-five layers of fiber after which four layers of 90° fiber were added for compaction. The final O.D. of the wound sleeve cylinder was 11.078". The thickness per layer was 0.0078".

The same steel mandrel and materials used to fabricate the bore seal sleeves were used to fabricate the coil support. The winding setup and procedures were the same as used for the bore seal sleeves with the exception that no fiberglass fabric is used in the structure. Seventy-eight layers of OCF S-2 fiberglass was required to achieve a finished O.D. of 11.387". The inner layer was of 90° fiber. The winding sequence subsequent to this was $\pm$ 45°/90°/90°. The cure schedule was as follows:

12 hours - 80°C
4 hours -120°C
12 hours -160°C

This cure schedule was required by the thick wall section of the wound cylinder.

Bore Seal, Sleeve and Coil Support Machining

The bore seal, sleeves and coil supports were successfully machined at Tooling Specialists, Inc., Latrobe, PA. Dimensional checks on the finished components by the Inspection Department qualified the components as per the following drawings:

(1) ED-363378
(2) ED-363480
(3) ED-383416

Twelve radial pilot holes were drilled in the sleeves using a horizontal indexing machine and a carbide drill bit. Fraying and fiber pull out on the exit hole side were eliminated by using a 1/8" thick Plexiglass backing sheet on the exit side.

APPENDIX B

COMPOSITE COMPONENT DESIGN

COMPOSITE COMPONENT DESIGN

J.E. BURSH

JUNE 14, 1975

FINAL REPORT

WORK PERIOD: APRIL 14, 1975 -JUNE 14, 1975

Prepared Under

CONTRACT NO. RP 15366-A

for

WESTINGHOUSE ELECTRIC CORPORATION RESEARCH LABORATORIES

BEULAH ROAD, CHURCHILL BOROUGH

PITTSBURGH, PENNSYLVANIA

by

HERCULES INCORPORATED

ALLEGHANY BALLISTICS LABORATORY

CUMBERLAND, MARYLAND

I. INTRODUCTION

This report was prepared for Westinghouse Electric Corporation Research and Development Center under Contract RP 15366-A. The objective of the work completed during this program was to design and analytically characterize the performance of a fiberglass/epoxy resin, filament wound bore seal tube intended for use in a prototype superconducting airborne electric generator.

II. SUMMARY

Manufacuring drawings for the bore seal, bore seal sleeves and bore seal assembly analyzed are found in Figures B·7, B·8 and B·9 respectively. The results of a stress analysis and strength analysis of this design indicate the bore seal will function satisfactorily under the predicted loads and environmental conditions.

III. BORE SEAL DESIGN

A. DESIGN CRITERIA

A meeting of Westinghouse and Hercules representatives was held to review preliminary engineering drawings of the electric generator and to accurately define the loads and environment under which the bore seal is expected to operate. As a result of this meeting, the information found in Table B·1, page 186, was computed, a tabulation of applied loads and environmental conditions which were considered significant factors in formulating a tentative design for analysis.

B. COMPOSITE MECHANICAL PROPERTIES

S-901 Fiberglass and DOW X·D-7818 epoxy resin had been specified by Westinghouse for use in the bore seal. Since little mechanical property data are available at this time, the necessary data for performing the design and analysis were determined analytically using the approach of Halpin-Tsai which is described in Reference (20). For fiberglass/epoxy composites, this approach has been found to yield good correlation between computed and experimental results. The equations used are summarized below.

Longitudinal Modulus:

$$E_{11} = E_R V_F + E_R \left[1 - V_F\right]$$

Transverse Modulus:

$$E_{22} = E_R \left[\frac{1 + \xi_E \eta_E V_F}{1 - \eta_E V_F}\right]$$

In-Plane Shear Modulus:

$$G_{12} = G_R \frac{1 + \xi_G \eta_G V_F}{1 - \eta_G V_F}$$

Poisson's Ratio;

$$\nu_{12} = \nu_f V_F + \nu_R (1 - V_F)$$

$$\eta_E \equiv \frac{\frac{E_F}{E_R} - 1}{\frac{E_F}{E_R} + \xi_E} \qquad \eta_G \equiv \frac{\frac{G_F}{G_R} - 1}{\frac{G_F}{G_R} + \xi_G}$$

Where:

E_F ≡ fiber longitudinal modulus of elasticity = 12.5×10^6 psi*

E_R ≡ resin longitudinal modulus of elasticity = $.55 \times 10^6$ psi**

G_F ≡ fiber shear modulus = 5.2×10^6 psi*

G_R ≡ resin shear modulus = $.19 \times 10^6$ psi**

V_F ≡ fiber volume fraction = .70

ν_f ≡ fiber Poisson's ratio = .22*

ν_R ≡ resin Poisson's ratop = .42**

ξ_E ≡ fiber transverse strength correction factor ≈ 1.0

ξ_G ≡ fiber shear strength correction factor ≈ .8

Therefore:

E_{11} ≡ composite longitudinal modulus of elasticity = 8.9×10^6 psi

E_{22} ≡ composite transverse modulus of elasticity = 2.5×10^6 psi

G_{12} ≡ composite longitudinal-transverse shear modulus = $.84 \times 10^6$ psi

ν_{12} ≡ composite Poisson's ratio = .266

* Data from Reference (21)

**Data provided by Westinghouse for Dow X·D-7818 @ 212°F

C. FIBER ORIENTATION AND COMPOSITE THICKNESS SELECTION

Based on (1) the predicted maximum operating loads and environment, (2) composite mechanical properties and (3) interface requirements imposed by Westinghouse, a preliminary design for the bore seal was formulated. Because

the majority of the loads were torsional shear and hoop compression, a combination of $\pm$ 45° and 90° windings approximately 0.18 inch thick in the tube were selected. Westinghouse recommended twenty "ears" machined into the built up portion at each end of the tube to slip into the end bells to transmit the torque load. It became apparent after analysis of this proposal that a considerable risk existed that the fiberglass/epoxy shear and bearing allowables would be exceeded if less than twenty of the ears contacted the end bell or if each ear did not transmit the load uniformly along the face. For this reason it was decided to incorporate a design using twelve radial bolts on both ends to join the bore seal to the end bells. A .50 inch thickness at each end built up by an equal number of $\pm$ 45° and 90° windings was selected for the initial design, but as will be shown later some modification of this approach was required.

D. THERMAL EXPANSION OF THE BORE SEAL

Thermal expansion of the bore seal is a function of fiber and resin mechanical and thermal properties and the winding pattern. Assuming a composite linear coefficient of thermal expansion of 3.5×10^{-6} in./in./°F parallel to the fiber and a coefficient of 12×10^{-6} in./in./°F transverse to the fiber, which are typical of S-901 fiberglass/epoxy composites, the following values were calculated using the method shown in Reference 20:

$\alpha_1 \equiv$ axial coefficient of thermal expansion = 10.11×10^{-6} in./in./°F

$\alpha_2 \equiv$ circumferential coefficient of thermal expansion = 3.75 x 10-6in./in./°F

$\alpha_3 \equiv$ radial coefficient of thermal expansion = 12×10^{-6} in./in./°F.

IV. STRESS ANALYSIS

A. FINITE ELEMENT ANALYSIS

A finite element analysis of the bore seal was conducted to determine the stress state present during fitting of the back iron and during transient loads at 212°F. These condiitons will be referred to as Condition I and Condition II respectively. The grid used to model the right-hand half of the bore seal and stack is shown in Figure B.1. During Condition I the boundary conditions on the bore seal are such that it can expand axially and radially outward. During Condition II, however, the boundary conditions on the bore seal will be determined by the means of attachment of the bore seal to the end bell. As the precise method of attachment was not determined at the time the grid was perpared it was decided to (1) set the boundary condi-tions during Condition II identical to those during Condition I such that the ends are axially and radially unrestrained, (2) determine the stress state in the bore seal during both the conditions, (3) compute the loads associated with selected means of attachment of the bore seal to the end bell in a conventional fashion, and (4) superimpose on the stress state computed by the finite element analysis these computed loads. Additionally, as the torsional shear loads created by motor operation in the axial-circumferential plane cannot be shown in the plane selected for analysis, these loads must be computed and superimposed on the loads calculated by the computer program.

It was necessary to calculate the mechanical and thermal properties of the materials which will fit on the bore seal to determine the stresses they will create in the seal during Conditions I and II. The "composite" properties of the stack were computed to be as follows:

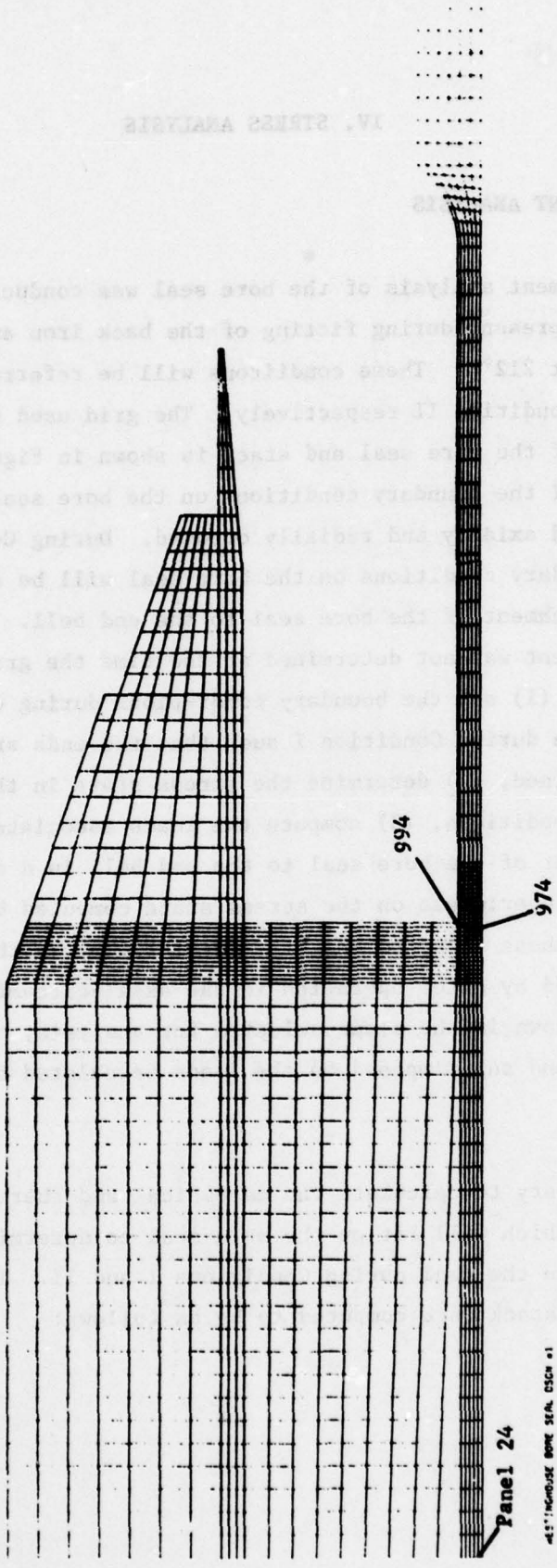


Figure B-1 Finite Element Grid of Right-Hand Portion of Bore Seal and Stator Stack

E_R ≡ radial modulus of elasticity = 5.9×10^6 psi

E_A ≡ axial modulus of elasticity = 8.24×10^6 psi

E_C ≡ circumferential modulus of elasticity = 3.75×10^6 psi

G_{all} ≡ shear modulus = 2.3×10^6 psi

ν ≡ Poisson's ration = .3

α_R ≡ radial coefficient of thermal expansion = 5.28 in./in./°F

α_A ≡ axial coefficient of thermal expansion = 5.42×10^{-6} in./in./°F

α_C ≡ circumferential coefficient of thermal expansion = 4.62×10^{-6} in./in./°F

These properties, in addition to the ones previously shown for the bore seal, constitute the input required to determine the stress state during Conditions I and II. Stress levels present in the seal during Conditions I and II are shown in Figures B.2 through B.6. Figure B.2 shows the axial stress in the seal during Condition I and Figure B.3 the hoop stress during this condition. Figures B.4, B.5, and B.6 show the axial, hoop and shear stresses respectively present during Condition II. Since the ends of the seal are totally restrained during this 1900 psi axial tensile load created by the differential expansion of bore seal and end bell (the end bell was assumed to have a thermal coefficient of thermal expansion of 13×10^{-6} in./in./°F) are algebraically added to the stress levels determined by the finite element analysis.

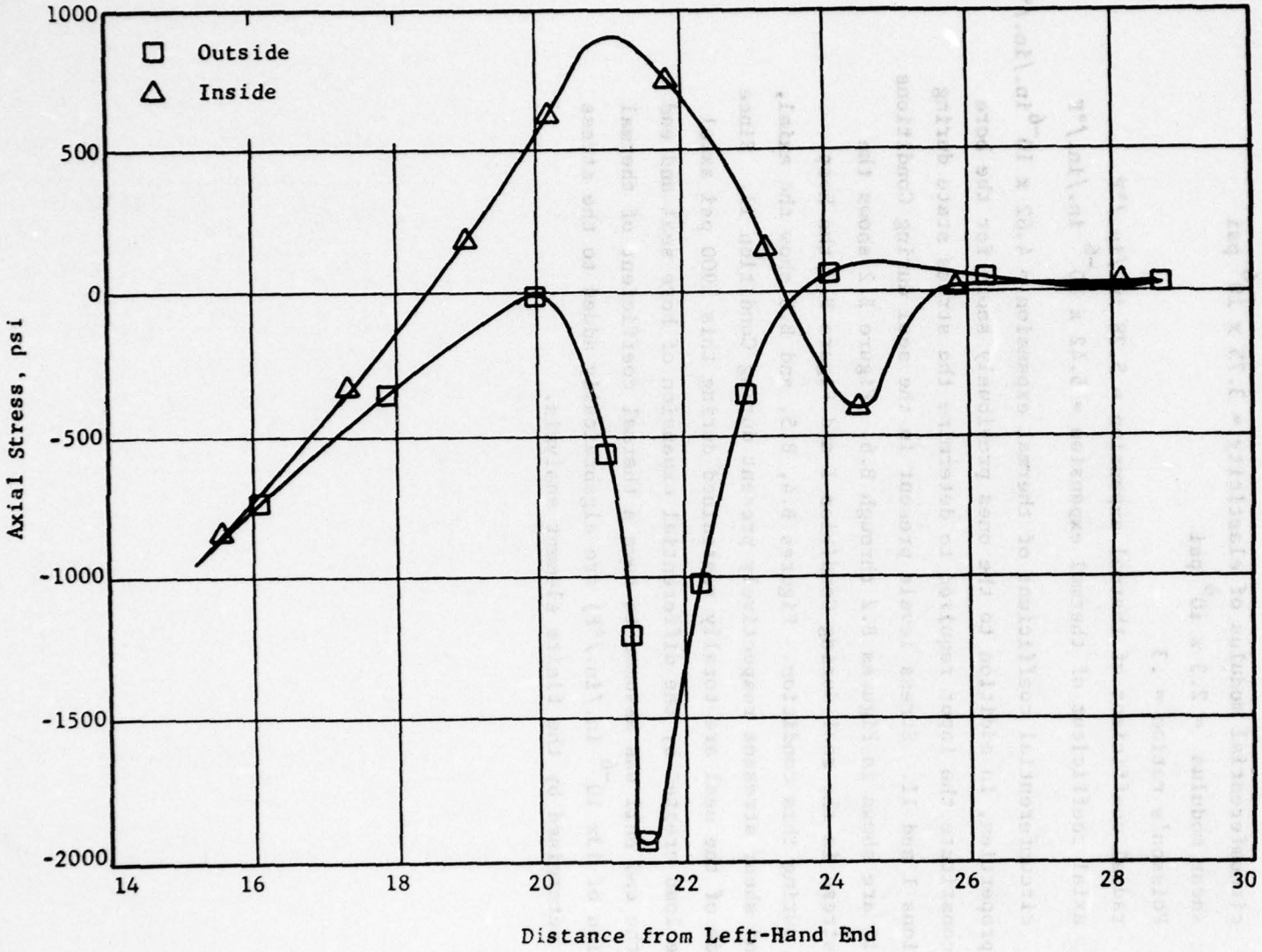


Figure B-2 Bore Seal Axial Stress Vs. Axial Length Condition I

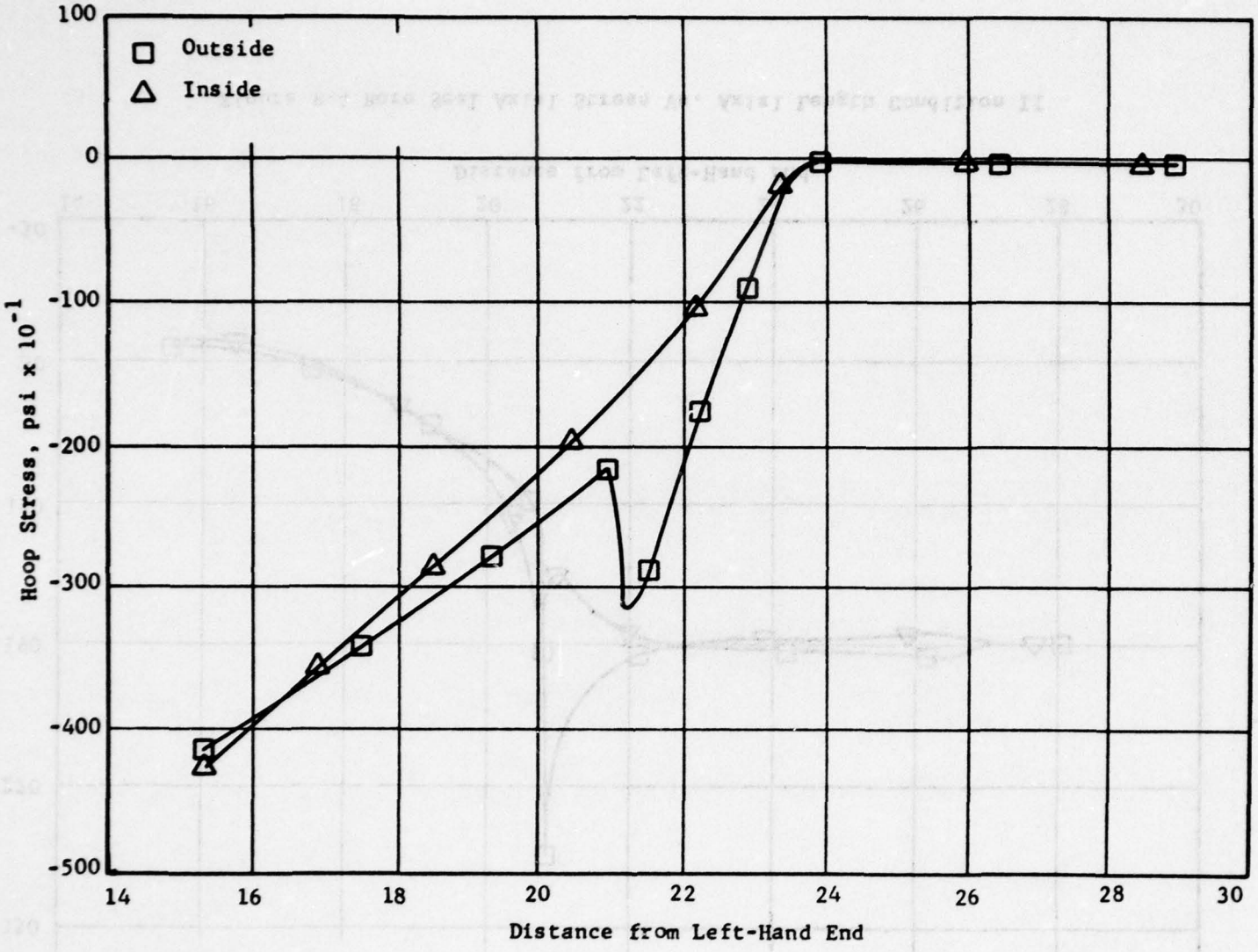


Figure B-3 Bore Seal Hoop Stress Vs. Axial Length Condition I

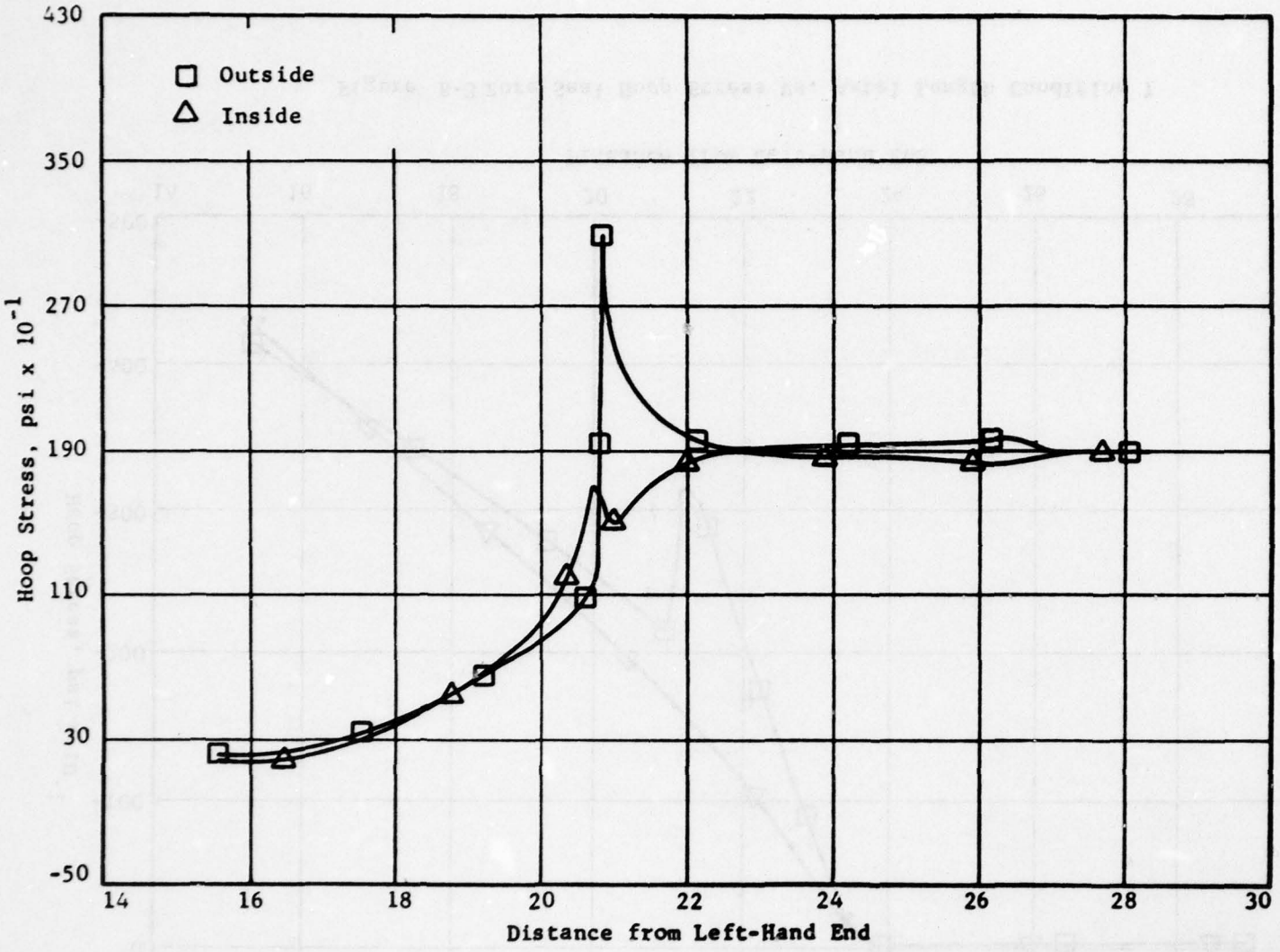
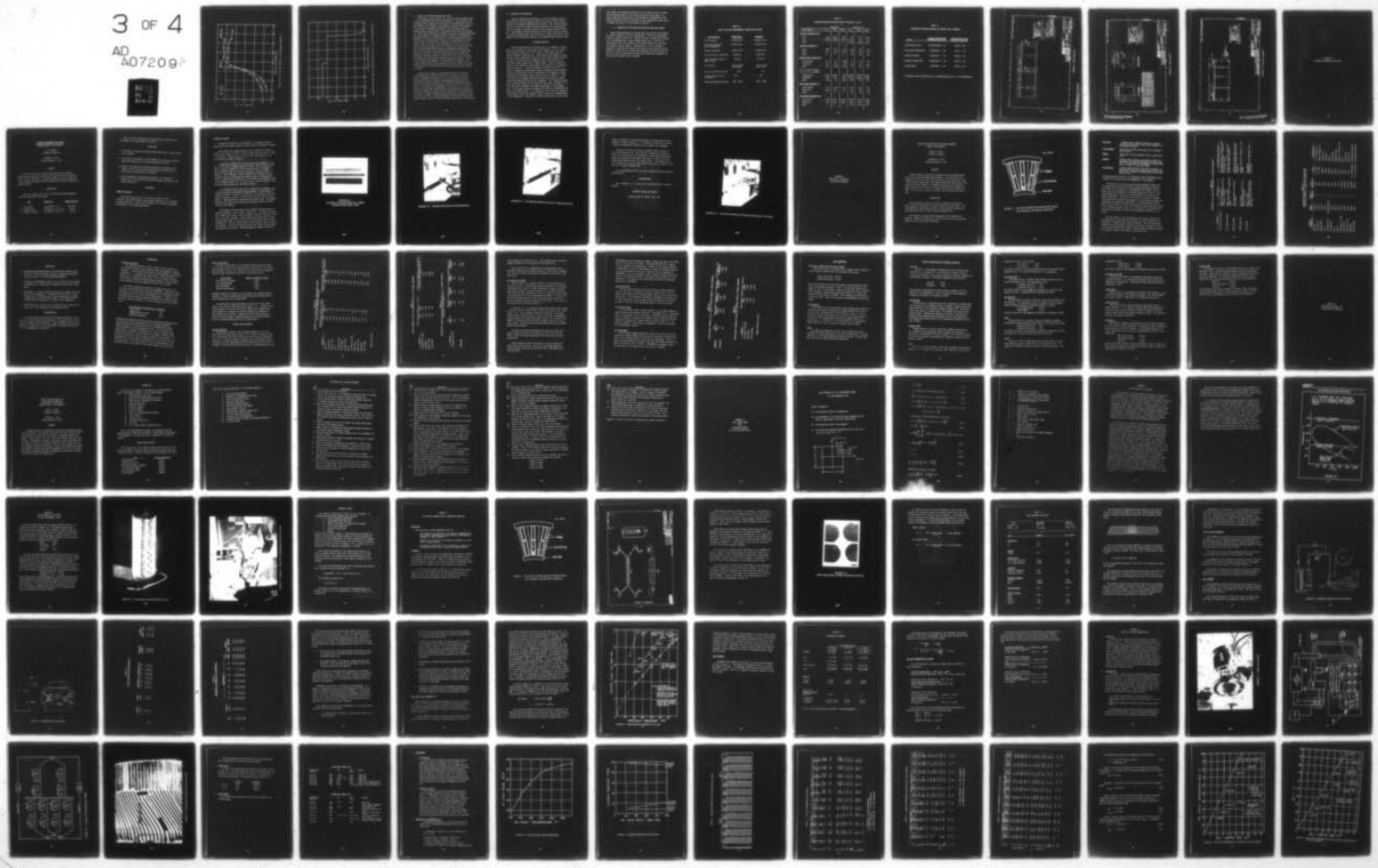


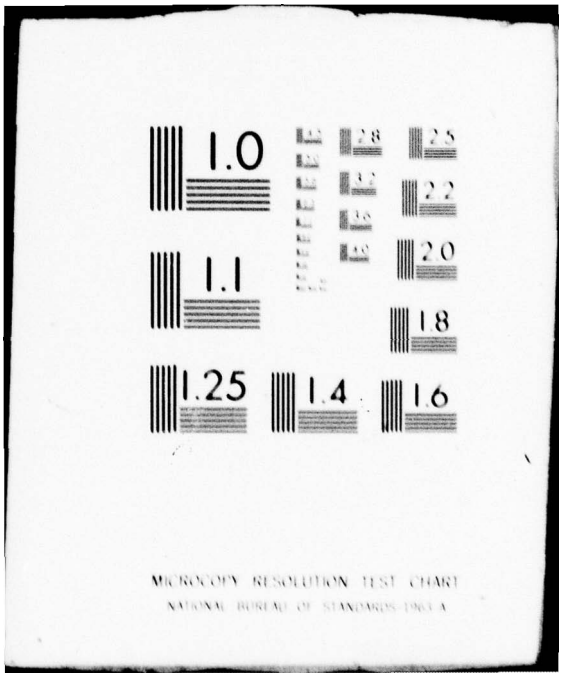
Figure B.4 Bore Seal Axial Stress Vs. Axial Length Condition II

AD-A072 093 WESTINGHOUSE ELECTRIC CORP LIMA OHIO AEROSPACE ELECT--ETC F/G 10/2
PROGRAM FOR THE DEVELOPMENT OF A SUPERCONDUCTING GENERATOR.(U)
FEB 79 J L MCCABRIA F33615-71-C-1591

UNCLASSIFIED AFAPL-TR-79-2012 NL

3 OF 4
AD A072093




1.0
1.1
1.25
1.4
1.6
2.8
2.5
2.2
2.0
1.8
MICROCOPY RESOLUTION TEST CHART
NATIONAL BUREAU OF STANDARDS 1963 A

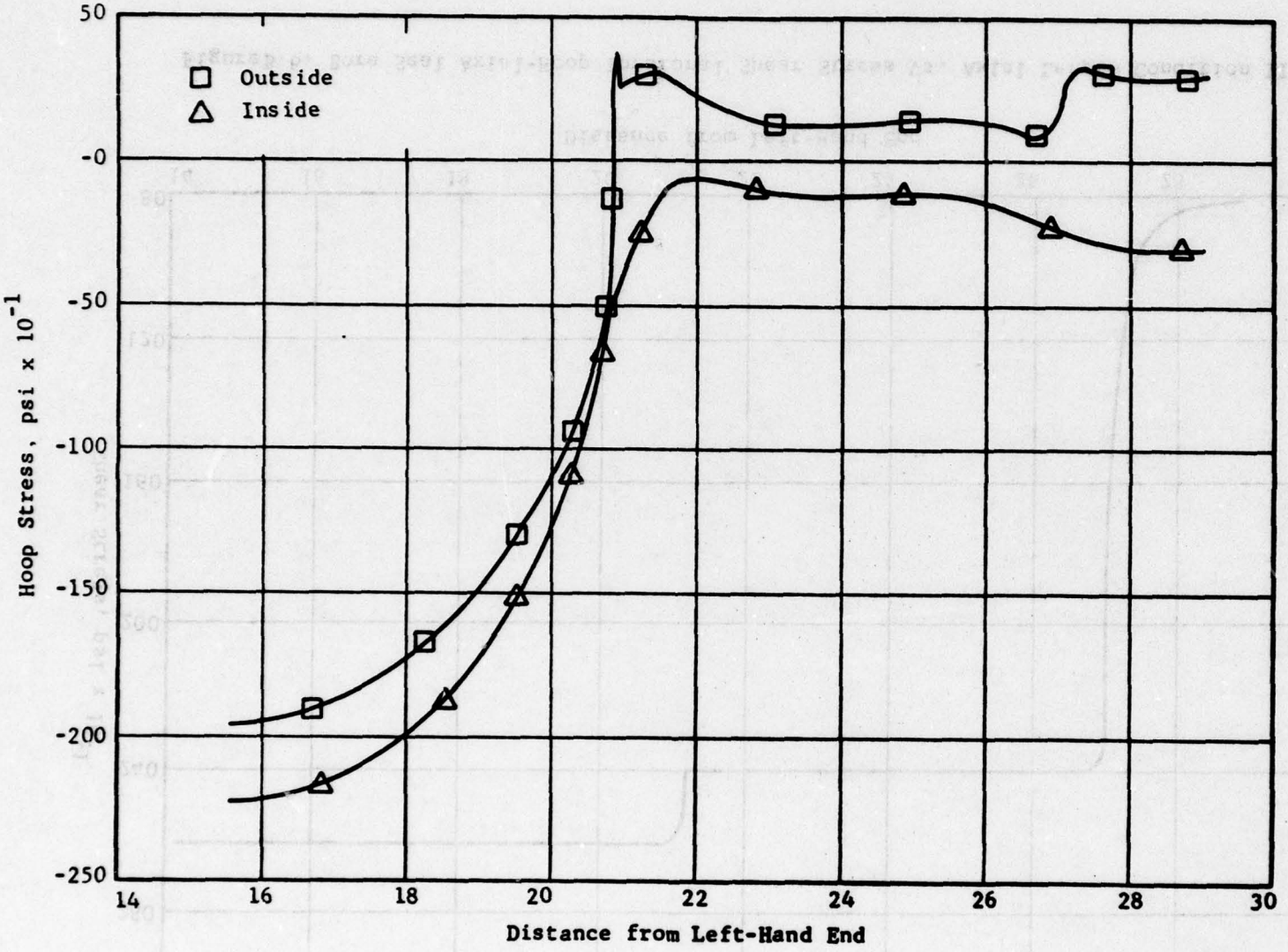
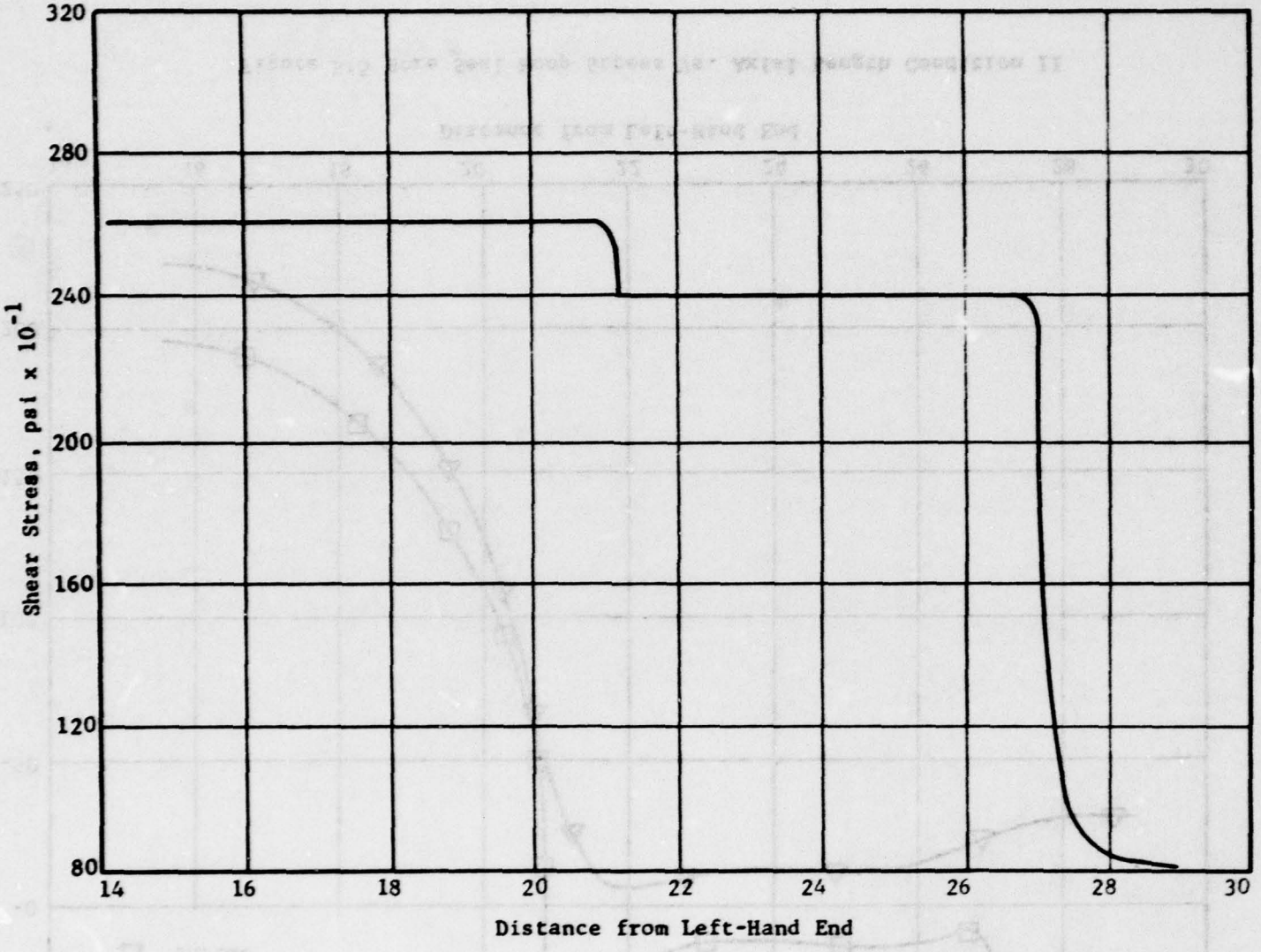


Figure B·5 Bore Seal Hoop Stress Vs. Axial Length Condition II



FigureB.6. Bore Seal Axial-Hoop Torsional Shear Stress Vs. Axial Length Condition II

B. ANALYSIS OF THE BORE SEAL-END BELL JOINT

The decision to bolt the bore seal to the end bell was based largely upon the favorable data found in Reference 22. By considering each attachment point a single lap bolted joint and calculating the ratios of edge distance, side distance, and thickness to the bolt hole diameter, it is possible to determine the adequacy of the bolting concept by comparing these critical ratios to acceptable ratios found in Reference 22. These values determine the ability of the joint to withstand bearing, tension and shear out. Assuming the load created by the differential expansion of the bore seal and end bell to be 2610 lb/bolt hole and the load created at transient motor operation to be 1200 lb/bolt hole the bearing, shear and tension in the composite at the joint can be calculated. Shear and tension loads were determined to be well below allowable loads determined during testing of fiberglass/aluminum joints, however, the bearing stress was approximately 25% of the demonstrated allowable of 130 ksi. The report however points out that when the thickness-to-bolt hole diameter ratios (t/d) of about .8 are exceeded bolt bending appears before the bearing allowable is reached. The t/d of this design of approximately 2.0 indicates that although the calculated bearing stress is high compared to the other loads at the joint it should pose no problem as the bolts will fail before this allowable is reached.

Optimal joint strength is achieved when half of the plies are oriented parallel to the load and half at a 45° angle to the load. Since the predominant load will be in an axial direction, plies of unidirectional cloth or filament wound broadgoods material with the strength in the axial direction, $\pm$ 45° helically wound layers and hoop layers in the sleeves are recommended in a ratio of 4:4:2. The hoop layers do not contribute significantly to the strength of the joint but are used to compact the cloth and helical layers and aid in producing a coefficient of thermal expansion in the sleeve which is similar to that in the bore seal tube. A marked difference in coefficients would cause excessive shear stresses in the joints which bond the tube to the sleeves.

C. BUCKLING OF THE BORE SEAL

Using the equations for buckling of thin wall cylinders found in Reference 23, critical buckling loads of the bore seal under external pressure and torsional loadings were determined. The critical buckling load for the bore seal under external pressurization is approximately 250 psi and under a torsional load the critical shear stress is 23,000 psi. The margins of safety indicated by these figures are high (205 psi for external pressurization and 20,400 psi for shear) thus the bore seal appears to be structurally capable of withstanding these critical loads.

V. STRENGTH ANALYSIS

Given the stress state in the bore seal, it is possible to determine at any location (1) the strain of the laminate, (2) the strain in each individual lamina and (3) the stress in each lamina using the method described in Reference 20. Three panels which appeared to have the most severe loading were selected for an in-depth strength analysis in order to determine how the computed strains and stresses in the individual lamina compare with allowable loads. Table B.2 shows the results of the analysis of these panels. The location of the panels is shown in Figure B.1. Using the information found in Table B.2, the ratios of maximum stress/allowable stress and maximum strain/allowable strain were calculated to give an indication of the margins of safety involved with this design. These values are seen in Table B.3. Table B.3 indicates all maximum predicted stresses and strains are considerably below experimentally derived allowables. The transverse tensile load of 1840 psi which occurs in the hoop layers during Condition II is the stress which represents the highest percentage of the allowable, 37%. All the other predicted stresses and strains are considerably less than the allowable values. It is important to note that the allowable values shown in Table B.3 represent typical values for fiberglass/epoxy at room temperature. Variations in manufacturing methods, fiber volume,

void content and properties peculiar to Dow X-D 7818 at 212°F can cause these allowable values to vary as much as 20% from those shown. As precise date which characterize the performance of fiberglass/X-D 7818 become available they can be inserted for the representative values used to compute the factors of safety shown in Table B-3.

VI. FABRICATION OF THE BORE SEAL TUBE AND BORE SEAL SLEEVES

Manufacturing drawings for the bore seal tube and bore seal sleeves are shown in Figures B-7 and B-8 respectively. The final sub-assembly drawing is shown in Figure B-9. Observe the left- and right-hand sleeves are to be machined from a single filament wound tube. Allow for an approximately .003 inch expansion of the inside diameter of both tubes upon removal from the mandrel. Additionally, it is not considered necessary to remachine the mandrel which will hold the bore seal during shrink fit as the .004 inch diametrical shrinkage of the tube during the shrink fit will be essentially the same as the diametrical expansion of the tube after removal from the mandrel.

TABLE B-1

DESIGN LOADS AND ENVIRONMENTAL CONDITIONS FOR STATOR

Load Condition	Steady State	Transient
Applied Torque	67,000 in.lb	268,400 in.lb
Torque Distributed to Seal (54% Applied)	36,234 in.lb	144,936 in.lb
Torque on Each End	18,117 in.lb	72,468 in.lb
Torsional Force on Each End	3,589 lbf	14,350 lbf
Torsional Shear Stress in Body of Tube	639 psi	2,557 psi
Oil Pressure	45 psig max @ tube center	45 psig max @ tube center
Back Iron 2G Inertial Load	1 psi	1 psi
Minimum Interference Fit on Tube OD	.006	.006
Operating Temperature Range	70°F - 212°F	70°F - 212°F

TABLE B-2

MAXIMUM STRESSES AND STRAINS DURING CONDITIONS I AND II

	Condition I			Condition II		
Panel Number	24	994	974	24	994	974
Composite Stresses, psi						
Axial	-954	2,045	927	175	3,102	1,668
Hoop	-4,300	3,098	-1,715	-2,227	233	-50
Shear	0	0	0	2,600	2,600	2,600
Composite Strains, %						
Axial	-.005	-.05	.05	-.02	.08	.02
Hoop	-.06	-.04	-.04	-.05	-.03	-.02
Shear	0	0	0	.18	.18	.18
Helical Lamina Strains, %						
Longitudinal	-.03	-.05	.005	.15	.21	.18
Transverse	-.03	-.05	.005	-.22	-.16	-.18
Shear	-.03	.005	-.05	.03	-.01	.02
Helical Lamina Stresses, psi						
Longitudinal	-2,932	-4,886	489	12,100	18,000	15,100
Transverse	-972	-682	162	-4,610	-2,660	-3,380
Shear	-252	42	-420	250	-80	170
Hoop Lamina Strains, %						
Longitudinal	-.06	-.04	-.04	-.05	-.03	-.02
Transverse	-.005	-.05	.05	-.02	.08	.02
Shear	0	0	0	.18	.18	.18
Hoop Lamina Stresses, psi						
Longitudinal	-5,488	-3,977	-3,295	-4,680	-2,180	-1,680
Transverse	-537	-1,552	-1,007	-850	1,840	380
Shear	0	0	0	1,512	1,512	1,512

TABLE B.3

COMPARISON OF MAXIMUM STRESSES AND STRAINS WITH ALLOWABLES

Stress	Maximum Stress (psi)* / Allowable Stress (psi)	Maximum Strain (%)* / Allowable Strain (%)
Longitudinal Tensile	18,000/250,000 = .07	.21/2.8 = .08
Longitudinal Compression	5,488/60,000 = .09	.06/.6 = .10
Transverse Tensile	1,840/5,000 = .37	.08/.33 = .24
Transverse Compression	4,610/25,000 = .18	.22/1.0 = .22
In-Plane Shear	1,512/6,000 = .25	.18/1.0 = .18

*Allowables found in Reference 15 for fiberglass/epoxy resin at room temperature.

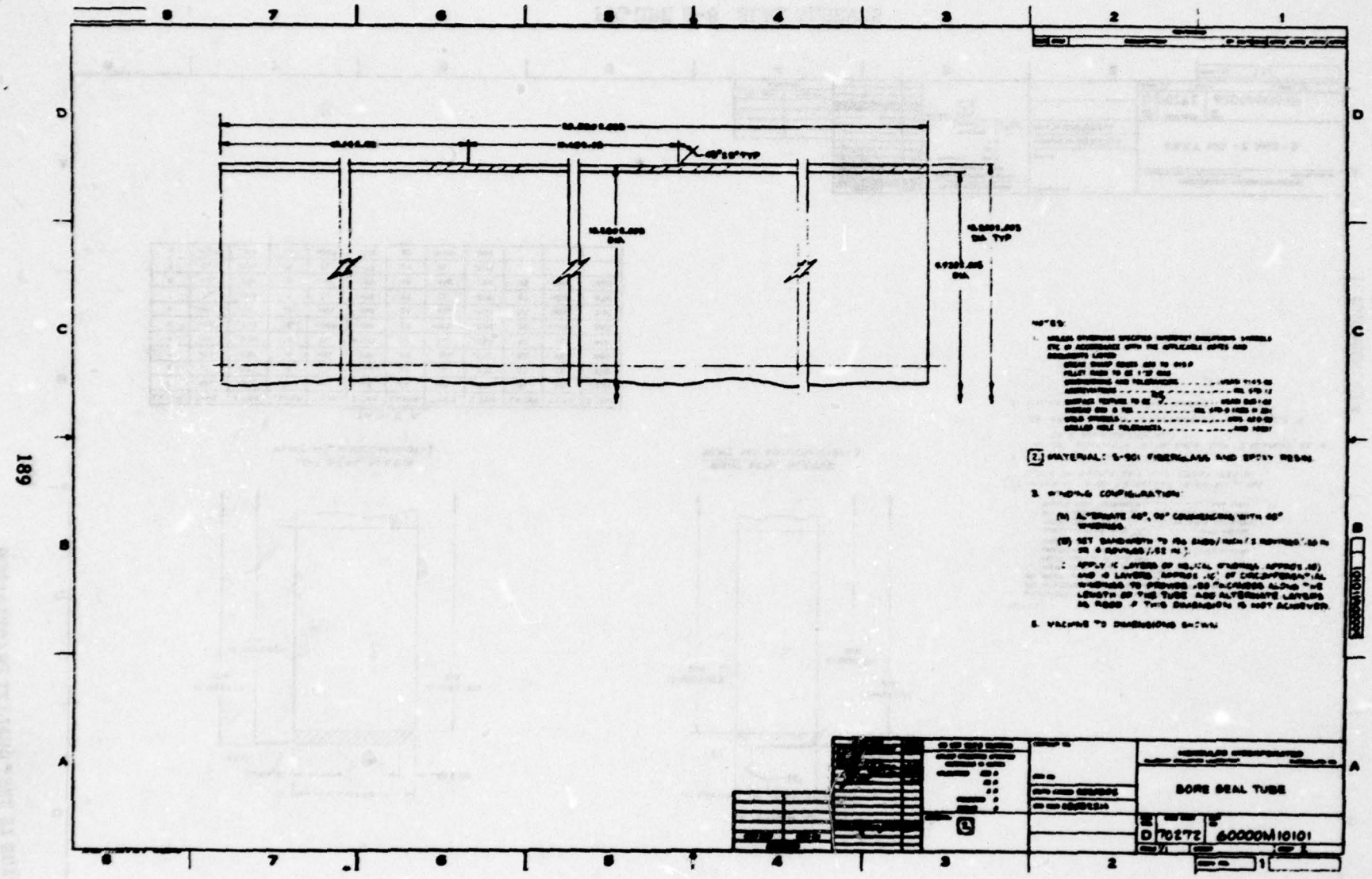


FIGURE B-7 BORE SEAL TUBE

THIS PAGE IS BEST QUALITY PRACTICABLE
FROM COPY FURNISHED TO DDC

THIS PAGE IS BEST QUALITY PRACTICABLE
FROM COPY FURNISHED TO DDC

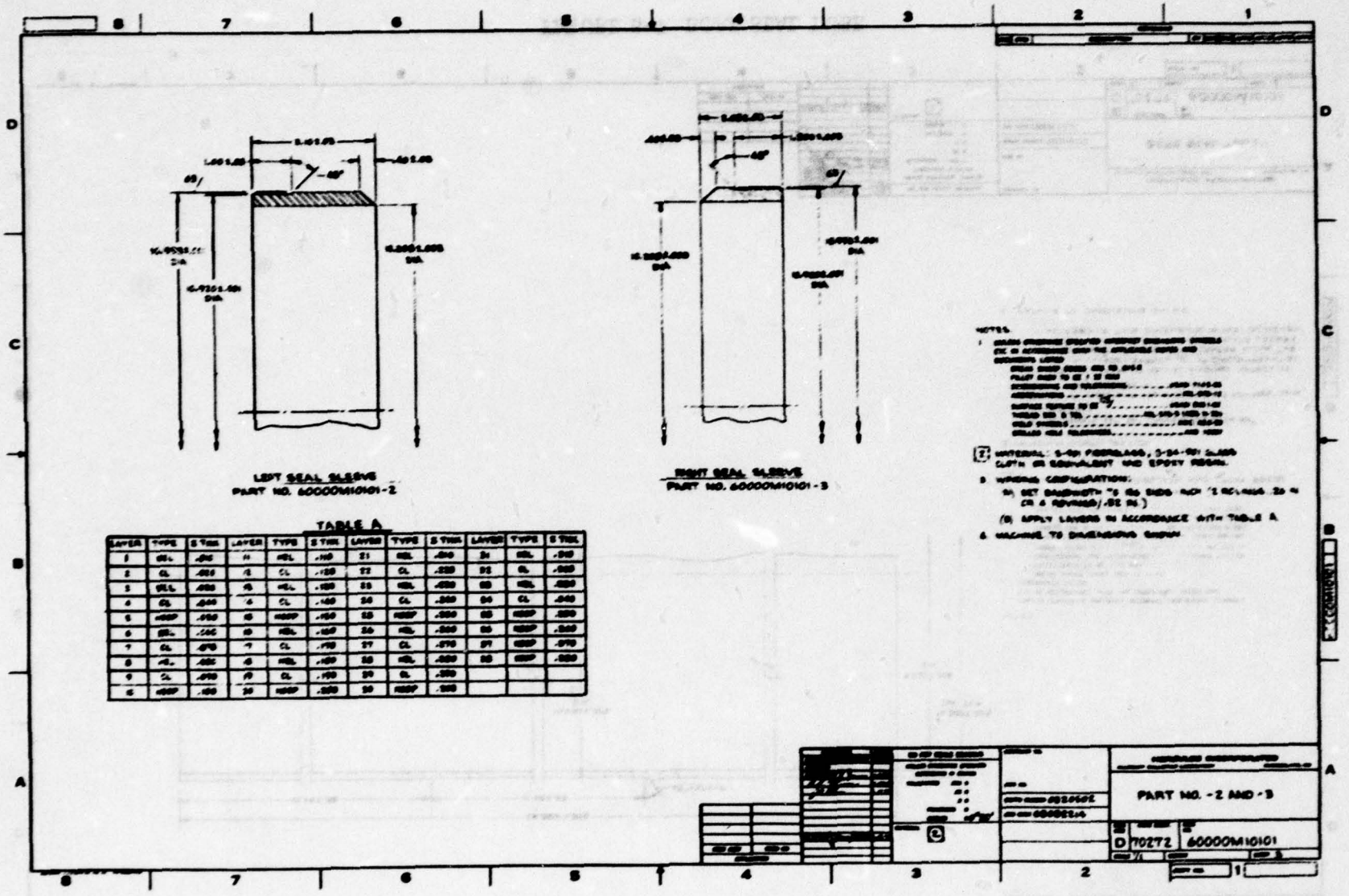


FIGURE B-8 SEAL SLEEVES

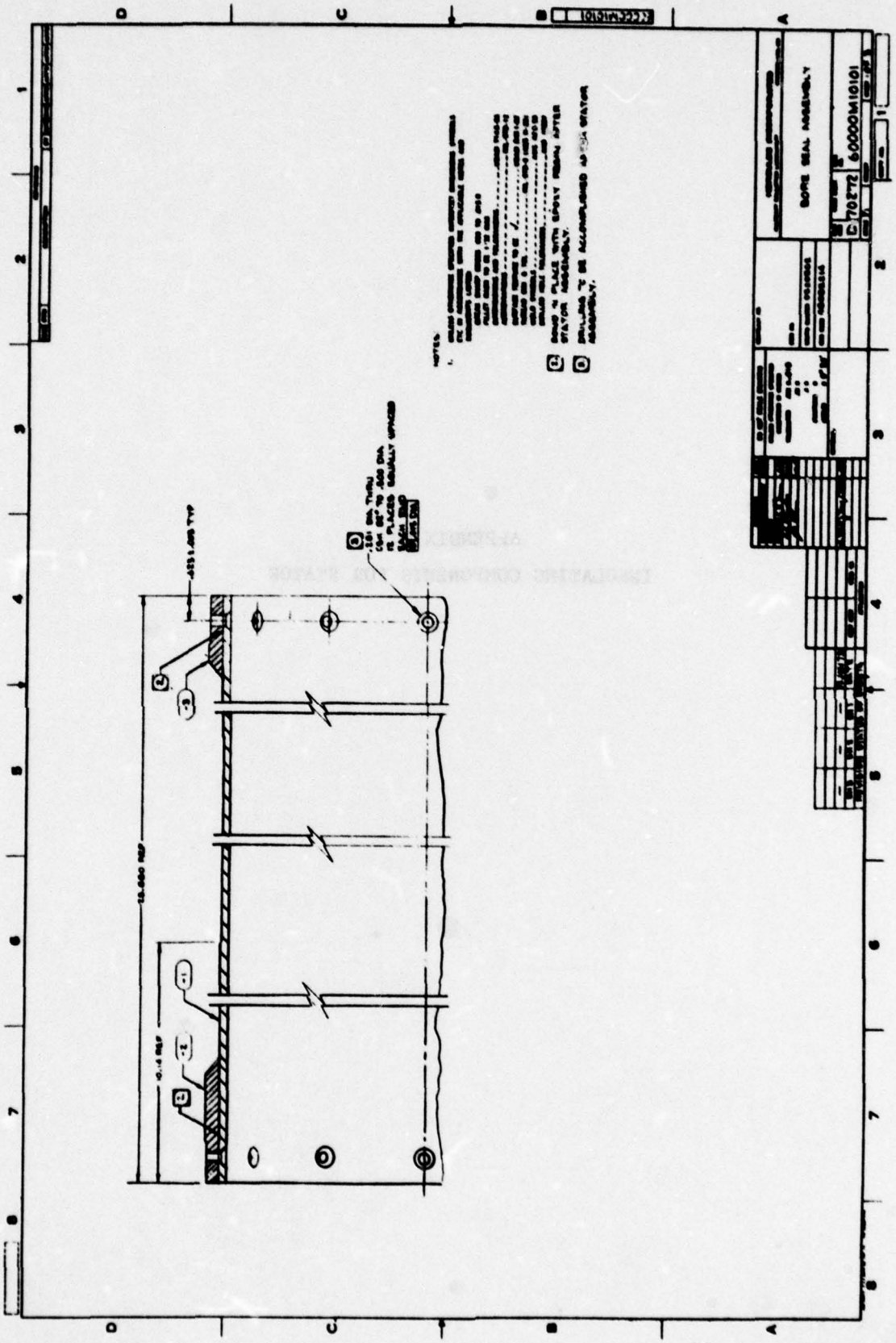


FIGURE B-9 BORE SEAL ASSEMBLY

THIS PAGE IS BEST QUALITY PRACTICABLE
FROM COPY FURNISHED TO DDC

APPENDIX C

INSULATING COMPONENTS FOR STATOR

INSULATION COMPONENTS FOR STATOR

RESEARCH REPORT 75-8B7-BORSE-R3

Z. N. Sanjana

Polymers & Plastics

November 11, 1975

Revised November 4, 1978

ABSTRACT

The stator has several non-structural insulating components. Materials were specified, obtained and machined for these components. For one of the components - a U-shaped channel which will contain the coils -tooling was designed and the channels were wound and machined to specifications.

INTRODUCTION

The stator design calls for the following insulating components which are described in this report:

Item	Drawing No.	Number Required
1. Coil Spacer	ED 362769 IT. 3 & 6	192 each
2. Channel Wedge	ED 383339 IT. 6,7,8, & 9	96 each
3 Conductor Channel	ED 383339 IT. 1,2,3, & 4	96 each

While no stress requirements were specified, the materials had to withstand the coolant (Wemco C) at 100°C.

CONCLUSIONS

1. The spacers and wedges were machined from NEMA grade G-11 glass cloth-epoxy laminate.

2. The channels were wound on a steel mandrel from a Class F polyester-glass tape supplied by the Industrial Materials Division.

3. Because of the small size and close dimensional tolerances on the channel, lower cost alternative manufacturing procedures such as pultrusion or extrusion were not feasible.

4. Injection molding or matched-metal molding of the channels is feasible but costs incurred would have been higher than those of the winding method used.

DISCUSSION

Wedges and Spacers

Since these materials had to be strong and rigid at 100°C in Wemco C oil, it was decided to make them of NEMA grade G-11 (44163AG) epoxy-glass laminate. Material was obtained in the required thicknesses and machined to the drawing dimensions.

Conductor Channels

The material selected for the channels is a B-staged polyester-glass fabric tape (5M54) obtained from the Industrial Materials Division.

The channels are U-shaped and have a wall thickness of 0.020" ± 0.004" and a height of 0.917" ± 0.010" for one type, and 0.867" ± 0.010" for the other. Channel width is 0.178 ± 0.001" and length is 5.14". The channels are shown in Figure C.1.

Originally we decided that by winding the correct number of plies on a 0.178" thick rectangular mandrel of width 1.754", we could obtain the two types of channels by cutting along the axis of the mandrel. This required a 0.010" cut and we were hoping to make the axial cut manually. After machining a sample mandrel from aluminum, it was determined that (a) we could not meet specifications on channel height when we cut the channels manually, and (b) without putting some pressure on the channels during cure, we could not get a cohesive wall nor could we obtain the necessary wall thickness tolerance.

It was decided that we would cut the channel off the mandrel using a carbide cutter on a horizontal milling machine. We also decided to design the mandrel to allow for a 0.025" cut. The cutting was facilitated by machining a groove of 0.030" width and 0.010" depth into the mandrel. Eight mandrels were made from cold rolled steel. The mandrels were made 20" long so that three pairs of channels could be obtained from one wound mandrel.

The channels were hand wound using a filament winding machine to rotate the mandrel. This is shown in Figure C.2. The glass cloth tape has a 0.004" thick fabric, thus five plies of tape are required to build up to the 0.020" thickness. After spraying the mandrel with a fluorocarbon release agent, the first layer of tape was butt wound, as shown in Figure C.2. The next pass was made by half-lapping, thus two layers were applied. The next two passes were both butt wound, thus providing the requisite five layers. The wound mandrel is shown in Figure C.3.

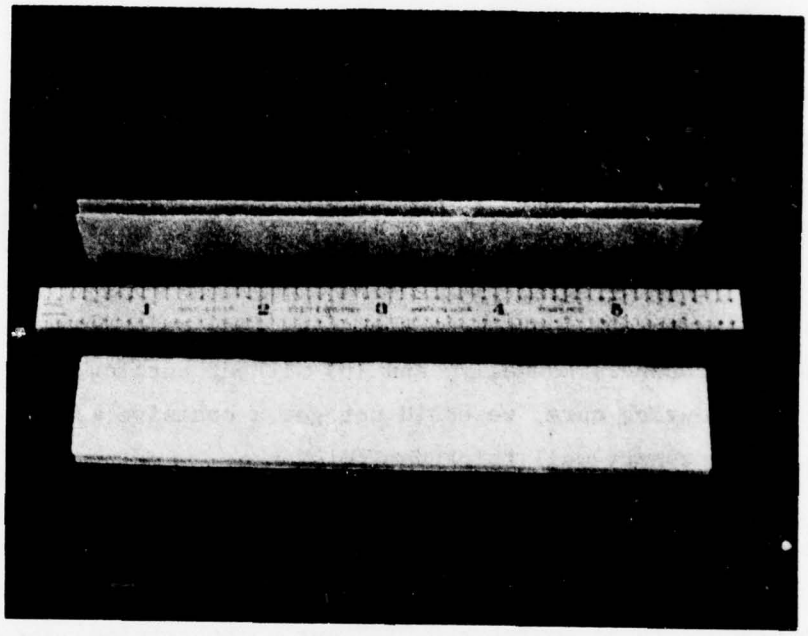


FIGURE C-1
Conductor Channels Made From 5M54
Polyester-Glass Fabric Tape



FIGURE C.2 - Winding Tape Onto the Steel Mandrel



FIGURE C.3 - The Mandrel With Five Layers of Tape Wound On

Finally, the mandrel was sandwiched between flat plates and bars and clamped, as shown in Figure C·4. The purpose of these was to allow us to meet the dimensional tolerances on the channel wall thickness.

The tape was cured by placing the assembly shown in Figure C·4 in a circulating air oven. Cure time was a minimum of 2.5 hours at 150°C. It was allowed to cool gradually to room temperature when the clamps were removed and the mandrel was taken to be cut on the horizontal milling machine along the mandrel groove. (The groove can be seen in Figure C·2.) The 18" long channels were cut to a length of 5.14" on a wet saw with a diamond wheel.

All channels fabricated by this method easily fell within required specifications.

ACKNOWLEDGMENT

Sincere thanks to R. L. Selby for the fabrication of the conductor channels.

PERMANENT RECORD BOOK ENTRIES

Figuring Book No. 206632...Pgs. 7274

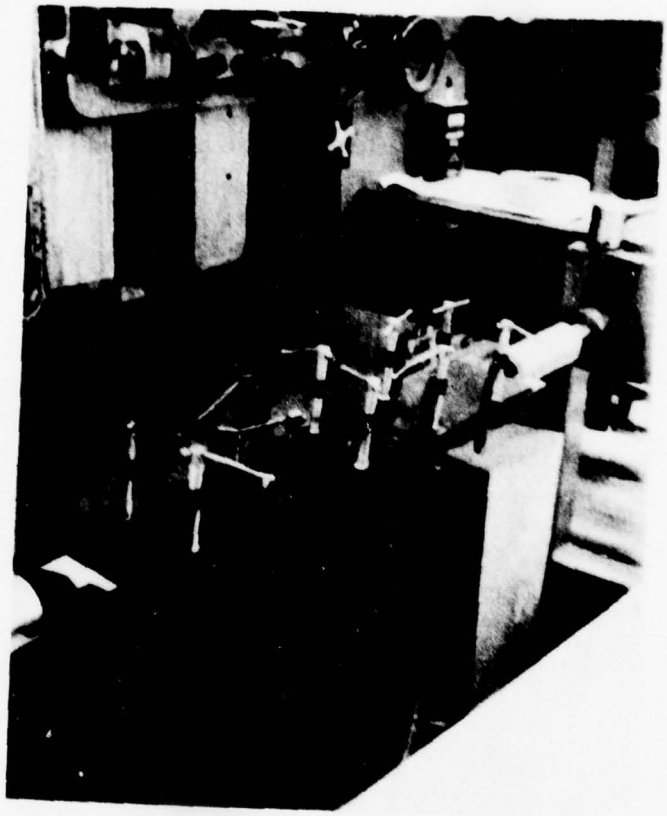


FIGURE C.4 - Tape Wound Mandrel Sandwiched Between Flat Plates

APPENDIX D

EVALUATION OF ADHESIVES FOR STATOR COMPONENTS

EVALUATION OF ADHESIVES FOR STATOR COMPONENTS
REPORT 75-8B7-BORSE R2

Edward M. Petrie
Polymers & Plastics

September 16, 1975
Revised November 4, 1978

ABSTRACT

Various adhesive systems were evaluated for use in manufacturing the stator for the superconducting generator. The substrates to be bonded include the bore seal, bore seal sleeves, and coil support rings (filament wound epoxy-glass); coil channels (polyester-glass tapes); and wedges (G-11 epoxy laminate). Candidate adhesives were evaluated for shear strength at 25°C and 100°C, strength retention after immersion in Wemco C oil at 100°C, fatigue, resistance, and processing characteristics.

INTRODUCTION

The all-composite nature of the stator components necessitates heavy reliance on adhesives to provide a monolithic construction. This investigation was undertaken to select the best adhesive candidate for each application and to provide related performance data.

The following composite stator components will be bonded by an adhesive. Figure D.1 illustrates an end view of the stator section and shows the most critical bond interfaces.

Dwg. 6364A92

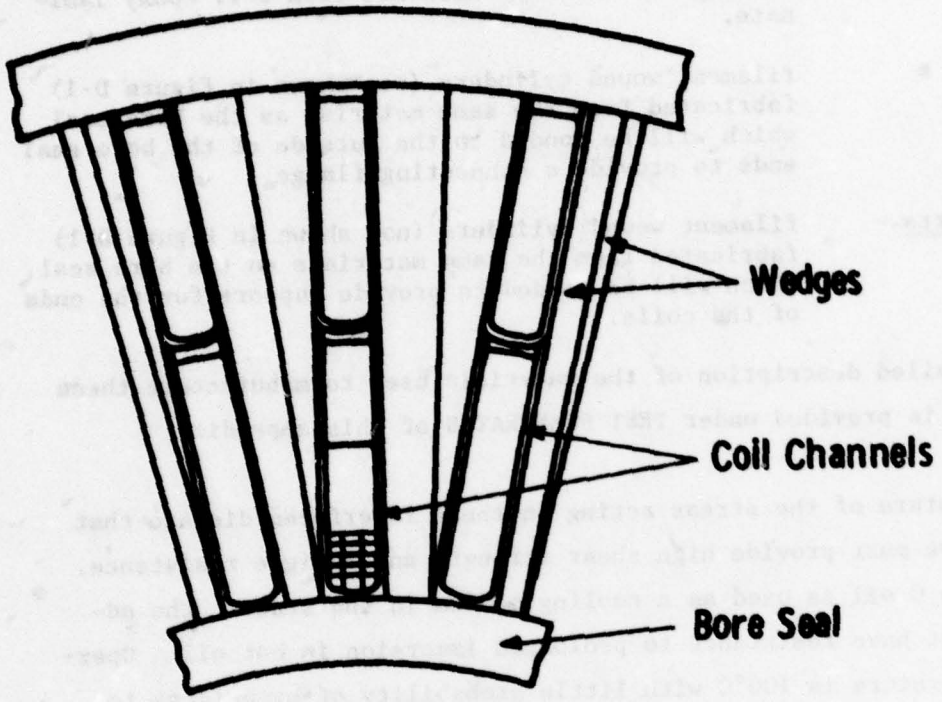


FIGURE D-1 END VIEW OF STATOR SECTION SHOWING WEDGE, COIL CHANNEL, AND BORE SEAL INTERFACES

Bore Seal - a filament wound cylinder consisting of S-glass roving reinforced with an epoxy resin designated by Westinghouse Research.

Coil Channels - tape wound U-channels fabricated from a polyester-glass prepreg.

Wedges - rectangular sections machined from G-11 epoxy laminate.

Sleeves - filament wound cylinders (not shown in Figure D·1) fabricated from the same material as the bore seal which will be bonded to the outside of the bore seal ends to provide a connecting flange.

Coil Supports - filament wound cylinders (not shown in Figure D·1) fabricated from the same materials as the bore seal which will be bonded to provide support for the ends of the coils.

A more detailed description of the materials used to manufacture these components is provided under TEST SUBSTRATES of this appendix.

The nature of the stress acting on these interfaces dictate that the adhesive must provide high shear strength and fatigue resistance. Since Wemco C oil is used as a cooling medium in the stator, the adhesives must have resistance to prolonged immersion in hot oil. Operating temperature is 100°C with little probability of excurisons to higher temperatures. Because of the details of the stator's assembly, the ashesive must possess varying degrees of thixotropy and working life depending on the particular application. Curing temperature requirements should be 300°F or less to avoid thermal stresses which may develop in the complex structure. Table D·1 is a matrix of the performance and processing requirements necessary for each adhesive interface in the stator.

The first phase of this investigation was to screen elevated and room temperature curing structural adhesives for bond strength and oil resistance on a general epoxy laminate substrate. The most appropriate candidates were then further evaluated on substrates equivalent to those of the actual generator with regard to shear strength, fatigue resistance and strength retention after aging in 100°C Wemco C oil.

TABLE D-1
PERFORMANCE AND PROCESSING REQUIREMENTS OF CANDIDATE ADHESIVES

Interface	Environment	Processing Characteristics
Bore Seal-Coil Channels	Wemco C oil at 100°C. Shear loads approximately 504 psi transient. Fatigue.	Long working life to provide for lay-up Gap-filling: 0-20 mils. Thixotropic for vertical lay-up.
Coil Channels-Wedges	Wemco C oil at 100°C. Slight shear loads of undetermined stress	Low viscosity liquid for negligible bondline allotment: 0-2 mils.
Bore Seal-Wedges	Same requirements as Bore Seal-Coil Channel.	Adhesive will be the same as used for Coil Channels-Wedges because of convenience.
Sleeves-Bore Seal	Air at 100°C. Shear loads will be minor due to mechanical fasteners.	Suitable viscosity to maintain a 5 mil bondline.
Coil Support	Wemco C at 100°C. No Shear Stress except for oil pressure, adhesive serves mainly as a seal.	Gap filling. Preferably a room temperature cure to avoid stress.

TABLE D·2
CANDIDATE ADHESIVES FOR BORE SEAL APPLICATIONS
(Detailed Description on Pages 215 through 219)

Adhesive Tradename	Generic Type	Number of Components	Cure Temperature	Form	Manufacturer
Tame 200	Acrylic	2	Room	Lt. Paste	B. F. Goodrich Co.
Versilok 506	Acrylic	1	Room	Lt. Paste	Hughson Chemical Co.
Trabond 2135D	Epoxy	2	Room	Liquid	Tra-Con, Inc.
A-271	Epoxy	2	Room	Liquid	Armstrong
Scotchweld 3520	Epoxy/Elastomer	2	Room	Liquid	3M Co.
RP-138/H-998	Epoxy	2	Room	Paste	Ren Plastics
#8751	Epoxy	2	Room	Liquid	Epoxylite Corp.
EA-934	Epoxy	2	Room	Paste	Hysol Div., Dexter Corp.
Scotchweld 2214 NMF	Epoxy	1	Elevated	Paste	3M Co.
Uniset 908-4	Epoxy	1	Elevated	Paste	Amicon Corp.
Uniset 2027-47D	Epoxy	1	Elevated	Paste	Amicon Corp.
XB2793/MDA	Epoxy	2	Elevated	Lt. Paste/Liquid	Westinghouse Research
XD7575.02/MDA	Epoxy	2	Elevated	Lt. Paste/Liquid	Westinghouse Research

CONCLUSIONS

1. XB2793/MDA (Westinghouse Research) has excellent adhesive properties on all of the polymeric composite substrates intended for use in the stator of the superconducting generator.

2. Resistance of XB2793/MDA to Wemco C oil at 100°C is also excellent. No degradation of tensile-shear strength was noticed after 1,000 hours.

3. XB2793/MDA is a two-part adhesive system with a working life of 48 hours at room temperature. Scotchweld 2214 NMF (3M Co.), whose strength and oil resistance were second to XB2793/MDA, provides a working life for application of 6 weeks at room temperature.

4. EA-934 (Hysol Div., Dexter Corp.) provided the best overall properties for a room temperature curing adhesive system.

RECOMMENDATION

It is recommended that XB2793/MDA (Westinghouse Research) be used on all the stator applications provided that the working life is sufficient for assembly of the components. Where XB2793/MDA connot be used because of working life or cure requirements, Scotchweld 2214 NMF (3M Co.) is recommended as a substitute.

EXPERIMENTAL

Screening Evaluation

The candidate adhesives listed in Table D.2 were selected for investigation because of their reported high bond strength to plastic laminates. A more detailed description of these adhesives is presented subsequently. A screening test was devised to limit the number of adhesives to a manageable number which could be evaluated in detail. The screening criteria were tensile-shear strength at 25°C and 100°C before and after 300 hours immersion in Wemco C oil at 100°C.

The substrate materials selected to be used in the stator construction are described fully under TEST SUBSTRATES. During the screening phase, the actual bore seal formulation was not used because it was not decided upon at the time of the screening tests. Instead, a substrate was used which was the preferred material at the time; the only difference being the absence of a reactive diluent in the final formulation.

Resin System For Screening Test Substrates	
XB2793 Epoxy	70 g
DGENPG Reactive Diluent	30 g
Methylene Dianiline	34 g

Laminates were prepared from this resin and tensile-shear specimens were then fabricated from this substrate with the candidate adhesives. Specimen geometry and testing procedure were per ASTM D1002 using a sample population of three specimens per test. The substrates were treated prior to bonding by abrayding with a 120X grit aluminum oxide sanding belt followed by a solvent wash with acetone. Bondline thickness was maintained at 5 mils by using a suitable bonding fixture. All specimens that required elevated temperature cure were cured in an air circulating oven. A positive pressure of ½ psi was maintained on the specimens during cure by means of dead weight loading on the bond area.

Final Testing Phase

The final testing phase of this program employed substrates identical to those chosen for the final generator construction. The following ASTM D1002 lap shear joint designs were prepared using the adhesives having superior properties as measured by the screening test:

Joint Design	Bondline Thickness, Inches
Bore Seal-Coil Channel	0.003
Coil Channel-Wedge	0.001
Bore Seal-Wedge	0.003
Barrier Ring-Aluminum	0.003

Bondline thickness was varied so as to represent the designed bondline allotment. Surface treatment and bonding procedures were identical to those followed under the screening phase.

The resulting lap shear specimens were tested at 25°C and 100°C after 0, 250, 500 and 1,000 hours aging in Wemco C oil. Because of the critical nature of the bore seal-to-coil channel joint, samples were also evaluated for resistance to fatigue loading (8 to 800 psi) at a rate of 80 cycles per minute. Samples were cycled until failure or until 10^6 cycles elapsed. Fatigue specimens were not aged in Wemco C oil or at elevated temperatures prior to being tested.

RESULTS AND DISCUSSION

Initial Screening

Tensile-shear strenths of the candidate adhesives at 25°C and 100°C before and after aging in Wemco C oil at 100°C are shown in Table D·3. The substrate was not the actual bore seal resin but differed by addition of a reactive diluent as explained in the Experimental section. Scotchweld 2214 NMF, XB2793/MDA and XC7575.02/MDA exhibited excellent strength at 25°C and 100°C and showed little or no degradation after 300

TABLE D·3
SCREENING TESTS OF CANDIDATE ADHESIVES; TENSILE-SHEAR STRENGTH
ON 0.063" EPOXY FIBERGLASS SUBSTRATES

Adhesive	Tensile-Shear Strength, psi, After No Environmental Aging; Tested at 25°C	Tensile-Shear Strength, psi, After No Environmental Aging; Tested at 100°C	Tensile-Shear Strength, psi, After 300 Hrs. Aging in 100°C Wemco C Oil; Tested at 25°C	Tensile-Shear Strength, psi, After 300 Hrs. Aging in 100°C Wemco C Oil; Tested at 100°C
Tame 200	2,527	300	1,930	990
Versilok 506	2,783	820	3,040	280
Trabond 2135D	3,003	193	2,950	127
A-271	2,167	643	1,940	1,170
Scotchweld 3520	3,297	377	3,850	330
EP-138/H-998	1,507	650	1,413	423
Epoxylite #8751	2,780	290	2,420	257
EA-934	1,717	617	1,403	1,153
Scotchweld 2214 NMF	2,580	2,473*	2,590	2,090
Uniset 908-4	3,123	877	1,837	327
Uniset 2027-47D	2,213	477	1,663	306
XB2793/MDA	2,233	2,000	2,117	2,463
XD7575.02/MDA	2,533	1,883	1,583	2,193*

*Substrate failure.

TABLE D.4
TENSILE STRENGTH OF BORE SEAL SUBSTRATE BONDED TO COIL CHANNEL SUBSTRATE

Adhesive	Tensile-Shear Strength, psi, Tested at 25°C	Tensile-Shear Strength, psi, Tested at 100°C	Tensile-Shear Strength, psi, After 300 Hrs. in Air at 100°C, Tested at 25°C
Scotchweld 2214 NMF	1,378	1,184	1,156
XB2793/MDA	1,538	1,266	1,216
XD7575.02/MDA	1,100	983	1,200
Uniset 908-4	620	466	1,070

TABLE D.5
TENSILE-SHEAR STRENGTH OF BORE SEAL SUBSTRATE BONDED TO COIL CHANNEL SUBSTRATE AFTER AGING IN 100°C WEMCO C OIL

Adhesive	Test Temp., °C	Tensil-Shear Strength, psi, After Aging in 100°C Wemco C Oil 0 Hours	250 Hours	500 Hours	1,000 Hours
Scotchweld 2214 NMF	25	1,378	927	900	1,033
	100	1,184	853	780	987
XB2793/MDA	25	1,538	1,797	1,670	1,613
	100	1,266	1,403	1,500	1,650

hours immersion in 100°C Wemco C oil. These adhesives were selected as primary candidates for the critical bore seal applications.

EA-934 and A-271 are room temperature setting adhesives which exhibited relatively good strength retention at 100°C and after aging in oil. These two systems were chosen as candidates for the barrier ring application.

Bore Seal-Coil Channel

The bore seal to coil channel interface is the most important in the stator because of its high load bearing requirements and relatively large bonded area. Table D·4 shows tensile-shear strength of the bore seal substrate bonded to the coil channel with the primary candidates. Uniset 908-4 was also evaluated as a basis for comparison and to confirm its unexpectedly poor elevated temperature performance. Scotchweld 2214 NMF and XB2793/MDA exhibited better overall properties and were subjected to extended aging tests in Wemco C oil at 100°C. The results of these aging tests are shown in Table D·5.

In general, all of the adhesives showed significantly lower strength on the bore seal-coil channel joints than on bore seal-bore seal joints (Table D·3). This is probably caused by the polyester coil channel substrate which is more difficult to bond to than epoxy. XB2793/MDA is clearly superior to Scotchweld 2214 NMF in the hot oil resistance tests. XB2793 is a hydantoin epoxy resin which is highly polar, and in fact, water soluble. The high polarity and good wetting properties of XB2793 provide strong adhesion.

Scotchweld 2214 NMF and XB2793/MDA joints were also subjected to tensile fatigue cycling of 8 to 800 psi at a rate of 80 cycles per minute. None of the joints failed after 10^6 cycles and the test was discontinued.

Lengthy working time may be necessary to lay-up the many coil channels around the bore seal. The effect of prolonged laboratory ambient exposure on uncured Scotchweld 2214 NMF or XB2793/MDA has not been determined.

XB2793/MDA may prove unsuitable, however, because once mixed, the working life is on the order of 48 hours. Scotchweld 2214 NMF has a working life of 6 weeks at room temperature. Because of the superior adhesion of XB2793/MDA, it would be advantageous to design the assembly operation so that this adhesive can be used. Because of the low viscosity of XB2793/MDA, it will be necessary to add a thixotropic agent such as Cab-O-Sil at 5-10 precent by weight to provide non-sag properties for this application. The addition of Cab-O-Sil will not affect the adhesive properties of XB2793/MDA.

Bore Seal-Sleeves

The bore seal-to-sleeve joint is not critical because operating loads are small due to mechanical fasteners through the bore seal and sleeve. Both substrates are filament wound cylinders using the bore seal resin matrix. Both Scotchweld 2214 NMF and XB2793/MDA are satisfactory for this application. Shear strength should approximate those realized in Table D.3 because of the epoxy-epoxy nature of the joint design.

Coil Channel-Wedge

The coil channel-wedge interface requires a low viscosity adhesive because of negligible bondline allotment. Scotchweld 2214 is a thixotropic paste and unsuitable for this application. XB2793/MDA without Cab-O-Sil filler, provides low viscosity and excellent shear strength and strength retention in wedge-to-coil channel joints as shown by Table D.6. The adhesive bondline in these tests was maintained at 0.001" as explained in the Experimental section.

Bore Seal-Wedge

The bore seal-to-wedge application is minor in terms of total bond area and the adhesive must be the same as that selected to bond the bore seal to coil channels because of the stator's construction. Table D.7 shows the bond strength of Scotchweld 2214 NMF, XB2793/MDA and XD7575.02/MDA in this joint at 25°C and 100°C. XB2793/MDA will adequately bond the bore seal to the wedges as well as to the coil channels.

TABLE D.6

TENSILE-SHEAR STRENGTH OF COIL CHANNEL SUBSTRATE BONDED TO WEDGE SUBSTRATE

Adhesive	Test Temp. °C	Tensile-Shear Strength, psi, After Aging in 100°C Wemco C Oil			
		0 Hours	250 Hours	500 Hours	1,000 Hours
XB2793/MDA	25	1,840	1,849	1,677	1,920
	100	1,524	1,600*	1,453	1,580

TABLE D.7

TENSILE-SHEAR STRENGTH OF BORE SEAL SUBSTRATE BONDED TO WEDGE SUBSTRATE

Adhesive	Tensile-Shear Strength, psi, Tested at	
	25°C	100°C
Scotchweld 2214 NMF	1,656	1,240
XB2793/MDA	1,480	1,156*
XD7575.02/MDA	1,463	1,316*

*Wedge Substrates Failed.

TEST SUBSTRATES

Bore Seal, Sleeves and Coil Support Rings

These parts will be constructed from a filament wound cylinder of S-glass roving reinforced with the following resin system:

XB2793 Epoxy Resin	100 pbw
Methylene Dianiline	34 pbw

For test substrates, this resin was coated on Style 181/A1100 E-glass fabric and B-staged 60 minutes at 80°C. The resulting prepregs were molded at 177°C for 60 minutes. Mechanical stops were used to maintain 1/16" thickness. Seven prepreg sheets were necessary to obtain the desired flow and laminate thickness. The laminates were postcured for 16 hours at 160°C. Final resin content was approximately 40 percent by weight.

Coil Channels

Coil channels will be constructed by hand winding glass reinforced polyester tape around an appropriately designed mandrel and curing 4 hours at 135°C. Thickness of the coil channels is 20 mils. For test substrates, actual coil channels were cut into 1" strips and bonded to the edge of 1/32" aluminum sheet with EA-934 adhesive (Hysol Div., Dexter Corp.). In this way a lap shear substrate was achieved with minimal material, and the actual coil channel could be tested.

Wedge

The wedge test substrates were cut from the same stock used to fabricate the actual wedges used in the stator construction. The wedge material is a G-11 epoxy laminate supplied by NVF Corp. A 1/16" thick sheet was used for ASTM tensile-sheal substrates.

DETAILED DESCRIPTIONS OF CANDIDATE ADHESIVES

Tame 200

Tame 200 is a two-component thermosetting acrylic adhesive manufactured by B. F. Goodrich Co. The adhesive is claimed to have excellent bond strength to most plastic substrates, good peel strength and environmental resistance. The mixing formulation was as follows:

Tame 200	97 pbw
Catalyst C	3 pbw

which yields a creamy paste of 9,000 cps with a working life of 50 minutes at room temperature. Cure was 16 hours at room temperature followed by a postcure of 30 minutes at 200°F.

Versilok 506

Versilok 506 is a thermosetting acrylic catalyzed by a primer which can be coated onto the substrates prior to bonding. Adhesive and primer (Accelerator No. 4) are supplied by Hughson Chemical Corp. The thixotropic paste gels in 5 minutes after it is brought into contact with a primed surface. Complete cure develops in 48 hours. The primer was applied to both substrates and completely dried at room temperature. The adhesive was cured 16 hours at room temperature followed by 30 minutes at 200°F.

Trabond 2135D

Trabond 2135D is a two-part liquid epoxy adhesive from Tra-Con, Inc. claimed to have high impact bonds to epoxies and polyesters. It was used as a pre-weighed kit from the supplier. Pot life is 60 minutes and cure was 16 hours at room temperature followed by a postcure of 30 minutes at 200°F.

A-271

A-271 is a flexible, two-part liquid epoxy available from Armstrong Products. It is claimed to be useful for most plastics at service tem-

peratures to 225°F. The mix ratio

A-271 Part A	7 pbw
A-271 Part B	3 pbw

was cured 16 hours at room temperature followed by 30 minutes at 200°F. Working life of a 1 lb mass is 60 minutes at room temperature.

Scotchweld 3520

Scotchweld 3520 is a two-part liquid adhesive believed to be an epoxy-polyurethane alloy. The following mix ratio

Scotchweld 3520 Part A	5 pbw
Scotchweld 3520 Part B	6 pbw

was cured 16 hours at room temperature followed by a postcure of 30 minutes at 200°F. Scotchweld 3520 is available from 3M Co.

RP-138/H-998

RP-138/H-998 is a two-part thixotropic epoxy paste available from Ren Plastics. The following mix ratio is claimed to yield a slightly flexible adhesive suitable for bonding dissimilar substrates.

RP-138 Epoxy Resin	100 pbw
H-998 Hardner	40 pbw

Cure was 16 hours at room temperature followed by 30 minutes at 200°F.

#8751

Epoxylite #8751 is a two-part liquid epoxy adhesive claimed to provide high strength metal-to-plastic bonds. The following mix ration

Epoxylite #8751 Part A	4 pbw
Epoxylite #8751 Part B	1 pbw

was cured 16 hours at room temperature followed by 30 minutes at 200°F. The adhesive is available from the Epoxylite Corporation.

EA-934

EA-934 is a two-part light paste epoxy system claimed to provide high temperature service (300°F) with a room temperature cure. The adhesive is available from Hysol Division of Dexter Corporation. The

following mix ratio

EA-934 Part A	100 pbw
EA-934 Part B	33 pbw

was cured 16 hours at room temperature followed by 30 minutes at 200°F.

Scotchweld 2214 NMF

Scotchweld 2214 NMF is a one-component thixotropic epoxy paste available from 3M Co. It is noted for excellent shelf life and low temperature curing ability. Scotchweld 2214 NMF joints were cured for 40 minutes at 250°F.

Uniset 908-4

Uniset 908-4 is a one-component thixotropic epoxy adhesive. It is unfilled and claimed to have high peel strength. The curing schedule was 2 hours @ 280°F. Uniset 908-4 is available from Amicon Co.

Uniset 2027-47D

Uniset 2027-47D is a thick thixotropic epoxy system which is single component. It is claimed to provide exceptional toughness and resiliency after cure with excellent adhesion to plastics and elastomers. Uniset 2027-47D was cured 60 minutes at 250°F. The adhesive is available from Amicon Corporation.

XB2793/MDA

XB2793/MDA is composed of essentially the same resin and hardener as used in the bore seal resin matrix. Viscosity and flow is controlled by the addition of Cab-O-Sil additive. The following formulation provided a light paste with a pot life of approximately 48 hours at room temperature.

XB2793 Epoxy Resin	100 pbw
Methylene Dianiline	36 pbw
Cab-O-Sil	10 pbw

Cure was achieved in 2 hours at 100°C followed by 2 hours at 150°C. The epoxy resin is available from CIBA-Geigy Corporation and the hardener is available from a variety of sources.

XD7575.02/MDA

This adhesive is similar to XB2793/MDA except that the epoxy resin, XD7575.02, forms a distinct two-phase system of epoxy and compatible elastomer. This system is claimed to impart toughness without degrading other properties. The following formulation provided a light paste with a pot life of approximately 48 hours at room temperature.

XD7575.02	100 pbw
Methylene Dianiline	30 pbw
Cab-O-Sil	10 pbw

The Cab-O-Sil content may be adjusted to provide various viscosities. Cure conditions were 2 hours at 100°C followed by 2 hours at 150°C. XD7575.02 is an experimental resin available from Dow Chemical Co.

APPENDIX E

WOUND STATOR ASSEMBLY FOR SUPERCONDUCTING GENERATOR

WOUND STATOR ASSEMBLY FOR SUPERCONDUCTING GENERATOR RESEARCH REPORT 76-8B7-BORSE-R1

Robert L. Kolek
Polymers & Plastics

December 27, 1976
Revised November 4, 1978

ABSTRACT

A complete stator coil assembly was fabricated and banded according to specifications. The assembly consisted of 12 coils, an inner fiberglass cylinder, sleeves, end turn supports, fiberglass channels and wedges, Teflon spacers and an outer fiberglass cylinder which was wound in place. Dimensional variations in the copper stator coils made necessary numerous tooling and component changes as well as modification of the assembly procedure specification. None of these changes was significant enough to prevent the successful assembly of the unit. This report describes the assembly procedures, techniques and tools used to produce the finished stator coil assembly unit.

DESCRIPTION

The wound stator assembly is described by Lima AED drawing ED 362759. The assembly consists of the following elements:

1. Fiberglass/epoxy bore seal.
2. Right and left fiberglass/epoxy sleeves.
3. Right and left fiberglass coil supports.
4. Twelve stator coils.
5. Conductor channels.
6. Conductor spacers.
7. Conductor wedges.
8. Outer coil fiberglass/epoxy cylinder.
9. Teflon baffles.
10. Teflon spacers.
11. Fiberglass lacing tape.
12. Bus bars.
13. No. 36 chrome-alumel thermocouple wire.

All of the fiberglass/epoxy elements, coil supports, had been fabricated and are described in Appendix A 75-8B7-BORSE-R1 and Appendix C 75-8B7-BORSE-R3. The adhesives used for assembly are described in Appendix D.

TOOLING AND FACILITIES

The tooling used in this assembly operation was conceived so as to reduce the number of fixtures, future cleaning and operation time, and to improve accuracy. The main building tools are identified as follows:

Tool	Research Drawing No.
Building Fixture	114E274
Bearing Ring Fixture	8513D12
Bearing Ring Fixture Assembly	8513D13
Top Clamp Ring Assembly	8513D22
Top Clamp Ring Details	8513D15
Clamp Weldment	1681B52

Other tools used and fabricated on a need basis consist of:

1. Bore seal winding mandrel.
2. Fiberglass oil manifold back-up ring.
3. Teflon oil manifold spacers.
4. Delrin AF center pins.
5. Hard maple temporary wedges.
6. Assorted steel band hose clamps.
7. Oven loading steel cart.
8. Movable stator assembly transfer cart.
9. Coil end turn support blocks.
10. Assorted Teflon cushioning pads.
11. Disposable plastic syringes for adhesive application.
12. Assorted clamps.

SCG STATOR COIL BUILDING PROCEDURE

Step No.	Operation
1.	Slip channels onto coil conductors.
2.	Locate coil on the O.D. of a horizontal, dummy bore seal by slipping the bus bar shoes over properly positioned locating pins.
3.	Insert tapered Delrin AF center spacing pins between conductors to properly panograph and space the conductors.
4.	Move channels against each side of the properly positioned center pins to achieve a 0.5" center gap between channels and band the conductors down on each end to prevent movement.
5.	Insert a properly shaped 0.1" thick Teflon sheet into the center gaps cut down from the tops of the Delrin AF pins. This creates a 0.1" barrier across the circumferential center line of each conductor.
6.	Place the spacers on top of the channels and locate them against each side of the Teflon barrier.
7.	Apply a bead of Scotchweld 2214 NMF adhesive along both edges of the spacers using a disposable syringe.
8.	Band down the spacers to prevent movement and cure the assembly for 40 mins at 250°F.
9.	Repeat this process to complete attachment and location of channels and spacers for all 12 coils.
10.	Locate and bond the sleeves and coil supports to the bore seal using the Scotchweld 2214 NMF adhesive. Cure for 2 hrs at 250°F.
11.	Locate, drill and chamfer 12 radial through-holes in each end of the bore seal.
12.	Slip the bore seal onto the vertically mounted coil assembly building fixture and cover the outer diameter with Scotchweld 2214 NMF adhesive.
13.	Locate the coils around the bore seal by means of the locating pins in the bottom support plate and by selectively engaging the proper top holding clamp. The upper and lower Teflon baffles are inserted during this operation.

Step No.	Operation
14.	Loosely attach two upper and two lower banding rings around the O.D. of the coil assembly.
15.	Insert the Delrin AF center spacing pins and tighten the banding rings to pull the coils into the bore seal. Verify the dimension required by measuring the distance from the bore seal outer diameter to the top of the coils.
16.	Remove bottom two banding rings and insert the temporary wood wedges to achieve proper alignment of the coil conductors. Reattach the banding rings and tighten.
17.	Repeat step 16 for the top half of the coil assembly.
18.	Begin insertion of the permanent fiberglass wedges after verifying all dimensional specifications.
19.	Remove the lower two banding rings and about one fourth of the wood wedges.
20.	Using a long, thin tool, apply a thin coating of Scotchweld 2214 NMF adhesive to the sides of the channels on the top conductor. Apply a thin coating of the same adhesive to the mating surfaces of the two fiberglass wedge halves and press together. Apply a thin coating of the same adhesive to the surfaces of the wedges which will contact the sides of the channels on the bottom conductors. Insert the wedge and tap in place.
21.	Repeat step 20 until all of the wedges have been inserted.
22.	Re-band the bottom of the completed coil assembly.
23.	Repeat steps 20, 21, and 22 for the top half of the coil assembly.
24.	After completion of the insertion process for the fiberglass wedges, verify the completed outer dimension of the assembly and insert the Teflon end turn spacers.
25.	Insert suitable fiberglass shims coated with the Scotchweld adhesive on top of those wedges which need shimming to bring them to the tops of the coil conductors.
26.	Place the entire assembly in a walk-in oven and cure for 1 hr. at 212°F and 4 hrs. at 250°F. Timing of the cure should start after 2 hrs. and 20 mins., which is the time required to get the assembly to temperature.

Step No.	Operation
27.	After cure, place the bore seal/coil assembly, which is mounted on the winding mandrel-building plate tooling, into the McClean-Anderson W-1 winding machine.
28.	Remove the banding and center spacing Delrin AF pins.
29.	Using a hand grinder, remove excess shim material from each of the wedges to provide a uniform outside diameter around the circumference of the coil assembly.
30.	Using a run-out gauge, determine the highest conductor in the end turn region and size the bearing ring figures accordingly to fit around the end turn area without damaging the conductors.
31.	Bond six, 24" long thermocouples to the neutral coils on each side of the center maifold area. Tape the wire down to the neutral conductor and fasten with tie wire to the appropriate conductor at the end turns. Use the Scotchweld 2214 NMF adhesive.
32.	Attach the bearing rings to both ends of the coil assembly.
33.	Attach a 0.75" wide by 0.75" thick split fiberglass ring around the center manifold area to serve as a back-up plate for a 0.10" wide by 0.75" thick split Teflon ring. This assembly is located to maintain the glass free manifold opening. It is secured with a metal banding clamp. Six axial braces are provided between the fiberglass ring and the aluminum bearing ring fixture on the end which is to be banded last.
34.	Filament wind a fiberglass/epoxy shell over one half of the coil assembly. Wind the flat conductor area first and move in steps up the tapered region of the coils with final completion of the winding occurring at the barrier ring.
35.	After filament winding one half of the coil assembly, the unit is cured in a walk-in oven using the following cure schedule: 2 Hours at 212°F 2 Hours at 250°F 2 Hours at 300°F 2 Hours at 350°F

Step No.	Operation
36.	After cure, steps 31 through 35 are repeated for filament winding the second half of the assembly. Step 33, however, is modified. The fiberglass ring and axial braces are no longer required to back up the split Teflon ring since the fiberglass winding, now in place, serves their function.
37.	After winding and cure of the second half of the coil assembly, the completed fiberglass shell is machined to drawing dimensions.
38.	Install the bus bar phase connections with the neutral connections insulated from the bus ring. Immerse in oil and conduct the three phase-to-phase dielectric tests at 11 kV, 60 Hz for 1 min. This operation completes the wound stator assembly, Lima Drawing 362759.

Figures 7, 8, and 9 of Section II illustrate the assembly operations.

APPENDIX F
EDDY CURRENT LOSS
FOR A
RECTANGULAR STRAND
IN A TWO-COMPONENT FIELD

EDDY CURRENT LOSS FOR A RECTANGULAR STRAND IN A TWO-COMPONENT FIELD

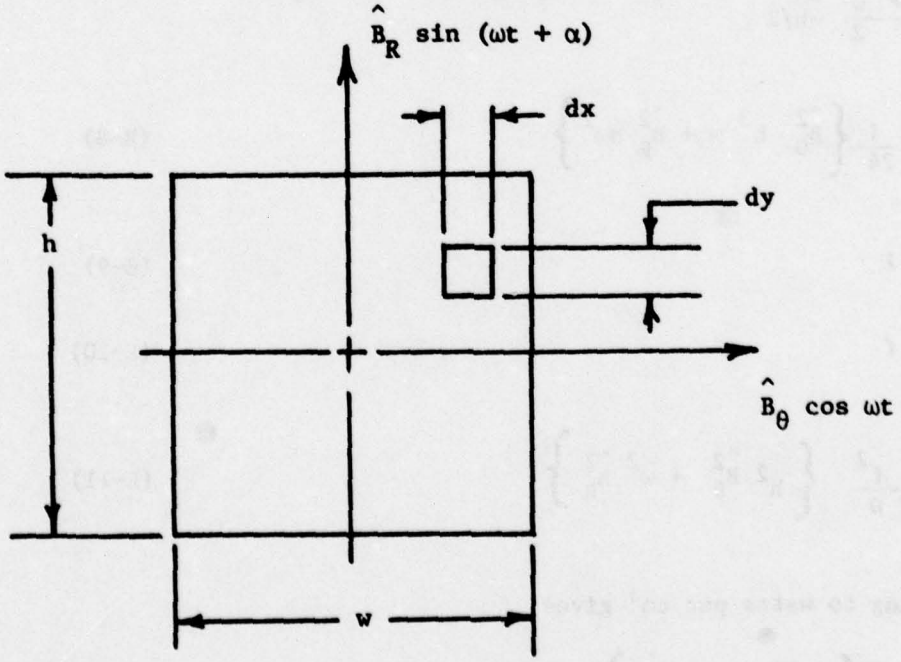
Specific Assumption:

(1) The transverse fields are homogeneous.

(2) The dimensions of the strand are small compared with the depth of penetration of the time varying field.

(3) The conductive strand is non-magnetic.

4) The fields are pulsating perpendicular as $B_\theta = \hat{B}_\theta \cos \omega t$ and as $B_R = \hat{B}_R \sin (\omega t + \alpha)$.



$$e = -\frac{d\phi}{dt} \tag{E-1}$$

$$\phi = 2\ell\chi \hat{B}_R \sin(\omega t + \alpha) + 2\ell y \hat{B}_\theta \cos \omega t \tag{E-2}$$

$$\frac{d\phi}{dt} = 2\ell\omega\chi \hat{B}_R \cos(\omega t + \alpha) - 2\ell\omega y \hat{B}_\theta \sin \omega t \tag{E-3}$$

$$e = 2\ell\omega \left\{ y \hat{B}_\theta \sin \omega t - \chi \hat{B}_\theta \cos(\omega t + \alpha) \right\} \tag{E-4}$$

$$e^2 = 4\ell^2\omega^2 \left\{ y^2 \hat{B}_\theta^2 \sin^2 \omega t - z\chi y \hat{B}_\theta \hat{B}_R \sin \omega t \cos(\omega t + \alpha) + \chi^2 \hat{B}_2^2 \cos^2(\omega t + \alpha) \right\} \tag{E-4}$$

Considering the time average value of each term

$$e^2 = 2\ell^2\omega^2 \left\{ y^2 \hat{B}_\theta^2 + \chi y \hat{B}_\theta \hat{B}_R \sin \alpha + \chi^2 \hat{B}_R^2 \right\} \tag{E-5}$$

$$dp = \frac{e^2}{R} = \frac{e^2}{2P\ell} dy\, d\chi \tag{E-6}$$

$$P = \frac{\ell\omega^2}{\rho} \int_{-\frac{w}{2}}^{\frac{w}{2}} \int_{-h/2}^{h/2} (y^2 \hat{B}_\theta^2 + \chi y \hat{B}_\theta \hat{B}_R \sin \alpha + \chi^2 \hat{B}_\theta^2)\, dy\, d\chi \tag{E-7}$$

$$P = \frac{\ell\omega^2}{\rho} \frac{1}{24} \left\{ \hat{B}_\theta^2 h^3 \omega + \hat{B}_R^2 h\omega^2 \right\} \tag{E-8}$$

$$V = h\, \omega\, \ell \tag{E-9}$$

$$\omega = 2\pi f \tag{E-10}$$

$$\frac{P}{V} = \frac{\pi^2}{6} \frac{f^2}{\rho} \left\{ h^2 \hat{B}_\theta^2 + \omega^2 \hat{B}_R^2 \right\} \tag{E-11}$$

Converting to watts per cm^3 gives

$$\frac{P}{V} = \frac{\pi^2}{6} \frac{f^2}{\rho} \left\{ h^2 \hat{B}_\theta^2 + \omega^2 \hat{B}_R^2 \right\} \times 10^{-7} \tag{E-12}$$

B = Magnetic field, gauses

$\hat{B}$ = Amplitude of magnetic field, gauses

e = voltage around a closed loop, abvolts

e_a = time average value of voltage around a closed loop, abvolts

f = frequency, Hz

h = height of conductor, cm

l = one-half the length of closed loop, cm

p = power, ergs per second

P = power, watts

R = resistance of closed loop, abohm

t = time, seconds

V = volume of conductor, cm^3

w = width of conductor, cm

Φ = magnetic flux, lines

α = phase angle between time varying components

ω = $2\pi f$

ρ = resistivity, abohm-cm

APPENDIX G

HELIUM COOLING COIL FAILURES

A 304L stainless tubing was used for the helium cooling coils on the subassembly. This low carbon stainless (analyzed at 0.020% C) reduced the problem of carbide precipitation during welding and permitted the use of this steel in the as-welded condition. The 304 type stainless steels in general offer excellent corrosion resistance if the chromium and carbon remain in solution. Precipitation of the chromium by combination with carbon forms chromium carbide which depletes the chromium level in areas adjacent to the grain boundaries thus allowing susceptibility to intergranular attack. Unfortunately a series of events occurred which created the necessary conditions for possible corrosive attack of the 304L stainless helium cooling tubes.

The 718 alloy was received in a forged condition which was intermediate in strength and hardness relative to a solution treated and fully age hardened condition. The furnace brazing of the 304L tubing to the 718 thermal transition piece (TTP) not only satisfied the braze requirement but also solution treated the 718. The furnace braze was carried out at 1080°C followed by a rebraze at 1010°C. This brazing which also solution treated the 718 did not affect the chromium dispersion in the 304L (see Figure G·1). On the other hand, in order to obtain full strength for the 718 an aging treatment was necessary. This treatment was performed at 650°C x 20 hours followed by an air cool. At this temperature, however, dependent on the chromium, nickel, and carbon levels precipitation would have "sensitized" the stainless which in effect would have reduced its corrosion resistance. The stainless tubing was exposed to a corrosive environment by the subsequent copper plating solution which contained highly corrosive fluoroborates. Although an attempt was made to protect the tubing during plating, evidence of corrosion was noted after the plating was completed. It is thus concluded that aging heat treatment on the 718 degraded the corrosion resistance of the 304L allowing subsequent attack during the copper plating on the sleeve of the TTP.

Dye penetrant inspection of the tubing did not show evidence of intergranular attack. The attack was apparently confined to pin holes produced most likely by a defect related pitting failure. Repair of the pin holes was not successful requiring removal of the tubing.

It is suspected that the earlier tubing leakage in the anti-drive end was also related to the same corrosion problem as discussed above. It is important to note, however, that corrosion to the anti-drive end was markedly reduced as it was plated after the drive end. Additional effort was made to prevent corrosion on the anti-drive end after viewing the initial corrosion effects on the drive end. This effort, although improved, was not completely successful in eliminating all corrosive attack as evidenced by the resultant failure of the large tubes. A higher level of carbon in the large tubing in the anti-drive end accentuated the problem, i.e., the large tubing which failed in the anti-drive end was fabricated from 304 having an 0.06% carbon level. Sensitization of the stainless is much easier due to the higher carbon level.

WESTINGHOUSE ELECTRIC CORPORATION

TTS - DIAGRAMS FOR 304 STAINLESS (18-8, 18-10) SHOWING SENSITIZATION REGIONS AS A FUNCTION OF CARBON LEVEL.

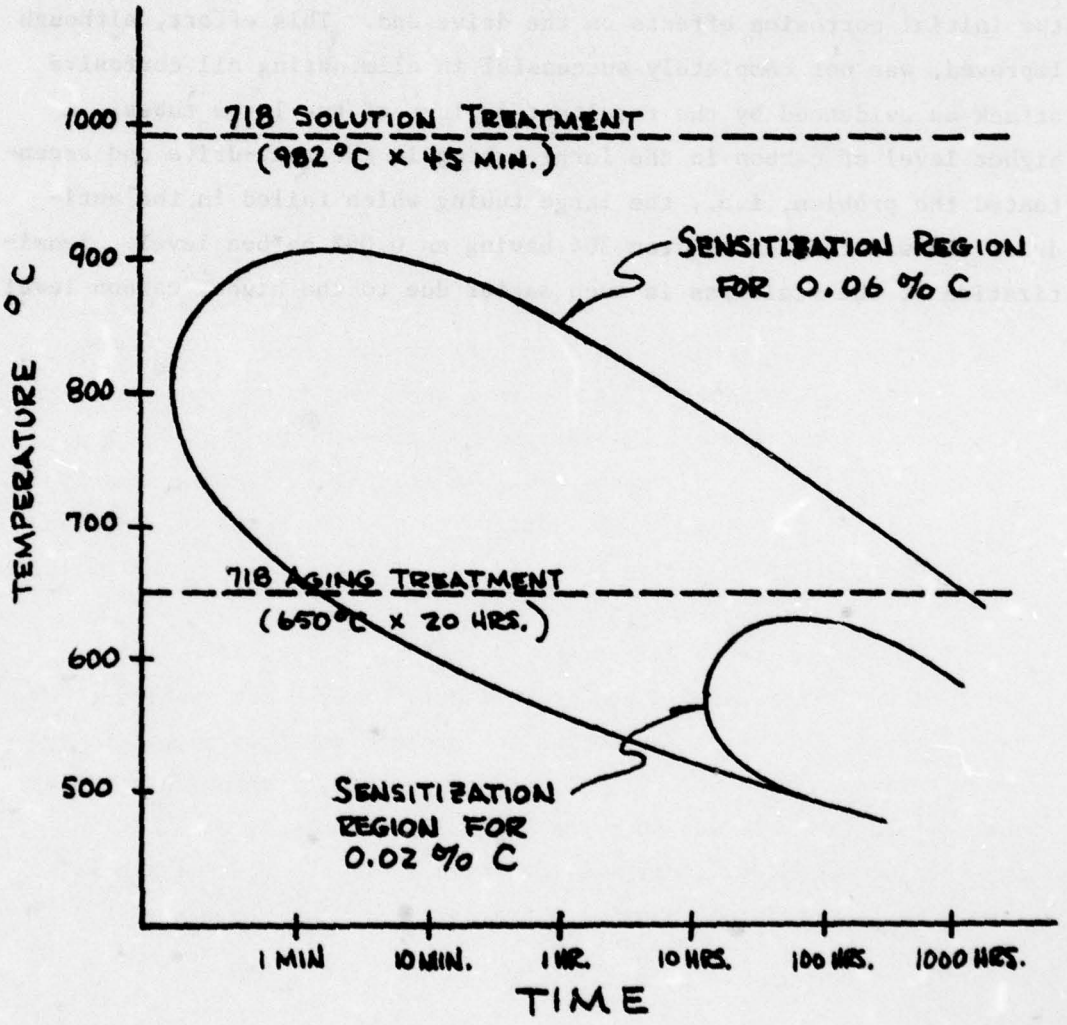


FIGURE G.1

APPENDIX H

TEST CYLINDER FOR AN OVERWRAP ON THE ELECTROTHERMAL SHIELD

The 304 stainless steel fiber was supplied as multifilament, continuous yarn as shown in Figure H·1. The filament diameter was 8 microns and the yarn consists of 1159 filaments. Filament winding of a 5.75" I.D. by 10.0" long by 0.060" thick test cylinder was accomplished on a McClean-Anderson W-1 winding machine so shown in Figure H·2. The cylinder was wound on a hollow steel mandrel capable of being internally heated or cooled. The winding conditions were:

Speed:	40 rpm
Band Width:	0.075
No. Layers:	15
Tension:	4 lbs.

A branson ultrasonic horn was positioned over the fiber just before exit from the resin bath. This horn excites the fiber and resin, causing rapid agitation to occur. This movement accelerates the wetting of the fiber with the resin and expels extraneous gaseous voids allowing a void-free composite to be fabricated. Additional uniformity is achieved by rotation of the wound assembly during cure. The resin system used was a room temperature curing epoxy resin with the following formulation:

Dow Epoxy Resin 330 - 100 ppH
Jaffamine T - 403 - 36 ppH

which has been used in advanced composites. We have observed that this resin demonstrates excellent mechanical properties after repeated cryogenic cycling. The wound cylinder was allowed to cure for 24 hours at room temperature. It was then post cured for six hours at 120°C in air. The completed cylinder was then pushed off the winding mandrel using a McClean-Anderson mandrel extractor.

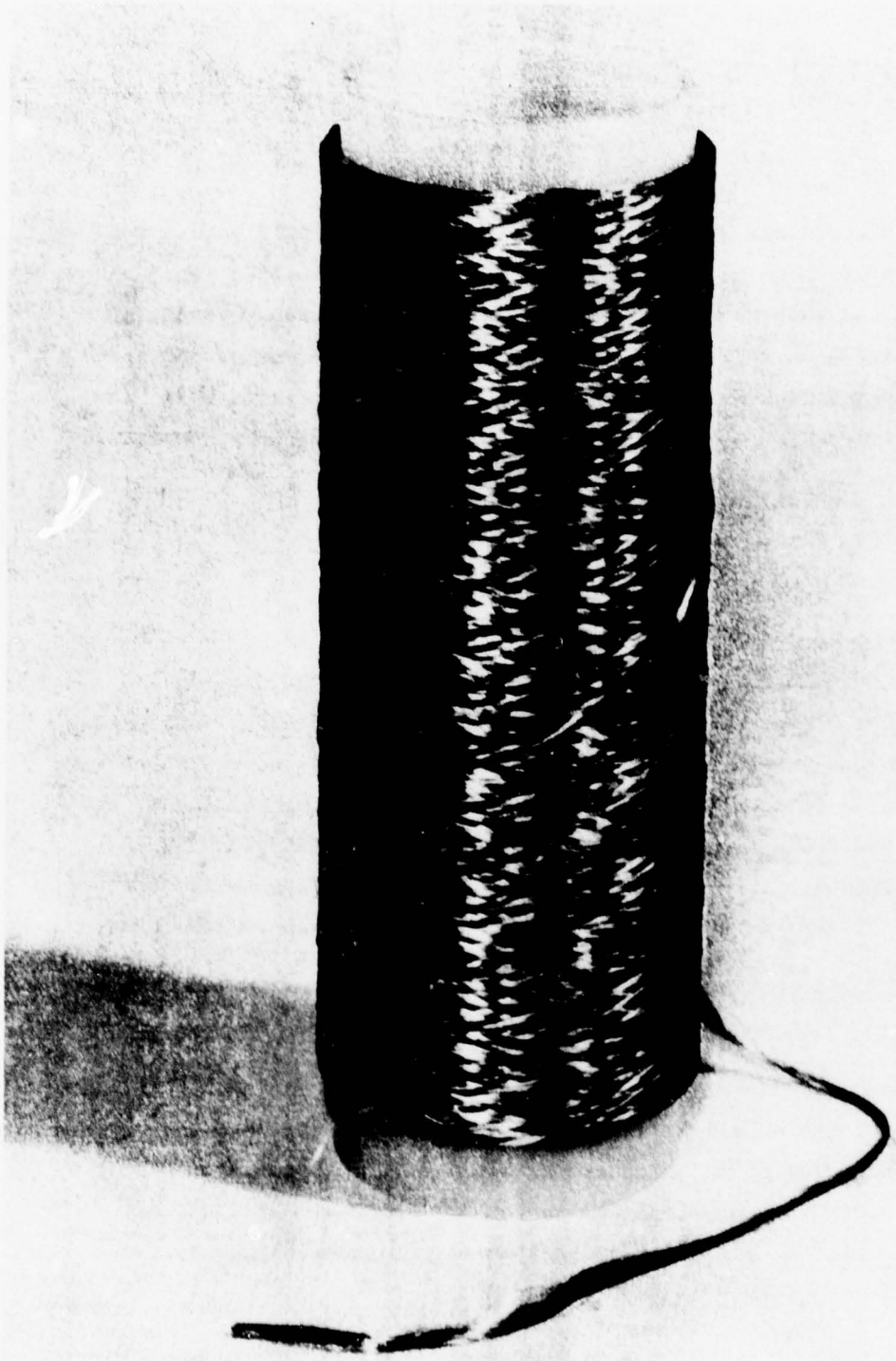


FIGURE H.1 - 304 Stainless Steel Multifilament Yarn

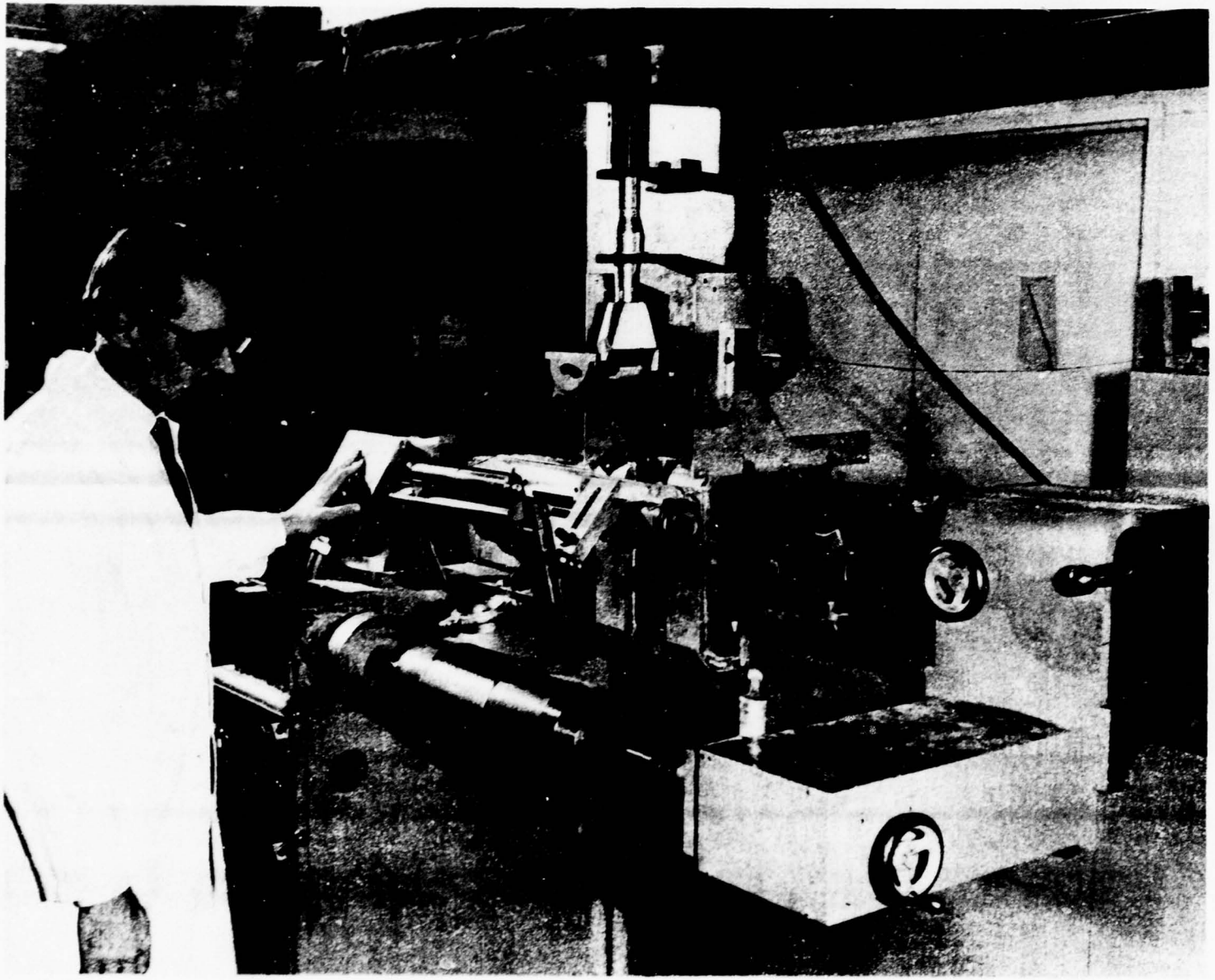


FIGURE H.2 - McClean—Anderson W-1 Winding Machine and Test Cylinder

COMPOSITE TESTING

The completed cylinder was sectioned into test specimens. The following tests were then conducted which included:

1. Tensile properties ASTM D2290
2. Interlaminar shear ASTM D2344
3. Thermal coefficient of expansion (78 to 485°K)
4. Fiber content ASTM D2584
5. Electrical resistivity
6. Magnetic.

The test data is shown in Table 4. The mechanical test data was performed at room and liquid nitrogen temperatures with no apparent difference at the lower temperature. The tensil strength on the composite was within 10% of the predicted value. The tensile modulus was within 20% as calculated by the rule of mixtures, i.e., 14 versus 17 psi x 10^6. The density of the composite was measured at 5.34 gm/cc.

The electrical resistance of the composite was measured on an $\sim$ 0.040 in. (eight layers of fiber yarn) thick cylinder ($\sim$6.5 cm long) mounted on micarta. The resistance was measured transverse to the winding direction by attaching two copper plates to either end of the cylinder.

The resistance was markedly higher than an equivalent 304 stainless steel cylinder of the same dimension, i.e.,

$$\rho \text{ (composite)} = 170 \times \rho \text{ (304 stainless steel)}$$

The transverse resistivity is

$$\sim 12 \times 10^{-3} \Omega\text{-cm}$$

The magnetic saturation was measured in the hard-worked or as received condition in a Foner magnetometer and showed at 4.2°K a 12.5 kG saturation.

APPENDIX I

OIL FLOW AND THERMAL TESTS ON ARMATURE CONDUCTORS

OBJECTIVES

The objectives of these experiments were to:

- Gain experience for bonding of the composite components with the adhesive recommended in Research Report 75-8B7-BORSE-R2, September 16, 1975, Appendix D.
- Measure the flow rate of oil through the conductor as a function of supply pressure.
- Determine the temperature of the conductors as a function of the applied current with a constant oil supply pressure.

APPARATUS

An array of six conductors was constructed. This mock-up included the conductor channels, wedges, and spacers which were made to secure the conductors in the stator. Figure I.1 illustrates how these parts and the conductors appear in the stator and Figure I.2 (ED383710) shows how a mock-up of a typical array of these parts was constructed.

In a stator slot, one-half (three) of the conductors are from one side of a coil and the other half are from the opposite side of a different coil. For convenience, the six conductor array shown in Figure I.2 was made from opposite sides of the same coil.

Dwg. 6364A92

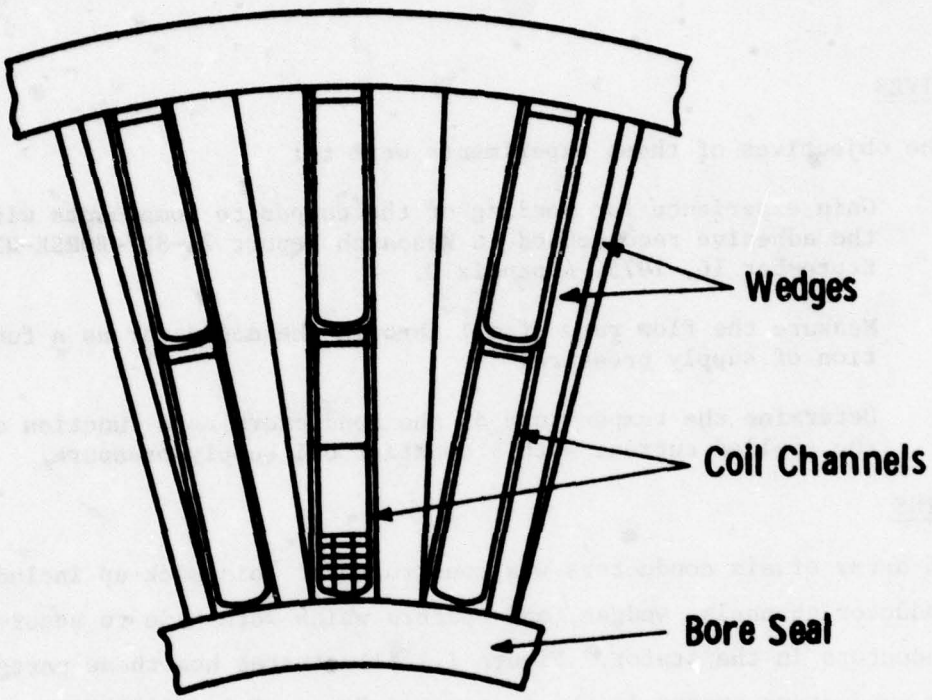


FIGURE I-1 END VIEW OF STATOR SECTION SHOWING WEDGE, COIL CHANNEL, AND BORE SEAL INTERFACES

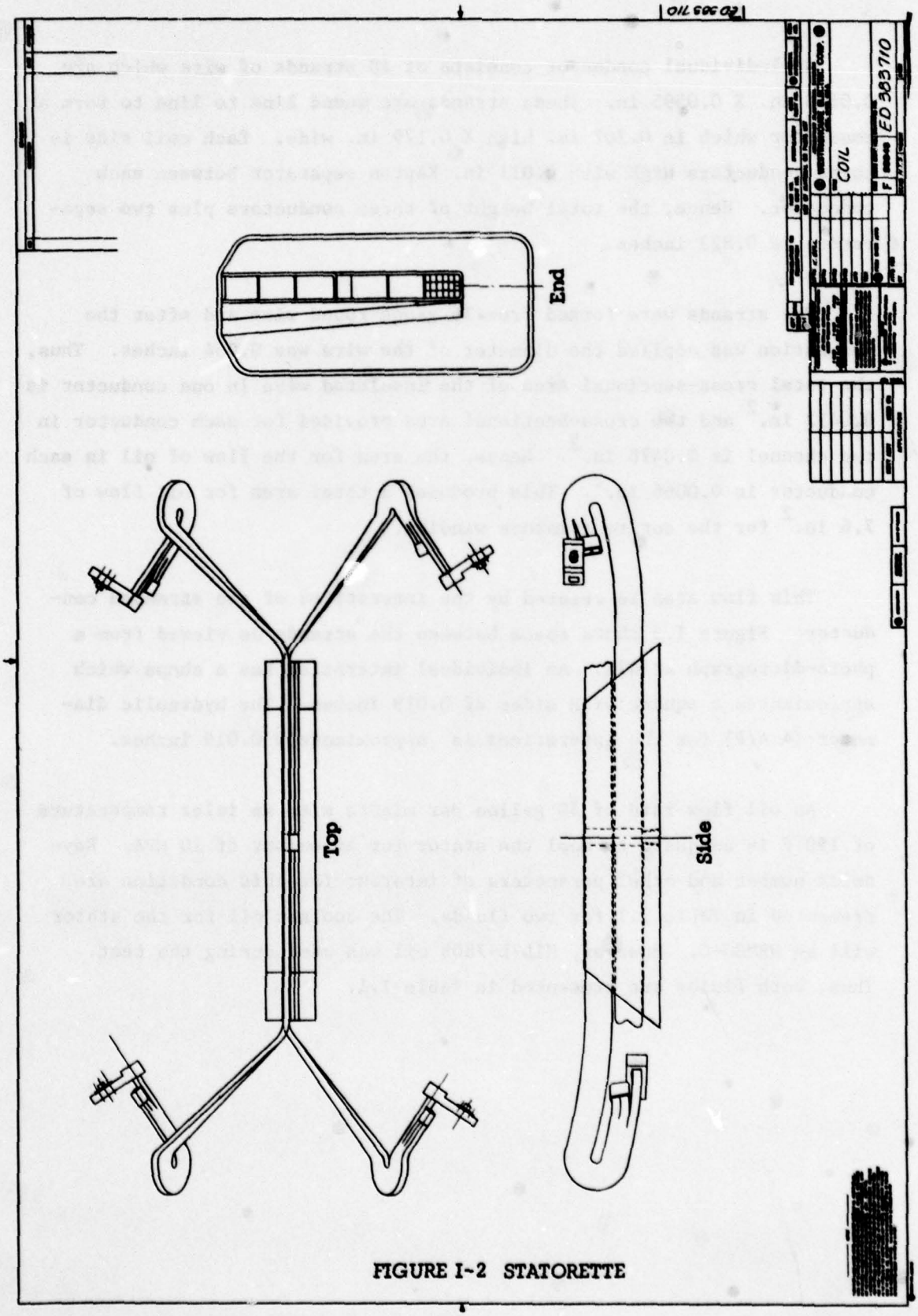


FIGURE I-2 STATORETTE

An individual conductor consists of 18 strands of wire which are 0.0445 in. X 0.0595 in. These strands are wound line to line to form a conductor which is 0.267 in. high X 0.179 in. wide. Each coil side is three conductors high with 0.011 in. Kapton separator between each conductor. Hence, the total height of three conductors plus two separators is 0.823 inches.

The strands were formed from 16 gauge round wire and after the insulation was applied the diameter of the wire was 0.054 inches. Thus, the total cross-sectional area of the insulated wire in one conductor is 0.0412 $in.^2$ and the cross-sectional area provided for each conductor in the channel is 0.0478 $in.^2$. Hence, the area for the flow of oil in each conductor is 0.0066 $in.^2$. This produces a total area for oil flow of 7.6 $in.^2$ for the entire armature winding.

This flow area is created by the interstices of the stranded conductor. Figure I.3 shows space between the strands as viewed from a photo-micrograph at 42X. An individual interstice has a shape which approximates a square with sides of 0.019 inches. The hydraulic diameter (4 A/P) for the interstices is approximately 0.019 inches.

An oil flow rate of 50 gallon per minute with an inlet temperature of 150°F is adequate to cool the stator for an output of 10 MVA. Reynolds number and other parameters of interest for this condition are presented in Table I.1 for two fluids. The coolant oil for the stator will be WEMCO-C. However, MIL-L-7808 oil was used during the test. Thus, both fluids are presented in Table I.1.

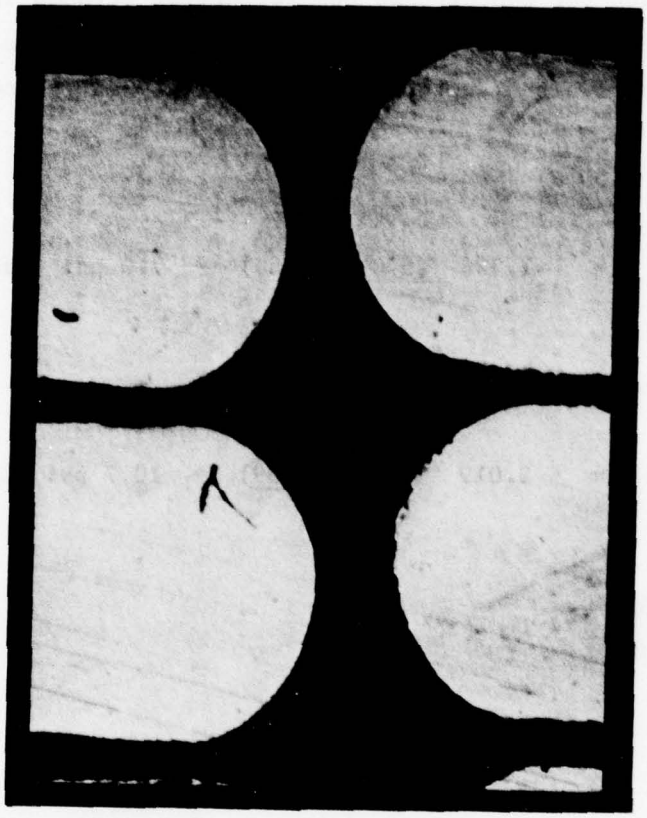


FIGURE I-3
Photo Micrograph of Stator Stranded Conductor

In order for the oil to exit the conductor, it must travel the length of the conductor channel and around the bend line in the coil. At this point the oil can exit from the conductor. The minimum length of the oil path for top strands and for bottom strands is 4.59 and 6.00 inches respectively. It can be noted from Table I.1 the following pressures are required to force the fluids through the conductors:

WEMCO-C (150°F)

$$\Delta P = 1.326 \frac{(6.00 + 4.59)}{2} = 7.0 \text{ psi (minimum)}$$

MIL-L-7808 (150°F)

$$\Delta P = 2.019 \frac{(6.00 + 4.59)}{2} = 10.7 \text{ psi (minimum)}$$

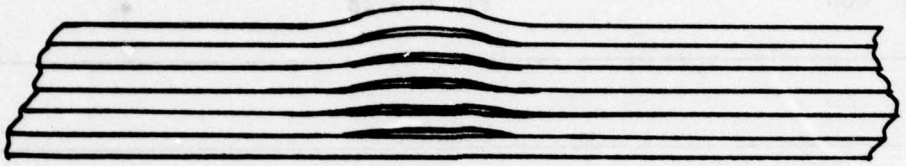
TABLE I·1

FLOW PARAMETERS FOR STATOR

FLOW	FLOW AREA	VELOCITY
Gal/Min. 50	IN^2 7.6	FT/Hr 7581
FT^3/Hr. 400	FT^2 0.0528	FT/Sec. 2.106

FLUID	WEMCO-C	MIL-L-7808
Temperature		
°F	150	150
°C	65.5	65.5
Density		
Lbm/Ft^2	54.1	55.5
Dynamic Press		
$1/2\ \rho\ V^2/gc\ (Lbf/Ft^2)$	3.725	3.821
$1/2\ \rho\ V^2/gc\ (Lbf/In^2)$	0.0258	0.0265
Viscosity		
Absolute (Lbm/Ft-Hr)	9.84	15
Kinematic (Ft^2/Hr)	0.182	0.27
Hydraulic Diameter		
Inches	0.0190	0.019
Feet	0.00158	0.00158
Reynolds Number	65.8	44.4
Friction Factor		
$64/R_N$	0.972	1.443
ΔP/L		
Lbf/Ft^3	2293	3489
Lbf/In^3	1.326	2.019

The oil enters the interstices in the conductor at the center of the coil. Five spacers (0.005" X 0.25") were placed between adjacent layers of strands in each conductor when the coil was wound as shown below:



After the strands were bonded together by melting the polysulfone coating on the wire, these spacers were removed leaving a gap between the layers at these locations. The total area of these gaps per conductor is:

$$5 \text{ X } 0.005 \text{ X } 0.25 = 0.0062 \text{ In}^2$$

which is approximately equivalent to the area of the interstices within the conductor.

The channels were located between the bend lines at each end of the straight length with a one-half inch gap in the center of the coil. A one-half inch gap was also provided in the center of the coil by channels and wedges.

The composite components were bonded together and to the aluminum frame with a one-component thixotropic epoxy paste, Scotchweld 2214 NMF available from the 3M Company. This is a thick adhesive (paste) which is noted for excellent shelf life and low temperature curing ability. The joints were cured for approximately 40 minutes at 250°F.

Unfortunately, it was difficult to coat the components with this particular epoxy since it is a thick paste and could not be applied as a thin film. The paste was applied with a spatula as the parts were placed in the aluminum form. Considerable force was required to cause them to assume their correct position. This caused the excess paste to flow into the manifold region and out of the ends of the assembly. Subsequently, most of the excess paste was removed with acetone on a cotton swab.

TEST SITE AND EXPERIMENTS

MIL-L-7808G oil was supplied via a gear pump as shown schematically in Figure I.4. The oil supply was maintained at approximately 150°F with a thermostatically controlled electric heater in the supply tank. Oil flow rates were determined by measuring the times required to accumulate five pounds of oil in a sump on a scale.

The level of oil in the sump was maintained above the statorettes and was periodically lowered to prevent overflow of the sump.

The temperature of the conductor was measured at five locations (TC #1 through TC #5) and the oil temperature was measured in the supply tank (TC #7) and in the sump (TC #6) as shown in Figure I.5.

400 HZ power was supplied to the statorette by way of a step-down transformer (29 to 1) and a generator which was excited separately to obtain the specified currents for the conductors in the statorette.

TEST PERFORMED

Flow measurements were made with 20,40 and 60 psi pressure in the central manifold. The current in the conductor was adjusted to maintain the maximum temperature of the conductors to 200°F. The results of the tests are given in Table I.2.

With a maniflod pressure of 60 psi, the current was varied from 0 to 600 amps. The results of this calibration is given in Table I.3.

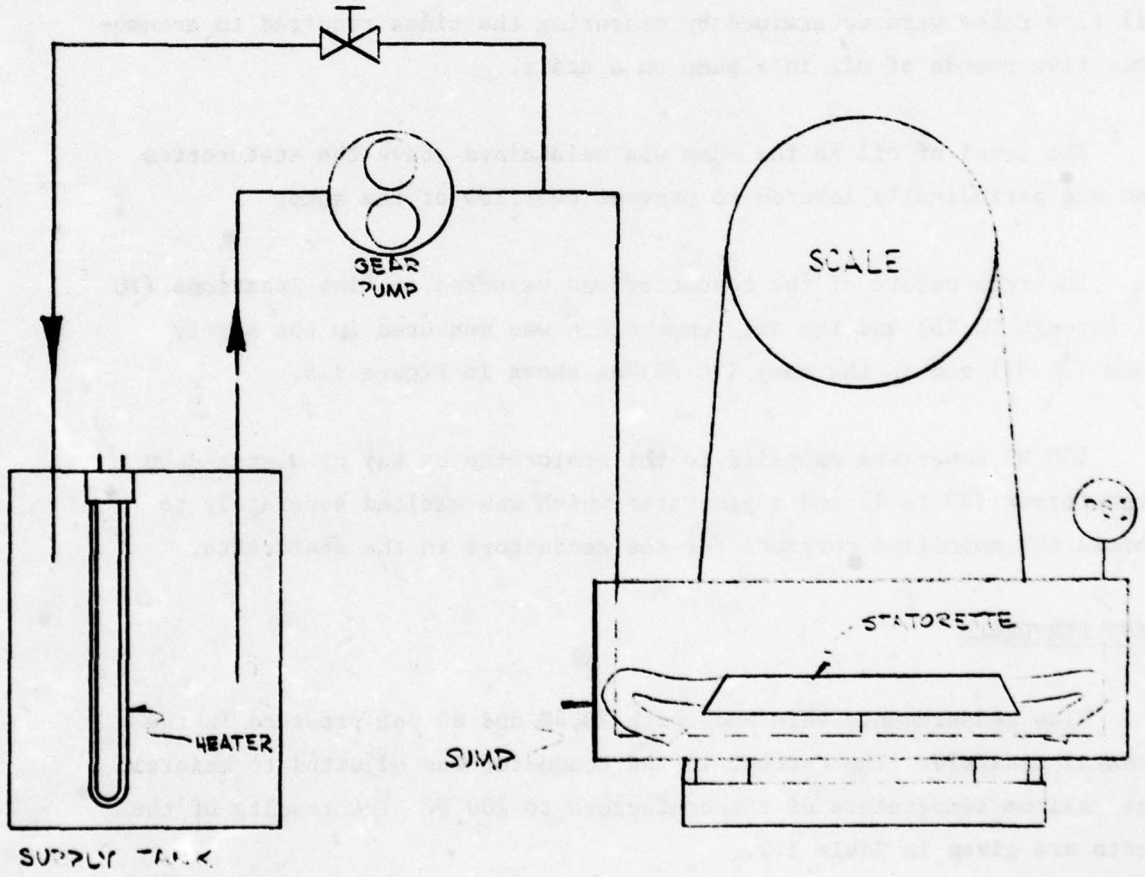


FIGURE I-4 SCHEMATIC DIAGRAM OF OIL FLOW TESTS

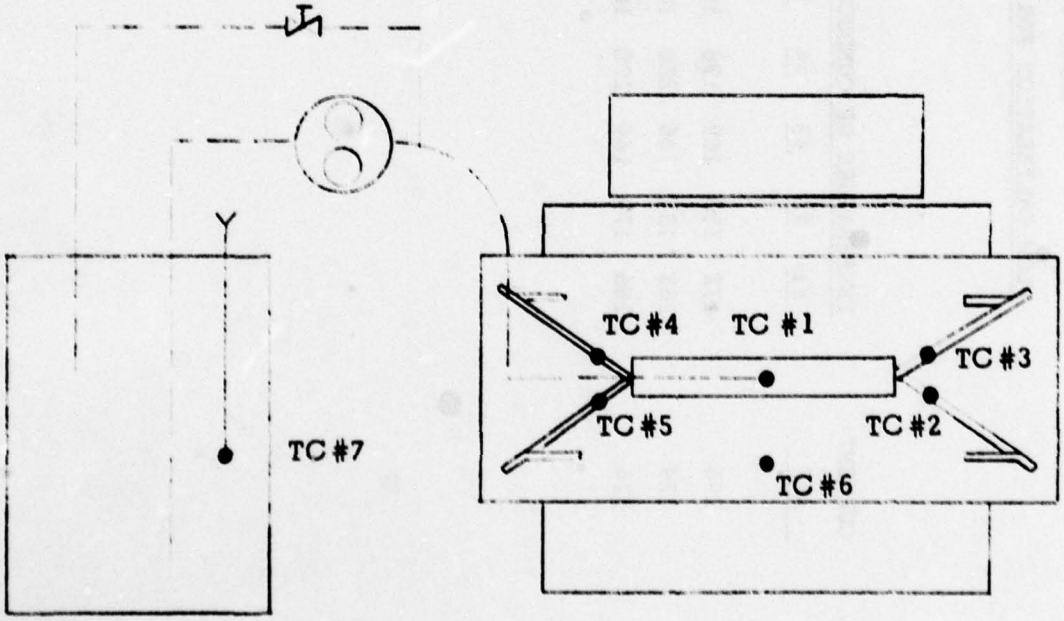


FIGURE I-5 THERMOCOUPLE LOCATIONS

TABLE I.2

FLOW CALIBRATION FOR STATORETTE #1

PRESSURE	CURRENT	TEMPERATURE OF CONDUCTORS (°F)						STATORETTE	STATOR	
PSI	AMP	#1	#2	#3	#4	#5	#7	#/MIN	#/MIN	GPM
20	294	172	180	169	198	187	154	0.108	10.4	1.40
40	329	163	181	166	200	188	149	0.278	26.7	3.61
60	324	166	179	169	200	189	151	0.490	47.0	6.35

TABLE I.3

TEMPERATUKE CALIBRATION OF STATORETTE #1

I	PRESSURE	TEMPERATURE °F							FLOW	STATOR	
AMP	PSI	#1	#2	#3	#4	#5	#6	#7	#/MIN	#/MIN	GAL/MIN
0	60	142	—	—	—	—	—	155	0.293	28.1	3.80
312	60	166	179	169	200	189	—	151	0.490	47.0	6.35
500	60	188	274	218	247	309	145	161	0.508	48.8	6.59
552	60	202	289	230	264	328	161	168	0.524	50.3	6.80
600	60	230	324	263	352	366	183	164	0.582	55.8	7.54

The results from the flow test with MIL-L-7808 oil in the mock-up did not agree with anticipated rate. In fact, the observed flow rate was about 1.2% of the anticipated flow rate at 10.7 psi. Increasing the pressure to 50 psi only produced approximately 10% of the design flow rate (50 gallon per minute). The variance between the anticipated results of the observed flows suggest the discrepancy may be due to the following factors:

1. The oil flow test in the statorette may not have been a realistic evaluation due to excessive sealing of the interstices by the adhesive paste, and

2. The strands outside of the conductor channels may have been bonded in a tight array and the oil was unable to get out of the interstices within the conductor.

These factors were investigated and a discussion of the observations are presented here. Firstly, the strands outside of the conductor channel were separated into a very loose array. This had a little, if any, effect upon the oil flow rate through the statorette with 60 psi pressure in the manifold.

Subsequent to this test, the statorette was disassembled. In general, a considerable amount of the epoxy adhesive was found in and around the conductors which blocked the oil passages. In the manifold region, one side of the stranded conductor was completely filled with epoxy. In fact the 0.005 inch separations between the strands were for the most part filled with epoxy. Blockage of the interstices was also observed at the ends of the conductor channels.

New emphasis was placed upon the fabrication of a second statorette using the procedures outlined below.

1. The aluminum form was cleaned in a sand blast to remove all of the old adhesive.

2. New sections of the conductors were removed from the scrapped coil and coated with MIL-L-7808 oil to prevent bonding between the conductors and the adhesives.

3. U-Channels were placed around the conductors and a G-11 laminate was bonded to each channel to form a conduit for each array of three conductors. The joints between the U-Channel and the laminate was made by applying Scotchweld 2214 NMF paste with a hypodermic syringe. The parts were clamped before the paste was applied and during the cure at 250°F for 40 minutes.

4. The thickness of wedge with parallel side was reduced by .010 inches.

5. The resin was applied to the conductor channels and the sides of the aluminum form with a brush. The wedges were not coated with resin. These parts were cured one (1) hour at 100°F. A positive pressure was maintained on the channel-wedge interface and the wedge-aluminum interface by virtue of the taper on one of the two wedges.

6. Sealing of the statorette was accomplished by wrapping the aluminum form with three layers of a prepregnated glass tape. The final assembly was cured for eight (8) hours at 190°F.

TEST RESULTS FOR STATORETTE #2

Room temperature oil was pumped through the statorette at pressure up to 60 psi. The time required to accumulate 20 or more pounds of oil in a sump was measured for various values of the manifold pressure. This data was converted to gallons per minute for the entire stator as shown in Figure 1·6.

The room temperature calibration showed a linear variation in flow with manifold pressure. A pressure of approximately 76 psi would pro-

duce a flow of 50 gallon per minute with MIL-L-7808 oil at 82°F. The viscosity of this oil at 82°F is approximately 48 Lbm/Ft-Hr. Hence, the flow rate with 150°F oil would have been greater. An attempt was made to supply the statorette with 150°F oil. This was accomplished by heating the oil in the tank until the temperature reached 150°F. It required 12 hours to bring the oil (approximately 50 gallon) up to this temperature due to the limitation of the electric heater and the heat loss from the oil drum. Subsequently, the pump was started and the by-pass was set to provide 30 psi at the manifold. This pressure produced approximately 0.35 gpm in the transfer system. The temperature of the oil in the system stabilized at approximately 125°F at the pump outlet and approximately 108°F at the manifold. A flow versus manifold pressure calibration was performed with these conditions. This data is graphically illustrated in Figure I.6. In general, the flow increase caused by heating the oil from room temperature to approximately 108°F was in accordance with change in the viscosity of the oil from 48 Lbm/Ft-Hr at 82°F to 30 Lbm/Ft-Hr at 108°F. Unfortunately it was not practical to obtain a higher oil temperature with the equipment used for this test. Therefore, it was necessary to estimate the pressure required to produce the design condition of 50 gallon per minute with 150°F oil.

As noted in Figure I·6, a pressure of 24 psi would probably produce 50 gpm with MIL-L-7808 oil at 150°F. This pressure is within the safe operating limit of the stator and can easily be supplied by an external pump. The viscosity of WEMCO-C oil is less than MIL-L-7808. Hence, the pressure required for this oil becomes, as noted in Table I·1.

$$(\Delta P)\ \text{WEMCO-C} = \Delta P\ \text{MIL-L-7808} \times \frac{1.326}{2.019}$$

$$= 24 \times 0.657 = 15.8\ \text{psi}$$

The final test performed on Statorette #2 was an evaluation of the division of the flow between the left and right side of the statorette. Previous observation indicated the flow was not evenly divided. The oil from each end of the statorette was collected in separate sumps for a

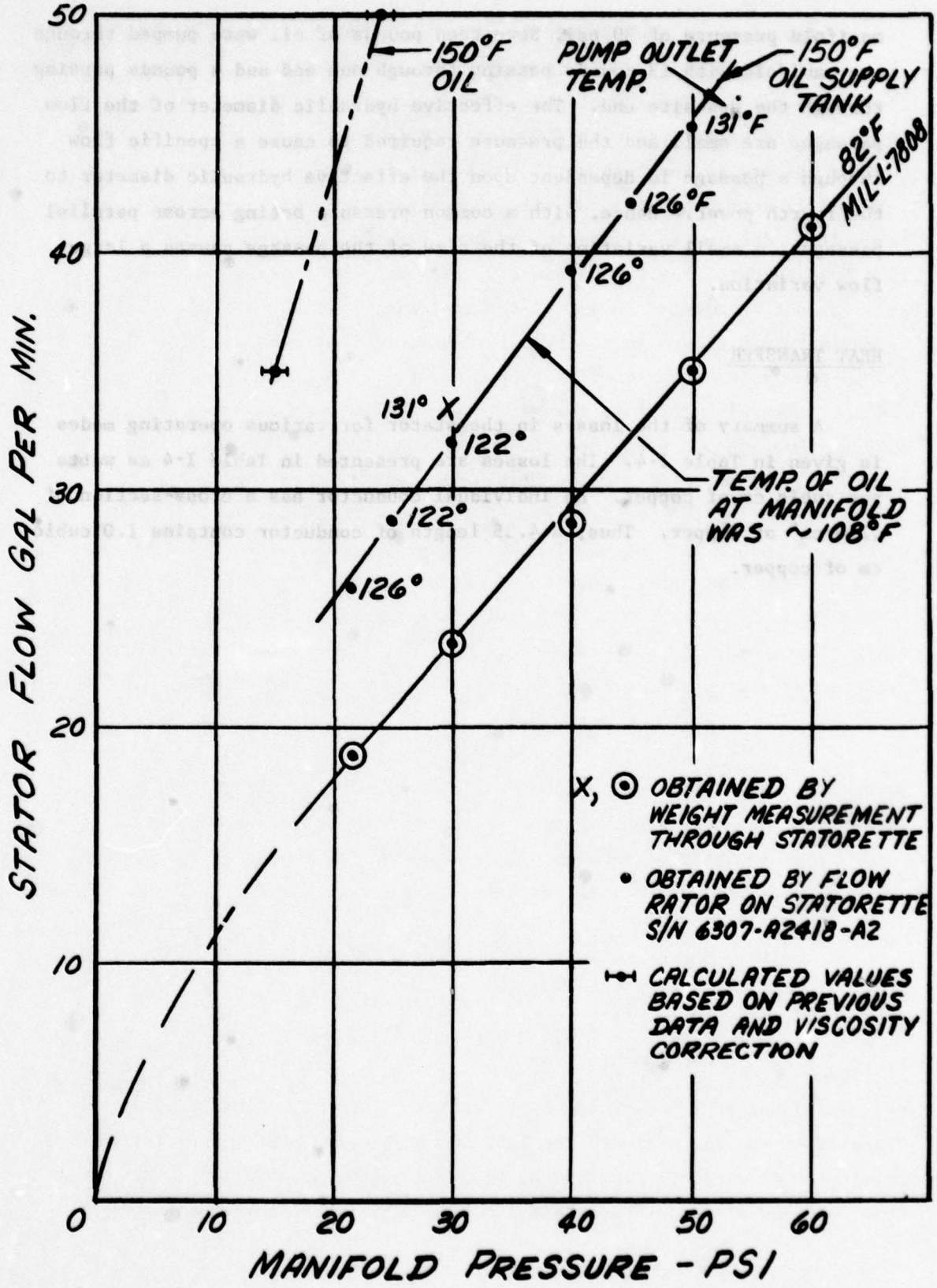


FIGURE I-6 STATOR MANIFOLD PRESSURE VS OIL FLOW

manifold pressure of 30 psi. Seventeen pounds of oil were pumped through the manifold with 13 pounds passing through one end and 4 pounds passing through the opposite end. The effective hydraulic diameter of the flow passages are small and the pressure required to cause a specific flow through a passage is dependent upon the effective hydraulic diameter to the fourth power. Hence, with a common pressure acting across parallel passages, a small variation of the size of the passage causes a large flow variation.

HEAT TRANSFER

A summary of the losses in the stator for various operating modes is given in Table I·4. The losses are presented in Table I·4 as watts per cubic cm of copper. An individual conductor has a cross-section of .230 cm^2 of copper. Thus, a 4.35 length of conductor contains 1.0 cubic cm of copper.

TABLE I-4

SUMMARY OF LOSSES

Source	OPERATING MODE: Full Load 9.728 MVA I_f = 246A	No Load I_f = 246A	No Load Max. Excitation I_f = 300A
Iron	8.263 KW	10.314 KW	15.339 KW
I^2R	109.455 KW	0	0
Eddy Currents	46.368 KW	57.879 KW	86.071 KW
Total	164.086 KW	68.193 KW	101.410 KW
ΔT Oil			
50 gpm	51.7°F	21.5°F	31.9°F
80 gpm	32.3°F	13.4°F	19.9°F
Power Loss Density, W/cm^3			
End Turns	13.74	0	0
U-Channels			
Average	13.74 + 13.01	16.24	24.15
Maximum	13.74 + 17.81	17.97	26.72

NOTE: Eddy current losses calculated by method of Appendix F.

The maximum specific power density in the U-channels occurs under full-load at the bore of the winding. For this case, the specific power density is 31.55 watts/cm^3 and the ΔT becomes

$$\Delta T = \frac{31.55 \frac{\text{watts}}{\text{cm}^3} \times \frac{1.8°F}{°C}}{12.7\ \text{cm}^{-1} \times .14 \frac{\text{watts}}{\text{cm}^2 °C}} = 31.9°F$$

HOT SPOT TEMPERATURES IN STATOR

For 9.728 MVA output, 50 gallon per minute flow, and 150°F oil inlet temperature:

Oil Outlet Temperature = 150° + 52° = 202°F

Maximum Conductor Temperature = 202° + 73° = 275°F in end turns

Maximum oil outlet Temperature = 150 + 43 = 193
From U-Channels with Balanced Flow

Maximum Conductor Temperature = 193 + 32 = 225
in U-Channel

Maximum Oil Outlet Temperature
From U-Channels with a 4/17 and = 150 + 91 = 241°F
13/17 Flow Unbalance

Maximum Conductor Temperature
in U-Channels = 241 + 32 = 273°F

The No-Load tests at the Westinghouse Research Laboratories are performed with an oil pump with the following rating:

Flow = 80 gpm
Head = 137 Feet = 47.5 psi
S. G.= .8
Kinematic Viscosity = 120 SSU

The pressure drop across the oil filters will be approximately 3.0 psi and with this oil pump, the oil flow into the stator is near 80 gallon per minute in place of 50 gpm as previously assumed. The hot spot temperature for this flow rate are given below for output of 9.728 MVA.

Oil Outlet Temperature	= 150 + 32 = 182°F
Maximum Conductor Temperature in End Turns	= 182 + 73 = 255°F
Maximum Oil Outlet Temperature from U-Channels with balanced flow	= 150 + 27 = 177°F
Maximum Conductor Temperature in U-Channels	= 177 + 32 = 209°F
Maximum Oil Outlet Temperature from U-Channels with a 4/17 and 13/17 Flow Unbalance	= 150 + 57 = 207°F
Maximum Conductor Temperature in U-Channel	= 207 + 32 = 239°F

APPENDIX J
STATOR OIL FLOW AND THERMAL TESTS

A. TEST SITE

The stator was connected to the cooling system as shown in Figures J·1 and J·2. This cooling system contained 120 gallons of transformer oil with 4·2 gallon (33 pounds) in the stator. A vent into the ambient atmosphere was provided by way of the storage tank. A positive pressure was maintained in the system since the tank was approximately 10 feet above the pump inlet. Flow was measured by a ITT Bell and Gossett gauge (SCR 153-894-1) with a 3 inch circuit setter valve after the oil passed through a bank of 10 microns filters. All tests were performed with the by-pass valve closed so the entire flow in the cooling circuit passed through the stator. The pressures at stator inlet and outlet manifolds were measured with conventional gauges.

B. THERMOCOUPLES

The stator contained twenty-four Chromel-Alumel thermocouples which were placed on the winding and back-iron during the fabrication of the stator. All thermocouples were operational during the tests except one couple which was located between the back-iron and the wrapping around the winding. This couple was open inside of the stator. The locations of the thermocouples (twenty) on the winding are shown in Figure J.3. Three positions on typical conductors are represented by these sensor locations:

- the knuckle (often referred to as the hairpin turn),
- the straight length of the conductors which connect to the bus rings,
- the straight length of the conductor where it exits from the cells.

The thermocouple junctions were placed on the conductors and covered with an epoxy cement. Figure J·4 shows the installation of a couple at the end of the cells before the winding was wrapped.

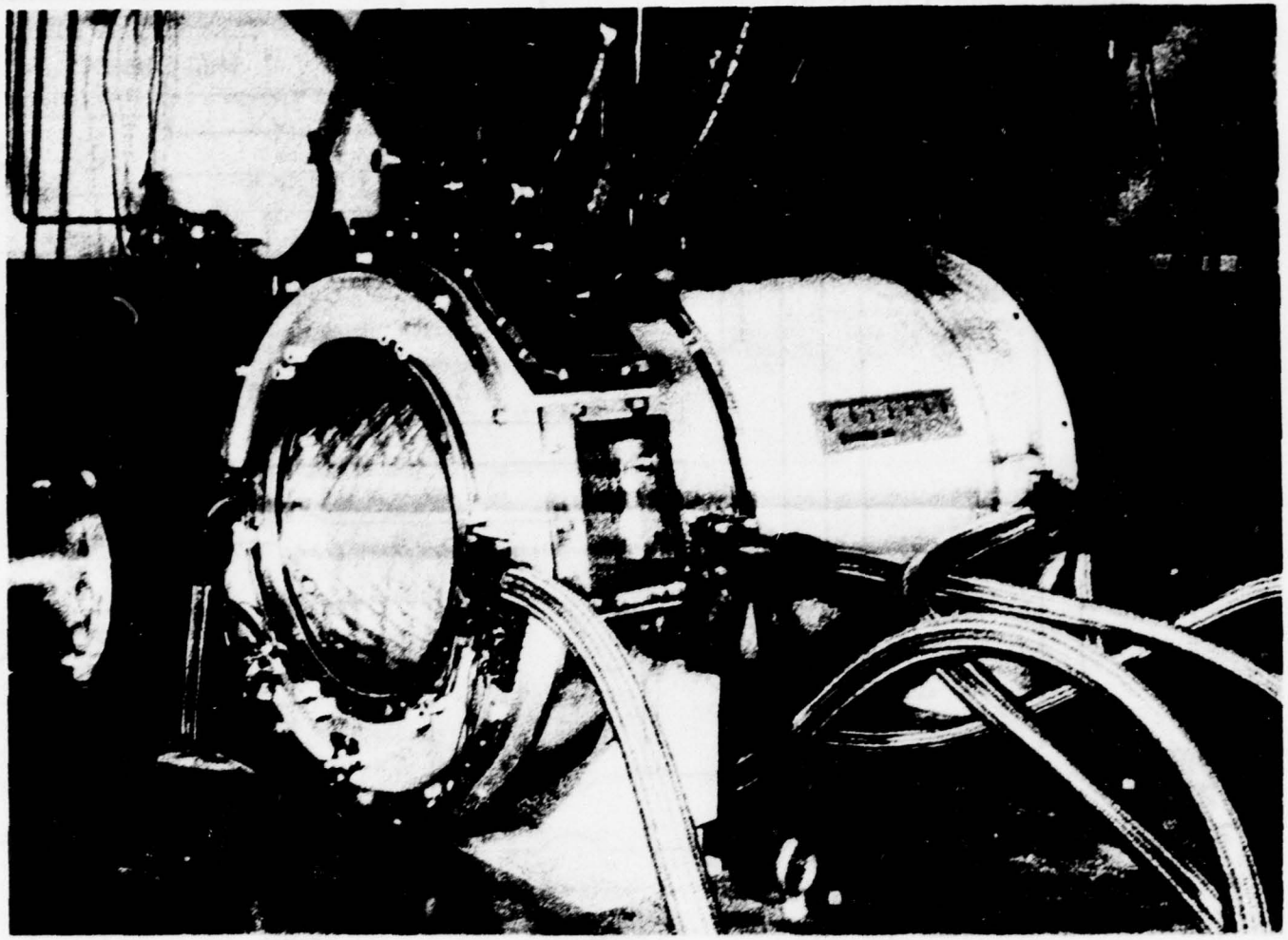


FIGURE J.1 - Stator On Test Bed

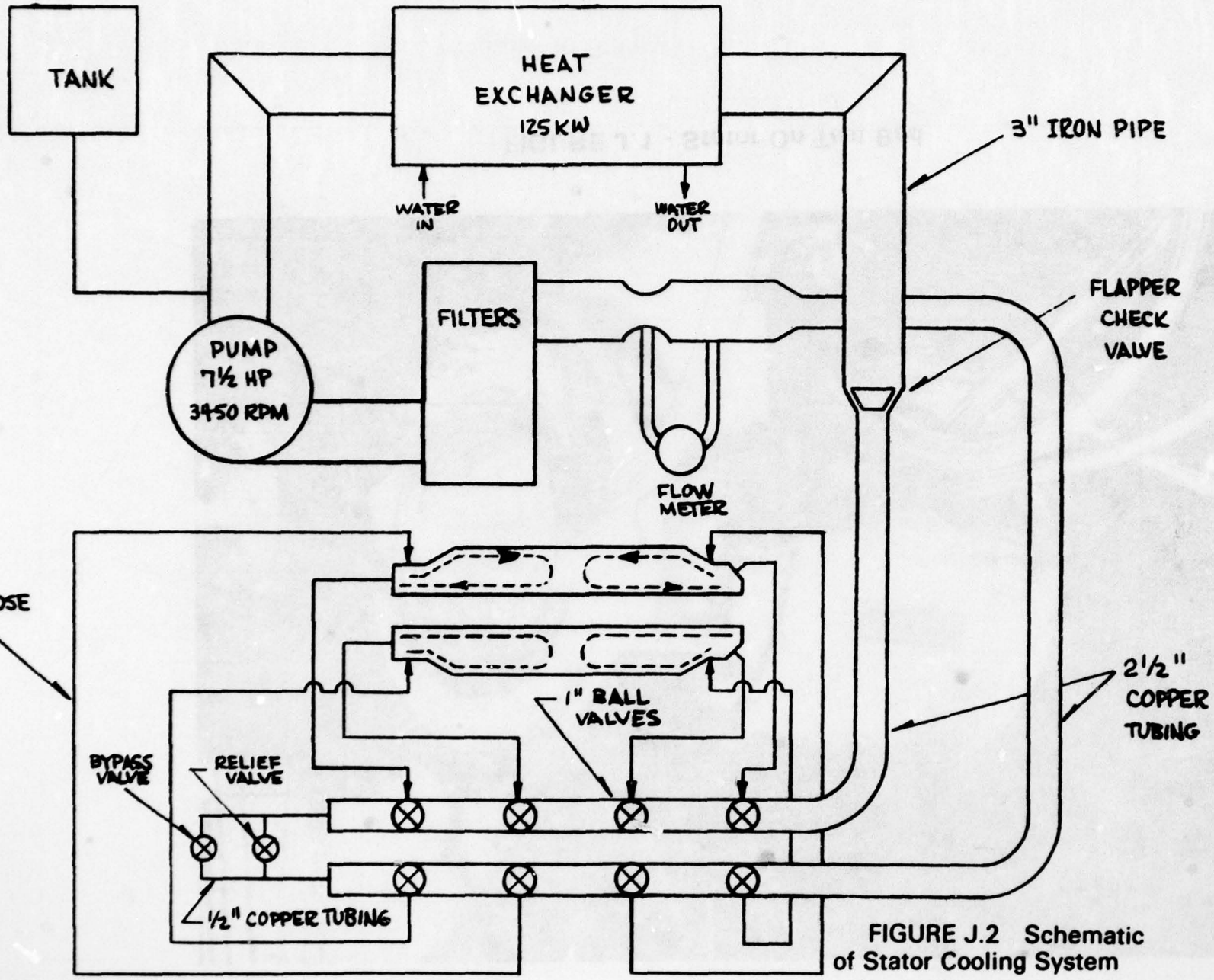


FIGURE J.2 Schematic of Stator Cooling System

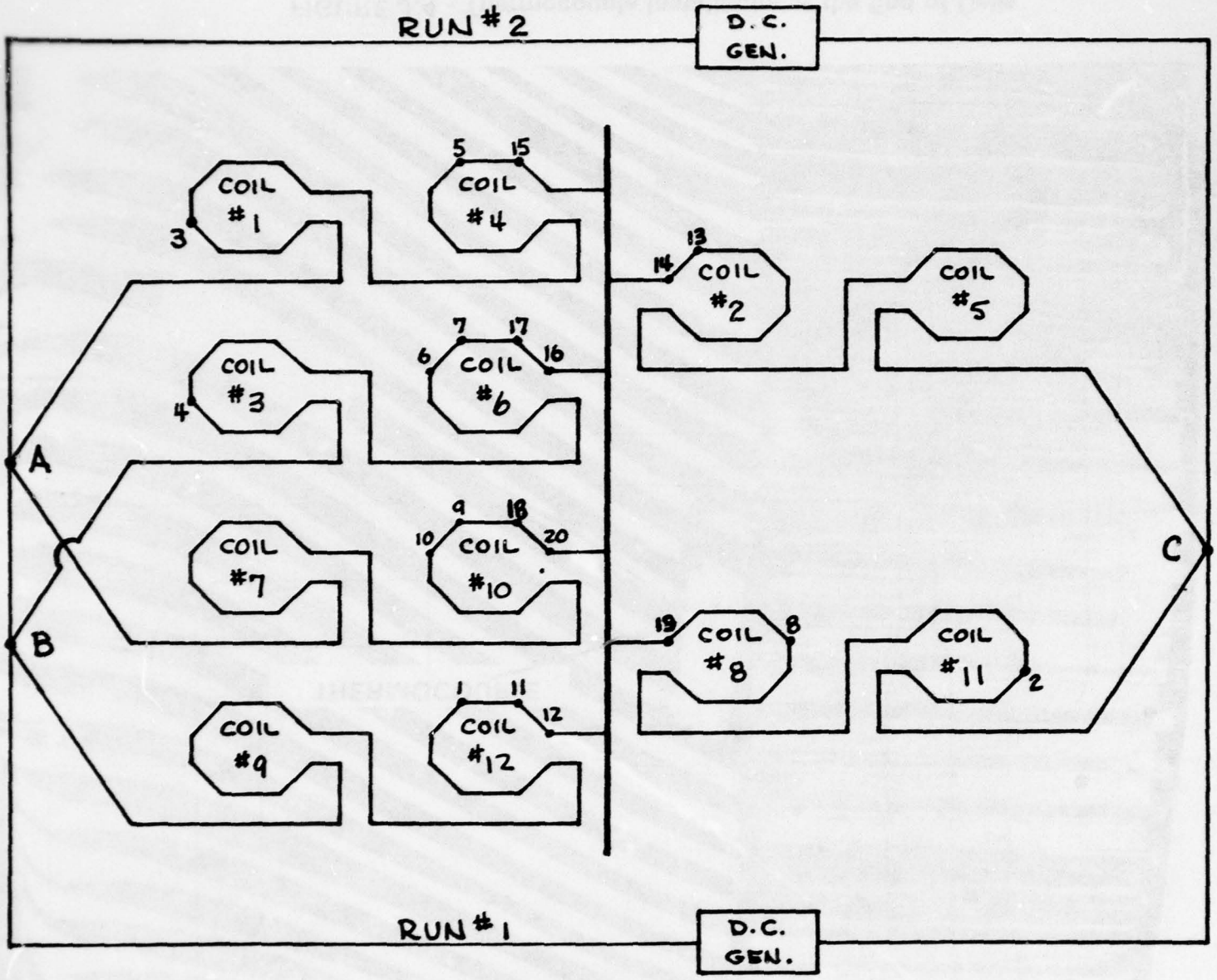


FIGURE J.3 Location of Thermocouples in Stator

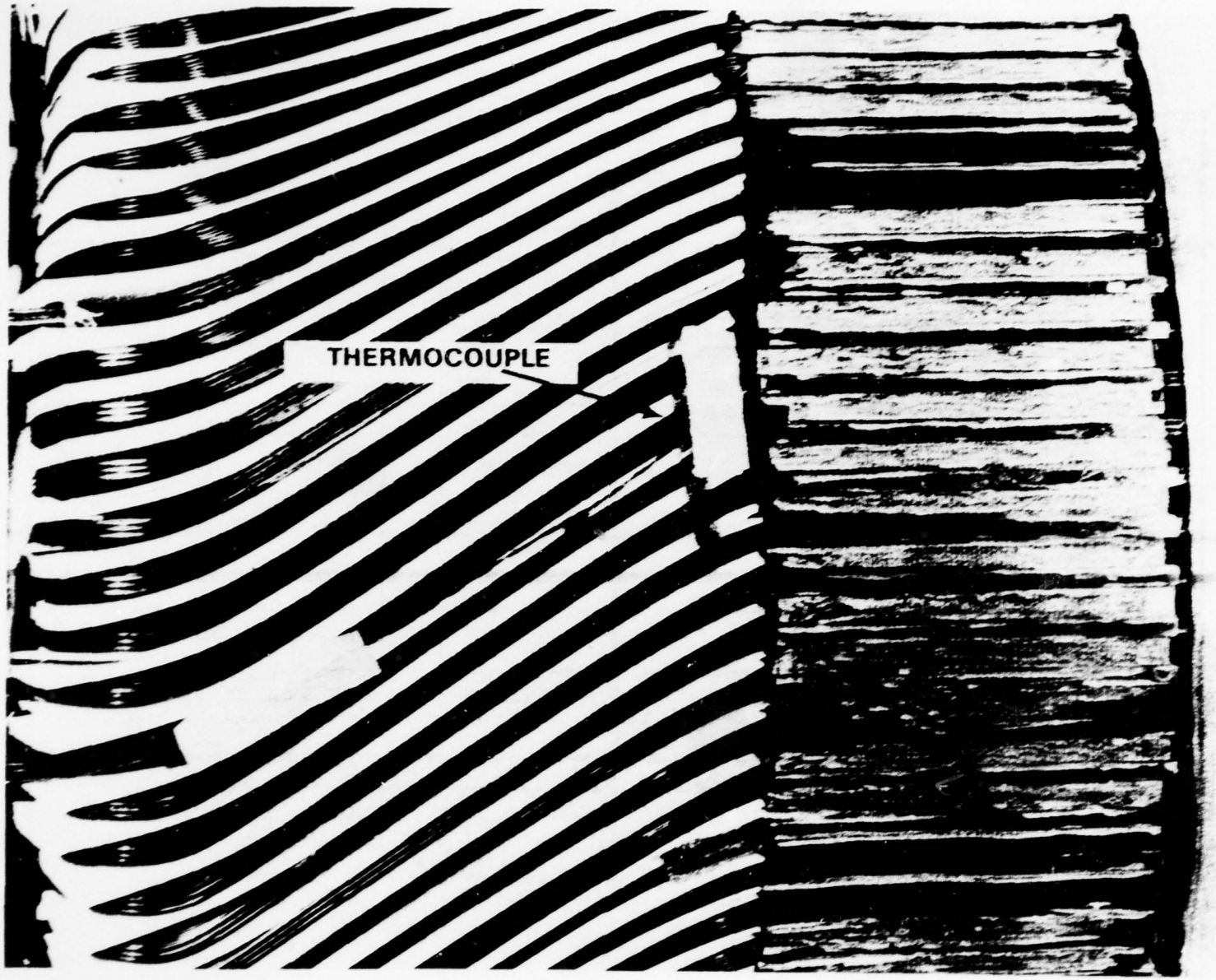


FIGURE J.4 - Thermocouple Installation at the End of Cells

The electromotive force (millivolts) from the thermocouples was recorded with a multichannel cyclic instrument.

C. POWER SUPPLY

A direct current generator was used as a power supply for the thermal test. The power leads were connected to phases B and C for the first run and C and A for the second run. The resistance of each phase was measured at room temperature and found to be:

	Current	Resistance
A - N	20A	.02325 Ω
B - N	20A	.02355 Ω
C - N	20A	.02325 Ω

D. TEST SCHEDULE

The elapsed time and currents for each run are listed on the following page.

FIRST RUN, PHASES B & C

Elapsed Time (Minutes)	I	KW	GPM Flow	Remarks
0 to 15	200	1.89	74.5	Water Off
15 to 35	400	7.89	78.3	Water Off
35 to 62	600	18.7 to 19.6	90.0	Water Off
62 to 77	800	35.6	90.0	Water Off
77 to 92	800	32.9	76.1	Water on but throttled low
92 to 114	1000	51.3	65.2	Water on but throttled low
114 to 132	1156	69.9	63 to 68.5	Water on but throttled low

SECOND RUN, PHASES A & C

Elapsed Time (Minutes)	I	KW	GPM Flow	Remarks
0 to 14	700	24.7	76.1	Water Off
14 to 20	700			Water turned on slightly oil in temp. 130°F
20 to 25	1000	53.3	83.7	Oil inlet @ 135
25 to 30	1000		89.1	Oil inlet stabilized at 148°F
30 to 32	1000		90.0	Oil inlet stabilized at 150°F
32 to 51	1156	75.1 to 79.4	90 to 95.6	Oil inlet temperature 150 to 195
51 to 55	1156		95.6 to 84.7	Water adjusted to stabilize oil inlet at 150°F
55 to 65	1156		84.7	

E. TEST RESULTS

1. Oil Flow Rate

The oil flow rate through the stator increased when the temperature of the oil increased as shown in Figure J·5. This trend reflected the influence of oil viscoisty and density upon the pump and throttling charateristics of the system. The pressure drop observed across the stator manifolds is given in Figure J·6 as a function of flow rate which varied with oil temperature as given in Figure J·5. In general the pressure drop between the stator outlet manifold and the pump inlet increased with the flow rate whereas the head across the stator decreased with increasing oil temperature and flow rate.

2. Temperature Records

The electromotive force for each thermocouple was converted to degrees Fahrenheit and listed by Chart numbers in Table J·1. Subsequently, the thermocouples with a common position on the conductors were listed together in individual tables. Table J·2 gives the thermocouple readings for the knuckles; Table J·3 gives the straight lenghts of conductor which connects to the bus rings; and Table J·4 gives the thermocouple readings for the straight length of the conductors where they exit from the cells. Two sets of temperatures are given for the thermocouples on Phase A and B - one with current flowing and one without current in the conductors.

F. CORRELATION OF TEMPERATURE DATA

The observed temperatures (θ) at each position in the winding were plotted against power density (p/v) in the conductor where

θ = Temperature of Conductor - oil inlet temperature °F

$\frac{P}{V} = I^2 \rho L/4A$

I = Phase Current = 2X Conductor Current, Amp

A = Area of Copper in conductor = .230 cm^2

L = Length of Conductor per unit volume, 4.35 cm^{-1}

ρ = Resistivity of Copper at the observed temperature, ohm-cm

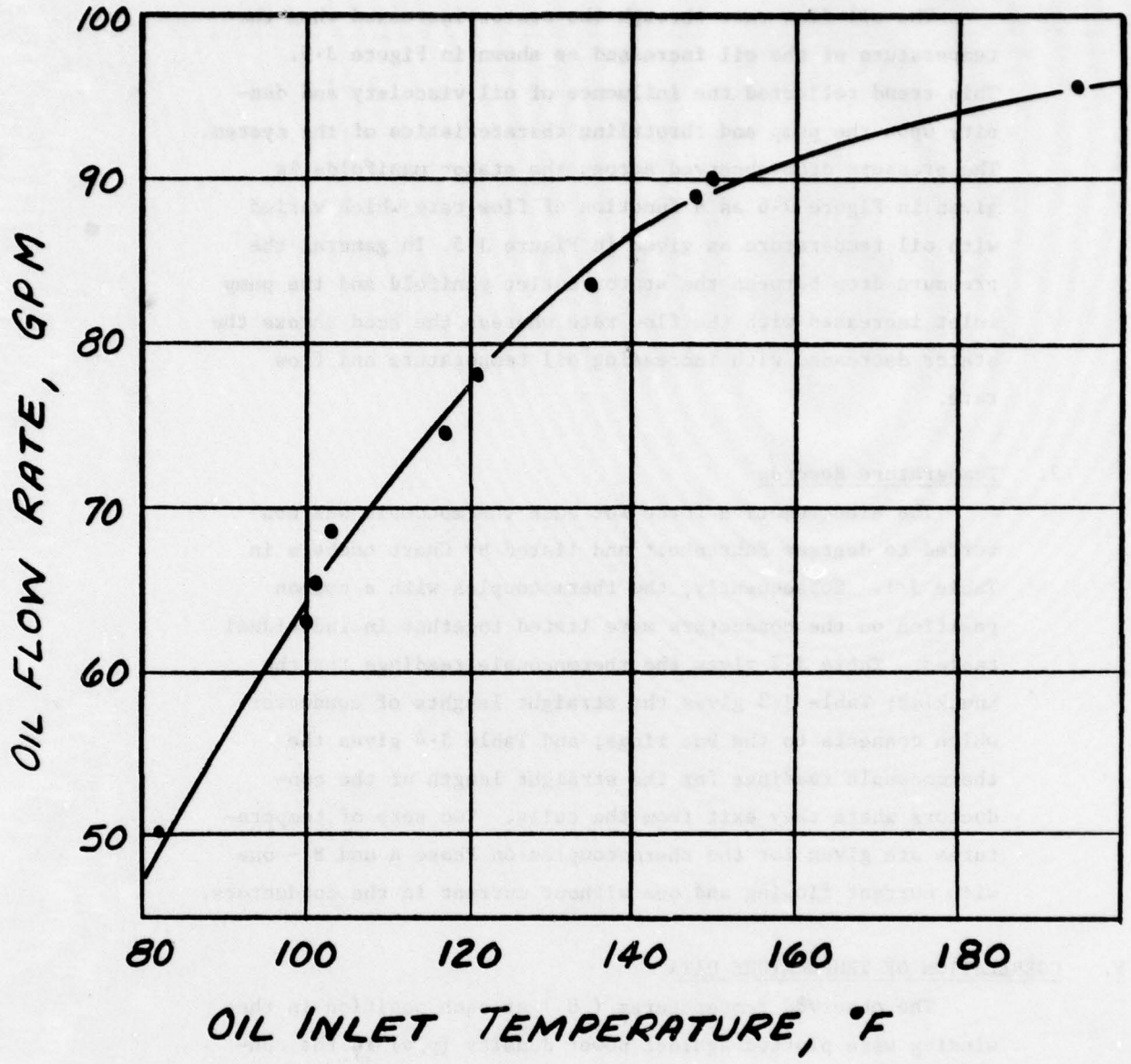


FIGURE J-5 OIL FLOW VS OIL INLET TEMPERATURE

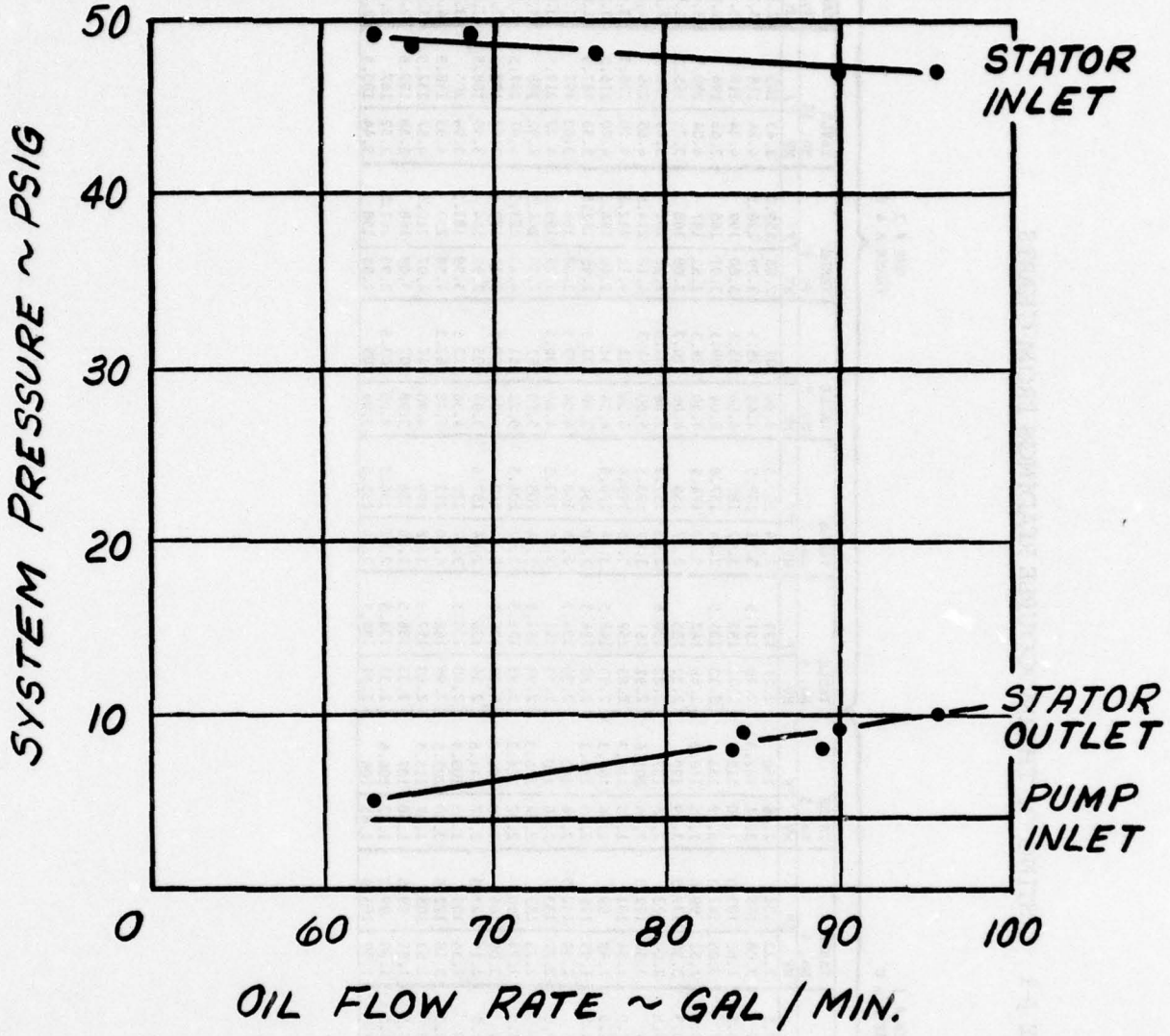


FIGURE J-6 SYSTEM PRESSURE VS OIL FLOW RATE

TABLE J-1 LISTING OF THERMOCOUPLE READINGS FROM CHARTS

RUN # 1
PHASE B & C

RUN # 2
PHASE A & C

T.C. No.	TABLE No. 1		TABLE No. 2		TABLE No.3		TABLE No. 4		TABLE No. 5		TABLE No. 6		TABLE No. 7		TABLE No. 8		TABLE No. 9		TABLE No. 10		TABLE No. 11	
	MV	°F	MV	°F	MV	°F	MV	°F	MV	°F	MV	°F	MV	°F	MV	°F	MV	°F	MV	°F	MV	°F
1	3.03	166	4.02	208.5	2.03	122.5	2.23	131	2.66	150	2.27	133	2.74	153.5	3.84	201	2.88	159.5	3.43	183	2.78	155
2	3.10	169	4.09	211.5	2.64	149	3.08	168	3.41	182.3	2.70	151.5	3.53	187.5	4.66	236.5	3.79	198.5	4.24	218	3.73	196
3	2.89	160	3.69	194.5	1.67	106.6	1.60	103.3	1.80	112.5	2.71	152	3.52	187	4.64	235.5	3.80	199	4.24	218	3.74	196.5
4	3.20	173.3	4.03	209	2.59	147	3.06	167.3	3.49	186	2.33	135.5	2.84	157.6	4.04	209.5	3.01	165	3.68	194	2.86	158.5
5	2.86	158.5	3.68	194	1.60	103.6	1.51	99.6	1.75	110.3	2.48	142	3.23	174.5	4.50	229.5	3.52	187	4.04	209.5	3.40	182
6	3.29	177	4.47	228	2.90	160.3	3.30	177.3	3.59	190	2.32	135	2.87	159	4.06	210.3	3.08	168	3.71	195.3	2.92	161
7	3.04	166.5	3.96	206	1.96	119.5	2.04	123	2.36	137	2.22	130.6	2.83	157.3	3.88	202.5	2.92	161	3.49	186	2.83	157.3
8	3.13	170.3	4.09	211.5	2.75	154	3.34	179.3	3.86	201.6	2.92	161	3.67	193.5	5.00	251.3	4.16	214.5	4.65	236	4.05	210
9	2.90	160.3	3.70	195	1.69	107.5	1.54	101	1.75	110.3	2.85	158	3.35	179.6	4.54	231	4.11	212.5	4.20	216.5	3.95	205.5
10	2.85	158	3.67	193.5	1.64	105.5	1.49	99	1.66	106.3	2.63	148.5	3.34	179.3	4.54	231	3.69	194.5	4.20	216.5	3.55	188.5
11	2.95	162.5	3.86	201.6	1.85	114.5	1.95	119	2.30	134.3	2.30	134.3	2.80	156	3.90	203.5	2.95	162.5	3.53	187.5	2.80	156
12	3.13	170.3	4.13	213.3	2.32	135	2.49	142.5	2.96	163	2.30	134.3	2.85	158	4.04	209.5	3.08	168	3.63	192	2.90	160.3
13	3.12	170	4.11	212.5	2.14	127.6	2.27	133	2.66	150	2.59	147	3.39	181.5	4.66	236.5	3.74	196.5	4.27	219.5	3.60	190.5
14	3.20	173.3	4.19	216	2.34	136	2.73	153	3.27	176.3	2.93	161,5	3.94	205	5.22	261	4.39	244.5	4.92	248	4.30	220.6
15	2.85	158	3.74	196.5	1.78	111.5	1.74	110	2.07	124.3	2.93	161.5	3.97	206.5	5.22	261	4.45	227.3	4.91	247.5	4.32	201.5
16	3.25	175.5	4.28	220	2.52	144	3.03	166	3.50	186.3	2.40	138.5	2.94	162	4.04	209.5	3.14	170.6	3.67	193.5	2.98	164
17	3.13	170.3	4.06	210.6	2.03	122.5	2.14	127.3	2.47	141.8	2.34	136	2.84	157.6	3.94	205	2.98	164	3.55	188.5	2.84	157.6
18	2.93	161.5	3.71	195.3	1.70	108	1.54	101	1.73	109.5	2.40	138.5	3.12	170	4.36	223.5	3.39	181.5	3.94	205	3.25	175.5
19	3.24	175	4.30	220.6	2.65	149.5	3.18	172.5	3.90	203.5	2.94	162	4.10	212	5.28	263.3	4.58	233	4.93	248.3	4.53	230.6
20	2.96	163	3.77	198	1.74	110	1.63	105	1.87	115.5	2.83	157.3	3.68	194	4.90	247	4.07	210.6	4.57	232.5	3.94	205
21	2.86	158.5	3.69	194.5	1.64	105.5	1.51	99.6	1.68	107	2.35	136.5	2.85	158	3.98	207	3.08	168	3.58	189.6	2.90	160.3
22	2.86	158.5	3.70	195	1.62	104.5	1.50	99.3	1.67	106.6	2.33	135.5	2.81	156.5	3.90	203.5	2.93	161.5	3.52	187	2.80	156
23	2.91	160.6	3.57	189.6	1.72	109	1.59	103.6	1.65	106	2.31	134.6	2.74	153.5	3.94	205	2.85	158	3.44	183.5	2.77	154.6

TABLE J.2. LISTING OF TEMPERATURES FOR KNUCKLES

	RUN # 1 - PHASE B AND C					RUN # 2 - PHASE A AND C					
T.C. No.	600 A °F	800 A °F	800 A °F	1000 A °F	1156 A °F	700 A °F	1000 A °F	1156 A °F	1156 A °F	1156A °F	1156 A °F
2	169	211.5	149	168	182.3	151.5	187.5	236.5	198.5	218	196
3						152	187	235.5	199	218	196.5
4	173	209	147	167	186						
6	177	228	160.	177.3	190						
8	168	211.5	149	168	182.3	161	193.5	251.3	214.5	236	210
10						148.5	179.3	231	194.5	216.5	188.5
AVG	171.8	215	151.3	170.1	185.2	153.3	186.8	238.6	201.6	222.1	197.8
	170	216.17	147.7								
2											
3	160	194.5	106.6	103.3	112.5						
4						135.5	157.6	209.5	165	194	158.5
6						135	159	210.3	168	195.3	161
8											
10	158	193.5	105.5	99	106.3						
AVG	159	194	106	101	109.4	135.2	158.3	209.9	166.5	194.7	159.8
OIL TEMP	159	192.3	106.8	101.5	106.3	135.1	155	204.3	159.8	185.3	155.3
$\bar{\theta}$	12.8	22.7	44.5	68.5	78.9	18.2	31.8	34.3	41.8	36.8	42.5
θ_M	18.	35.7	53.2	75.8	83.7	25.9	38.5	47	54.7	50.7	54.7
θ_{Me}	18.	34	54	76.3	80.6	25.8	35.2	41.4	48.0	41.3	50.2
$\bar{\theta}_s$	1.1	22.17	41.7	67							

θ = TEMPERATURE - OIL INLET TEMPERATURE

$\bar{\theta}$ = AVERAGE TEMPERATURE - OIL INLET TEMPERATURE

θ_M = MAXIMUM TEMPERATURE - OIL INLET TEMPERATURE

TABLE J.3. LISTING OF TEMPERATURES FOR CONDUCTOR/BUS RING CONNECTION

	RUN # 1 - PHASE B AND C					RUN # 2 - PHASE A AND C					
T.C. No.	600 A TABLE #1 °F	800 A TABLE #2 °F	800 A TABLE #3 °F	1000 A TABLE #4 °F	1156 A TABLE #5 °F	700 A TABLE #6 °F	1000 A TABLE #7 °F	1156 A TABLE #8 °F	1156 A TABLE #9 °F	1156 A TABLE #10 °F	1156 A TABLE #11 °F
12	170	213.3	135	142.5	163						
14	173	216	136	153	176.3	161.5	205	261	224.5	248	220.6
16	175.5	220	144	166	186.3						
19	175	220.6	149.5	172.5	203.5	162	212	263.6	233	248.3	230.6
20	———	———	———	———	———	157.3	194	247	210.6	232.5	205
AVG.	173.4	217.5	141.1	158.5	182.3	160.3	203.7	257.2	222.7	242.9	218.7
12	———	———	———	———	———	134.3	158	209.5	168	192	160.3
14	———	———	———	———	———						
16	———	———	———	———	———	138.5	162	209.5	170.6	193.5	164
19	———	———	———	———	———	———	———	———	———	———	———
20	163	198	110	105	115.5	———	———	———	———	———	———
AVG.	163	198	110	105	115.5	136.4	160	209.5	169.3	192.8	162.2
OIL TEMP.	159	192.3	106.8	101.5	106.3	135.1	155	204.3	159.8	185.3	155.3
$\bar{\theta}$	14.4	25.2	34.3	57	76	25.2	48.7	52.9	62.9	57.6	63.4
θ_M	16.5	28.3	42.7	71	97.2	26.9	57	59.3	73.2	63	75.3

$\bar{\theta}$ = AVERAGE TEMPERATURE - OIL INLET TEMPERATURE

θ_M = MAXIMUM TEMPERATURE - OIL INLET TEMPERATURE

TABLE J-4 LISTING OF TEMPERATURES AT THE EXIT OF THE CELLS

		RUN # 1 - PHASE B AND C					RUN # 2 - PHASE A AND C					
	T.C. No.	CHART #1 @660 A °F	CHART #2 @800 A °F	CHART #3 @800 A °F	CHART #4 @1000 A °F	CHART #5 @1156 A °F	CHART #6 @700 A °F	CHART #7 @1000 A °F	CHART #8 @1156 A °F	CHART #9 @1156 A °F	CHART #10 @1156 A °F	CHART #11 @1156 A °F
AT CURRENT SHOWN	1	166	208.5	122.5	131	150						
	5						142	174.5	229.5	187	218	196.5
	7	166.5	206	119.5	123	137						
	9						158	179.6	231	212.5	216.5	205.5
	11	162.5	201.6	114.5	119	134.3						
	13	170	212.5	127.6	133	150	147	181.5	236.5	196.5	219.5	190.5
	15						161.5	206.5	261	227.3	247.5	201.5
	17	170.3	210.6	122.5	127.3	141.5						
	18						138.5	170	223.5	181.5	205	175.5
	AVG.	167	207.8	121.3	126.7	142.6	149.4	182.4	236.5	201.0	221.3	193.9
NO CURRENT	1						133	153.5	201	159.5	183	155
	5	158.5	194	103.6	99.6	110.3						
	7						130.6	157.3	202.5	161	186	157.3
	9	160.3	195	107.5	101	110.3						
	11						134.3	156	203.5	162.5	187.5	156
	13											
	15	158	196.5	111.5	110	124.3						
	17						136	157.6	205	164	188.5	157.6
	18	161.5	195.3	108	101	109.5						
	AVG.	159.6	195.2	107.6	102.9	113.6	133.5	156.1	203	161.8	186.3	156.5
	OIL TEMP.	159	192.3	106.8	101.5	106.3	135.1	155	204.3	159.8	185.3	155.3
	θ_M	11.3	20.3	20.8	31.5	43.7	26.4	51.5	56.7	67.5	62.2	50.2
	θ_{avg}	8	15.5	14.5	25.2	36.3	14.3	27.4	32.2	41.2	36	38.6

The resistivity as function of temperature was calculated by

$$\rho = 1.72 \times 10^{-6} (390.1 + t/467.1) \quad \text{(J-1)}$$

t = Temperature, °F

Figure J·7 gives this information for the knuckles using the data from Table J·2. A correlation for the maximum temperature of the knuckles is given by

$$\theta_M \leq 8.67 \ (P/V) \quad \text{(J-2)}$$

Similarly, a correlation for the average temperature of the knuckles gives

$$\theta_{avg} = 4.07 \ (P/V) \quad \text{(J-3)}$$

Figure J·8 gives a plot of the data from Table J·3 for the maximum temperature observed at the junction of the straight length of the conductor and the bus ring. A correlation of the maximum temperatures and the average temperatures gives

$$\theta_M = 7.25 \ (P/V) \quad \text{(J-4)}$$

$$\theta_{avg} = 4.62 \ (P/V) \quad \text{(J-5)}$$

Figure J·9 gives a plot of the data from Table J·4 for the maximum conductor temperatures observed at the end of the cells. A correlation of the temperatures gives

$$\theta_M = 4.42 \ (P/V) + 5 \quad \text{(J-6)}$$

$$\theta_{avg} = 2.66 \ (P/V) \quad \text{(J-7)}$$

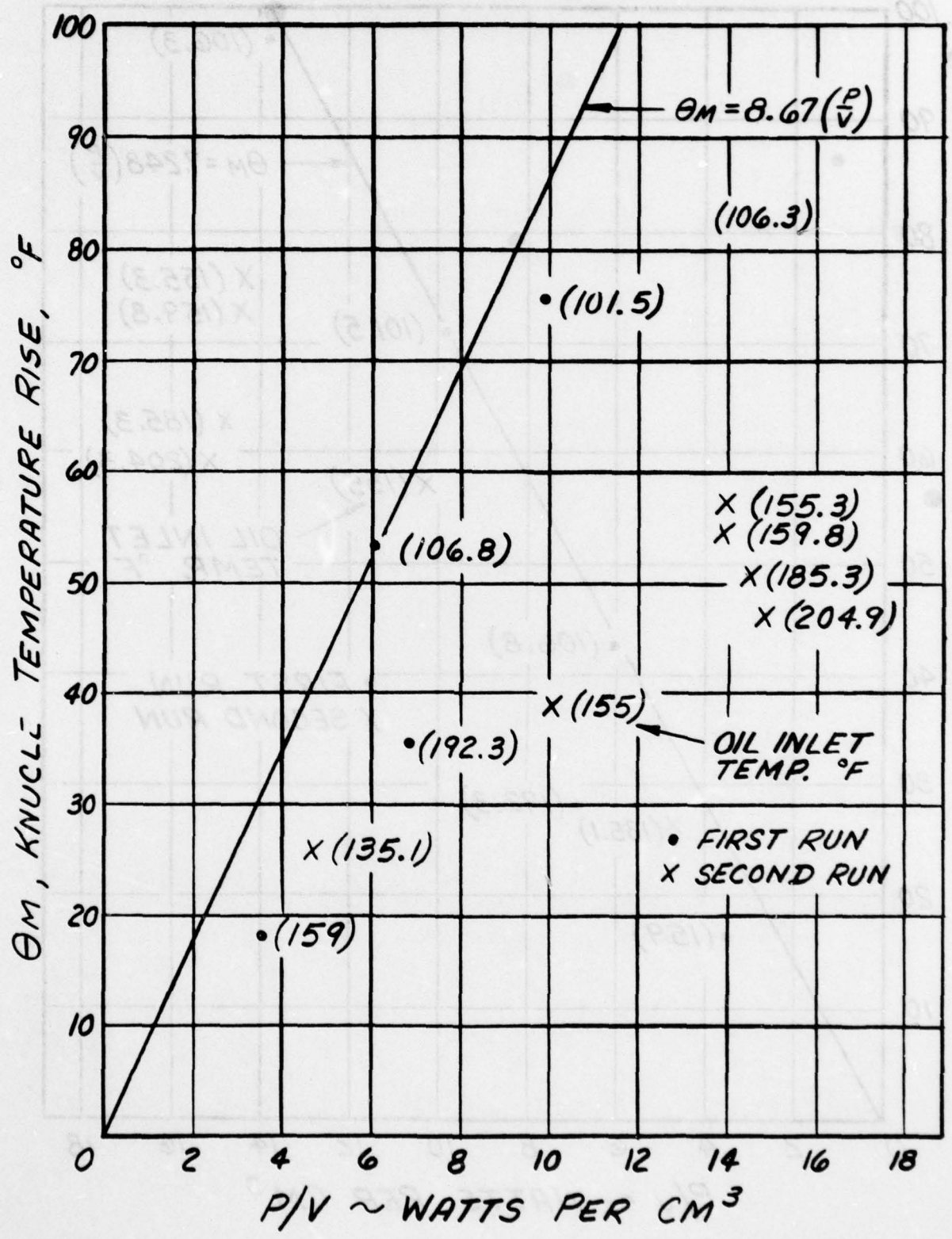


FIGURE J-7 HOT SPOT TEMPERATURE OF KNUCKLE VS POWER DENSITY

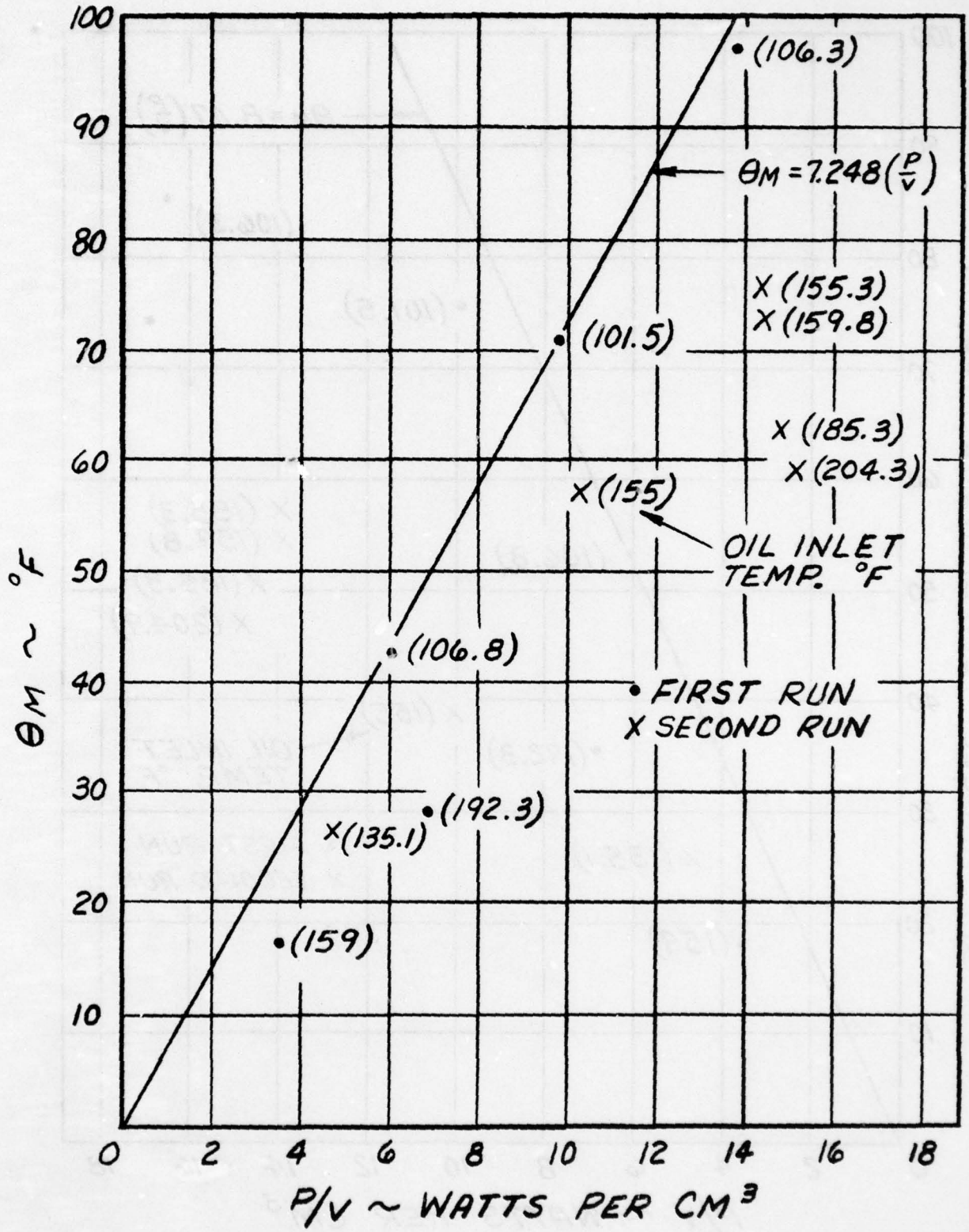


FIGURE J-8 HOT SPOT TEMPERATURE OF CONDUCTOR BUS RING JUNCTION VS POWER DENSITY

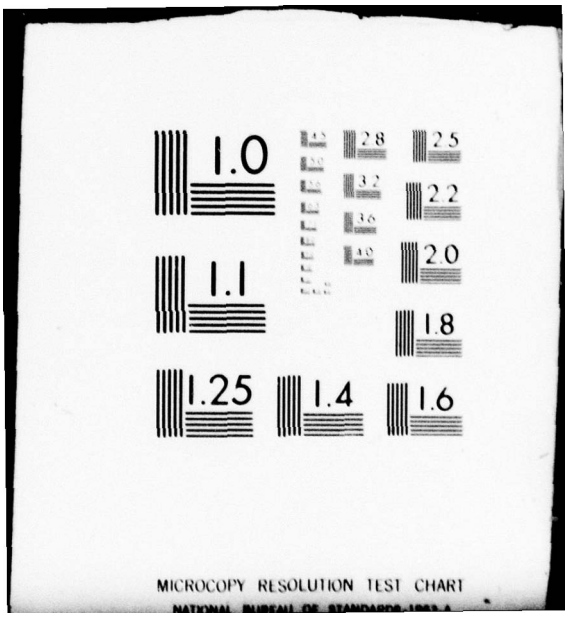
AD-A072 093 WESTINGHOUSE ELECTRIC CORP LIMA OHIO AEROSPACE ELECT--ETC F/G 10/2
PROGRAM FOR THE DEVELOPMENT OF A SUPERCONDUCTING GENERATOR.(U)
FEB 79 J L MCCABRIA F33615-71-C-1591

UNCLASSIFIED AFAPL-TR-79-2012 NL

4 OF 4
AD A072093



END
DATE FILMED
9-79
DDC


1.0
1.1
1.25
1.4
1.6
2.8
3.2
3.6
2.5
2.2
2.0
1.8
MICROCOPY RESOLUTION TEST CHART

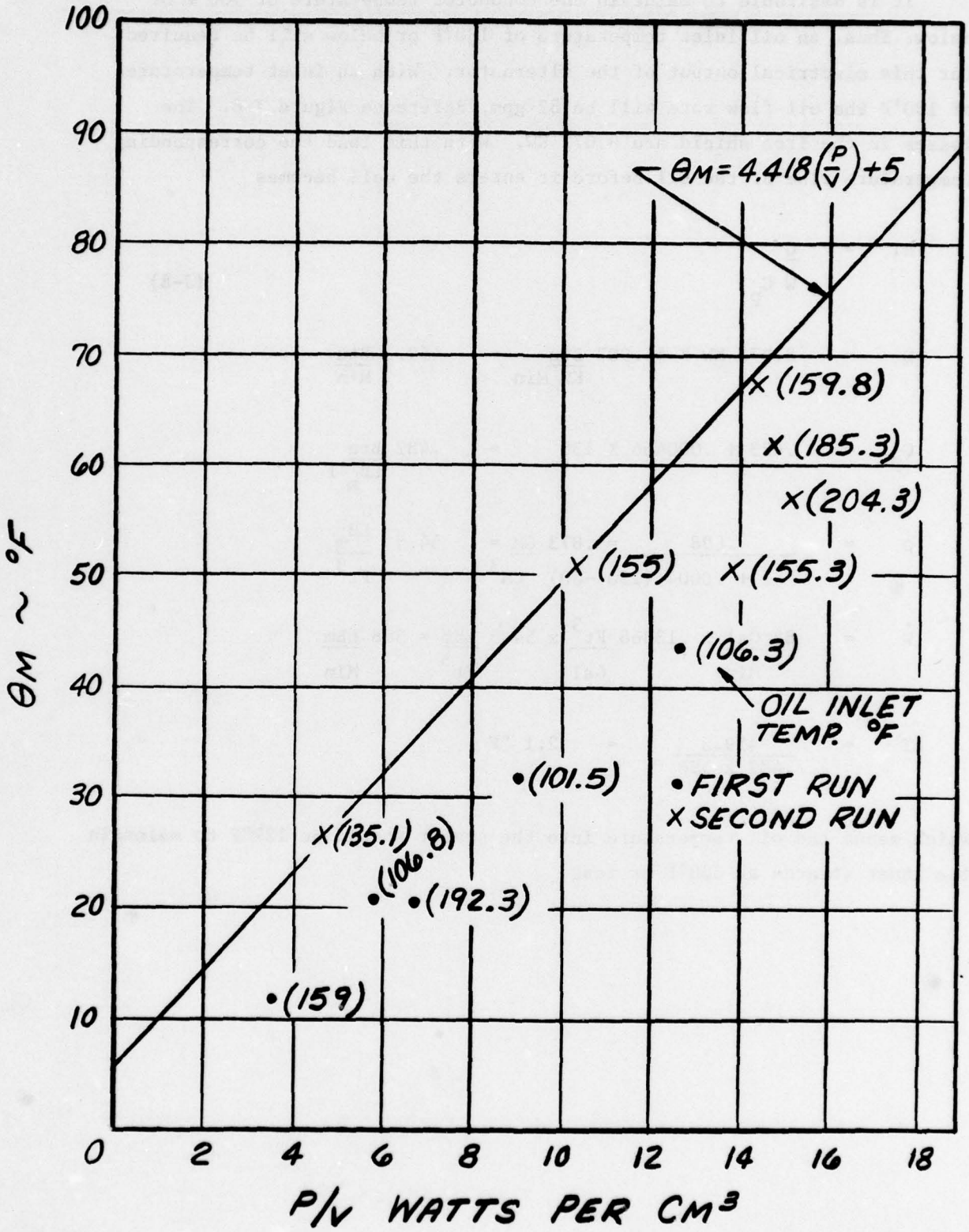


FIGURE J-9 HOT SPOT TEMPERATURE AT END OF CELLS VS POWER DENSITY

It is desirable to maintain the conductor temperature at 300°F or below. Thus, an oil inlet temperature of 130°F or below will be required for this electrical output of the alternator. With an inlet temperature of 130°F the oil flow rate will be 82 gpm, Reference Figure J·6. The losses in the iron shield are 8.072 KW. With this load the corresponding temperature rise of the oil before it enters the cell becomes

$$\Delta T = \frac{Q}{\dot{W} C_p} \qquad \text{(J-8)}$$

$$Q = 8.072 \text{ KW} \times 56.907 \frac{\text{Btu}}{\text{KW Min}} = 459.3 \frac{\text{Btu}}{\text{Min}}$$

$$C_p = .423 + .000456 \times 130 = .482 \frac{\text{Btu}}{\text{LB}_m\,^\circ\text{F}}$$

$$\rho = \frac{.898}{1 + .0004\,(130 - 60)} = .873 \frac{\text{GM}}{\text{CM}^3} = 54.5 \frac{\text{LB}_m}{\text{Ft}^3}$$

$$\dot{W} = 82 \frac{\text{Gal}}{\text{Min}} \times .13368 \frac{\text{Ft}^3}{\text{Gal}} \times 54.5 \frac{\text{LBm}}{\text{Ft}^3} = 598 \frac{\text{LBm}}{\text{Min}}$$

$$\Delta T = \frac{459.3}{.482 \times 598} = 2.1\ ^\circ\text{F}$$

Which means the oil temperature into the stator should be 129°F to maintain the inner strands at 300°F or less.

K. SUMMARY

The oil flow through the stator was 89 gpm with an oil inlet temperature of 150°F and 82 gpm when the oil temperature was decreased to 129°F. It was anticipated from previous tests on a statorette that the coolant pump at the Westinghouse Research Lab test site would produce a flow of about 80 gpm when the temperature of the oil at the inlet ports was above 135°F. The test results on the full scale stator are in agreement with previous projections.

The maximum temperature difference between the conductor and the oil with a uniform power (loss) density in the conductor occurs in the end extensions as anticipated from previous heat transfer calculations. At 5 MVA, 5000 Volts, the hot spot in the end extensions will not exceed 193°F with a 129°F oil inlet temperature.

The power density due to eddy currents by virtue of the time varying field in this stator were calculated from a new formulation for this problem. The eddy current loss at the inner radius of the winding is increased by a factor of 1.69 (5 MVA, 5000V) when compared with the old method for calculating this loss.

The combined loss per unit volume for the inner strands is 37.04 watts cm^{-3} at 5 MVA, 5000V. An oil inlet temperature of 129°F or less is required to maintain the conductors at the inner radius of the winding at 300°F or less.

A line-to-line voltage of 5000 volts is not optimum for the stator from the standpoint of the critical loss density in the winding. Reducing the speed or the field current to obtain 5 MVA at 3000 to 3300 volts would reduce the maximum heat rate in the stator by a factor of .74 or more.

APPENDIX K

TEST PROCEDURES

PROOF-OF-INTEGRITY TEST PROCEDURE

This procedure is intended to explain and establish specific methods for proof-of-integrity tests on Superconducting Generator ED 363428. These tests will be performed by Westinghouse Electric Corporation for the Aero Propulsion Laboratory, Wright-Patterson Air Force Base, Dayton, Ohio, under USAF Contract No. F33615-71-C-1591. The tests will be performed at the Westinghouse Research Laboratories, Churchill Borough, Pittsburgh, Pennsylvania, 15235.

1.0 WARM ROTOR TESTS

1.1 After assembly of generator in test bed, alignment will be carefully checked by placement of an indicator on the rotor shaft and manually rotating the shaft. A squareness of .001 TIR or less and concentricity of .002 TIR or less relative to the output shaft on the gearbox will be obtained by shifting and shimming the cradle on the bed.

1.2 After alignment has been achieved, the cradle will be pinned and bolted to the "I" beams.

1.3 After the cradle has been secured, the generator will be removed from the cradle, the drive spindle will be installed, and the generator will be reinstalled in the cradle.

1.4 Oil line, cooling air, and water line connections will be completed and subsequently checked for leakage.

1.5 All brushes, dc power leads, cryogenic seals, and the transfer bayonet shall be installed. Apply 3 volts d-c to field power terminals to check continuity of field connections.

1.6 All instrument outputs, such as seal and bearing thermometry and vibration pick-ups will be connected.

1.7 After assembly of generator in test bed, rotor will be run at 600 rpm checking on instrumentation slip rings, current slip ring, general operation of oil supply and scavenge, unusual noises, and the operation of the rotating vacuum pump-down seal.

1.8 Rotor speed will be increased up to 4000 rpm checking general operation of system at intermediate speeds. All emergency shut-down provisions will be activated during this run. X and Y vibration (displacement) at each of the main bearings and the rotational speed will be recorded during the run-up and run-down. This test will be concluded by making a permanent trace of vibration (acceleration) at each bearing on a two channel X-Y recorder. The X axis shall be driven by a tachometer generator.

2.0 ROTOR COOL-DOWN

2.1 The rotor will be cooled to a superconducting state after a satisfactory warm rotor spin-up has been achieved. The rotor shall be cooled by introducing liquid helium via the bayonet on the external transfer line from the CTI system. Before cryogenic helium is introduced, the helium compartments within the rotor shall be purged of ambient gas by the procedure outline in Section 2.2.

2.2 Purge of Rotor

2.2.1 Cap helium vents on thermal transition tubes (eight ports).

2.2.2 Connect house vacuum to one of the current lead discharge ports and to the inlet helium transfer line at union connection.

2.2.3 Connect a regulated supply of helium gas to the second current lead discharge port.

2.2.4 Pump helium compartment in the rotor down to 10^{-3} torr and back-fill with helium gas.

2.2.5 Repeat Step 2.2.4 until the rotor has been back-filled with helium gas.

2.2.6 With vacuum pump down lines closed, pressurize rotor via current lead exhaust port. Slowly increase pressure in rotor until outer seal opens and allows gas to flow. Record pressure in rotor where seal opens. Decrease pressure until the seal closes. Record pressure at which the seal closes.

2.2.7 Repeat Step 2.2.4 and continue with Step 2.2.8.

2.2.8 Maintain a positive pressure (2.0 psig) of helium gas within the rotor and remove caps on vents on the thermal transition tubes (eight ports).

2.2.9 With positive pressure in generator by way of the current lead exhaust port, connect union in transfer line from the CTI (ref. Attachment A-1).

2.3 Purge CTI of Ambient Gas

Prior to Step 2.2.9 the CTI shall be purged of ambient gas and made ready for liquid helium by the procedure outlined here.

2.3.1 Evacuate space between outer vacuum jacket and internal Dewar.

2.3.2 Evacuate vacuum spaces around pipe penetrations.

2.3.3 Evacuate internal piping assembly and back-fill with helium gas.

2.3.4 Evacuate internal Dewar and back-fill with helium gas.

2.3.5 Circulate LN_2 to cool radiation shield and internal Dewar.

2.3.6 Connect CTI to helium supply Dewar.

2.3.7 Fill helium bath.

2.3.8 Connect generator to transfer line (see Step 2.2.9).

2.4 Introduction of Helium into Rotor

2.4.1 Delete.

2.4.2 Pressurize helium supply dewar to 20 psig and simultaneously open outlet valve in CTI.

2.4.3 Discontinue pressurization of rotor by way of the current lead exhaust port. Open exhaust vent until the pressure at lead exhaust is slightly less than the outer seal closure pressure obtained in Step 2.2.6.

2.4.4 Increase helium supply pressure until the ΔP across the inner seal is two times the opening pressure differential for the outer seal.

2.4.5 After a superconducting state has been achieved, the rotor speed will be increased to 4000 RPM checking the general operation of the machine and the ability of the vacuum pump to maintain a satisfactory vacuum within the rotor. Activate all bearing and gearbox lubrication and rotate rotor at 4000 rpm.

2.4.6 Helium thermometer readings shall be recorded every 15 minutes during the cool-down mode of operation. A plot of log temperature versus time shall be made and a plot of helium consumed versus cool down time shall be maintained. The apparatus and meters shown in Attachment A-2 shall be connected to the slip ring to obtain thermometer readings. The locations of the temperature indicators within the rotor are presented in Attachment A-3. The temperature indicators in the external helium management system, see Attachment A-1, shall be recorded during cool-down, also.

2.4.7 **Increase the field excitation at a rate not to exceed 25 Amps/minute until the field current reaches 50 amps (maximum). Allow the field current to drift to a constant current. Adjust input voltage to DC motor to maintain a speed of 4000 ± 120 RPM. Simultaneously read and record the:**

- **field current**
- **terminal voltage**
- **rotor speed**
- **clock time**

Mark on the cyclic recorder charts and strip charts this clock time. Allow the temperatures of the stator to stabilize and simultaneously read and record:

- **ΔT across the oil manifold**
- **Δp across the oil flow meter**
- **terminal voltage**
- **clock time (mark on charts)**

LOW POWER TEST PROCEDURE

This procedure is intended to explain and establish specific methods for measurement of parameters during the low power tests on Superconducting Generator ED363428. These tests will be performed by Westinghouse Electric Corporation for the Aero Propulsion Laboratory, Wright-Patterson Air Force Base, Dayton, Ohio, under USAF Contract No. F33615-71-C-1591. The tests will be performed at the Westinghouse Research Laboratories, Churchill Borough, Pittsburgh, Pennsylvania, 15235, after the proof-of-integrity tests have been successfully completed and approval has been granted by the USAF to run the low power tests.

SPECIAL NOTE*: The steps outlined in paragraphs 1 and 2 herein are the same procedures for the prior proof-of-integrity tests; the actual low power tests begin with paragraph 3 herein. The preparatory steps prior to running the first low power test of paragraph 3 are basically as outlined in paragraphs 1 and 2; thus, these two paragraphs are included intact herein for the sake of completeness of test preparation information. Their inclusion should not be construed to mean that the proof-of-integrity tests must be repeated prior to beginning the low power test per paragraph 3.

The low power tests per Revision C differ from those in Revision B in the following basic areas:

a. The tests start with paragraph 3,

b. The maximum test speed will be 8000 rpm instead of 12,000 or 13,200 rpm.

c. Initial tests will be at 4000 rpm at conditions well away from possible quench conditions. These initial tests are (by paragraph number):

   3. Open Circuit Tests
   4. Short Circuit Tests
   5. Sudden Application of Short Circuits.

d. Concluding tests will be at 8000 rpm at conditions that will result in a quench. These concluding tests are (by paragraph number):

   6. Open Circuit Tests (repeat of original test but at higher speed)
   7. Unbalanced Load Test, L-N Short Circuit
   8. Short Circuit Rectifier Bridge Test.

---

* Revision D added the special note on this page only.

Rev. A 4/25/77
Rev. B 5/12/77
Rev. C 4/5/78
Rev. D 4/7/78

1.0 WARM ROTOR TESTS

1.1 After assembly of generator in test bed, alignment will be carefully checked by placement of an indicator on the rotor shaft and manually rotating the shaft. A squareness of .001 TIR or less and concentricity of .002 TIR or less relative to the output shaft on the gearbox will be obtained by shifting and shimming the cradle on the bed.

1.2 After alignment has been achieved, the cradle will be pinned and bolted to the "I" beams.

1.3 After the cradle has been secured, the generator will be removed from the cradle, the drive spindle will be installed, and the generator will be reinstalled in the cradle.

1.4 Oil line, cooling air, and water line connections will be completed and subsequently checked for leakage.

1.5 All brushes, dc power leads, cryogenic seals, and the transfer bayonet shall be installed. Apply 3 volts d-c to field power terminals to check continuity of field connections. B

1.6 All instrument outputs, such as seal and bearing thermometry and vibration pick-ups will be connected.

1.7 After assembly of generator in test bed, rotor will be run at 600 rpm checking on instrumentation slip rings, current slip ring, general operation of oil supply and scavenge, unusual noises, and the operation of the rotating vacuum pump-down seal. C

1.8 Rotor speed will be increased up to 4000 rpm checking general operation of system at intermediate speeds. All emergency shut-down provisions will be activated during this run. X and Y vibration (displacement) at each of the main bearings and the rotational speed will be recorded during the run-up and run-down. This test will be concluded by making a permanent trace of vibration (acceleration) at each bearing on a two channel X-Y recorder. The X axis shall be driven by a tachometer generator. C

2.0 ROTOR COOL-DOWN

2.1 C

The rotor will be cooled to a superconducting state after a satisfactory warm rotor spin-up has been achieved. The rotor shall be cooled by introducing liquid helium via the bayonet on the external transfer line from the CTI system. Before cryogenic helium is introduced, the helium compartments within the rotor shall be purged of ambient gas by the procedure outline in Section 2.2.

2.2 Purge of Rotor

2.2.1 Cap helium vents on thermal transition tubes (eight ports).

2.2.2 Connect house vacuum to one of the current lead discharge ports and to the inlet helium transfer line at union connection.

2.2.3 Connect a regulated supply of helium gas to the second current lead discharge port.

2.2.4 Pump helium compartment in the rotor down to 10^{-3} torr and back-fill with helium gas.

2.2.5 Repeat Step 2.2.4 until the rotor has been back-filled with helium gas.

2.2.6 With vacuum pump down lines closed, pressurize rotor via current lead exhaust port. Slowly increase pressure in rotor until outer seal opens and allows gas to flow. Record pressure in rotor where seal opens. Decrease pressure until the seal closes. Record pressure at which the seal closes.

2.2.7 Repeat Step 2.2.4 and continue with Step 2.2.8.

2.2.8 Maintain a positive pressure (2.0 psig) of helium gas within the rotor and remove caps on vents on the thermal transition tubes (eight ports).

2.2.9 With positive pressure in generator by way of the current lead exhaust port, connect union in transfer line from the CTI (ref. Attachment A-1).

2.3 Purge CTI of Ambient Gas

Prior to Step 2.2.9 the CTI shall be purged of ambient gas and made ready for liquid helium by the procedure outlined here.

2.3.1 Evacuate space between outer vacuum jacket and internal Dewar.

2.3.2 Evacuate vacuum spaces around pipe penetrations.

2.3.3 Evacuate internal piping assembly and back-fill with helium gas.

2.3.4 Evacuate internal Dewar and back-fill with helium gas.

2.3.5 Circulate LN_2 to cool radiation shield and internal Dewar.

2.3.6 Connect CTI to helium supply Dewar.

2.3.7 Fill helium bath.

2.3.8 Connect generator to transfer line (see Step 2.2.9).

2.4 Introduction of Helium into Rotor

2.4.1 Delete. C

2.4.2 Pressurize helium supply dewar to 20 psig and simultaneously open outlet valve in CTI.

2.4.3 Discontinue pressurization of rotor by way of the current lead exhaust port. Open exhaust vent until the pressure at lead exhaust is slightly less than the outer seal closure pressure obtained in Step 2.2.6.

2.4.4 Increase helium supply pressure until the ΔP across the inner seal is two times the opening pressure differential for the outer seal.

2.4.5 After a superconducting state has been achieved, the rotor speed will be increased to 4000 RPM checking the general operation of the machine and the ability of the vacuum pump to maintain a satisfactory vacuum within the rotor. Activate all bearing and gearbox lubrication and rotate rotor at 4000 rpm. C

2.4.6 Helium thermometer readings shall be recorded every 15 minutes during the cool-down mode of operation. A plot of log temperature versus time shall be made and a plot of helium consumed versus cool down time shall be maintained. The apparatus and meters shown in Attachment A-2 shall be connected to the slip ring to obtain thermometer readings. The locations of the temperature indicators within the rotor are presented in Attachment A-3. The temperature indicators in the external helium management system, see Attachment A-1, shall be recorded during cool-down, also.

3.0 OPEN CIRCUIT TESTS AT 4000 RPM C

3.1 General. The purpose of this test is to obtain the no-load output voltage versus the field amperes at rated speed. This calibration will be used to compare the actual voltage with computer calculations. The other parameters obtained from this test are (1) phase balance (voltage), (2) field current for normalization of the field at design speed, (3) the no-load electrical losses in the stator, (4) the stator coolant flow rate, and (5) the voltage wave form. C

3.2 Apparatus

3.2.1 The signals generated by a 60 tooth wheel directly coupled to the rotor shaft shall be counted over a one second period to measure the revolution per minute.

3.2.2 The instrumentation shown in Attachment B will be used to measure the open-circuit voltages (line-to-neutral) and the field current.

3.2.3 The apparatus shown in Attachment C will be connected to the stator to circulate and measure the oil flow through the stator.

3.2.4 The apparatus and meters shown in Attachment A will be used to record and observe the output of the calibrated, resistance thermometers in the rotor and the external helium management system.

3.2.5 The meters shown in Attachment D will be used to cyclic record the temperatures of the stator cooling oil, back-iron, and armature conductor temperatures. The location of the thermocouples in the stator are shown in Attachment D, also.

3.3 Procedure

3.3.1 Operate stator coolant pump with water valve in the full on position without excitation in the generator until the stator and cooling system reach constant temperatures.

3.3.2 Operate generator at 4000 RPM until bearings and helium cooling system reach a constant temperature. C

3.3.3 Increase field excitation at a constant rate of 25 ± 2 A/min. until the field current given below is reached and allow the field current to drift to a constant current for each rheostat position. Adjust input voltage to DC motor to maintain a speed of 4000 ± 120 RPM. Field current for readings: 0, 25, 50, 100, 150, and 200A. See Attachment J. C B, C

3.3.4 As soon as the field current reaches a constant value for each rheostat position and the speed is set at 4000 ± 120 RPM, simultaneously read and record the field current, terminal voltages, rotor speed and clock time. C

Mark on the cyclic recorder charts and the strip charts this clock time. Allow the temperatures of the stator to stabilize and simultaneously read and record:

- Δ T across the oil mainfold
- Δ p across the oil flow meter
- field current
- terminal voltage
- rotor speed
- clock time (mark on charts)

With a field current of 15 amperes obtain data at the generator terminals for a voltage wave form analysis. The L-N voltage will be approximately 70 volts for 15 amperes field current. C B C

~~3.3.5 Caution: Do not maintain an over excitation at 12,000 rpm long enough to cause overheating of the armature conductors. Any combination of rotor speed and field current which generates a line to neutral voltage > 3400 V can cause overheating of the armature. At 12,000 rpm a field current greater than 245A may cause overheating of the armature conductors.~~ C A

3.3.6 Superconductor Normalization

3.3.6.1 If normalization does not occur at 245A or less at 12,000 rpm during Step 3.3.4, reduce field current to zero and allow stator temperature to stabilize.

3.3.6.2 Ramp field current at a rate of 250A/min. at 12,000 rpm until field normalization occurs or until 275 amp field current is reached. Reduce field current to zero at a moderate rate immediately after a 275A field current is reached and allow stator temperature to stabilize.

3.3.6.3 If normalization did not occur during Step 3.3.6.2, reduce rotor speed to 11,000 rpm and ramp field current at a rate of 250A/min until field normalization occurs or 325A is reached. Reduce field current to zero at a moderate rate immediately after 325A is reached. If normalization does not occur at 325A or less at 11,000 RPM, additional field ramps at reduced speed may be specified by the test engineer.

3.4 Results

3.4.1 A plot with armature terminal voltage/RPM on the vertical axis and field current on the horizontal axis shall be made. C

3.4.2 A plot of stator oil flow and the temperature difference across the oil manifolds versus field current will be made. Finally a plot of stator losses versus terminal voltage squared will be made.

3.4.3 A plot of conductor temperature rise versus an eddy current loss parameter will be made. B

3.4.4 The input power to the d-c motor less the input power to this motor with generator disconnected from the output shaft of the high speed gearbox will be used to determine the total losses in the generator. B
The input power with the generator disconnected has been correlated with the output speed of the gearbox prior to this test. C C

The input power to the dc motor with the generator excited less the input power unexcited will be used to determine the stator losses.

4.0 SHORT CIRCUIT TESTS

4.1 General. The synchronous impedance test shall be made to determine the field current necessary to produce a given armature current when the generator is operating short-circuited. This calibration is used with the open circuit calibration to determine the reactance (X_d) for regulation calculations. In addition, the armature conductors are subjected to currents long enough to reach a steady state temperature. This temperature data is used to verify the calculation for the armature cooling system.

4.2 Apparatus. The apparatus used for this test is the same as that defined in 3.2 except the instruments and meter of Attachment B are replaced with those shown in Attachment E.

4.3 Procedure

4.3.1 With the armature terminals short-circuited as shown in Attachment E, and with the valve in the stator cooling system in the full-on position, operate the generator at the speed and field currents shown in Para. 4.4.4. A C

4.3.2 Delete C

4.3.3 Delete C

4.3.4 Record instrument reading as soon as field current reaches a constant value and rotor speed at the specified value. Simultaneously read and record field current, phase currents, rotor speed and clock time. Mark on cyclic recorder and the strip chart this clock time. Allow the temperature of the stator to stabilize and simultaneously read and record: C

ΔT across the oil manifold
Δp across the oil flow meter
field current
phase currents
rotor speed
clock time (mark on charts)

4.3.5 Reduce the field current in steps to obtain approximately 1000, 800, 600, 300, and 0 amperes phase current. Record all instrument readings at each reduction step as defined in Step 4.3.4. C

4.3.6 If phase currents observed in Step 4.3.3 are within 3% of the mean and the conductor temperatures observed in Step 4.3.3 were less than 300°F, increase the field current until 1400A flows in the armature conductors. Record all instrument readings as defined in Step 4.3.4. Additional tests with increased overload currents may be specified by the test engineer. C

4.3.7 Caution: Do not maintain overload currents long enough to cause overheating of the armature. If a conductor temperature reaches 325°F, reduce excitation and discontinue this test.

4.4 Results

4.4.1 A plot of generator short-circuit current (vertical axis) versus field current (horizontal axis) shall be made. The temperatures of the armature winding will be plotted against phase current.

4.4.2 A plot of the temperature of the armature winding versus the power loss density in the conductor will be made.

4.4.3 The short-circuit ratio and the reactance X_d will be determined by the method defined in MIL-STD-705A, Section 420.1 and Section 421.1.

4.4.4 Reference Attachment K C

If	RPM
0	2400
16	2400
33	2400
49	2400
66	2400
82	3200
92	4000

5.0 SUDDEN APPLICATION OF SHORT-CIRCUITS

5.1 General. A three-phase contactor shall be used for the sudden application of phase-to-phase short-circuits. The transient current records obtained by application of these short-circuits shall be used to determine:

Direct-Axis Transient Reactance, X'd
Direct-Axis Sub-Transient Reactance, X"d
Direct-Axis Transient Short-Circuit Time Constant, T'd
Direct-Axis Subtransient Short-Circuit Time Constant, T"d
Short-Circuit Time Constant of Armature Winding, T'a

5.2 Apparatus. The apparatus used for this test is the same as that defined in 4.2 except the instruments and meters of Attachment E are replaced with those in Attachment F.

5.3 Procedure

5.3.1 Operate the generator at 4,000 rpm and excite the field with 5 amperes dc current. Record the three line-to-neutral voltages (~ 23 volts), field current, and speed. C C

5.3.2 Adjust the oscillograph for proper timing and current calibration (~ 50 amps steady state) using current transformers and ammeter. B

5.3.3 Take oscillograph record to show the zero position of oscillograph current elements and timing wave. Remove current transformers after calibration. B

5.3.4 Close the contactor switch and record the transient and sustained currents.

5.3.5 Record line-to-neutral voltage, phase current, speed, and field current when steady-state short-circuit conditions are achieved.

5.4 Results

5.4.1 Direct-Axis Transient Reactance - This parameter shall be evaluated by the method defined in MIL-STD-705A, Section 425.1.4 as modified by paragraph 5.4.6 below. B

5.4.2 Direct-Axis Subtransient Reactance - This parameter shall be evaluated by the method defined in MIL-STD-705A, Section 426.1.4 as modified by paragraph 5.4.6 below. B

5.4.3 Direct-Axis Transient Short-Circuit Time Constant - This parameter shall be evaluated by the method defined in MIL-STD-705A, Section 427.1.4.

5.4.4 Direct-Axis Subtransient Short-Circuit Time Constant - This parameter shall be evaluated by the method defined in MIL-STD-705A, Section 428.1.4.

5.4.5 Short-Circuit Time Constant of Armature Winding - This parameter shall be evaluated by the method defined in MIL-STD-705A, Section 432.1.

5.4.6 The values calculated for the reactances will be modified by the ratio of the open circuit voltage with I_f = 5 amperes to rated open circuit voltage. B

5.4.7 The values calculated for the reactances from the test data will be compared with the values obtained from the design program. B

6.0 OPEN CIRCUIT TESTS AT 8000 RPM (ADDED PARA.): C

6.1 General. The purpose of this test is to obtain the no-load output voltage versus the field amperes at rated speed*. This calibration will be used to compare the actual voltage with computer calculations. The other parameters obtained from this test are (1) phase balance (voltage), (2) field current for normalization of the field at 8000 rpm, (3) the no-load electrical losses in the stator, and (4) the stator coolant flow rate.

6.2 Apparatus

6.2.1 The signals generated by a 60 tooth wheel directly coupled to the rotor shaft shall be counted over a one second period to measure the revolution per minute.

6.2.2 The instrumentation shown in Attachment B will be used to measure the open-circuit voltages (line-to-neutral) and the field current.

6.2.3 The apparatus shown in Attachment C will be connected to the stator to circulate and measure the oil flow through the stator.

6.2.4 The apparatus and meters shown in Attachment A will be used to record and observe the output of the calibrated, resistance thermometers in the rotor, and the external helium management system.

6.2.5 The meters shown in Attachment D will be used to cyclic record the temperatures of the stator cooling oil, back-iron, and armature conductor temperatures. The location of the thermocouples in the stator are shown in Attachment D, also.

6.3 Procedure

6.3.1 Operate stator coolant pump with water valve in the full on position without excitation in the generator until the stator and cooling system reach constant temperatures.

6.3.2 Operate generator at 8000 rpm until bearings and helium cooling system reach a constant temperature.

---

* Note that we will now prove 5 MW capability at 8000 rpm instead of at 12,000 rpm. See Figure 11 of Monthly Report #20 of Phase IIB for period ending November 30, 1976 for correlative conditions. Note on that Figure that the L-L voltage will be about 3000.

6.3.3 Increase field excitation at a constant rate of 25 ± 2 A/min. until the field current given below is reached and allow the field current to drift to a constant current for each rheostat position. Adjust input voltage to DC motor to maintain a speed of 8,000 ± 1%. Field current for readings: 0, 5, 50, 100, 150, 200, 225, and 245A.

6.3.4 As soon as the field current reaches a constant value for each rheostat position and the speed is set at 8,000 rpm ± 1%, simultaneously read and record the field current, terminal voltages, rotor speed, and clock time.

Mark on the cyclic recorder charts and the strip charts this clock time. Allow the temperatures of the stator to stabilize and simultaneously read and record:

ΔT across the oil manifold
Δp across the oil flow meter
field current
terminal voltage
rotor speed
clock time (mark on charts)

6.3.5 Caution: Do not maintain an over excitation of 8000 rpm long enough to cause overheating of the armature conductors. Any combination of rotor speed and field current which generates a line to neutral voltage > 3400V can cause overheating of the armature. At 8000 rpm a field current greater than 367A may cause overheating of the armature conductors.

6.3.6 Superconductor Normalization

6.3.6.1 If normalization does not occur at 245A or less at 8,000 rpm during Step 6.3.4, reduce field current to zero and allow stator temperature to stabilize.

6.3.6.2 Ramp field current at a rate of 250A/min. at 8000 rpm until field normalization occurs or until 275 amp field current is reached. Reduce field current to zero at a moderate rate after a 275A field current is reached and allow stator temperature to stabilize.

3.4 Results

3.4.1 A plot with armature terminal voltage on the vertical axis and field current on the horizontal axis shall be made.

6.4.2 A plot of stator oil flow and the temperature difference across the oil manifolds versus field current will be made. Finally a plot of stator losses versus terminal voltage squared will be made.

6.4.3 A plot of conductor temperature rise versus an eddy current loss parameter will be made.

6.4.4 The input power to the d-c motor less the input power to this motor with generator disconnected from the output shaft of the high speed gearbox will be used to determine the total losses in the generator. The input power with the generator disconnected shall be correlated with the output speed of the gearbox prior to the Warm Rotor Test of Paragraph 1.0.

The input power to the dc motor with the generator excited less the input power unexcited will be used to determine the stator losses.

7.0 UNBALANCED LOAD TEST, L-N SHORT-CIRCUIT *

7.1 General. The generator will be subject to an unbalanced load by shorting one phase terminal to neutral terminal. This unbalanced load will cause a time varying electromagnetic field relative to the rotor. Heating of the rotor electromagnetic shield will occur. The thermal state of the shield under a steady-state unbalanced load will be compared with design calculations.

7.2 Apparatus. The apparatus used for this test is the same as that defined in Section 5.2 except the instruments and meters of Attachment F are replaced with those in Attachment G.

7.3 Procedure

7.3.1 Operate the generator at 8000 rpm without excitation until steady-state thermal state exists within the field winding and at the cooling stations for the electromagnetic shield. Record the output of the resistance thermometers in the rotor.

7.3.2 Increase field current until a 35 amp current is obtained in the shorted phase.

7.3.3 Allow the output of the resistance thermometers at the cooling stations for the electromagnetic shield to stabilize and record a complete set of readings. Obtain a calibrated trace of the field current during this mode of operation.

7.3.4 Increase field current in steps to obtain 40, 45, 50, 55, and 60 amp current in the shorted phase and repeat Step 7.3.3.

7.3.5 Caution: Heating of the electromagnetic shield may exceed the capacity of the cooling system. Therefore, the thermometers at the cooling stations should be monitored continuously. If the temperature of a cooling station reaches 80K, the field current must be reduced at a moderate rate immediately and the test should be discontinued.

7.4 Results

A plot of electromagnetic shield temperatures versus the shorted phase current will be made.

---

* Originally Paragraph 6.0 C

8.0 SHORT-CIRCUIT RECTIFIER BRIDGE TEST *

8.1 General. A three phase, full-wave rectifier bridge will be connected to the terminals of the generator. The dc output terminals of the bridge will be short-circuited through an inductor. This load will produce odd time harmonics, excluding the third and its multiples, in the phase currents. The harmonic currents produce time varying fields relative to the rotor and cause heating in the electromagnetic shield. The heating data obtained from this test will be compared with the calculated data.

8.2 Apparatus. The apparatus required for this test is the same as the apparatus defined by Section 7.2 except the equipment shown in Attachment G is replaced by the equipment shown in Attachment H .

8.3 Procedure

8.3.1 Operate the generator at 8000 without excitation until steady-state thermal state within the field winding and at the cooling stations for the electromagnetic shield. Record the output of the resistance thermometers in the rotor.

8.3.2 Increase field excitation until a dc short circuit current at 50 amperes is obtained.

8.3.3 Obtain a calibrated trace of the ac component of the alternator field current at each operating condition.

8.3.4 Obtain a calibrated trace of the phase currents and the dc current during each operating condition.

8.3.5 Allow the output of the resistance thermometers at the cooling stations for the electromagnetic shield to stabilize and record a complete set of readings.

8.3.6 Repeat Step 8.3.2 through 8.3.5 for dc currents of 100, 150, and 200 amperes. Additional tests with increased dc currents may be specified by the test engineer.

---

* Originally Paragraph 7.0

C

8.3.7 Caution: Heating of the electromagnetic shield may exceed the capacity of the cooling system. Therefore, the thermometers at the cooling stations should be monitored continuously. If the temperature of a cooling station reaches 80K, the field current must be reduced at a moderate rate immediately and the test should be discontinued.

8.3.8 Results

8.3.8.1 A plot of shield temperature versus dc output from the rectifier bridge will be made.

8.3.8.2 The phase current harmonic will be determined.

8.3.8.3 The harmonic on the dc current will be determined.

8.3.8.4 The heating of the electromagnetic shield based upon the measured phase current harmonic shall be calculated.

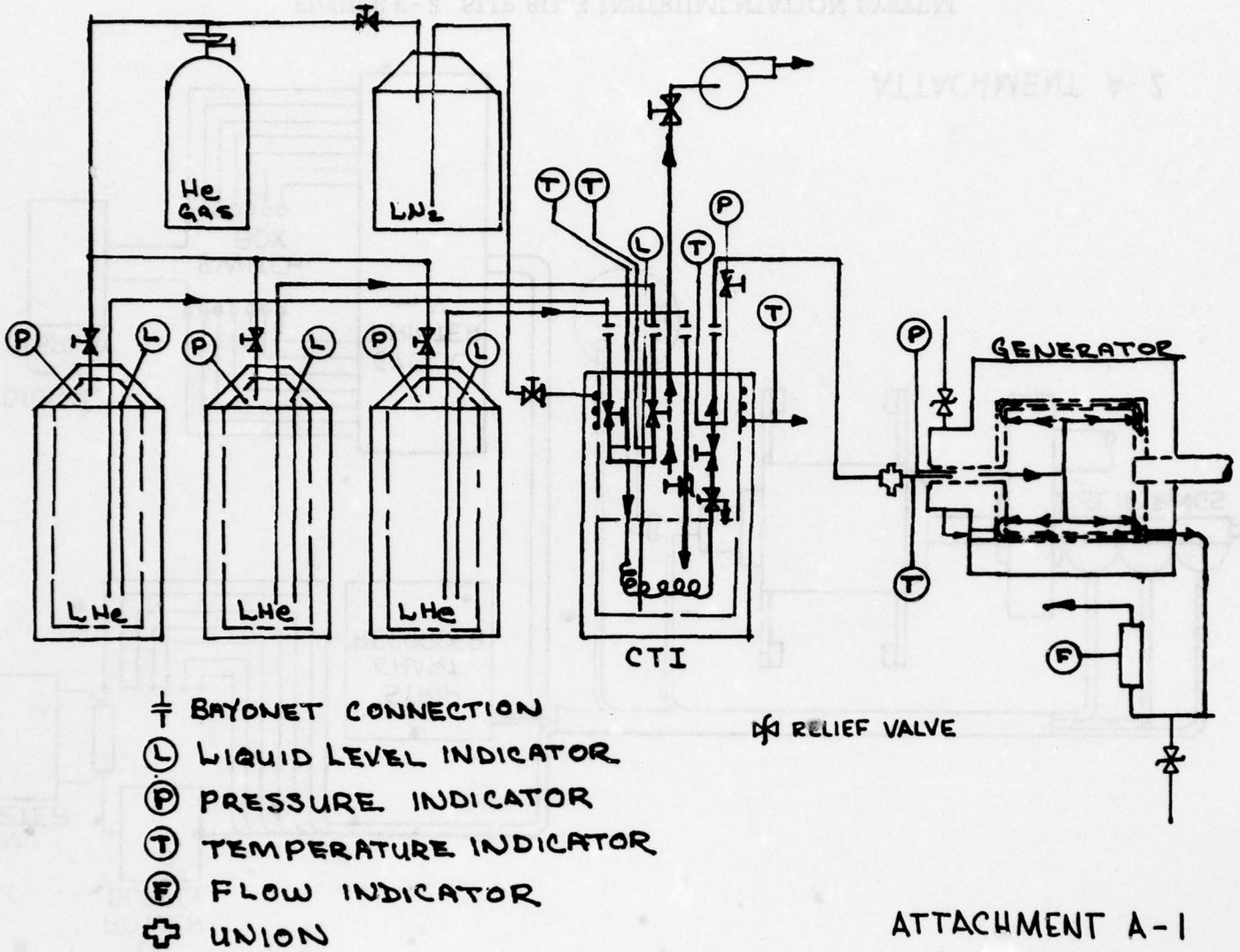


FIGURE K-1 EXTERNAL HELIUM SUPPLY SYSTEM

PRECEDING PAGE BLANK

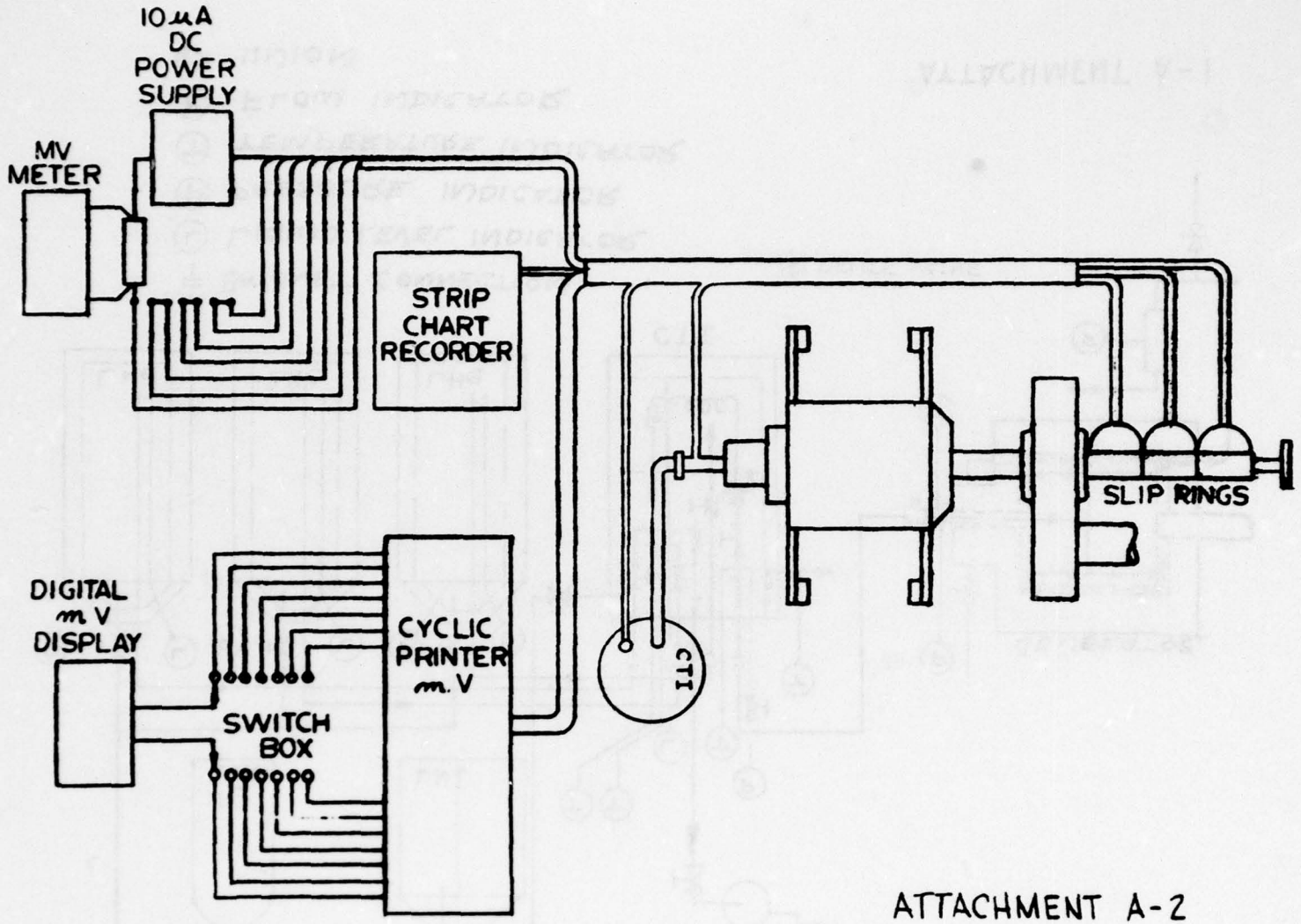


FIGURE K-2 SLIP RING INSTRUMENTATION SYSTEM

SKETCH SHEET
FORM 28577

WESTINGHOUSE ELECTRIC CORPORATION

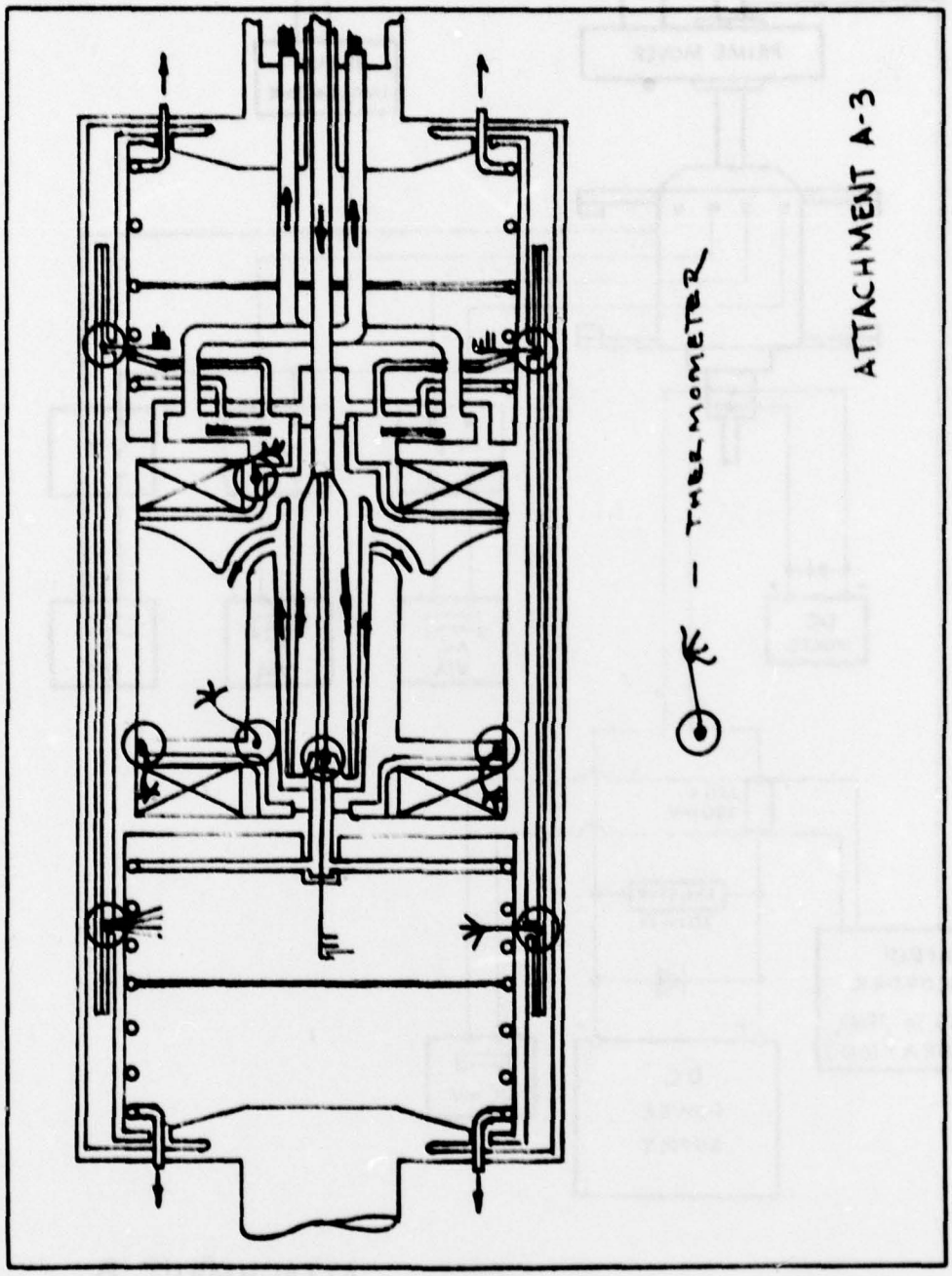
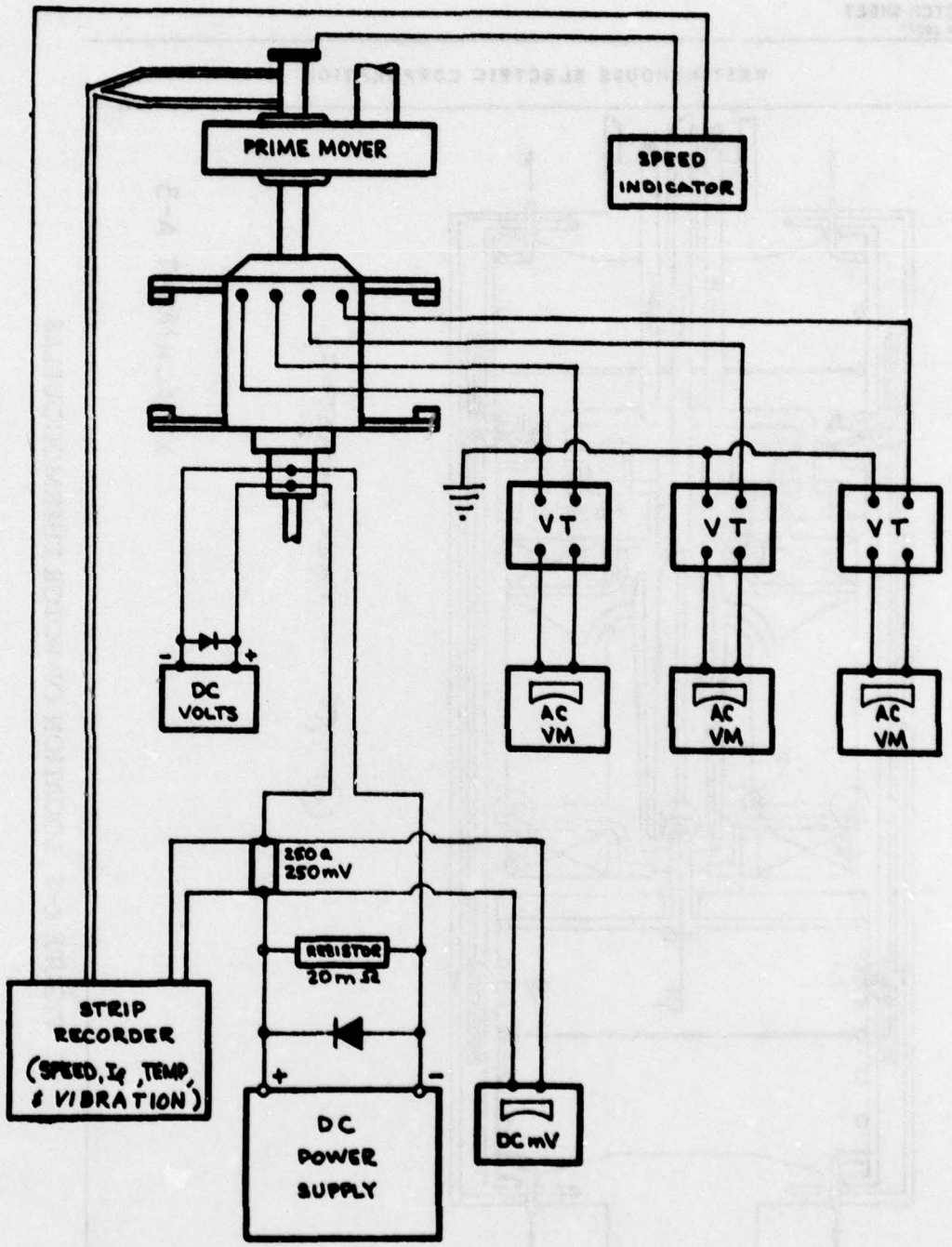


FIGURE K-3 LOCATION OF ROTOR THERMOCOUPLES



ATTACHMENT B

FIGURE K-4 OPEN CIRCUIT TEST INSTRUMENTATION

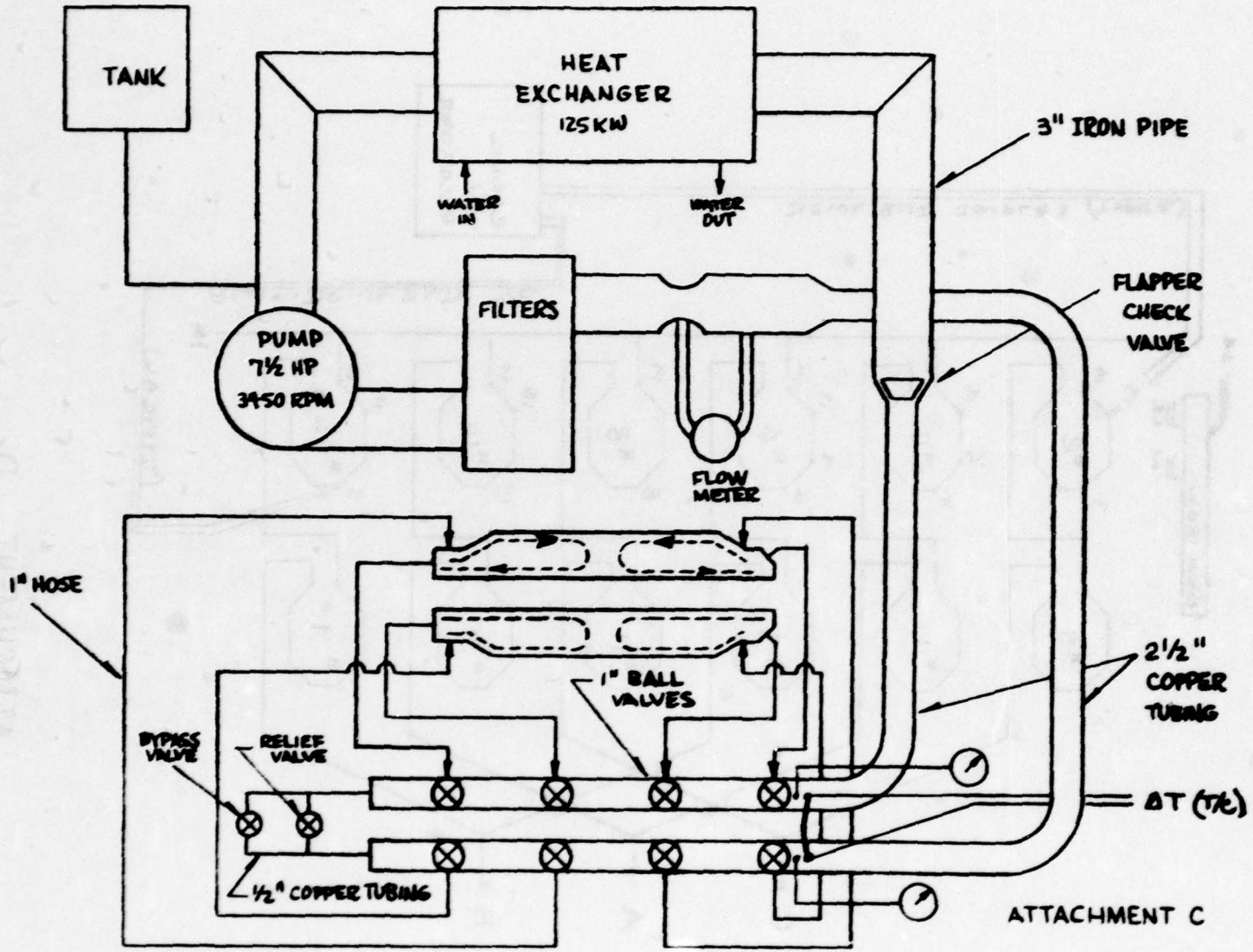
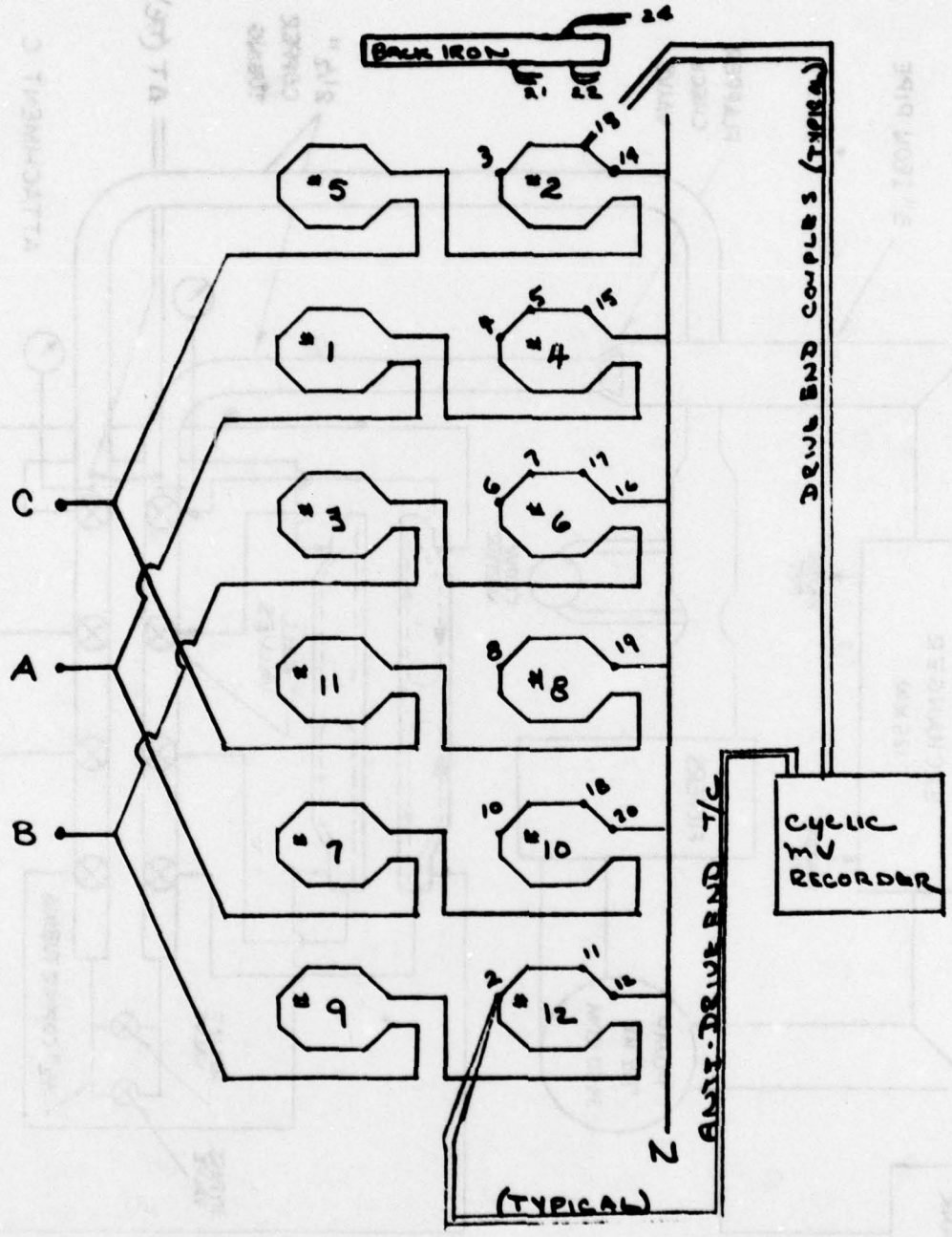
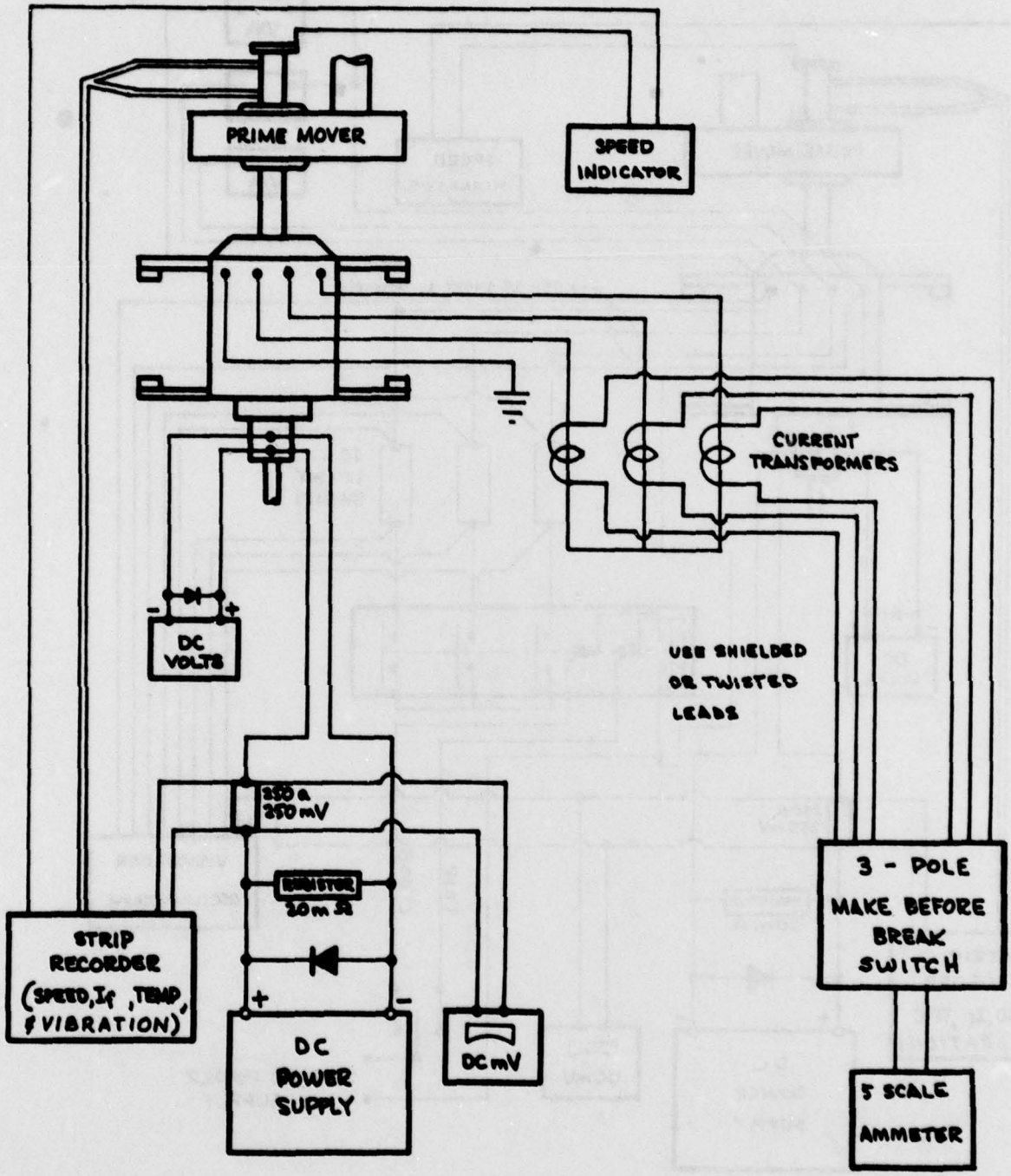


FIGURE K-5 STATOR COOLING SYSTEM



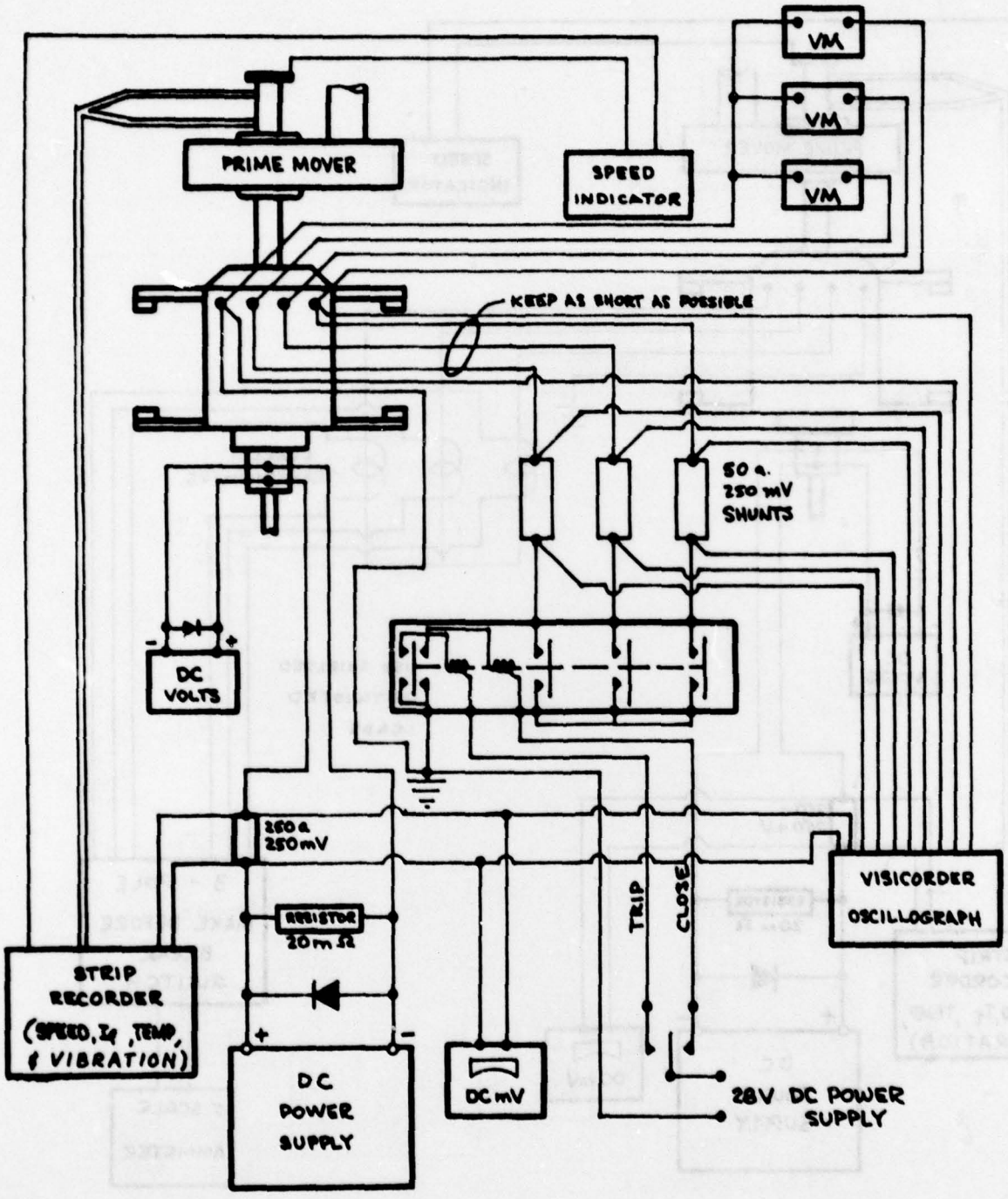
ATTACHMENT D

FIGURE K-6 THERMOCOUPLE LOCATIONS IN STATOR



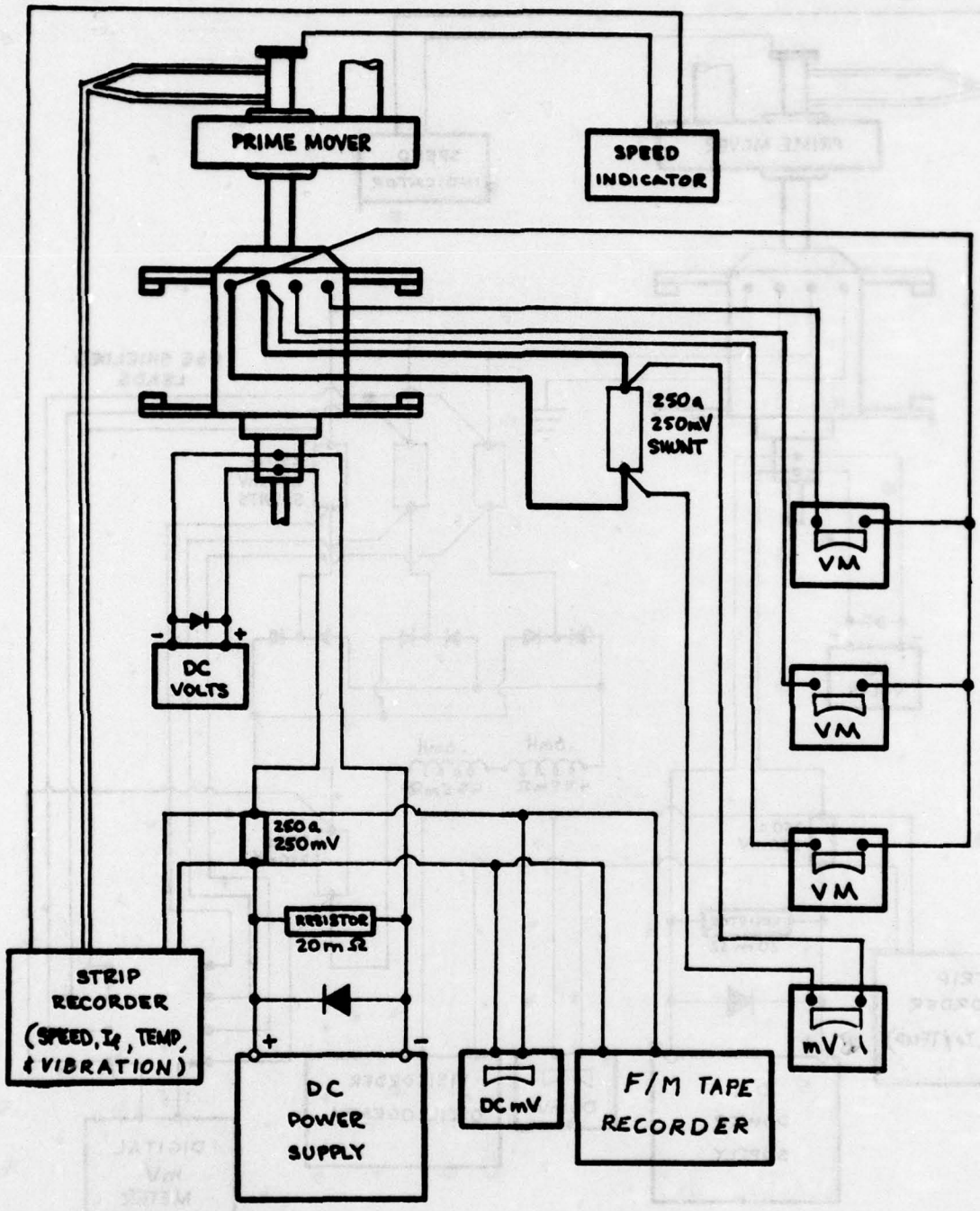
ATTACHMENT E

FIGURE K-7 SHORT CIRCUIT TEST INSTRUMENTATION



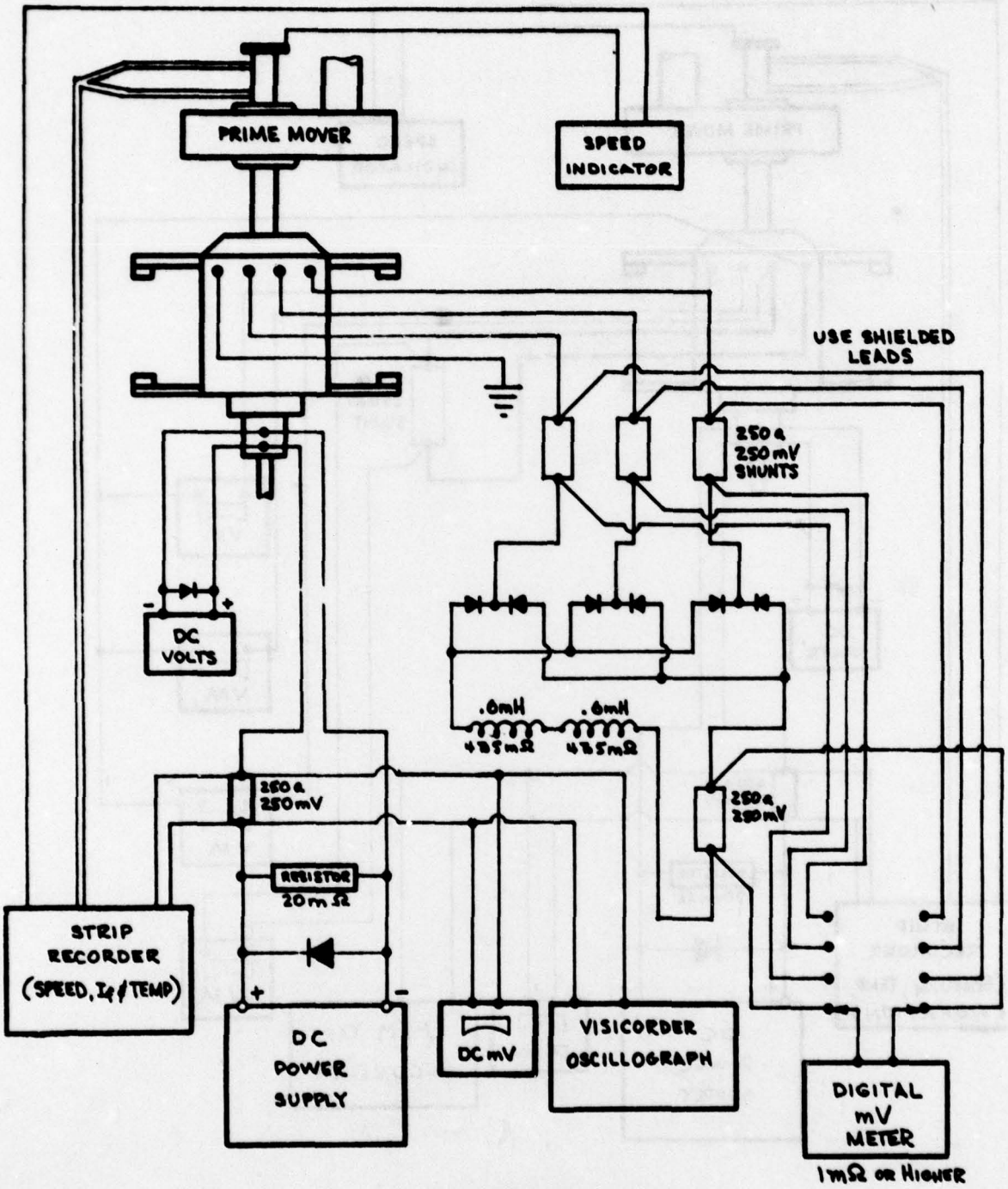
ATTACHMENT F

FIGURE K-8 INSTRUMENTATION FOR SUDDEN APPLICATION OF SHORT CIRCUIT TESTS



ATTACHMENT G

FIGURE K-9 UNBALANCED LOAD TEST INSTRUMENTATION



ATTACHMENT H

FIGURE K-10 INSTRUMENTATION FOR RECTIFIED LOAD TEST

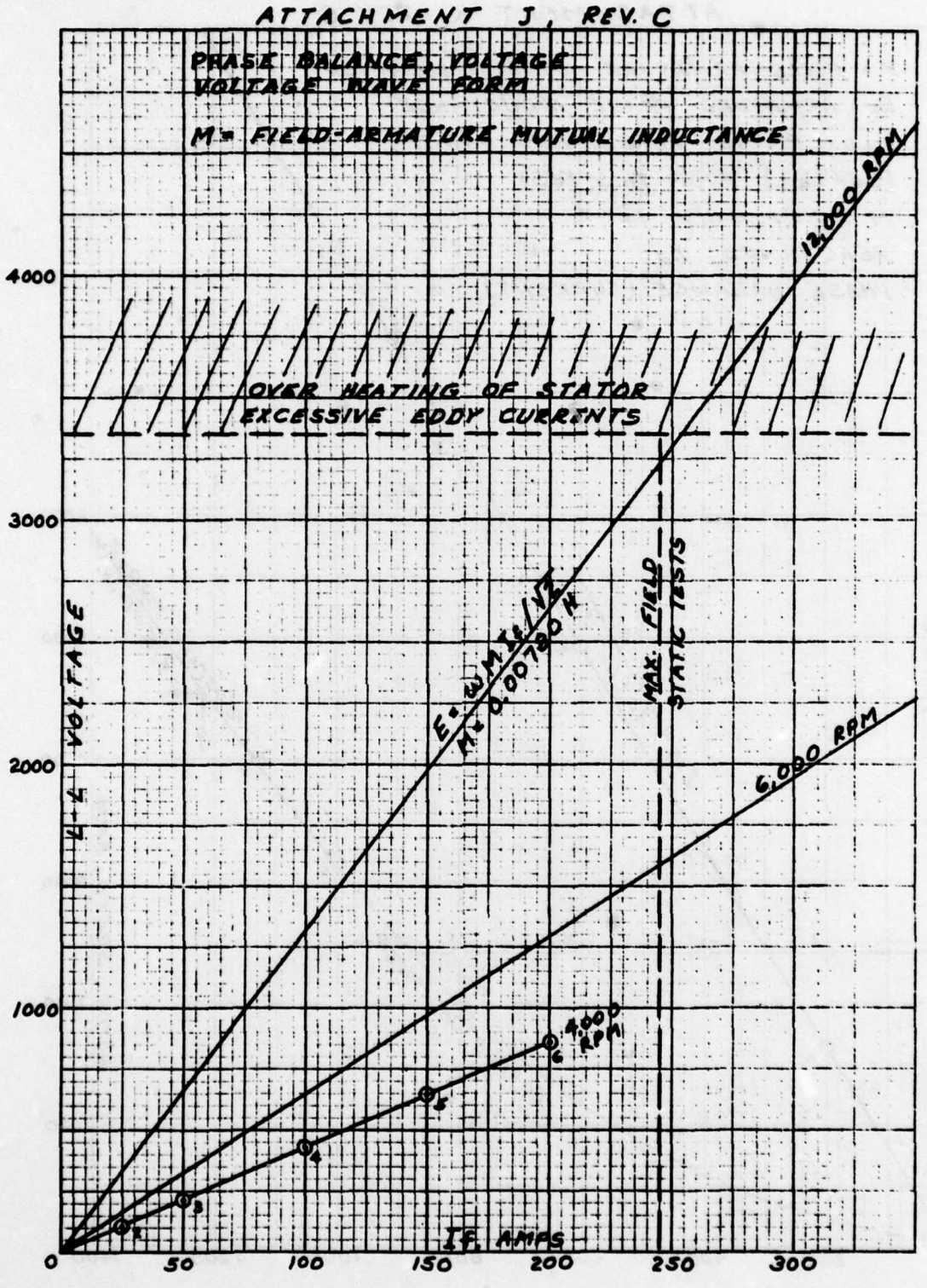


FIGURE K-11 VOLTAGE PARAMETERS FOR NO LOAD TEST

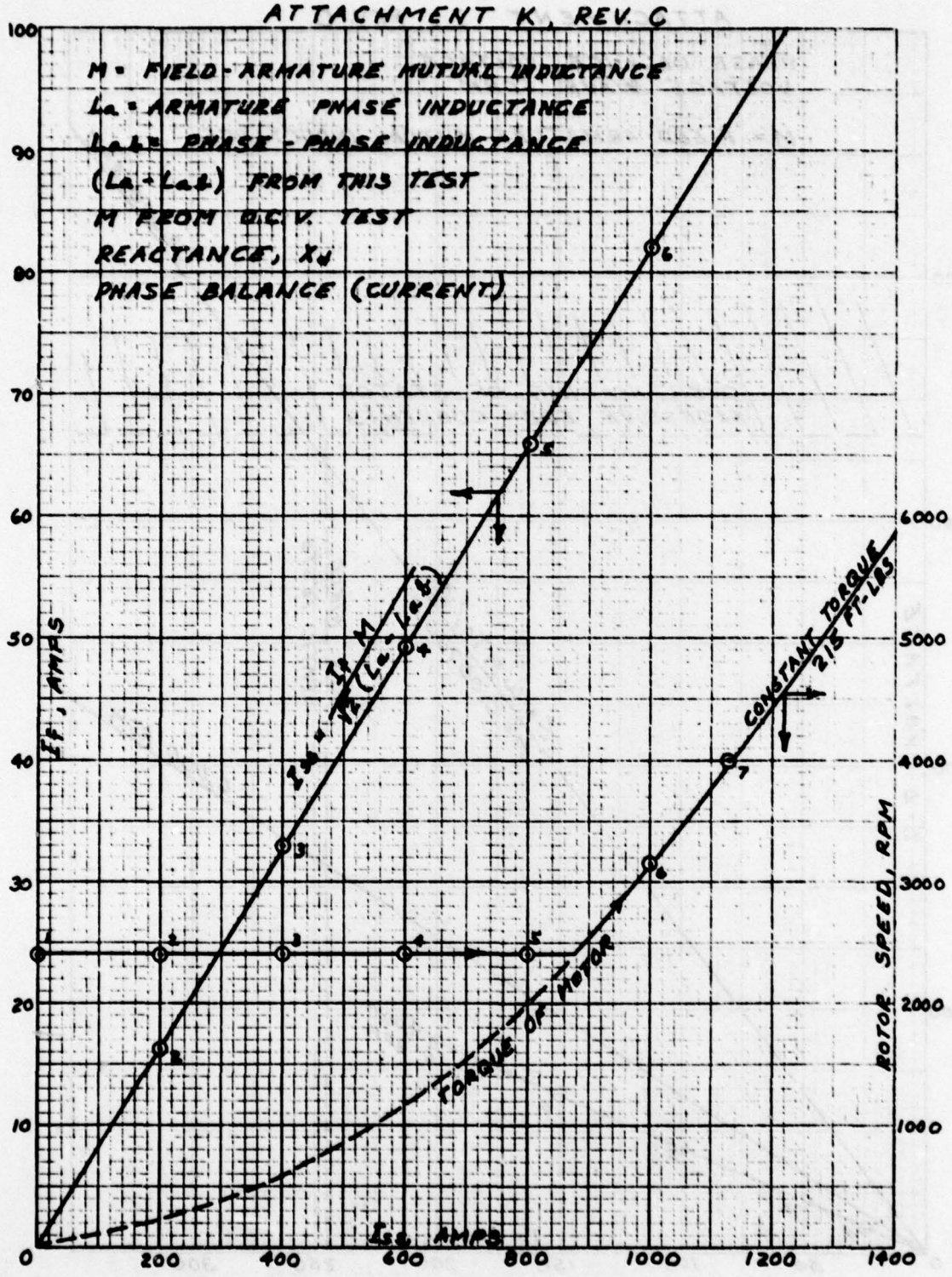


FIGURE K-12 FIELD CURRENT PARAMETERS FOR SHORT CIRCUIT TESTS

REFERENCES

1. Woodson, H. H., Smith, J. L., Jr., Thullen, P., Kirtley, J. L., Jr., "The Application of Superconductors in the Field Windings of Large Synchronous Machines", Vol. PAS-90, No. 2, pp. 620-627, IEEE Trans. Power Apparatus and Systems, March/April 1971.

2. Stekley, Z. J. J., Woodson, H. H., Hatch, A. M., Hoppie, L. O., Halas, E., "A Study of Alternators with Superconducting Field Windings: II Experiment", Vol. PAS-85, No. 3, pp. 274-280, IEEE Trans. Power Apparatus and Systems, March 1966.

3. Thullen, P., Dudley, J. C., Greene, D. L., Smith, J. L., Jr., Woodson, H. H., "An Experimental Alternator with a Superconducting Field Winding", IEEE Power Group, September 1969.

4. Litz, D. C., Jones, C. K., "Cryogenic Considerations in the Development and Operation of a Large Superconducting Synchronous Generator", Vol. 20, Advances in Cryogenics, (to be published).

5. Sterrett, C. C., Mole, C. J., "A Superconducting Machine for General Station Power Generation", Vol. 35, pp. 1035-1047, Proceedings of the American Power Conference, 1973.

6. Smith, J. L., Jr., Kirtley, J. L., Jr., Thullen, P., Woodson, H. H., "EEI Program on Large Superconducting Synchronous Machine", IEEE No. 72CH0682-5-TABSC, Proc. Applied Superconductivity Conference, Annapolis, 1972.

7. Proceedings of the Fifth International Cryogenic Engineering Conference, Kyoto, Japan, May 7-10, 1974.

8. Parker, J. H., Jr., Blaugher, R. D., Patterson, A., Vecchio, P. D., McCabria, J. L., "A High Speed Superconducting Rotor", Vol. MAG-11, No. 2, pp. 640-645, IEEE Trans. on Magnetics, March 1975.

9. McCabria, J. L., Blaugher, R. D., Parker, J. H., Jr., "Superconducting Generator Development", Proceedings of the IEEE National Aerospace and Electronics Conference, June 1975.

10. Blaugher, R. D., McCabria, J. L., Parker, J. H., Jr., "Program for the Development of a Superconducting Generator, Part I, Phase I Report", Air Force Technical Report AFAPL-TR-74-84, October 1974.

11. Blaugher, R. D., et al, "High Speed Superconducting Generator", Vol. MAG-13, No. 1, IEEE Trans. on Magnetics, January 1977.

12. McCabria, J. L., et al, "High Speed Superconducting Generator Development", Proceedings of the IEEE National Aerospace and Electronics Conference, May 1975.

13. Moskowitz, R., "Designing with Ferromagnetic Fluids", 74 DE-5, The ASME Design Engineering Conference, Chicago, Illinois, 1974.

14. Echert and Drake, Heat and Mass Transfer, page 194, McGraw-Hill Publishing Co., Second Edition.

15. Jiri Lammeraner and Milos Stafl, Eddy Currents, pp. 91-98, Iliffe Books, Ltd., 1966.

16. Patterson A. E., et al, "High Speed Helium Transfer System - Evaluation and Testing", Vol. 23, Cryogenic Engineering, 1973.

17. Blaugher, R. D., "Superconducting Spin-Test Rotor", Air Force Technical Report AFAPL-TR-77-39, (release pending).

18. Scott, R. B., Cryogenic Engineering, D. Van Nostrand Co., Princeton, N. J., 1959.

19. Dunbar, W. G., Seabrook J. W., "High Voltage Design Guide for Airborne Equipment", AFAPL-TR-76-41, June 1976.

20. Ashton, Halpin, Petit, Primer on Composite Materials: Analysis, Techonomic Publishing Co., Inc., Stamford, Conn., 1969.

21. Vicario, A. A., "Trident I (C-4) Composite Materials Characterization Program", Hercules Incorporated, Allegany Ballistics Laboratory, Cumberland, Maryland, February 1973.

22. Lehman, Hawley, et al., "Investigation of Joints in Advanced Fibrous Composites for Aircraft Structures", Volume 1, Technical Report AFFDL-TR-69-43, 1969.

23. Anon., "Buckling of Thin-Walled Circular Cylinders", NASA SP-8007, August 1968.

☆U.S.Government Printing Office: 1979 — 657-002/707